MINISTRY OF EDUCATION AND SCIENCE OF UKRAINE
DNIPRO UNIVERSITY OF TECHNOLOGY

K. Zabolotnyi
V. Symonenko
O. Panchenko
M. Rutkovskiy

JUSTIFICATION OF THE CALCULATION METHOD FOR CYLINDRICAL DRUMS OF MINE HOISTING MACHINES

Monograph

Dnipro
Jurfond
2024

UDC 622.673.1:621.778.27

J95

Recommended for publication by the Academic Council of the Dnipro University of Technology (protocol No. 9 of 24 July 2024).

Reviewers:

I.V. Belmas - Doctor of Technical Sciences, Professor, Head of the Department of Machinery Technologies and Engineering at Dniprovsky State Technical University;

G.O. Shevchenko - Doctor of Technical Sciences, Head of the Department of Mechanics of Machines and Mineral Raw Processing at the Polyakov Institute of Geotechnical Mechanics of the National Academy of Sciences of Ukraine,

L.N. Shyrin - Doctor of Technical Sciences, Professor, Head of the Department of Transport Systems and Energy-Mechanical Complexes, Dnipro University of Technology.

Zabolotnyi K.S.

J95

Justification of the Calculation Method for Cylindrical Drums of Mine Hoisting Machines: monograph / K.S. Zabolotnyi, V.V. Symonenko, O.V. Panchenko, M.A. Rutkovskiy; Ministry of Education and Science of Ukraine, National Technical University "Dnipro Polytechnic." - D : Dnipro, Jurfond, 2024. - 190 p.

ISBN 978-966-934-571-4

The paper presents the results of research aimed at substantiating and developing a method for determining the design loads when winding a rope on a cylindrical drum of mine hoisting machines, taking into account the influence of the geometric and strength characteristics of its reinforced structure and the change in the stress-strain state that occurs there under the influence of rope turns. It is proved for the first time that by determining the average values of stresses in the structurally orthotropic shell of the drum, it is possible to select data for further refined calculation of its parameters by the FEM method. A methodology for calculating drums of non-standard designs of mine hoisting machines has been developed and substantiated on the example of the drum of the TsR-6.75×6.2/1.95 machine. The error of the method of simplified calculation: the method of averaging with increased thickness of the lobes is estimated.

For students, teachers, engineers, technicians, scientists and designers involved in heavy engineering.

ISBN 978-966-934-571-4

CONTENTS

INTRODUCTION

The relevance of the topic covered in this monograph can be explained, first of all, by the great importance of underground cargo movement to the surface. It is known that the main means for this purpose are mine hoisting systems.

It is these complex units that link the underground mine workings to the day surface. The key part of each of them is the mine hoisting machine (MHM). In modern conditions, this is the most energy-intensive and power-consuming stationary equipment at the mine. For example, the power of the electric drive of such a machine can exceed 2000 kW. At coal mines and mines of the mining industry most often use a hoisting machine equipped with cylindrical drums. In fact, the largest modern domestic drum MHM can provide a useful lifting capacity of up to 35 tonnes from a depth of up to 1000 m, developing lifting speeds of up to 20 m/s. Cylindrical drum as an actuating organ of the MHM is called to perceive high static and dynamic loads. That is why its design is often subject to special requirements. For example, European manufacturers of MHM's use drums of relatively simple designs, as a rule, smooth cast drums, the thickness of the shell of which reaches 160 mm. In domestic practice, it is customary to increase the strength and rigidity of drums by means of various types of reinforcements (braces, ribs, spandrels). Thus, Ukrainian manufacturers produce MHM's, drums of which have more complex welded construction, but have much lower mass compared to foreign analogues, and the thickness of the shell of these objects does not exceed 55 mm. It is clear that, on the one hand, there is a significant competitive advantage of the domestic MHM, but at the same time there is a problem of correct installation of drum reinforcements, which is constantly faced by designers. In case of failure of such operations, welded drums can reduce their service life in comparison with imported analogues. Meanwhile, correctly calculated parameters and well-defined drum design, as well as its operating conditions, largely determine the service life of the mechanical part of the hoisting machine.

As practice shows, in the process of operation of these installations such malfunctions of winding organs may occur: deformation of the shell, drum creaking,

cracks in the shell, drum knocking during operation, increased axial displacement of the shaft, slipping of the rope from the drum surface, wear of its loose hub.

Many famous scientists, in particular B.I. Davydov, B.S. Kovalsky, Z.M. Fedorova, A.P. Nesterov, F.L. Shevchenko, V.I. Dvornikov, V.I. Samusya, K.S. Zabolotny, N.M. Fidrovskaya [1], have been engaged in improving the design of MHM drums in their time. The solution of these issues is reflected in the whole set of methodological recommendations developed by the above-mentioned specialists. The methods of verification calculations of MHM drums operation contained in the literature are of an evaluative nature. Often these data are insufficient to optimise the drum design. That is why it was decided to apply structural design optimisation techniques to develop the existing methods. For example, the essence of the Zabolotny K.S. method consists in building a simplified generalised-parametric model of a drum of a grinding machine with the subsequent optimisation of its parameters and introduction of appropriate changes in the design of this object. In the process of realisation of this approach there was a necessity to develop an effective method of determination of design loads acting on the drum. At the same time, the influence of geometric and stiffness characteristics of structural reinforcements of the drum, as well as changes in its stress-strain state (STS) under the influence of rope turns should be taken into account. This method was recognised as a computational algorithm (designer's ARM), the use of which on the basis of mathematical models of deformation of the reinforced drum and rope winding makes it possible to calculate the operating parameters of these objects and to design rational designs of working bodies of the machine. Taking into account the above, the purpose of the research considered in this monograph is to solve a very urgent scientific problem.

The authors of the monograph aimed to determine the influence of geometric and stiffness characteristics of the reinforced drum structure, as well as to trace the change in its stress-strain state under the influence of rope turns in terms of developing a method for calculating design loads, creating an engineering methodology for determining the parameters of operation of these objects and designing rational designs of the working bodies of MHM.

1 ANALYSING THE STATE OF THE ART AND SETTING THE SCIENTIFIC CHALLENGE

1.1 Relevance of the technical problem calculation of drum parameters of typical MHM designs

In the process of solving very important issues for our time, devoted to the development of new methods of design of prospective mining machines, the authors focused on mine hoisting machines as the main part of the mine hoisting plant. The practice of underground mining confirms the special importance of shaft hoisting machines in the continuity of production. Thus, the forced stoppage of the hoisting machine is the cause of the actual cessation of work in the mine, bringing huge losses. This determines high requirements to the technical level of lifting machines and the quality of their manufacture.

In the conditions of the modern mining equipment market, mine hoists of domestic production are inferior to foreign analogues in terms of quality, reliability and cost. High metal intensity, low durability compared to imported analogues, all this does not allow our hoists to compete in the foreign market. European manufacturers, as a rule, equip MHM with drums of relatively simple designs. Often they are smooth cast, with shell thickness not exceeding 160 mm.

In order to reduce the impact of the existing design deficiencies on the operation of the MHM, domestic specialists are forced to increase the strength and rigidity of drums by means of various types of reinforcements (braces, ribs, spandrels). As a result, domestic hoist drums are rather complex welded structures, at the same time they are much lighter than their foreign analogues, having at the same time a shell not thicker than 55 mm.

As noted above, modern MHM’s are the most powerful of all stationary mining equipment. Thus, the electric drive of a hoisting machine can have a capacity from 1000 to 2000 kW. At the same time, it consumes up to 40 per cent of all electricity

used in the mine. In addition, the hoisting machine is installed for the entire life of the mine, and the weight of this equipment can range from 20 to 300 tonnes.

The vessels lifted by the machines move in the shaft at a speed of 15 - 20 m/s (54 - 72 km/h). Approximately the same speed is developed by a railway train. But since in the first case the movement is limited to a short distance (equal to the length of the mine shaft), the lifting machines must have a very reliable control system and fail-safe braking devices.

In mine and quarry operations, the most commonly used MHM's are those equipped with cylindrical or bicylindroconical drums.

The most powerful of the modern domestic drum hoisting machines can provide a useful lifting capacity of up to 35 tonnes, moving materials from depths of up to 900 m and developing speeds of up to 14 m/s.

For the last 35 years in the Ukrainian Donbass the depth of mine shafts has reached 1200 - 1500 m, for comparison, in the mines of South Africa this indicator is 3000 - 4200 m. At the same time, the load capacity of MHM vessels at coal mines is equal to 35 tonnes, and at iron ore pits - 50 tonnes, and the vessels move at a speed of at least 16 m/s. In addition, the power of electric drive of hoists in some cases can reach 6000 -10000 kW.

It is known from the experience of new coal mines of FRG that there the speed of skip movement reaches 20 m/s. And if in 1950 the lifting capacity of these vessels did not exceed 12 tonnes, by 1985 it doubled, and now it reaches 35 tonnes. A similar trend of lifting transport development is observed in other countries.

It was noted that the rope capacity of bicylindrical conical drums (BCC), with which domestic hoists are equipped, is very difficult to increase. For this reason, they are significantly inferior to machines with cylindrical drums (CD) in terms of many operating and physical parameters (fly moment, machine weight, etc.). It turned out that these lifts cannot successfully compete with the machines of the TsR type (shortened from the name of cylindrical split drum).

At the same time, modern designers are developing hoisting machines with

lifting capacities of 75...100 tonnes, as well as machines that can operate in very deep mines.

As the main mode of transport linking the underground mine workings with the day surface, hoisting plants play a crucial role in mining technology.

Any MHM includes the following objects: main shaft with winding organ, shifting mechanism and main bearings; braking device; couplings; gearbox; electric drive; control, protection and interlocking equipment.

The winding organ (drum) is the most important element of a hoisting machine, as it supports high static and dynamic loads. The mechanical life of the hoisting machine depends to a large extent on the correct calculation and design of the drum, as well as the operating conditions.

As noted by Fedorova Z.M., the drum is the most massive and heavily loaded unit of the lifting machine, which is a closed cylindrical shell supported by stiffening rings. Each cylindrical drum has such structural elements:

- shell, i.e. a profiled cylindrical shell, which is attached to the rim of the frontal and is intended for winding the rope;

- frontal, which is a set of circular discs that form the sides of a drum with circular holes for mounting and a central hole connected to the hub;

- reinforcements - thin-walled bodies (braces, ribs, spandrels) that increase the stiffness of the drum in axial and annular directions;

- hubs connected to the shaft by means of keyways on wedged drums and loosely seated on sliding drums.

Historically, there have been two fundamental trends in the design of MHM drums, which have been preserved to this day: Western - cast designs and domestic - welded.

Cast drums are most common in mining operations in the USA and Europe. Cast steel drums have a shell thickness of up to 160 mm, which gives them sufficient rigidity, strength and durability, but at the same time they have a very high mass and high flywheel torque compared to welded drums.

Welded drums are produced at the Novokramatorsk Machine Building Plant (NKMZ). Taking into account technological considerations, the shells of welded drums are made up to 55 mm thick, which provides less massiveness compared to cast ones, but causes the need to compensate for design deficiencies by adding various reinforcements. The latter are installed in accordance with the stress intensity calculations.

The simplest in design are two-drum hoisting machines of 2C type, where each rope is wound on a separate drum. Let us designate the rope that lifts the payload as the working rope, otherwise we will call it the idle rope. From the point of view of shell theory, such drums are thin and long because their parameters correspond to such dependences:

$$\frac{l}{R}\cdot\beta = 1{,}31\frac{l}{R}\cdot\sqrt{\frac{R}{h}} = 8\text{K } 20 > 1{,}5\pi; \quad \frac{R}{h} = 60\text{K } 80,$$

where *R is* the shell radius; *h is* the thickness; *l is* the width; β is a dimensionless parameter determining the thinness of the shell.

Cylindrical cut cylindrical drum of the MHM of the TsR type, unlike the 2C type, consists of two parts, a wedged and a repositioned one. To visualise the structure of the welded drum, Fig. 1.1 shows the general view and section of the cylindrical split drum of the TsR -6×3.4 machine. The drum has a repositioning mechanism, by means of which the repositioning part of the drum is disconnected from the machine shaft to adjust the length of the rope, which is performed when changing horizons, as well as when it is necessary to pull out the rope and cut it for testing. The shifting mechanism can be located either on the outside of the shifting part or inside the drum.

Both the tipping part 11 and the wedged part 12 of the drum have a screw thread for the rope 13 on the outer surface. The lower rope 2 fixed to the wedged part of the drum can be coiled only up to the cut, i.e. up to the tipping part. The upper rope 1 secured to the slack part of the drum goes over the cut. This rope can be an idle rope and the lower rope can be a working rope, or vice versa: the upper rope can be a

working rope and the lower rope can be an idle rope. The first variant of rope use is more often used.

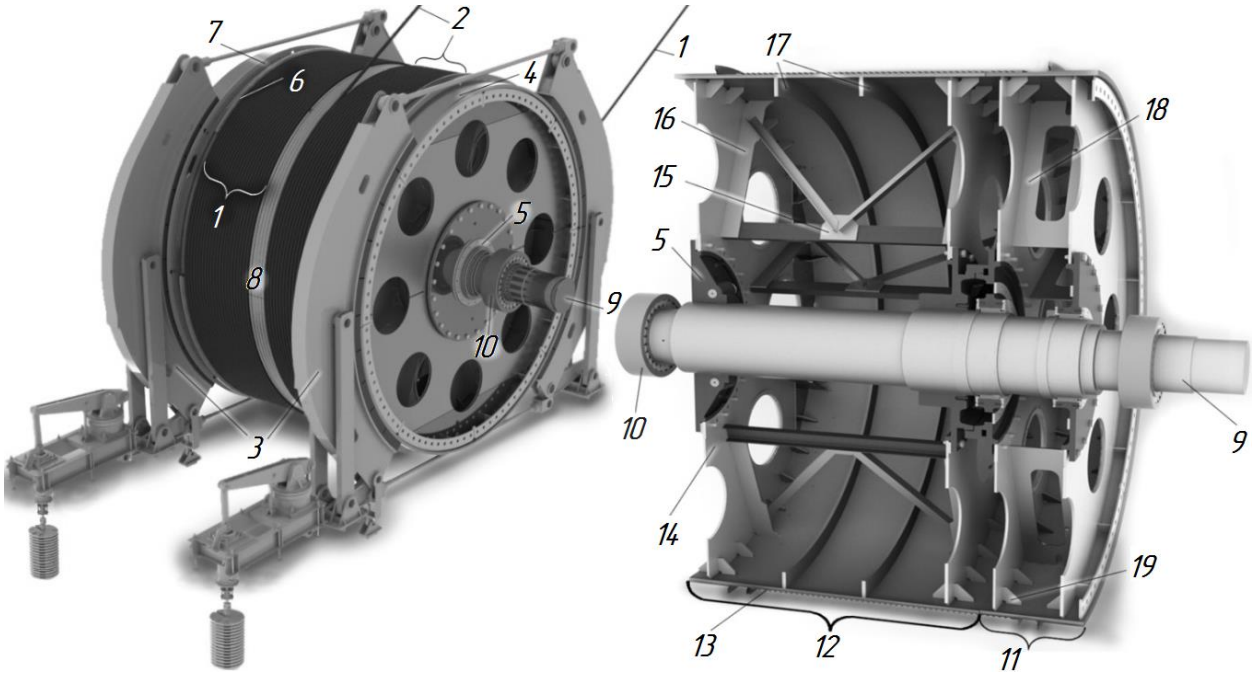

Fig. 1.1. General view and section of the MHM drum of the TsR type:
1 - working rope; 2 - idle rope; 3 - brake shoes;
4 - brake fields; 5 - hubs; 6 - small flange; 7 - large flange;
8 - shell; 9 - shaft; 10 - bearings; 11 - shifting part of the drum;
12 - wedged part of the drum; 13 - screw groove; 14 - lobes;
15 - channels with braces; 16 - ribs of the wedged part; 17 - spandrels; 18 - ribs of the repositioned part; 19 - braces

The TsR type machines are equipped with two brakes 3, which act on the friction surfaces 4. They are located on the outer sides of the wedged and shifting parts of the drum, being at the same time an extension of the shell.

The shell 8 of the TsR -type machine has the form of a cylinder, rolled from thick sheet metal, on the outer surface of which a screw groove for laying the hoisting rope is pre-cut. The lobes 14 are connected to the main shaft 9 with its two outer and two inner hubs 5 by means of bolts. The spars are connected to the shell by means of welded seams.

As already mentioned, this type of drum needs to be stiffened. Most of them are reinforced by installing continuous spacer rings made of I-beam section, as well as sheet or angle metal (so-called spandrels or ring ribs). To relieve the weld seams between the shell and the lobes, braces 13 are welded on the inner surface. The stiffness of the shell and the surface between the holes of the bows is increased by welding ribs 17 (rectangular or with curved transition).

During the operation of the split drum (as opposed to the use of two drums), the working rope is wound and the idle rope is unwound simultaneously. A gap of three to five turns is provided between the ropes so that the ropes do not cross during operation. In addition, the rope from the rewind part to the slack rope enters the cut groove, which is achieved by increasing the pitch of the last turn of the rewind part of the drum. Crossing the cut, the rope moves to the section of the wedged part of the drum and falls into the shaped section of the first groove, and pressing against its edge, passes into the ordinary groove of the wedged part. One of the main differences in the design of split drums from other drums is the use of a cantilever section on which the rope is wound.

As you can see, the drum of a hoisting machine is a very complex technical object with a large number of structural elements that provide load transfer from ropes and brakes.

On the one hand, the relatively low weight of domestic welded drums is a significant competitive advantage, but, at the same time, effective reinforcement of these objects is a complex technical problem that designers have to solve all the time. Thus, in case of unsuccessful installation of reinforcements, welded drums fail faster than their imported counterparts.

One of the examples of unsuccessfully designed construction is the drum of the TsR-6×6,4/1,8 skip MHM manufactured at PJSC NKMZ. Since 2003 it has been operated at the Tishinsky mine of MPP in Kazakhstan. During operation premature wear of the device was observed. For example, during its entire service life, the welded seams of the braces and stiffeners broke every year, thus necessitating repair of the drum steel structures. In addition to cracks, there was severe wear of the shell

(up to 56 %) in the welds, in particular in the troughs of the rifling in the places where the rope branches running up and down simultaneously impacted the shell. Thus, due to the wear of the shell and reinforcements the operation of the drum TsR - 6×6,4/1,8 was terminated in 2013 after ten years of service instead of the required twenty-five years.

The stages of drum wear are shown in Table 1.1.

Methods of strength calculation of nominal stresses using machine characteristics do not take into account many factors, such as local mechanical stress, duration, repetition and non-stationarity of operating modes, initial and developing defects, action of working environments, changes in structure and properties of materials, etc.

According to PJSC NKMZ specialists who inspected the worn shell and drum from the outside and inside, the critical wear was caused by the following reasons:

1. Increased vibration of the rope, due to increase of its string length up to 93 m in relation to the average 65 m; radial and end runout of the header pulleys; radial runout of the support rollers on the rope-supporting mast.

2. intensive wear at the points of impact on the shell of the concurrently advancing and escaping rope branches.

3. weakened control over the performance of routine works by the personnel of Tishinsky mine and equipment repair shop of RGOP of Kazzinc Remservice LLP.

The research revealed the most common faults of the winding organs are deformation of the shell, drum creaking, cracks in the shell, knocking in the drum during operation, increased axial displacement of the shaft, slipping of the rope on the drums of hoisting machines, wear of the loose hub.

1.2 Analysis of methods for calculating drum parameters of typical MHM designs

B.I. Davydov, B.S. Kov valsky, F.L. Shevchenko, Z.M. Fedorova, A.P. Nesterov, V.I. Dvornikov, V.I. Samusya, K.S. Zabolotny, N.M. Fidrovskaya have

Table 1.1

Wear stages of the drum TsR-6×6,4/1,8 installed in 2003.

at Tishinsky mine

Date	**Results of repairs and surveys**
2004	Repair of 6 drum cracks performed
2007	The drum metal structures were repaired: • welding of joint seams of stiffeners made of channel No. 18 in the amount of 7 pcs. • welding of joint seams of drive drum reinforcement braces in the amount of 50 pcs. • welding of joint seams of trapezoidal shaped braces for drum reinforcement in the amount of 6 pcs.
2008	The drum metal structures were repaired: • welding of joint seams of stiffeners made of channel No. 18 in the amount of 12 pcs. • welding of 15 joints of the drive drum reinforcement braces. • reinforcement of welded joint seams of braces in the amount of 4 pcs.
2009	Welding of joints of 36 braces, 12 stiffeners
2010	Welding of joints of 54 braces, 15 stiffeners
2011	Repair of metal structures of the drum: • removal of welds with cracks, crack cutting on the base metal • Welding of joints 57 braces , 17 stiffeners
2012	As a result of magnetic particle inspection and ultrasonic examination, progressive cracks with transition to the main metal of the drum shell in the places of previous repairs were detected in the welded joints of the stiffening ribs and reinforcement braces of the drum, examination of the wear of the shell channels did not show critical deviations.
2013	According to the results of the survey it was found that out of the total number of threading turns (90 pcs.) 29 pcs. (26 % of the total number) are worn out. The actual wear of such elements was determined by the troughs of the threading: of the first shell (left) within a tolerance of 2.5 to 10 %; of the second shell is out of tolerance from 40 to 56 %; of the third shell within a tolerance of 2.5 to 10 %. According to strength calculations the residual wall thickness should be at least 16.98 mm, in fact it is 19.1 mm. Taking into account that the average annual wear rate of the shell is 2 mm, the approximate service life of the drum will be 1.2 years

developed a whole set of methodological recommendations for the selection of rational parameters of hoisting units, in particular, MHM drums. But due to the complexity of the design object the use of these developments does not allow to achieve the necessary results.

In view of the drum radius, different lobbin designs are used: cast (for smaller sizes) and welded (for larger sizes). In addition, the number of holes is increased from two to six or eight in order to ensure a more uniform distribution of stresses and deformations.

The MHM drum is subject to the following factors: rope load distributed over part of its width; concentrated rope forces; braking force distributed at an angle; torsional and bending moments caused by different rope tensions, weight of skips, load and shaft.

Due to the actuation of the brake, the force is mainly absorbed by the head and the rope load prevails among the loads acting on the shell. Since the radial stiffness of the head is many times greater than the radial stiffness of the shell, it is sufficient to determine these drum values:

1) bending stiffness of the frontal;

2) stresses in the shell and the distributed shear force acting on the lobe, considering the shell as a beam on an elastic base under the influence of a uniform transverse load, the previous figure is also taken into account;

3) stresses in the lobes arising from the combined action of braking forces and shell pressure (the forces can be assumed to be uniformly distributed over the rim of the lobes).

The book by B.I. Davydov was a peculiar result of the practice of calculating the performance indicators of MHM drums according to the outlined scheme.

B.A. Morozov and B.G. Klimov investigated the effect of frontals and annular stiffeners on the magnitude of the stress state of the MHM drum shell, taking into account the reduction of rope tension as a result of the reduction of the shell radius under it during subsequent winding. In the process of research, frontals were defined as structures that consist of non-interacting spokes in the form of cantilever beams,

which are rigidly embedded in hubs and their edges are subjected to flywheel moment.

The mentioned authors tried to take into account in their calculations the presence of welded ring strip or braces to the shell at the place of their attachment to the frontal. It is known that these devices are able to reduce bending stresses in the drum shell.

In addition, it was found that, while the radial stiffness of the frontal is many times higher than that of the shell at different design features (therefore, the radial stiffness of the frontal is taken to be infinitely large in the calculation of shell parameters), the bending stiffness in both elements is quite commensurate.

Studies have shown that in an infinite shell uniformly loaded rou by external pressure, a momentless stress-strain state (SSS) arises, in which compressive stresses uniformly distributed over the shell thickness *h* dominate. They can be defined as follows: $\sigma^* = q \cdot R/h,$ here rope pressure $q = P_r/(R \cdot t),$ in turn *t is* the rope winding pitch; P_r is its tension.

Meanwhile, in the shell of a semi-infinite shell hinged to the lobe, the maximum reduced stresses $\sigma_q^{\max} = 1,27\sigma^*$. In this case, the distance from the edge of the shell $\chi^* = 1,13\sqrt{R \cdot h}$, and in case of its rigid termination $\sigma_q^{\max} = 1,82\sigma^*$. Under these conditions, by changing the design of the frontal, it is possible to influence the value of the maximum stresses in the shell within a wide enough range.

B.A. Morozov came to the conclusion that in a semi-infinite cylindrical shell, under conditions when the bending stiffness coefficient of the frontal $k_t > 0.65$, the stresses increase sharply. The value of the parameter k_t is determined from the following relation:

$$k_t = 1/\left(2\beta_1 D/c_f + 1\right),$$

where *D is* the bending stiffness of the shell; c_f is the bending stiffness of the frontal; β_1 is the coefficient of the characteristic length of the shell. Here:

$$\beta_1 = \sqrt[4]{\frac{3\left(1-\mu^2\right)}{R^2 \cdot h^2}}, \qquad D = \frac{E \cdot h^3}{12\left(1-\mu^2\right)}.$$

Since the bending stiffness is mainly determined by the height of the ribs, it is advisable to choose such geometrical dimensions of the ribs that, on the one hand, the frontal can withstand a given uniform radial load from the joint action of the brakes and the shell, and, on the other hand, that its bending stiffness is relatively small.

The method of determining the parameters of the drum developed by A.N. Dukhov provides that the function of the shape of the shell is the deflection of a continuous ribless circular disc. This is suitable only for the study of lobes without holes and with a sufficiently frequent arrangement of ribs.

In L.N. Dyadyk's studies, when determining the influence of the drum ribs on the creation of conditions of joint deformation, only normal interaction forces that satisfy this condition pointwise are considered. This approach, on the one hand, requires numerical solution of an infinite system of algebraic equations on a computer, and on the other hand, the results of the solution are far from accurate, in particular, it concerns the areas near the ribs. In addition, the method does not provide for the evaluation of the obtained error.

A large amount of research to improve the method of calculating the parameters of drum and multi-rope hoisting machines was carried out under the leadership of F.L. Shevchenko. The obtained results allow us to state that with an error of no more than 8 % it is possible to neglect the forces of friction of coils, non-uniformity of cargo movement, and in conditions of single-layer rope winding with an error of 11 % it is possible not to take into account the weakening of rope pressure caused by their deformation together with the sheath. It also turned out that it is necessary to take into account the bending ductility of cast lobes of all existing structures, and at the same time their radial ductility. It is recommended not to take into account the latter parameter in the calculation of welded lobes. F.L. Shevchenko, taking into account the use of ribs in welded lobes and calculating their influence by a method

similar to the one proposed by L.N. Dyadyk, comes to the conclusion that in determining the conditions of conjugation of the shell with the lobes it is possible to neglect the non-axisymmetric component of the angles of rotation of the latter. In addition, an insignificant (up to 9 %) reduction of the frontal stiffness in the presence of circular holes, and the use of radial ribs increases its stiffness almost 30 times. If the ribs are not welded to the shell, the stiffness decreases by 79 %.

The mentioned sources contain important conclusions about the operation of drums of hoisting machines of the designs considered by the authors, namely:

1) if the geometrical parameters of the shell are suitable for drums of lifting machines, the loss of stability of these devices is impossible within the permissible stresses, due to which the installation of intermediate annular stiffeners only worsens the performance of the structure;

2) The use of a stiffening tube also leads to deterioration of the MHM drum;

3) To achieve the desired effect, it is sufficient to mount internal radial stiffeners on the drum lobes;

4) the main load on the drum was the uniform pressure of the winding rope (all other loads cause stresses below the design stresses in the drum);

5) in a rigidly fixed drum shell, the design bending moment is three times greater than in a hinged shell connected to the frontal;

6) oblique asymmetrical loading of the drum under the influence of rope tension and the mass of the structure is necessarily taken into account when determining the working parameters of the shaft and lobes, at the same time shaft deformation is not taken into account, in the calculation of the drum shell its lobes are considered to be rigidly fixed, not moving in the joints with the shaft.

The common disadvantage of all the above mentioned methods in determining the performance indicators of drum design is the impossibility of accurate assessment of the interaction between the ribs and the lobed disc, as well as the use of lobes in the form of ribs of simple shape for calculation as basic reinforcements. Thus, if the MHM drums are equipped with box reinforcements of the shell, lobes and flanges, the mentioned calculation methods are not suitable.

The issues of selection and calculation of drum lining parameters are considered in detail in the works of A.L. Zhupiev, V.V. Franchuk. Franchuk, where special attention is paid to the study of stress intensity in kapron lining at contact with rope.

Here, the plane strain theory was applied and the rope was considered as an absolutely solid incompressible body of strand and wire structure, in which the bending and torsional stiffness parameter was not taken into account. The rope was modelled as a material point at its geometric axis, loaded by a contact force and connected to the elastic drum lining by discrete springs. The stiffness of the springs was determined by solving the Hertz-Belyaev problem taking into account the curvature of the wire rope wires. Here the variational-difference method of discretisation of parameter determination was used, and for the solution of the obtained system of equations the modification of the method of successive upper relaxation was useful. The results of calculations have shown that the equivalent tangential stresses in the kapron lining of the drum, reaching their maximum value in the zone of contact of the latter with the wire rope wires, exceed the permissible tensile (compression) stresses. In the rest of the scallop they are insignificant.

The disadvantage of the discretisation method used by the authors was that it is poorly adapted for approximating calculations concerning curvilinear liner boundaries, which makes it impossible to densify the measurement grid in the vicinity of the contact point. In addition, the solution of the system of equations turned out to be rather labour-intensive and unsuitable for practical calculations.

Recently, numerical methods of SSS calculation have been intensively used, which are based on discretisation of the initial (continuum) problem, in which the unknowns are stress $\sigma^{ij}\left(\overset{1}{x},t\right)$, displacement $u_i\left(\overset{1}{x},t\right)$ and deformation $\varepsilon_{ij}\left(\overset{1}{x},t\right)$. Each of them should be defined on an infinite set (continuum) of points $\overset{1}{x}$ of the Ω region and in the considered time interval $t \in \left[0, t_{\max}\right]$. The solution of the discretised problem completely depends on the values of a finite set of numerical coefficients (parameters), which are related to the value of the desired function in a finite set of

points - nodes of some grid applied to the considered area. In this case we deal with numerical methods. Among them are the boundary element method, finite difference method, finite element method (FEM).

As a result of discretisation, a stationary, time-independent, continuum problem is reduced to solving a system of linear or nonlinear algebraic equations to determine the desired function at grid nodes or another finite set of parameters describing some object.

At the same time, the nonstationary problem after discretisation with respect to spatial coordinates is transformed into a system of differential, integral or integrodifferential equations to determine the dependence of the solution on the time parameter, which in turn, as a rule, has to be discretised.

The accuracy of numerical solution results is usually closely related to the number of grid nodes or depends on the values of other sought coefficients describing the discretised problem. It is clear that the more of them there are, the more accurate the result will be, all other things being equal. In this connection, the number of unknowns determines the volume of calculations when solving this problem. Thus, to determine the SSS of structural elements, it is necessary to solve problems with the number of unknowns from several tens to hundreds of thousands.

Comparison of grid methods for calculating parameters of technical objects allows us to draw the following conclusions:

- The boundary element method is effective for the study of semi-infinite, unbounded fields. It requires an effective solution of the inverse problem of calculating the parameters of the unbounded field. It is not possible to automate these calculations. As a rule, it has no independent application.
- The method of finite differences is usually used for accelerated solution of separate problems describing characteristics of bodies of simple shape in those cases when the boundary of the body coincides with coordinate lines. In the case of calculation of parameters for bodies of more complex shape, no means of automation is provided within this method.

- The finite element method (FEM), as one of the most effective numerical methods for strength and stiffness calculations of complex structures, has found wide application with the advent of computers.

In essence, the FEM is reduced to approximating the parameters of a continuous medium, characterised by an infinite number of degrees of freedom, by a set of subareas (or elements) that have a finite number of degrees of freedom. Then a relationship is established between these elements. At the same time, the application of the mentioned method is limited by the following circumstances: on the one hand, it is the necessity to break the structure into a finite element grid, as well as labour-intensive preparation of initial data, and on the other hand, high requirements to the memory capacity and speed of the computing equipment, on which the calculation is performed.

Another circumstance that complicates the direct application of FEM is that the MHM drum belongs to the class of structures that include elements of small, medium and large stiffness. When numerically solving the system of linear algebraic equations describing its characteristics, it leads to poor conditionality of calculations and large error of their results, and sometimes to impossibility to obtain them. In addition, the calculation scheme used may have varying degrees of detail. In this connection, as the design is refined, it becomes necessary to determine as accurately as possible the deformations and stresses in its elements, as well as the maximum stresses arising in the components. Naturally, it is necessary to use the most adequate method for each such calculation.

Depending on the type of the investigated node, either its stiffness matrix (modelled by the superelement method) or an algorithm for its partitioning into a finite element mesh corresponding to a given range of initial values is usually entered and stored in the database.

Effective application of the FEM in solving the problems of calculating the strength of MHM drums is possible only if there is a software package, the development of which requires considerable time and money. Two main approaches to the creation of such programmes are possible: the first one involves the

development of a software package for solving problems of a limited class, the second one involves the creation of a universal software package, which means that with its help it is possible to solve problems of quite a wide range.

Calculating the strength characteristics of parts of the hoist requires a correct approach to determining the design loads, usually taking into account the most severe operating conditions of the machine. If the design loads are not selected and implemented correctly at the design stage, the hoist will be built with an excessive safety margin or, conversely, overloaded machine parts will fail prematurely.

The choice of design loads should not only be based on their absolute value, but also take into account the frequency and duration of their action, as well as analyse the influence of the place of their application on the SSS arising in the components of the lifting machine.

In addition, in the process of rope winding and unwinding there is a probability of internal forces that can lead to uneven distribution of stresses in the drum. It is proved that these stresses reach the maximum value under the influence of wound rope coils, which depends on its initial value, which in turn is determined by the weight of the vessel and rope, features of the drum construction, rope stiffness, as well as by the scheme of its winding.

In the works by Zabolotny K.S., Zhupiev A.L., Panchenko E.V., the possibility of calculating the characteristics of drums by means of FEM using the Hot Spot Stress methodology was first substantiated. In particular, it is shown that the calculation scheme for determining the drum SSS should be selected from loading variants corresponding to different positions of lifting vessels in the barrel. To achieve this goal, the authors proposed a series of numerical experiments using FEM and subsequent interpolation of the obtained results. It should be noted that this method is rather labour-intensive, moreover, if the computational model is slightly changed, it is necessary to repeat the series of numerical experiments.

It is known that in the process of rope winding the tension of the previous coils is weakened. This may be due to the deflection of the drum in the radial direction

under the influence of forces arising in the coils, which causes a decrease in their deformation and, therefore, in tension.

B.S. Kovalsky proposed to take into account the tension weakening of the wound coils by the method of determining the rope loads on the MHM drum. This method provides to take into account in calculations the tension weakening in the rope coils due to the deformation of the drum as an infinite smooth unsupported axisymmetric shell. In addition, the author was able to prove that in the process of winding the rope on the drum the sliding of its coils can be neglected.

Based on the law of joint deformation and Hooke's law, B.S. Kovalsky derived an integral equation for calculating the variable pressure on the shell when winding a rope with a constant tension force, viz:

$$\int_0^s \psi(s,x)\cdot\eta(|u-x|)dx - \int_0^u \psi(u,x)\cdot\eta(u-x)dx = \frac{2}{\varepsilon}\cdot\left[1-\psi(s,u)\right], \qquad (1.1)$$

here the deformation of the shell $\varepsilon = E_r\cdot F_r / E\cdot\delta\cdot t$; E_r , F_r - modulus of elasticity and cross-sectional area of the rope; δ - thickness of the shell; t - winding step; deflection of the semi-infinite shell $\eta(x) = e^{-\beta\cdot x}\left(\cos(\beta\cdot x)+\sin(\beta\cdot x)\right)$; dimensionless values li $\psi(s,u) = p(l,r)/p_0$, $x = \beta$-z, $u = \beta$-r, $s = \beta$-l, $p(l,r)$ - load occurring at a distance r from the origin of coordinates when winding the rope on the section from zero to l; z - current coordinate from zero to r or to l; $p_0 = T_0/R\cdot t$ - load on the drum; $\beta = 1{,}28/\sqrt{R\cdot\delta}$ - displacement damping coefficient; T_0 - tension of the running end of the rope; R - drum radius.

From the analysis of equation (1.1), it follows that the radial rope load decreases due to the deformation of the shell, and its change can be estimated by means of a correction factor which is determined by the following formula:

$$\psi_0 = \frac{1}{\sqrt{1+\dfrac{E_r\cdot F_r}{E\cdot\delta\cdot t}}}. \qquad (1.2)$$

Then, using said coefficient, the rope load on the drum, in which the tension relaxation in the rope coils is taken into account, is determined from the following expression:

$$p = \frac{T_0}{R \cdot t} \psi_0 . \qquad (1.3)$$

In this calculation, it was assumed that the drum is a semi-infinite shell without lobes, spandrels and other reinforcing elements. This leads to some underestimation of the rope load and maximum stresses in the reinforcement region.

The theory of B.S. Kovalsky was developed in the works of E.V. Panchenko devoted to the theory of multilayer winding of rubber rope. Unlike the previous author, E.V. Panchenko considers the process of rope winding as a discrete process. winding of the rope as discrete, thus instead of spiral arrangement of turns, the author offers anisotropic ring layers to put on each other. each other. Here, too, the influence of lobes and reinforcing elements of the drum is not taken into account.

The mathematical models developed by the mentioned authors provide for a simplified configuration of the profiled drum shell. It should be noted that the latter is a complex mechanical object and models of SSS arising there have not yet been developed for it, with the help of which it is possible to optimise the design of the drum of the MHM. At the present stage of research in the mathematical description of complex objects, scientists use a semi-empirical approach, which makes it possible to create a simpler mathematical model of the object, which does not affect the reliability of the results obtained. In this case, the simplified model uses coefficients determined experimentally and selected in such a way that in the considered interval of parameter changes the calculated and experimental data are in good agreement.

To determine the radial displacements of the drum shell, we can use a system of canonical equations based on the force method. In matrix form, the system has the following form:

$$\{w\} = [W]\text{-}\{F\}, \quad (1.4)$$

where [*W*] *is the* pliability matrix, in which the component $W_{i,j}$ represents the radial displacement of the *j-th* groove caused by the application of a unit specific force to it (Fig. 1.2); *{F}* is the vector of specific forces applied to the grooves; {w} *is the* vector of displacements of the drum grooves. .

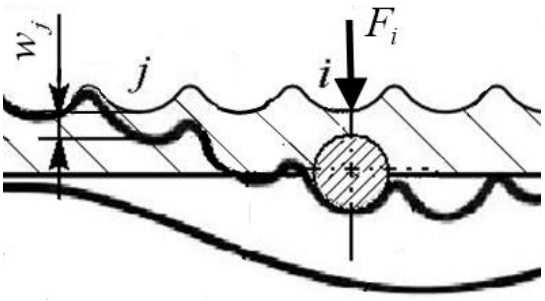

Fig. 1.2. Schematic diagram of groove deflection in the MHM drum

The value of the matrix [*W*] depends on the geometric shape of the drum, the design of the lobes, flanges, skewers, ribs, spandrels, as well as on the physical and mechanical properties of the materials from which the thin-walled reinforcements of the MHM drum are made. In this regard, the construction of the matrix is a complex technical task.

For example, in the work of Zabolotny K.S., in the study of SSS in the drum of the MHM of the TsR type, the matrix [*W*] was determined by conducting a series of numerical experiments, the results of which were processed by finite element analysis. It turned out that this method of construction is very labour-intensive, moreover, at insignificant change of the design model it was necessary to repeat a series of numerical experiments. This significantly complicates the process of optimising the design of the MHM drum. To reduce the volume of calculations, the authors of the monograph propose to use a semi-empirical approach in the research, which provides for the description of the object by creating an analytical model in which the coefficients determined by experience are applied, and their values are selected in such a way as to ensure the consistency of design and experimental data in some interval of changes in the design parameters.

The application of structural optimisation methods turned out to be a rather promising direction in design. For example, in the works of Zabolotny K.S., a simplified generalised-parametric model of a drum of a MHM created by the author is described, on the basis of which the optimisation of the performance of the structure is carried out, and then, taking into account the optimal values of generalised parameters, the structural development of the device is carried out. To realise this approach, it was necessary to create an effective method for determining the design loads on the drum, which would take into account the influence of geometric and stiffness characteristics of the reinforced drum structure, as well as changes in its SSS under the influence of rope turns. In order to implement the considered method, a computational algorithm (designer's workstation) was developed on the basis of mathematical models of the reinforced drum deformation and rope winding. With the help of this ARM, calculations were performed and rational designs of cylindrical drums were created. Thus, the present monograph continues the research on scientific substantiation and development of the method for determining the design loads of cylindrical MHM drums.

1.3 Defining the purpose and scientific objective of the study

The authors of the monograph conducted research aimed at developing methodological recommendations for the calculation of parameters and design of cylindrical drums of mine hoists.

In developing the involved method for determining the design loads in the drum, a semi-empirical approach was used, where the following assumptions were made: rope tension force is constant within a single coil; rope winding on the drum was modelled as a process of successive putting on with some tension of discrete rings; the force in the rope coil wound on the drum is equal to the tensile force in the rope plumb; insignificant axial movements of the drum and friction between the rope coils and the drum can be neglected.

In order to achieve the set goal, the following objectives were addressed in the

research:

1. Scientific substantiation and development of the method for determining the design loads arising during rope winding on a cylindrical drum.

2. to evaluate the validity of the method for calculating the rope pressure on the shell of cylindrical split drums by comparing the results of physical experiment and calculated data.

3. Creation of engineering methodology for calculation and design of cylindrical drums.

4. study of the influence of design parameters on the stress-strain state in the drum.

2 DEVELOPMENT OF A METHOD FOR DETERMINING DESIGN LOADS WHEN WINDING THE ROPE ON THE CYLINDRICAL DRUM OF A HOIST

2.1 Problem statement

The MHM's considered in the monograph have cylindrical split drums consisting of two parts - a wide wedged drum and a narrow sliding drum. The design of these machines provides for simultaneous winding and winding of rising and falling rope branches on the wedged drum. In order to avoid crossing of the branches during operation of the machine, a gap should be provided between them, the width of which corresponds to the total width of a certain number of grooves (it is called a zone of free grooves) of the spiral winding drum. As practice shows, in the course of the MHM operation the stress-strain state of the drum changes in time. The reason for such changes are the following factors: the number of friction turns N_{fr}, the number of grooves free of turns N_f , their location on the drum. The change in the SSS of the drum in turn affects the tension force of the rope coils wound on it and the radial pressure. A small number of rope coils are wound on the narrow cross-over part of the drum, so there is a slight weakening of the tension here.

Let's consider how the turns of the slack rope are distributed on the slack part of the MHM drum of the TsR type (Fig. 2.1). In general case it can be considered that the idle rope is wound on the slack part of the drum, and the working rope starts winding from the slack part.

N_p coils of the working rope are wound on the left side of the drum, and N_x coils of the idle rope are wound on the right side of the drum in the presence of already made friction coils N_{fr}. Between the coils of the idle and working ropes there is a gap consisting of N_f grooves, which prevents the possibility of crossing the ropes during the operation of the system. Under these conditions, the total number of grooves $N = N_p + N_f + N_x + N_{fr}$.

Fig. 2.1. Model of the distribution of turns on the wedged part of the MHM drum

The tension force in the friction coils of the idle rope N_x changes according to Euler's law in the circular direction. In further calculations we will accept the assumption used by NKMZ designers, according to which a linear law of change of the rope tension force is valid in the axial direction, when the load under the influence of friction coils will grow from zero to the value of the tensile force of the first winding coil of the idle rope under the influence of the final load.

In the general case there are two zones of coils on the slack part of the drum: the left one belongs to the working rope and the right one to the idle rope. Let us denote the number of the groove on which the rope is currently wound by *k.*

If the working rope is uncoiled and the idle rope is coiled, the coil zone of the working rope is from the first groove to the groove number $k - N_f$. At the same time, the coil zone of the idle rope is from the *k-th groove* to $N - N_{fr}$. When the idle rope is uncoiled and the working rope is reeled in, the coil area of the idle rope is in the

area of the drum from the first groove to groove number *k*, while the coils of the idle rope are in the area from groove $k + N_f$ to the groove labelled $N - N_{fr}$.

In order to calculate the parameters of complex systems, including the MHM drum, it is possible to use the method of physical discretisation, when the real existing system is replaced by a simplified physical model, and on its basis a finite set of equations is made and calculated.

In order to calculate the mentioned types of loads, you need to carry out such tasks:

- to develop a mathematical model of rope winding on a drum;
- build a mathematical model of the deformation of a reinforced drum;
- justify the design conditions that allow to estimate the drum SSS.

2.2 Development of a mathematical model of rope winding on the drum of the machine

The stress-strain state of the drum depends on the sequence of winding and unwinding of the rope, the scheme of laying the coils on the drum, as well as on the location of each of the coils of the load rope and the different positions of the lifting vessels in the shaft. Let's put in correspondence to the number of coils of the loaded rope the number of its loading variant. In this case, we will not take into account the asymmetry of the load under the influence of the rope.

In building the model, we make the following assumptions:

1. The winding of the rope along the helical line on the drum is represented as a process of successive putting on with tension of discrete rings, the stiffness of which is equal to E_r -S_r, where E_r is the modulus of elasticity of the rope, S_r is the cross-sectional area of all wires of the rope (the method is proposed by O.V. Panchenko).

2. The drum is modelled as an axisymmetric structural-orthotropic reinforced shell.

3. The force developed in the rope coil wound on the drum is equal to the tensile

force *T* occurring in the rope plumb line.

Next, let us proceed to the determination of the dependence of the interaction forces between the cylindrical drum and the rings successively put on it.

For this purpose, we formulate and solve the system of equations of joint deformation of elastic rings and reinforced drum shell.

Applying the methodology outlined in the paper, let us introduce a discrete coordinate system using the axis of integers, i.e. $X = 1,...,N$, with finite distances plotted on it, corresponding to the step of groove cutting on the drum *t*. Let us align the shell axis with the discrete axis of the drum (Fig. 2.2). On the basis of the points of the discrete axis, we construct the planes orthogonal to it, which, when intersecting with the shell surface, form coordinate lines whose numbers correspond to the numbers of the above-mentioned points.

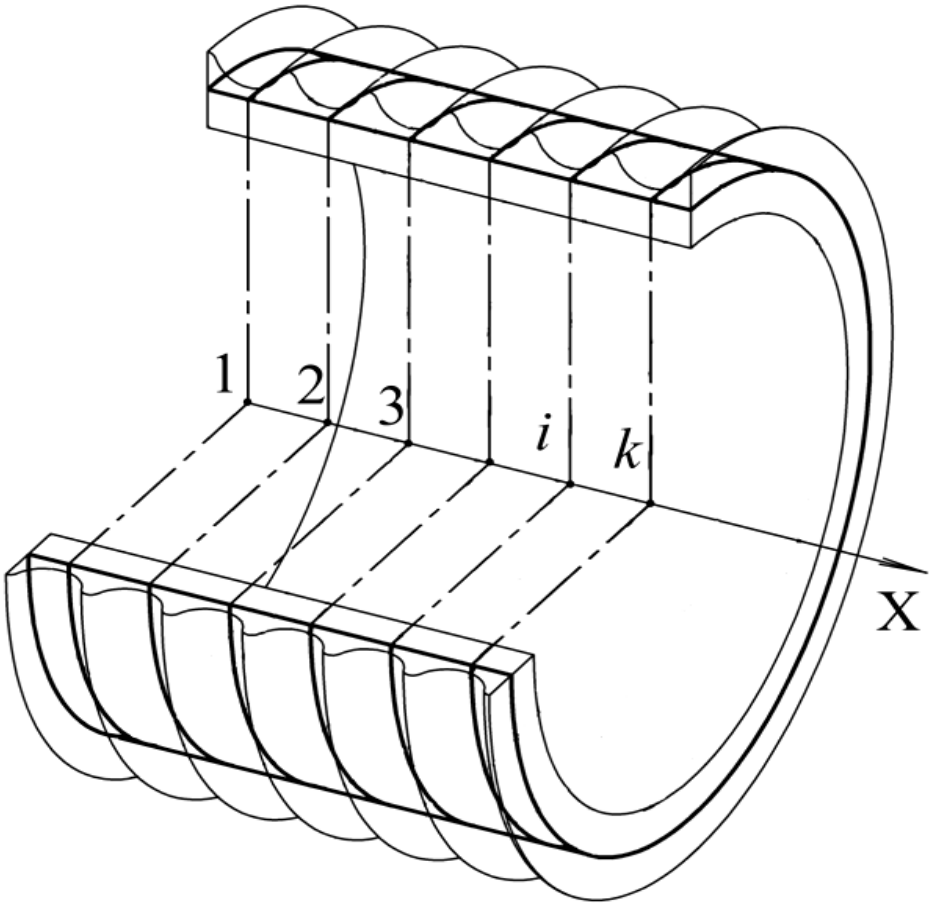

Fig. 2.2 Shell element with constructed discrete coordinate system

Let us introduce the following notations: *i* - number of the coordinate line of

the corresponding groove on the drum; *j* - number of the rope coil (or in our model the number of the ring put on the sheath); *k* - number of the coil of the rope (ring to be put on); R_o - radius of the shell along the axis of the rope coiling.

Let us correspond to the number of the working rope coil *k the* number of the loading variant *v.*

Fig. 2.3 shows the calculation scheme of the winding process. Between the *j-th* ring and the shell there is an interaction force $P_{j,k}$, causing deflection $w_{i,k}$ along the *i-th* coordinate line of the drum shell at the moment of putting on the k-th ring. *k-th* ring.

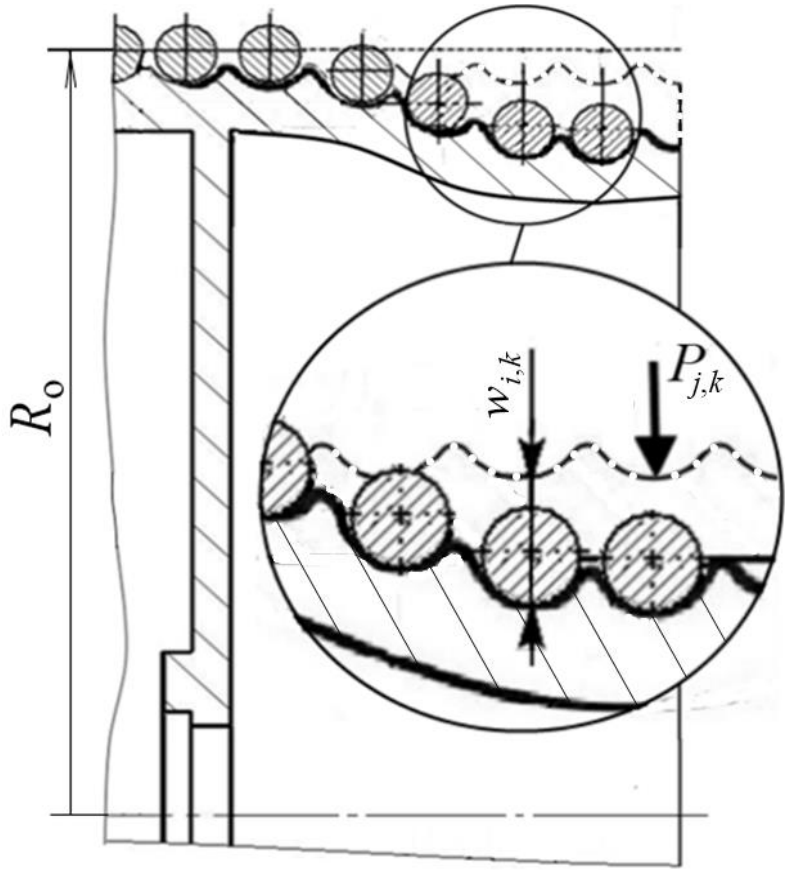

Fig. 2.3. Calculation diagram of the process of winding on the MHM drum loaded rope

Let [*W*] be the pliability matrix, whose components represent the displacement of coordinate line points on the drum shell under the influence of a unit force. This matrix can be defined by such a system of canonical equations:

$$\{w\} = [W]\text{-}\{F\},$$

where $\{w\}$ is the vector of radial displacements of the drum shell, $\{F\}$ is the vector of unit forces of interaction between the rings and the shell.

In view of the above, the expression for determining the deflection of the rope along the *i-th* coordinate line of the shell when putting on the *k-th* ring takes the following form:

$$w_{i,k} = \sum_{j=1}^{k} P_{j,k} \cdot W_{i,j} .$$

Since the force in the *k-th* ring put on the shell practically does not weaken and is equal to the force in the winding coil T_k , the equation describing the equilibrium of the ring and the shell has the following form:

$$P_{k,k} = \frac{T_k}{R_o}.$$

Thus, the circumferential deformation of the *j-th* ring put on the shell at the k-th ring put on

$$\varepsilon_{\theta_{j,k}} = P_{j,k} \cdot R_o / E_r \cdot S_r . \qquad (2.1)$$

On the other hand, according to Hooke's law, the circumferential deformation of the ring can be described by this equation:

$$\varepsilon_{\theta_{j,k}} = \Delta r_{j,k} / r_{j,k} , \qquad (2.2)$$

where $r_{j,k}$ is the radius of the undeformed ring; and the absolute elongation of the radius of the undeformed ring $\Delta r_{j,k} = (R_o - w_{i,k}) - r_{j,k}$.

Substituting formula (2.1) into equation (2.2), we obtain the expression, by which we can determine the force of interaction between the ring and the drum shell, i.e.

$$P_{j,k} = \left(E_r \cdot S_r / R_o\right) \cdot \left(\left(\left(R_o - w_{j,k}\right) / r_{j,k}\right) - 1\right),$$

and the radius of the undeformed *k-th* ring put on the drum

$$r_{k,k} = \left(R_o - w_{k,k}\right) / \left(1 + \varepsilon_{\theta_{k,k}}\right).$$

To create a mathematical model of rope winding on the drum, let us consider the conditional process of successive putting on the sheath of three rings with tension and generalise the results obtained with respect to *N* rings. Thus, when putting on the first ring (*k* = 1), we formulate the equation determining its equilibrium as follows: $P_{1,1} = T_1 / R_o$.

From the condition of joint deformations it follows that

$$w_{1,1} = P_{1,1} - W_{1,1}.$$

In this case, the circumferential deformation of the ring

$$\varepsilon_{\theta_{1,1}} = P_{1,1} \cdot R_o / E_r \cdot S_r .$$

And the radius of the undeformed ring

$$r_{1,1} = \frac{R_o - w_{1,1}}{1 + \varepsilon_{\theta_{1,1}}}.$$

The process of putting on the second ring when *k* = 2 requires the steps described below.

Let's make such a system of equations:

$$\begin{cases} P_{2,2} = \dfrac{T_2}{R_o}; \\ w_{1,2} = W_{1,1} \cdot P_{1,2} + W_{1,2} \cdot P_{2,2}; \\ w_{2,2} = W_{2,1} \cdot P_{1,2} + W_{2,2} \cdot P_{2,2}; \\ P_{1,2} = \dfrac{E_r \cdot S_r}{R_o} \cdot \left(\dfrac{R_o - w_{1,2}}{r_{1,1}} - 1 \right). \end{cases} \quad (2.3)$$

Let us introduce the following notations:

$$C_1 = w_{1,2},\ C_2 = w_{2,2},\ C_3 = P_{1,2},\ C_4 = P_{2,2}.$$

Taking them into account, the system of equations (2.3) will take the following form:

$$\begin{cases} C_1 - W_{1,1}\cdot C_3 - W_{1,2}\cdot C_4 = 0; \\ C_2 - W_{2,1}\cdot C_3 - W_{2,2}\cdot C_4 = 0; \\ \dfrac{E_r\cdot S_r}{R_o\cdot r_{1,1}} C_1 + C_3 = \dfrac{E_r\cdot S_r}{R_o}\cdot\left(\dfrac{R_o}{r_{1,1}} - 1\right); \\ C_4 = T_2 / R_o. \end{cases} \tag{2.4}$$

Let us write the system of equations (2.4) in matrix form, i.e.

$$[M]\text{-}\{C\}=\{H\}, \tag{2.5}$$

here

$$[M] = \begin{vmatrix} 1 & 0 & -W_{1,1} & -W_{1,2} \\ 0 & 1 & -W_{2,1} & -W_{2,2} \\ \dfrac{E_r\cdot S_r}{r_{1,1}\cdot R_o} & 0 & 1 & 0 \\ 0 & 0 & 0 & 1 \end{vmatrix}, \quad \{H\} = \begin{vmatrix} 0 \\ 0 \\ \dfrac{E_r\cdot S_r}{R_o}\cdot\left(\dfrac{R_o}{r_{1,1}} - 1\right) \\ T_2 / R_o \end{vmatrix}.$$

Using the Gauss elimination method, we obtain the result of solving the system of equations (2.5).

The magnitude of the shell deflections and ring tension forces can be found using the following expressions: $w_{1,2} = C_1$; $w_{2,2} = C_2$; $P = C_{1,2\,3}$; $P_{2,2} = C_4$.

After that we calculate the deformation of the second ring, i.e.

$$\varepsilon_{\theta\,2,2} = P_{2,2}\cdot R_o / E_r\cdot S_r,$$

as well as its radius in the undeformed state, viz:

$$r_{2,2} = \frac{R_o - w_{2,2}}{1 + \varepsilon_{\theta\,2,2}}.$$

The calculation of the process of putting on the third ring, i.e. when $k = 3$, is carried out in the sequence described below.

First, let's make the following system of equations:

$$\begin{cases} P_{3,3} = T_3 / R_o; \\ w_{1,3} = P_{1,3} \cdot W_{1,1} + P_{2,3} \cdot W_{1,2} + P_{1,3} \cdot W_{1,3}; \\ w_{2,3} = P_{1,3} \cdot W_{2,1} + P_{2,3} \cdot W_{2,2} + P_{3,3} \cdot W_{2,3}; \\ w_{3,3} = P_{1,3} \cdot W_{3,1} + P_{2,3} \cdot W_{3,2} + P_{3,3} \cdot W_{3,3}; \\ P_{1,3} = \left(E_r \cdot S_r / R_o\right) \cdot \left(\left(\left(R_o - w_{1,3}\right) / r_{1,1}\right) - 1\right); \\ P_{2,3} = \left(E_r \cdot S_r / R_o\right) \cdot \left(\left(\left(R_o - w_{2,3}\right) / r_{2,2}\right) - 1\right). \end{cases} \quad (2.6)$$

Then we introduce the following notations: $C_1 = w_{1,3}$; $C_2 = w_{2,3}$; $C_3 = w$; $C_{3,34} = P_{1,3}$; $C_5 = P_{2,3}$; $C_6 = P_{3,3}$. After using them, the system of equations (2.6) will take the following form:

$$\begin{cases} C_1 - C_4 \cdot W_{1,1} - C_5 \cdot W_{1,2} - C_6 \cdot W_{1,3} = 0; \\ C_2 - C_4 \cdot W_{2,1} - C_5 \cdot W_{2,2} - C_6 \cdot W_{2,3} = 0; \\ C_3 - C_4 \cdot W_{3,1} - C_5 \cdot W_{3,2} - C_6 \cdot W_{3,3} = 0; \\ \dfrac{E_r \cdot S_r}{R_o \cdot r_{1,1}} C_1 + C_4 = \dfrac{E_r \cdot S_r}{R_o} \cdot \left(\dfrac{R_o}{r_{1,1}} - 1\right); \\ \dfrac{E_r \cdot S_r}{R_o \cdot r_{2,2}} C_2 + C_5 = \dfrac{E_r \cdot S_r}{R_o} \cdot \left(\dfrac{R_o}{r_{2,2}} - 1\right); \\ C_6 = T_3 / R_o. \end{cases} \quad (2.7)$$

Moreover, in matrix form the system of equations (2.7) takes the form:

$$[M]\text{-}\{C\}=\{H\}.$$

Here

$$[M]=\begin{vmatrix} 1 & 0 & 0 & -W_{1,1} & -W_{1,2} & -W_{1,3} \\ 0 & 1 & 0 & -W_{2,1} & -W_{2,2} & -W_{2,3} \\ 0 & 0 & 1 & -W_{3,1} & -W_{3,2} & -W_{3,3} \\ \dfrac{E_r \cdot S_r}{r_{1,1} \cdot R_o} & 0 & 0 & 1 & 0 & 0 \\ 0 & \dfrac{E_r \cdot S_r}{r_{2,2} \cdot R_o} & 0 & 0 & 1 & 0 \\ 0 & 0 & 0 & 0 & 0 & 1 \end{vmatrix}, \quad \{H\}=\begin{vmatrix} 0 \\ 0 \\ 0 \\ E_r \cdot S_r \cdot \left(\dfrac{R_o}{r_{1,1}}-1\right) \\ E_r \cdot S_r \cdot \left(\dfrac{R_o}{r_{2,2}}-1\right) \\ T_3/R_o \end{vmatrix}.$$

Applying the Gauss elimination method, we obtain the results of solving the system of equations (2.7).

The magnitude of the shell deflections and ring tension forces can be determined using the following expressions: $w_{1,3} = C_1$; $w_{2,3} = C_2$; $w_{3,3} = C_3$; $P = C_{1,34}$; $P_{2,3} = C_5$; $P_{3,3} = C_6$.

Next, we calculate the deformation of the third ring as follows:

$$\varepsilon_{\theta\,3,3} = \frac{P_{3,3}}{E_r \cdot S_r}.$$

And also we define its radius in the undeformed state, i.e.

$$r_{3,3} = \frac{R_o - w_{3,3}}{1+\varepsilon_{\theta\,3,3}}.$$

When comparing the formulas describing the process of putting on the second and third rings, we conclude that the system of equations has become regular. For this reason, we can use a general form of formulas to describe the process of putting on rings, starting from the third ring.

After generalisation of the formulas with respect to successive putting on of N rings we obtain the following mathematical model of rope winding:

$$[M]\text{-}[C] = [H], \qquad (2.8)$$

where [*M*] is a cubic matrix, each element of which is a set of coefficients of the system of equations reflecting the process of putting on the *k-th* ring; *[H*] is a square matrix, each vector of which is in the right parts of the systems of equations describing the operation of putting on the *k-th* ring; *[C*] is a square matrix of unknown quantities to be determined.

The components of the matrix [*C*] correspond to the values of the radial displacement of the shell and drum of the weathering forces arising therefrom, viz:

$$C_{i,\,k} = w_{i,k}\,,\; C_{i+N,k} = P_{i,k}\;\; (i,\, k = 1...N). \qquad (2.9)$$

The intersection of the matrices [*M*] and [*H*], given a fixed value of the parameter *k* can be represented as follows:

$$[M_{\cdot\cdot k}] = \begin{bmatrix} [E] & -[W] \\ [D] & [E] \end{bmatrix}, \quad [H_{\cdot k}] = \begin{Bmatrix} \{0\} \\ \{Q\} \end{Bmatrix},$$

here [*E*] is the unit matrix of successive putting on the drum of *N* rings; [*W*] is the matrix of the drum pliability; [*D] is the* diagonal matrix of successive putting on of *N* rings, representing the forces caused by the shell deflection, ([*D*] = $E_к$ -$S_к$ -*diag{1/*$r_{1,1}$ *, 1/*$r_{2,2}$,..., 1/r ,..., 0,... , 0,... , 0}/R); {Q} are the forces caused by the tensile forces in the put on rings, where ,... ,..., *1/*$r_{k\text{-}1,k\text{-}1}$, 0,...,*0}/*R_0); {Q} are the forces caused by the tensile forces in the donning rings, with

$$\{Q\}^T = \frac{E_r \cdot S_r}{R_o} \cdot \left(\left(\frac{1}{r_{1,1}} - \frac{1}{R_o} \right), \left(\frac{1}{r_{2,2}} - \frac{1}{R_o} \right), ..., \left(\frac{1}{r_{k-1,k-1}} - \frac{1}{R_o} \right), \frac{T_k}{E_r \cdot S_r}, 0, ..., 0 \right).$$

The non-zero components of the matrix [*M*] and [*H*] are determined by the following expressions, provided that the values of the parameter *k* are in the range of 1 to *N*:

$$M_{i,i,k} = 1,\; M_{i,j+N,k} = -W_{i,j}\,,\; M_{i+N,i+N,k} = 1, \; (i,\, j = 1...N); \qquad (2.10)$$

$$M_{i+N,i,k} = \frac{E_r \cdot S_r}{r_{i,k} \cdot R_o} \qquad (i = 1...k - 1); \qquad (2.11)$$

$$H_{i+N,k} = E_r \cdot S_r \left(1/r_{i,k} - 1/R_o\right) \quad (i = 1...k - 1); \tag{2.12}$$

$$H_{k+N,k} = T_k / R_o . \tag{2.13}$$

Thus the radius of the k-th ring in the undeformed state

$$r_{k,k} = \left(R_o - w_{k,k}\right) / \left(1 + P_{k,k} \cdot R_o / E_r \cdot S_r\right). \tag{2.14}$$

Equations (2.8) - (2.14) form a mathematical model of rope winding, which allows us to determine many parameters, in particular, its radial displacements, deformations, forces of interaction between rings and sheath, as well as forces of interaction between the sheath and rope coils. At the same time, the solution of the system of equations (2.8) requires the construction of the drum shell pliability matrix [*W*].

Let's consider the process of winding the rope onto the drum and unwinding it (abbreviated as winding-unwinding).

The coils of the working and idle ropes are modelled as separate rings, the mathematical model of which is described above, with the zone of free coils on the drum modelled as rings with zero tension.

From expressions (2.10) - (2.14) it is clear that the rope winding-winding process is characterised by non-zero components of matrices [*M*] and [*H*], which is possible only under the following conditions:

$(i < k - N_f) \wedge [(i > k - N_f) \vee (i < k - N_{fr})]$ when the idle rope is wound and the working rope is unwound;

$(i < k) \wedge [(i > k + N_f) \vee (i < N - N_{fr})]$ in case of simultaneous winding of the working rope and unwinding of the idle rope.

To determine the characteristics of the friction coils, according to the adopted linear law of tension drop, the components of the matrix [*M*] correspond to such a relationship:

$$M_{2N-m,2N-Nfr} = -m/N_{fr} \qquad (m = 1...N_{fr}). \tag{2.15}$$

From the analysis of the mathematical model formulated by us (2.10) - (2.13) it follows that the values of coefficients in the systems of equations describing the operation of putting on each *k-th* ring depend on the solution of all the previous systems, which reflect the putting on of *k-1 rings*, so. the sequence of putting rings on the drum shell can be represented as a recurrent process described by the following system of equations:

$$\begin{cases} [M(r_{1,1},\ldots,r_{k-1,k-1})_{..k}]\cdot[C_{.k}]=[H(r_{1,1},\ldots,r_{k-1,k-1})_{.k}]; \\ r_{k,k}=\left(R_{\text{o}}-C_{k,k}\right)\Big/\left(1+P_{k,k}/E_r\cdot S_r\right). \end{cases} \quad (k = 2, \ldots, N - N_{\text{fr}} - N_{\text{f}}). \quad (2.16)$$

Since the *k-th* cross section of matrices [*M*] and [*H*] does not depend on the parameter $r_{k,k}$, with respect to matrix *C* it is found by solving a system of algebraic equations of order 2N, i.e.

$$[C_{.k}] = [M(r_{1,1},\ldots,r_{k-1,k-1})_{..k}]^{-1}[H(r_{1,1},\ldots,r_{k-1,k-1})_{.k}]. \quad (2.17)$$

The systems formulated above allow us to determine the displacements and forces occurring at the moment of putting the *k-th* ring on the drum shell, and then its radius $r_{k,k}$ in the undeformed state. The process ends with putting on the last ring, the serial number of which corresponds to the total number of coils of the working rope N_{r}.

As we can see, we have managed to construct a mathematical model of rope winding on the MHM drum in the form of systems of equations (2.8) - (2.17).

For its application it is necessary to develop an effective algorithm for constructing the ductility matrix of the axisymmetric shell of the MHM drum.

2.3 Construction of the mathematical model of deformation of the reinforced MHM drum

To begin with, let us determine for what distances the points of the coordinate lines on the drum shell move under the action of unit forces distributed along each of the mentioned lines.

For this purpose, we use the equations describing the joint deformations, as well as the equations reflecting the equilibrium of the shell and the elastic supports of the drum.

In making them, we make the following assumptions:

1) the physical model of a drum with a reinforced shell is a sequence of shells connected to each other in nodes, whose parameters are described below (see Section 2.4.);

2) elastic supports with equivalent characteristics are placed in the nodes corresponding to the lobes, flanges and spandrels of the drum.

So, according to the adopted assumption, let us represent the MHM drum as a sequence of structurally orthotropic axisymmetric shells (Fig. 2.4) with elastic supports connected to each other in nodes.

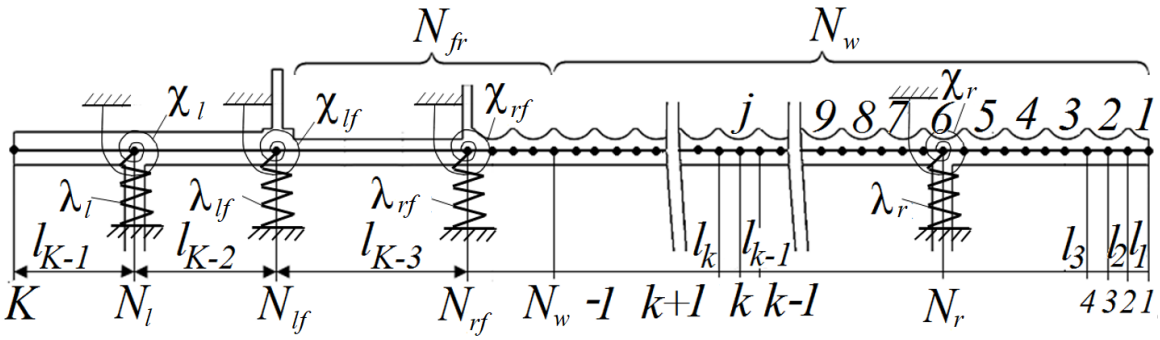

Figure 2.4. Physical model of the drum

In Fig. 2.4 shows: N_w - number of working grooves; N_{fr} - number of friction turns; K - number of nodes; N_l , N_r - numbers of nodes above the left and the right N_{lf}, N_{rf} - numbers of nodes above the left and right flanges; l_k - length of the *k-th* section of the shell; λ - stiffness of compression springs; χ - stiffness of torsion springs; L - total length of the shell.

As noted above, the elastic supports of the drum elements in the form of compression and torsion springs (they have constant stiffness characteristics) are placed in the nodes corresponding to the reinforcements (lobes, flanges, spandrels, etc.). We will assume that the loads acting on the drum grooves are applied to the nodes of the shell, which are assigned odd numbers.

The general expression for determining the deflection of the *k-th* section of the shell under the influence of a unit force along the *i-th* coordinate line ($i = 1...N$) takes the following form:

$$w_{i,k}(x) = e^{\beta_k \cdot x} \cdot \left(C_{i,4k-3} \cdot \sin(\beta_k \cdot x) + C_{i,4k-2} \cdot \cos(\beta_k \cdot x)\right) + \\ + e^{-\beta_k \cdot x} \cdot \left(C_{i,4k-1} \cdot \sin(\beta_k \cdot x) + C_{i,4k} \cdot \cos(\beta_k \cdot x)\right). \quad (2.18)$$

Here $\beta_k = \sqrt[4]{\frac{B_k}{4 \cdot R^2 \cdot D_k}}$ is the coefficient of reduction of the distance of displacement of the coils; B_k is the annular stiffness of the shell; D_k is the bending stiffness; and C are arbitrary constants.

The boundary values of the shell parameters can be described using a set of joint strain equations, as well as equations of equilibrium of the boundary nodes of the beams and supports, viz:

$$M_1(0) = 0, Q_1(0) = \delta^1_{8i-6} \cdot$$

$$\left.\begin{aligned} w_k(x_k) &= w_{k+1}(x_k), \\ \varphi_k(x_k) &= \varphi_{k+1}(x_k), \\ M_k(x_k) &= M_{k+1}(x_k) + \delta^k_{N_r} \cdot \chi_r \cdot \varphi_{N_r}(x_{N_r}) + \delta^k_{N_l} \cdot \chi_l \cdot \varphi_{N_l}(x_{N_l}) + \\ &\quad + \delta^k_{N_{rf}} \cdot \chi_{rf} \cdot \varphi_{N_{rf}}(x_{N_{rf}}) + \delta^k_{N_{lf}} \cdot \chi_{lf} \cdot \varphi_{N_{lf}}(x_{N_{lf}}), \\ Q_k(x_k) &= Q_{k+1}(x_k) - \delta^k_{N_r} \cdot \lambda_r \cdot w_{N_r}(x_{N_r}) - \delta^k_{N_l} \cdot \lambda_l \cdot w_{N_l}(x_{N_l}) - \\ &\quad - \delta^k_{N_{rf}} \cdot \lambda_{rf} \cdot w_{N_{rf}}(x_{N_{rf}}) - \delta^k_{N_{lf}} \cdot \lambda_{lf} \cdot w_{N_{lf}}(x_{N_{lf}}) - \mathrm{mod}(k,2) \cdot \delta^k_{8i-6} \end{aligned}\right\} \quad (2.19)$$

$M_{K-1}(L) = 0$, $Q_{K-1}(L) = 0$.

Here the number of the sheath node (with the total number of nodes K) $k = 2,...,$ K-1; the number of the node to which the force is applied, $i = 1...N$; φ is the angle of rotation; M is the bending moment that occurs in the rope coils; *Q is the* shear force; δ^k_i is the Kronecker symbol equal to one if i equals k, in other cases it is zero; mod (k, 2) is a function equal to zero at even value of parameter k and one at odd value.

Substituting the expression (2.18), corresponding to the deflection of the drum shell, into equations (2.19), describing the boundary conditions of its operation, we

obtain such systems of linear algebraic equations for determining the integration constants of the rope winding process on the drum: .

$$2D_{o1}\cdot\beta_1^{\,2}\left(C_3-C_1\right)=0;$$

$$2D_{o1}\cdot\beta_1^{\,3}\left(-C_1+C_2-C_3+C_4\right)=0{,}5\cdot\delta_1^m\cdot Q;$$

$$e^{\beta_{k-1}\cdot x_k}\left(C_{4k-7}\cdot\sin\left(\beta_{k-1}\cdot x_k\right)+C_{4k-6}\cdot\cos\left(\beta_{k-1}\cdot x_k\right)\right)+e^{-\beta_{k-1}\cdot x_k}\left(C_{4k-5}\cdot\sin\left(\beta_{k-1}\cdot x_k\right)+\right.$$

$$\left.+C_{4k-4}\cdot\cos\left(\beta_{k-1}\cdot x_k\right)\right)=e^{\beta_k\cdot x_k}\left(C_{4k-3}\cdot\sin\left(\beta_k\cdot x_k\right)+C_{4k-2}\cdot\cos\left(\beta_k\cdot x_k\right)\right)+$$

$$+e^{-\beta_k\cdot x_k}\left(C_{4k-1}\cdot\sin\left(\beta_k\cdot x_k\right)+C_{4k}\cdot\cos\left(\beta_k\cdot x_k\right)\right);$$

$$\beta_{k-1}\left[\begin{array}{l}\left(C_{4k-7}\cdot e^{\beta_{k-1}\cdot x_k}-C_{4k-4}\cdot e^{-\beta_{k-1}\cdot x_k}\right)\left(\cos\left(\beta_{k-1}\cdot x_k\right)+\sin\left(\beta_{k-1}\cdot x_k\right)\right)+\\+\left(C_{4k-6}\cdot e^{\beta_{k-1}\cdot x_k}+C_{4k-5}\cdot e^{-\beta_{k-1}\cdot x_k}\right)\left(\cos\left(\beta_{k-1}\cdot x_k\right)-\sin\left(\beta_{k-1}\cdot x_k\right)\right)\end{array}\right]=$$

$$=\beta_k\left[\begin{array}{l}\left(C_{4k-3}\cdot e^{\beta_k\cdot x_k}-C_{4k}\cdot e^{-\beta_k\cdot x_k}\right)\left(\cos\left(\beta_k\cdot x_k\right)+\sin\left(\beta_k\cdot x_k\right)\right)+\\+\left(C_{4k-2}\cdot e^{\beta_k\cdot x_k}+C_{4k-1}\cdot e^{-\beta_k\cdot x_k}\right)\left(\cos\left(\beta_k\cdot x_k\right)-\sin\left(\beta_k\cdot x_k\right)\right)\end{array}\right];$$

$$2D_{o_{k-1}}\cdot\beta_{k-1}^2\left[\begin{array}{l}\left(C_{4k-5}\cdot e^{-\beta_{k-1}\cdot x_k}-C_{4k-7}\cdot e^{\beta_{k-1}\cdot x_k}\right)\cos\left(\beta_{k-1}\cdot x_k\right)+\\+\left(C_{4k-6}\cdot e^{\beta_{k-1}\cdot x_k}-C_{4k-4}\cdot e^{-\beta_{k-1}\cdot x_k}\right)\sin\left(\beta_{k-1}\cdot x_k\right)\end{array}\right]=$$

$$=2D_{o_k}\cdot\beta_k^2\left[\begin{array}{l}\left(C_{4k-1}\cdot e^{-\beta_k\cdot x_k}-C_{4k-3}\cdot e^{\beta_k\cdot x_k}\right)\cos\left(\beta_k\cdot x_k\right)+\\+\left(C_{4k-2}\cdot e^{\beta_k\cdot x_k}-C_{4k}\cdot e^{-\beta_k\cdot x_k}\right)\sin\left(\beta_k\cdot x_k\right)\end{array}\right];$$

$$2D_{o_{k-1}}\cdot\beta_{k-1}^3\left[\begin{array}{l}\left(C_{4k-6}\cdot e^{\beta_{k-1}\cdot x_k}-C_{4k-5}\cdot e^{-\beta_{k-1}\cdot x_k}\right)\cdot\left(\cos\left(\beta_{k-1}\cdot x_k\right)+\sin\left(\beta_{k-1}\cdot x_k\right)\right)-\\-\left(C_{4k-7}\cdot e^{\beta_{k-1}\cdot x_k}-C_{4k-4}\cdot e^{-\beta_{k-1}\cdot x_k}\right)\cdot\left(\cos\left(\beta_{k-1}\cdot x_k\right)-\sin\left(\beta_{k-1}\cdot x_k\right)\right)\end{array}\right]=$$

$$=2D_{o_k}\cdot\beta_k^3\left[\begin{array}{l}\left(C_{4k-2}\cdot e^{\beta_k\cdot x_k}-C_{4k-1}\cdot e^{-\beta_k\cdot x_k}\right)\cdot\left(\cos\left(\beta_k\cdot x_k\right)+\sin\left(\beta_k\cdot x_k\right)\right)-\\-\left(C_{4k-3}\cdot e^{\beta_k\cdot x_k}-C_{4k}\cdot e^{-\beta_k\cdot x_k}\right)\cdot\left(\cos\left(\beta_k\cdot x_k\right)-\sin\left(\beta_k\cdot x_k\right)\right)\end{array}\right];$$

$$2D_{o_{K-1}}\cdot\beta_{K-1}^2\left[\left(C_{N-3}\cdot e^{-\beta_{K-1}\cdot L}-C_{N-1}\cdot e^{\beta_{K-1}\cdot L}\right)\cdot\cos\left(\beta_{K-1}\cdot L\right)+\right.$$

$$\left.+\left(C_{N-2}\cdot e^{\beta_{K-1}\cdot L}-C_N\cdot e^{-\beta_{K-1}\cdot L}\right)\sin\left(\beta_{K-1}\cdot L\right)\right]=0;$$

$$2D_{o_{K-1}}\cdot\beta_{K-1}^3\left[\left(C_{N-2}\cdot e^{\beta_{K-1}\cdot L}-C_{N-1}\cdot e^{-\beta_{K-1}\cdot L}\right)\cdot\left(\cos\left(\beta_{K-1}\cdot L\right)+\sin\left(\beta_{K-1}\cdot L\right)\right)-\right.$$

$$\left.-\left(C_{N-3}\cdot e^{\beta_{K-1}\cdot L}-C_N\cdot e^{-\beta_{K-1}\cdot L}\right)\cdot\left(\cos\left(\beta_{K-1}\cdot L\right)-\sin\left(\beta_{K-1}\cdot L\right)\right)\right]=0.$$

Applying to the processes occurring in the right frontal, we formulate such equations:

$$2D_{o_{N_r-1}}\cdot\beta^2_{N_r-1}\left[\begin{array}{l}\left(C_{4N_r-5}\cdot e^{-\beta_{N_r-1}\cdot x_{N_r}}-C_{4N_r-7}\cdot e^{\beta_{N_r-1}\cdot x_{N_r}}\right)\cdot\cos\left(\beta_{N_r-1}\cdot x_{N_r}\right)+\\ +\left(C_{4N_r-6}\cdot e^{\beta_{N_r-1}\cdot x_{N_r}}-C_{4N_r-4}\cdot e^{-\beta_{N_r-1}\cdot x_{N_r}}\right)\sin\left(\beta_{N_r-1}\cdot x_{N_r}\right)\end{array}\right]+$$

$$+\chi\cdot\beta_{N_r-1}\left[\begin{array}{l}\left(C_{4N_r-7}\cdot e^{\beta_{N_r-1}\cdot x_{N_r}}-C_{4N_r-4}\cdot e^{-\beta_{N_r-1}\cdot x_{N_r}}\right)\cdot\left(\cos\left(\beta_{N_r-1}\cdot x_{N_r}\right)+\sin\left(\beta_{N_r-1}\cdot x_{N_r}\right)\right)+\\ +\left(C_{4N_r-6}\cdot e^{\beta_{N_r-1}\cdot x_{N_r}}+C_{4N_r-5}\cdot e^{-\beta_{N_r-1}\cdot x_{N_r}}\right)\cdot\left(\cos\left(\beta_{N_r-1}\cdot x_{N_r}\right)-\sin\left(\beta_{N_r-1}\cdot x_{N_r}\right)\right)\end{array}\right]=$$

$$=2D_{o_{N_r}}\cdot\beta^2_{N_r}\left[\begin{array}{l}\left(C_{4N_r-1}\cdot e^{-\beta_{N_r}\cdot x_{N_r}}-C_{4N_r-3}\cdot e^{\beta_{N_r}\cdot x_{N_r}}\right)\cdot\cos\left(\beta_{N_r}\cdot x_{N_r}\right)+\\ +\left(C_{4N_r-2}\cdot e^{\beta_{N_r}\cdot x_{N_r}}-C_{4N_r-4}^{-\beta_{N_r}\cdot x_{N_r}}\right)\cdot\sin\left(\beta_{N_r}\cdot x_{N_r}\right)\end{array}\right];$$

$$\begin{aligned}2D_{o_{N_r-1}}\cdot\beta^3_{N_r-1}\Big[&\left(C_{4N_r-6}\cdot e^{\beta_{N_r-1}\cdot x_{N_r}}-C_{4N_r-5}\cdot e^{-\beta_{N_r-1}\cdot x_{N_r}}\right)\left(\cos\left(\beta_{N_r-1}\cdot x_{N_r}\right)+\sin\left(\beta_{N_r-1}\cdot x_{N_r}\right)\right)-\\ &-\left(C_{4N_r-7}\cdot e^{\beta_{N_r-1}\cdot x_{N_r}}-C_{4N_r-4}\cdot e^{-\beta_{N_r-1}\cdot x_{N_r}}\right)\left(\cos\left(\beta_{N_r-1}\cdot x_{N_r}\right)-\sin\left(\beta_{N_r-1}\cdot x_{N_r}\right)\right)\Big]+\\ &+\lambda\Big(e^{\beta_{N_r-1}\cdot x_{N_r}}\left(C_{4N_r-7}\cdot\sin\left(\beta_{N_r-1}\cdot x_{N_r}\right)+C_{4N_r-6}\cdot\cos\left(\beta_{N_r-1}\cdot x_{N_r}\right)\right)+\\ &+e^{-\beta_{N_r-1}\cdot x_{N_r}}\left(C_{4N_r-5}\cdot\sin\left(\beta_{N_r-1}\cdot x_{N_r}\right)+C_{4N_r-4}\cdot\cos\left(\beta_{N_r-1}\cdot x_{N_r}\right)\right)=\end{aligned}$$

$$\begin{aligned}=2D_{o_{N_r}}\cdot\beta^3_{N_r}\Big[&\left(C_{4N_r-2}\cdot e^{\beta_{N_r}\cdot x_{N_r}}-C_{4N_r-1}\cdot e^{-\beta_{N_r}\cdot x_{N_r}}\right)\left(\cos\left(\beta_{N_r}\cdot x_{N_r}\right)+\sin\left(\beta_{N_r}\cdot x_{N_r}\right)\right)-\\ &-\left(C_{4N_r-3}\cdot e^{\beta_{N_r}\cdot x_{N_r}}-C_{4N_r}\cdot e^{-\beta_{N_r}\cdot x_{N_r}}\right)\left(\cos\left(\beta_{N_r}\cdot x_{N_r}\right)-\sin\left(\beta_{N_r}\cdot x_{N_r}\right)\right)\Big].\end{aligned}$$

Regarding the left lob of the drum.

$$2D_{o_{N_l-1}}\cdot\beta^2_{N_l-1}\left[\begin{array}{l}\left(C_{4N_l-5}\cdot e^{-\beta_{N_l-1}\cdot x_{N_l}}-C_{4N_l-7}\cdot e^{\beta_{N_l-1}\cdot x_{N_l}}\right)\cos\left(\beta_{N_l-1}\cdot x_{N_l}\right)+\\ +\left(C_{4N_l-6}\cdot e^{\beta_{N_{\text{л}}-1}\cdot x_{N_l}}-C_{4N_l-4}\cdot e^{-\beta_{N_l-1}\cdot x_{N_l}}\right)\sin\left(\beta_{N_l-1}\cdot x_{N_l}\right)\end{array}\right]+$$

$$+\chi\cdot\beta_{N_l-1}\left[\begin{array}{l}\left(C_{4N_l-7}\cdot e^{\beta_{N_l-1}\cdot x_{N_l}}-C_{4N_l-4}\cdot e^{-\beta_{N_l-1}\cdot x_{N_l}}\right)\left(\cos\left(\beta_{N_l-1}\cdot x_{N_l}\right)+\sin\left(\beta_{N_l-1}\cdot x_{N_l}\right)\right)+\\ +\left(C_{4N_l-6}\cdot e^{\beta_{N_l-1}\cdot x_{N_l}}+C_{4N_l-5}\cdot e^{-\beta_{N_l-1}\cdot x_{N_l}}\right)\left(\cos\left(\beta_{N_l-1}\cdot x_{N_l}\right)-\sin\left(\beta_{N_l-1}\cdot x_{N_l}\right)\right)\end{array}\right]=$$

$$=2D_{o_{N_l}}\cdot\beta^2_{N_l}\left[\begin{array}{l}\left(C_{4N_l-1}\cdot e^{-\beta_{N_l}\cdot x_{N_l}}-C_{4N_l-3}\cdot e^{\beta_{N_l}\cdot x_{N_l}}\right)\cos\left(\beta_{N_l}\cdot x_{N_l}\right)+\\ +\left(C_{4N_l-2}\cdot e^{\beta_{N_l}\cdot x_{N_l}}-C_{4N_l-4}\cdot e^{-\beta_{N_l}\cdot x_{N_l}}\right)\sin\left(\beta_{N_l}\cdot x_{N_l}\right)\end{array}\right];$$

$$2D_{o_{N_l-1}}\cdot\beta_{N_l-1}^3\left[\left(C_{4N_l-6}\cdot e^{\beta_{N_l-1}\cdot x_{N_l}}-C_{4N_l-5}\cdot e^{-\beta_{N_l-1}\cdot x_{N_l}}\right)\left(\cos\left(\beta_{N_l-1}\cdot x_{N_l}\right)+\sin\left(\beta_{N_l-1}\cdot x_{N_l}\right)\right)-\right.$$
$$-\left.\left(C_{4N_l-7}\cdot e^{\beta_{N_l-1}\cdot x_{N_l}}-C_{4N_l-4}\cdot e^{-\beta_{N_l-1}\cdot x_{N_l}}\right)\left(\cos\left(\beta_{N_l-1}\cdot x_{N_l}\right)-\sin\left(\beta_{N_l-1}\cdot x_{N_l}\right)\right)\right]+$$
$$+\lambda\left(e^{\beta_{N_l-1}\cdot x_{N_l}}\left(C_{4N_l-7}\cdot\sin\left(\beta_{N_l-1}\cdot x_{N_l}\right)+C_{4N_l-6}\cdot\cos\left(\beta_{N_l-1}\cdot x_{N_l}\right)\right)+\right.$$
$$+\left.e^{-\beta_{N_l-1}\cdot x_{N_l}}\left(C_{4N_l-5}\cdot\sin\left(\beta_{N_l-1}\cdot x_{N_l}\right)+C_{4N_l-4}\cdot\cos\left(\beta_{N_l-1}\cdot x_{N_l}\right)\right)\right)=$$
$$=2D_{o_{N_l}}\cdot\beta_{N_l}^3\left[\left(C_{4N_l-2}\cdot e^{\beta_{N_l}\cdot x_{N_l}}-C_{4N_l-1}\cdot e^{-\beta_{N_l}\cdot x_{N_l}}\right)\cdot\left(\cos\left(\beta_{N_l}\cdot x_{N_l}\right)+\sin\left(\beta_{N_l}\cdot x_{N_l}\right)\right)-\right.$$
$$-\left.\left(C_{4N_l-3}\cdot e^{\beta_{N_l}\cdot x_{N_l}}-C_{4N_l}\cdot e^{-\beta_{N_l}\cdot x_{N_l}}\right)\cdot\left(\cos\left(\beta_{N_l}\cdot x_{N_l}\right)-\sin\left(\beta_{N_l}\cdot x_{N_l}\right)\right)\right].$$

To describe the processes occurring in the right bearing rib, we compose such a system of equations:

$$2D_{o_{N_{rf}-1}}\cdot\beta_{N_{rf}-1}^3\left[\left(C_{4N_{rf}-6}\cdot e^{\beta_{N_{rf}-1}\cdot x_{N_{rf}}}-C_{4N_{rf}-5}\cdot e^{-\beta_{N_{rf}-1}\cdot x_{N_{rf}}}\right)\left(\cos\left(\beta_{N_{rf}-1}\cdot x_{N_{rf}}\right)+\right.\right.$$
$$+\left.\sin\left(\beta_{N_{rf}-1}\cdot x_{N_{rf}}\right)\right)-\left(C_{4N_{rf}-7}\cdot e^{\beta_{N_{rf}-1}\cdot x_{N_{rf}}}-C_{4N_{rf}-4}\cdot e^{-\beta_{N_{rf}-1}\cdot x_{N_{rf}}}\right)\left(\cos\left(\beta_{N_{rf}-1}\cdot x_{N_{rf}}\right)-\right.$$
$$-\left.\left.\sin\left(\beta_{N_{rf}-1}\cdot x_{N_{rf}}\right)\right)\right]+\lambda\left(e^{\beta_{N_{rf}-1}\cdot x_{N_{rf}}}\left(C_{4N_{rf}-7}\cdot\sin\left(\beta_{N_{rf}-1}\cdot x_{N_{rf}}\right)+C_{4N_{rf}-6}\cdot\cos\left(\beta_{N_{rf}-1}\cdot x_{N_{rf}}\right)\right)+\right.$$
$$+\left.e^{-\beta_{N_{rf}-1}\cdot x_{N_{rf}}}\left(C_{4N_{rf}-5}\cdot\sin\left(\beta_{N_{rf}-1}\cdot x_{N_{rf}}\right)+C_{4N_{rf}-4}\cdot\cos\left(\beta_{N_{rf}-1}\cdot x_{N_{rf}}\right)\right)\right)=$$

$$=2D_{o_{N_{rf}}}\cdot\beta_{N_{rf}}^3\left[\left(C_{4N_{rf}-2}\cdot e^{\beta_{N_{rf}}\cdot x_{N_{rf}}}-C_{4N_{rf}-1}\cdot e^{-\beta_{N_{rf}}\cdot x_{N_{rf}}}\right)\left(\cos\left(\beta_{N_{rf}}\cdot x_{N_{rf}}\right)+\sin\left(\beta_{N_{rf}}\cdot x_{N_{rf}}\right)\right)-\right.$$
$$-\left.\left(C_{4N_{rf}-3}\cdot e^{\beta_{N_{rf}}\cdot x_{N_{rf}}}-C_{4N_{rf}}\cdot e^{-\beta_{N_{rf}}\cdot x_{N_{rf}}}\right)\left(\cos\left(\beta_{N_{rf}}\cdot x_{N_{rf}}\right)-\sin\left(\beta_{N_{rf}}\cdot x_{N_{rf}}\right)\right)\right].$$

In the left flange

$$2D_{o_{N_{lf}-1}}\cdot\beta_{N_{lf}-1}^3\left[\left(C_{4N_{lf}-6}\cdot e^{\beta_{N_{lf}-1}\cdot x_{N_{lf}}}-C_{4N_{lf}-5}\cdot e^{-\beta_{N_{lf}-1}\cdot x_{N_{lf}}}\right)\cdot\left(\cos\left(\beta_{N_{lf}-1}\cdot x_{N_{lf}}\right)+\right.\right.$$
$$+\left.\sin\left(\beta_{N_{lf}-1}\cdot x_{N_{lf}}\right)\right)-\left(C_{4N_{lf}-7}\cdot e^{\beta_{N_{lf}-1}\cdot x_{N_{lf}}}-C_{4N_{lf}-4}\cdot e^{-\beta_{N_{lf}-1}\cdot x_{N_{lf}}}\right)\left(\cos\left(\beta_{N_{lf}-1}\cdot x_{N_{lf}}\right)-\right.$$
$$-\left.\left.\sin\left(\beta_{N_{lf}-1}\cdot x_{N_{lf}}\right)\right)\right]+\lambda\left(e^{\beta_{N_{lf}-1}\cdot x_{N_{lf}}}\cdot\left(C_{4N_{lf}-7}\cdot\sin\left(\beta_{N_{lf}-1}\cdot x_{N_{lf}}\right)+C_{4N_{lf}-6}\cdot\cos\left(\beta_{N_{lf}-1}\cdot x_{N_{lf}}\right)\right)+\right.$$
$$+\left.e^{-\beta_{N_{lf}-1}\cdot x_{N_{lf}}}\left(C_{4N_{lf}-5}\cdot\sin\left(\beta_{N_{lf}-1}\cdot x_{N_{lf}}\right)+C_{4N_{lf}-4}\cdot\cos\left(\beta_{N_{lf}-1}\cdot x_{N_{lf}}\right)\right)\right)=$$
$$=2D_{o_{N_{lf}}}\cdot\beta_{N_{lf}}^3\left[\left(C_{4N_{lf}-2}\cdot e^{\beta_{N_{lf}}\cdot x_{N_{lf}}}-C_{4N_{lf}-1}\cdot e^{-\beta_{N_{lf}}\cdot x_{N_{lf}}}\right)\cdot\left(\cos\left(\beta_{N_{lf}}\cdot x_{N_{lf}}\right)+\sin\left(\beta_{N_{lf}}\cdot x_{N_{lf}}\right)\right)-\right.$$

$$-\left(C_{4N_{lf}-3}\cdot e^{\beta_{N_{lf}}\cdot x_{N_{lf}}}-C_{4N_{lf}}\cdot e^{-\beta_{N_{lf}}\cdot x_{N_{lf}}}\right)\cdot\left(\cos\left(\beta_{N_{lf}}\cdot x_{N_{lf}}\right)-\sin\left(\beta_{N_{lf}}\cdot x_{N_{lf}}\right)\right)\Big].$$

Let us represent the system of linear algebraic equations for determining the integration constants C in matrix form, i.e.

$$[A]\text{-}[C]=[C], \tag{2.20}$$

where $[A]$ is the matrix of the system, which is formed by substituting the general solution (2.18) into the system of equations (2.19), viz:

$$[A]=\begin{bmatrix}
A_{1,1} & A_{1,2} & A_{1,3} & A_{1,4} & & & & \\
A_{2,1} & A_{2,2} & A_{2,3} & A_{2,4} & & & & \\
. & . & . & . & . & . & . & . \\
A_{4k-5,4k-7} & A_{4k-5,4k-6} & A_{4k-5,4k-5} & A_{4k-5,4k-4} & A_{4k-5,4k-3} & A_{4k-5,4k-2} & A_{4k-5,4k-1} & A_{4k-5,4k} \\
A_{4k-4,4k-7} & A_{4k-4,4k-6} & A_{4k-4,4k-5} & A_{4k-4,4k-4} & A_{4k-4,4k-3} & A_{4k-4,4k-2} & A_{4k-5,4k-1} & A_{4k-4,4k} \\
A_{4k-3,4k-7} & A_{4k-3,4k-6} & A_{4k-3,4k-5} & A_{4k-3,4k-4} & A_{4k-3,4k-3} & A_{4k-3,4k-2} & A_{4k-4,4k-1} & A_{4k-3,4k} \\
A_{4k-2,4k-7} & A_{4k-2,4k-6} & A_{4k-2,4k-5} & A_{4k-2,4k-4} & A_{4k-2,4k-3} & A_{4k-2,4k-2} & A_{4k-3,4k-1} & A_{4k-2,4k} \\
. & . & . & . & . & . & . & . \\
 & & & & A_{N-1,N-3} & A_{N-1,N-2} & A_{N-1,N-1} & A_{N-1,N} \\
 & & & & A_{N,N-3} & A_{N,N-2} & A_{N,N-1} & A_{N,N}
\end{bmatrix}.$$

In this case, the components of the mentioned matrix acquire such values:

$$A_{1,1}=-2\cdot\beta_1^2\cdot D_1\cdot e^{\beta_1\cdot x_1}\cos\left(\beta_1\cdot x_1\right);$$

$$A_{1,2}=2\cdot\beta_1^2\cdot D_1\cdot e^{\beta_1\cdot x_1}\sin\left(\beta_1\cdot x_1\right);$$

$$A_{1,3}=2\cdot\beta_1^2\cdot D_1\cdot e^{-\beta_1\cdot x_1}\cos\left(\beta_1\cdot x_1\right);$$

$$A_{1,4}=-2\cdot\beta_1^2\cdot D_1\cdot e^{-\beta_1\cdot x_1}\sin\left(\beta_1\cdot x_1\right);$$

$$A_{2,1}=2\cdot\beta_1^3\cdot D_1\cdot e^{\beta_1\cdot x_1}\cdot\left(\cos\left(\beta_1\cdot x_1\right)-\sin\left(\beta_1\cdot x_1\right)\right);$$

$$A_{2,2}=-2\cdot\beta_1^3\cdot D_1\cdot e^{\beta_1\cdot x_1}\cdot\left(\cos\left(\beta_1\cdot x_1\right)+\sin\left(\beta_1\cdot x_1\right)\right);$$

$$A_{2,3}=2\cdot\beta_1^3\cdot D_1\cdot e^{-\beta_1\cdot x_1}\cdot\left(\cos\left(\beta_1\cdot x_1\right)+\sin\left(\beta_1\cdot x_1\right)\right);$$

$$A_{2,4}=-2\cdot\beta_1^3\cdot D_1\cdot e^{-\beta_1\cdot x_1}\cdot\left(\cos\left(\beta_1\cdot x_1\right)-\sin\left(\beta_1\cdot x_1\right)\right).$$

Then in expression (2.20) [*B*] is the load matrix, the components of which can be written in the following form:

$$B_{i,j} = \delta_{i,2} \big/ 2R + \delta_{i,8j-6} \big/ R, \text{N/m}. \qquad (2.21)$$

Here, the value of the indices is within these limits: $1 \le i \le N$, and $1 \le j \le N$.

Now we find the matrix of integration constants, namely:

$$[C] = [A]^{-1} \text{-}[C]. \qquad (2.22)$$

The distances by which the characteristic points of the coordinate lines of the MHM drum shell shell move under the influence of unit forces can be determined from equation (2.18), provided that $x = 0$, and the values of the integration constants are substituted from expression (2.22), thus,

$$W_{i,j} = C_{i,j8-6} + C_{i,8j-4} \qquad (2.23)$$

where $i, j = 1...N$.

Using equation (2.23), we determine the components of the pliability matrix [*W*], the values of which depend on the parameters of the structural-orthotropic shell of the drum and its elastic supports.

Expression (2.23) can be transformed into matrix form, i.e.

$$\{w\} = [\Phi]\text{-}\{C\},$$

in which the non-zero components of the matrix [F]

$$\Phi_{k,4k-2} = \Phi_{k,4k} = 1.$$

Now the general equation describing the pliability matrix has the following form:

$$[W] = [\Phi]\text{-}[A]^{-1} \text{-}[B]. \qquad (2.24)$$

As a result, we obtained a mathematical model of deformation of the shell of the MHM drum under the influence of rope load in the form of equations

(2.22) - (2.24). Within the framework of the research problem it is necessary to determine the unknown parameters D, B, λ, χ, using modern methods of structural mechanics, and for this purpose we need a physical model of the MHM drum. Its creation is the most important stage of this research.

2.4 Development of a physical model of a profiled reinforced drum

The MHM drum, equipped with a spiral rope thread, is a complex spatial thin-walled reinforced structure. It consists of a shell and reinforcements in the form of ribs, braces, flanges, lobes and spandrels.

Here we assume that the model is axisymmetric and that it is a set of physical models of the drum subsystems (see Fig. 2.5); in particular, the shell and reinforcements, which we develop separately, taking into account the peculiarities of the function of each of the structural elements.

Constructive orthotropy, many scales method and semi-empirical approach were used to create these simplified models.

We bring the structure to the axisymmetric form we envisaged by averaging the mechanical characteristics of its reinforcements.

So, building a physical model of the drum is impossible without solving the following subproblems:

1) Determination of possible errors in the operation of the structure when the screw groove of the drum is replaced by an axisymmetric model with a sequence of annular grooves.

2) Construction of a physical model of the shell.

3) Development of physical models of drum reinforcements.

2.4.1 Determination of SSS error occurring in drum with annular grooves

Since it was found that the non-axisymmetric component of the drum shell displacements is small enough, it became possible to model on it, instead of a spiral groove, a sequence of annular grooves (see Fig. 2.6).

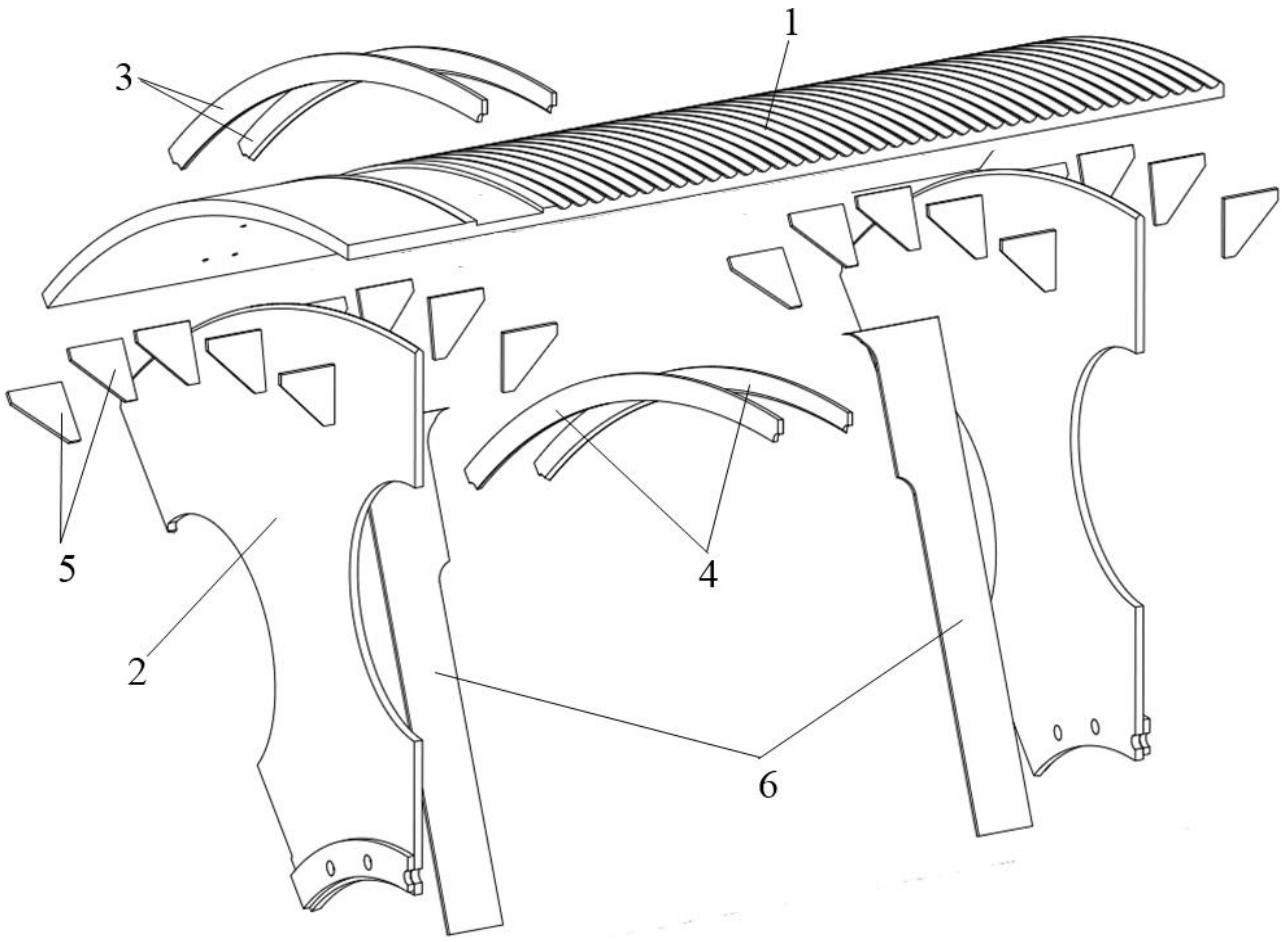

Figure 2.5. Schematic diagram of the MHM drum structure:
1 - shell; 2 - frontale; 3 - flanges; 4 – bearing ribs; 5 - gussets; 6 - ribs

Taking into account the given range of changes in the geometrical parameters of the MHM drum, we will perform calculations of SSS arising in the design with a helical groove, as well as in the model in the presence of a sequence of annular grooves, after which we will estimate the error of the result.

The calculations were performed by means of *a* computational experiment using FEM, taking into account the following assumptions:

1. The load on the shell under the influence of the rope coils is represented as a uniform radial pressure distributed along the bottom of the groove.

2. In the study of the non-axisymmetric shell caused by the presence of the spiral groove, we do not consider the effect of the drum reinforcements.

3. The joint between the frontal and the hub is a rigid termination.

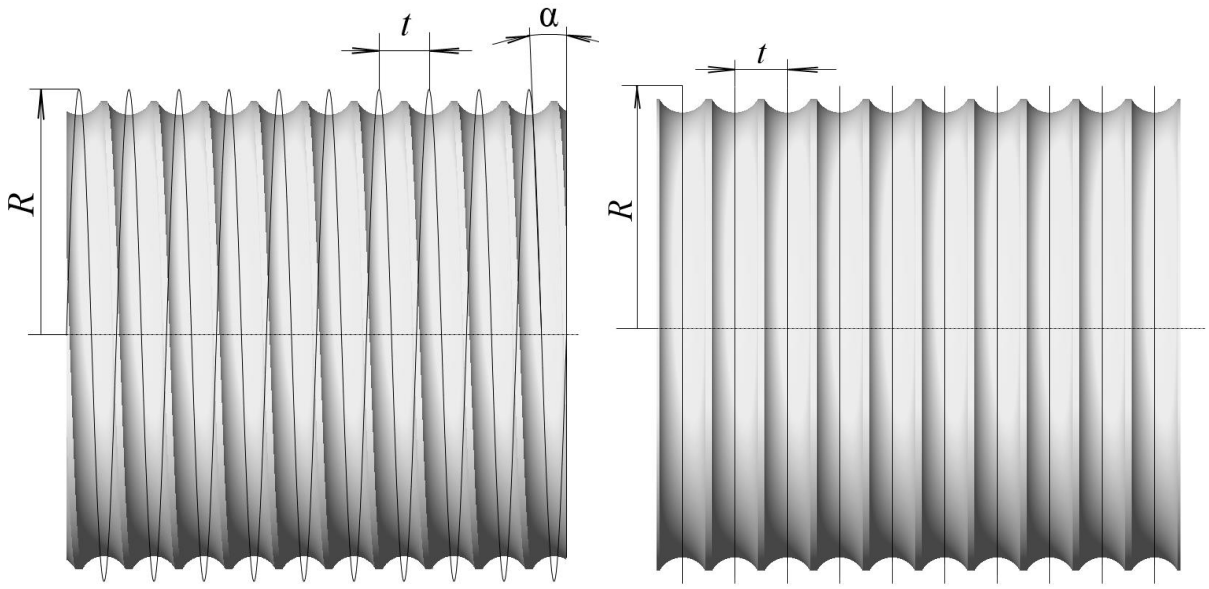

Fig. 2.6. Model of a drum shell with spiral (*a*)
and annular grooves (*b*)

The following parameters of the drum helical groove profile are required for calculations: *t* - groove cutting step; R_o - radius of winding; α - cutting angle

$$\alpha = \frac{t}{2\pi \cdot R_o}.$$

At that, α = 2.6 - 3.6° for drums of large MHM's.

Let us reduce the above considered parameters of the drum to dimensionless parameters, i.e.

$$\tilde{B} = B/R_o, \quad 0{,}8 \le \tilde{B} \le 1{,}15;$$

$$\tilde{h} = h/R_o, \quad 0{,}017 \le \tilde{h} \le 0{,}02;$$

$$\tilde{h}_l = h_l/R_o, \quad 0{,}01 \le \tilde{h}_l \le 0{,}0175,$$

where *B is* the drum width; *h is the* thickness of the shell; $h_л$ is the thickness of the frontal.

According to the computational experiment plan, the range of values of angle α consists of 11 levels and all other parameters consist of three levels.

The calculation scheme provides for the following conditions:

1) finite element models of the drum reflect the spiral and annular structure of the grooves;

2) the faces of the lobes adjacent to the hubs are pinched;

3) a radial pressure equal to 2 MPa is applied to the bottom of each groove.

As a result of the experiment, we determine displacements and stresses in the drum shells corresponding to the two types of groove placement (see Fig. 2.7, *a, b*).

On the basis of the conducted computational experiment, curves of dependence of the error δ on the groove cutting angle α were obtained (Fig. 2.8).

As shown in the figure, due to the change of the groove angle from 2.6° to 3.6°, the relative errors of the results increase monotonically, not exceeding 6 % when measuring the maximum displacements, and 10 % - in the case of maximum intensity of stresses in the drum shell. Thus, the use of a drum model with annular grooves provides a solution that agrees with the results of the study of a drum with a spiral groove.

Taking into account the above mentioned, we replace spiral grooves with annular grooves in SSS modelling and conclude that in the range of investigated parameters the error of results does not exceed 10 %. The spread of values of relative error of change of intensity of stresses and displacements in the shell, provided that the value of the groove cutting angle is constant, as well as taking into account dimensionless parameters (drum width, thickness of the shell and head), do not exceed 0.6 %.

2.4.2 Building a Physical Model of the MHM Drum Shell

According to the previous findings regarding the analytical definition of the shell pliability matrix, it is necessary to formulate analytical expressions for the calculation of its coefficients.

In developing the physical model of the shell, we will take into account the analytical expressions for calculating its deflection and the intensity of stresses arising

there.

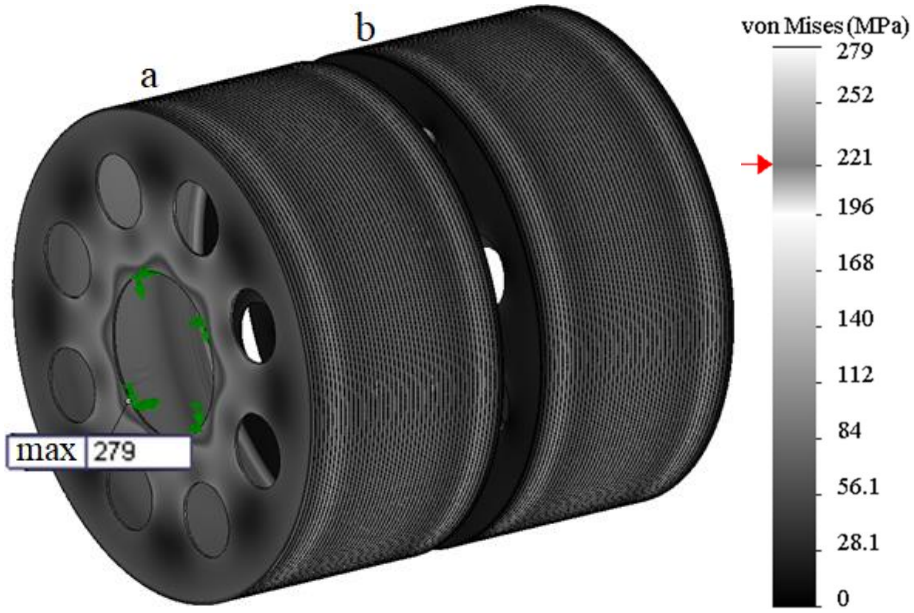

Figure 2.7. General view of the model and diagram of stress intensity
in drums with spiral groove (*a*)
and a sequence of annular grooves (*b*)

The model construction is based on the application of the idea of semi-empirical approach [2], which allows to simplify the mathematical model of the object, in which the coefficients calculated experimentally and selected in such a way that in a certain interval of parameter changes the calculated and experimental data agree well.

The methods of averaging, two scales, computational experiment, and finite element method (FEM) were used to create the model.

Let us assume that it is possible to model the profiled shell as a shell of variable thickness by relying on the Kirchhoff-Liave hypotheses.

Let us consider the bending of a shell with a profiled outer surface described by the function $f_z\ (x)$ with the following parameters: mean radius R, and thickness h, *while* the shell experiences a uniform radial pressure q. Let us extract an element from the shell (see Fig. 2.9) by means of two cross sections located at a distance dx and two radial sections forming an angle $d\varphi$ between them. Let us position the

coordinate system so that the *x-axis is* parallel to the drum axis and the *z-axis is* directed inwards along the radius, starting from the medial surface of its smooth shell having thickness *h*. Let us denote the displacements of the obtained element in the *x-axis* direction by *u* and in the *z-axis* direction by *w*.

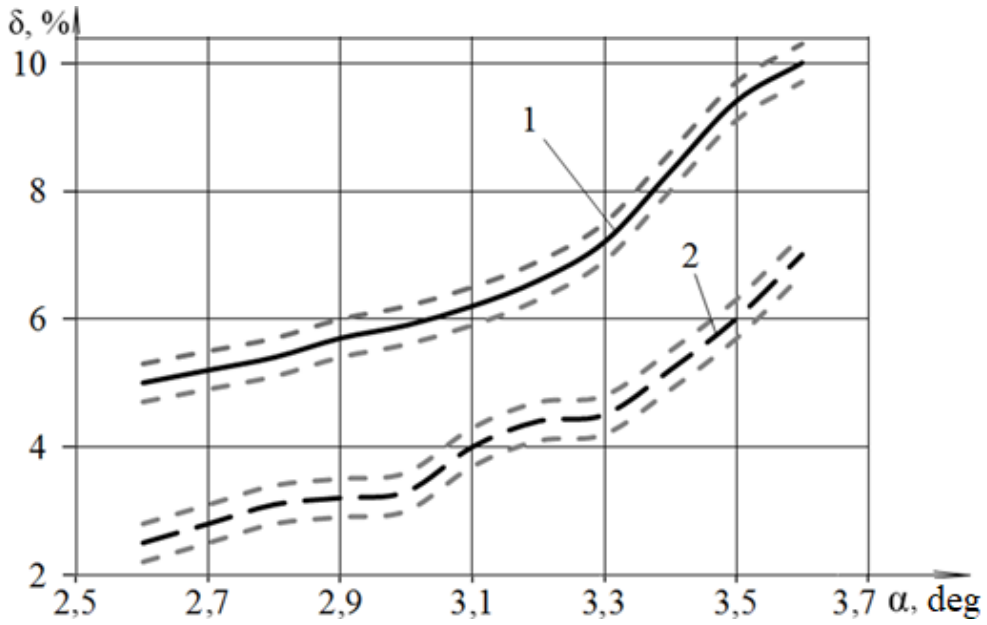

Fig. 2.8. Plots of dependence of the error of the results of the parameter δ determination on the cutting angle α taking into account the values of stress (1) and displacement (2)

Since the cylindrical shell and radial load are axisymmetric, the transverse forces Q_φ and torques M_φ are zero, and the longitudinal force N_φ is constant along the length of the circle.

Applying the static Kirchhoff-Liave hypothesis (τ , $\sigma_{xzz} = 0$), we obtain an expression for determining the variation of the internal potential energy of the shell.

Thus, the internal potential energy of deformation of the profiled shell of length *l*

$$\delta U_k = R\int_0^{l_k}\int_0^{2\pi}\int_{-f_z(x)}^{\frac{h}{2}+h_k}\left[\sigma_x\cdot\delta\varepsilon_x+\sigma_\varphi\cdot\delta\varepsilon_\varphi\right]dx\cdot d\varphi\cdot dz\,, \qquad (2.25)$$

where $f_z(x)$ *is a* function describing the bending of the groove profile; *R is the* radius

of the medial surface of the smooth shell; *h is* the thickness of the shell; longitudinal strain $\varepsilon_x = \partial u / \partial x$; circumferential strain $\varepsilon_\varphi = -w/R$.

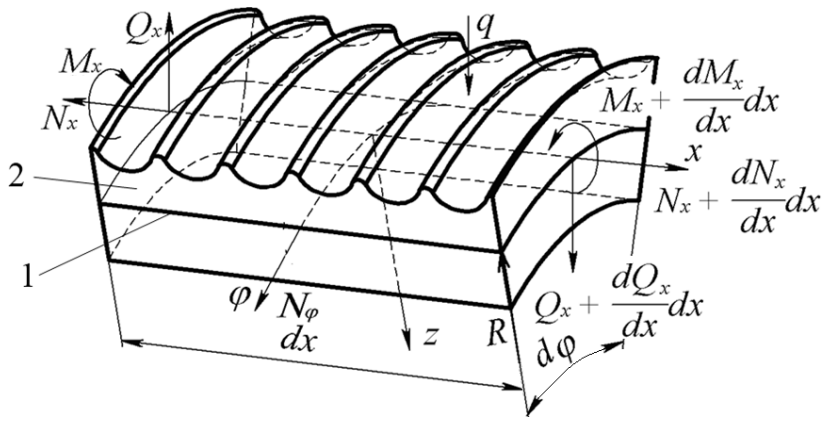

Fig. 2.9. Scheme for calculating the parameters of the shell element (1), equivalent to a part of the profiled shell of the MHM (2)

According to the literature, the bending of the groove profile (see Fig. 2.10) can be described by such a function:

$$f_z(x) = \begin{cases} y_1 + r_d - \sqrt{{r_d}^2 - x^2}, \text{ if } 0 \le x < x_2; \\ \dfrac{(x - x_2)\cdot(y_3 - y_2)}{(x_3 - x_2)} + y_2, \text{ if } x_2 \le x < x_3; \\ y_4 - r_f + \sqrt{{r_f}^2 - (x - x_4)^2}, \text{ if } x_3 \le x < x_4. \\ y_4, \text{ if } x_4 \le x < x_5. \end{cases} \quad (2.26)$$

Here *x* and *y are* the coordinates of the conjugate points determined from such expressions:

$x_1 = 0$; $y1 = 0.5\text{-}h - h_f$;

$x_2 = r_d\text{-}\sin(\varphi)$; $y_2 = y_1 + r_d\text{-}(1 - \cos(\varphi))$;

$x_3 = x_2 + a\text{-}sin(\varphi)$; $y_3 = y_2 + b\text{-}sin(\varphi)$;

$x_4 = x_3 + r_f\text{-}\sin(\varphi)$; $y_4 = y_3 + r_f\text{-}(1 - \cos(\varphi))$;

$x_5 = x_4 + b$; $y_5 = y_4$,

where r_d is the radius of the groove bottom; radius of the groove scallop $r_f = 1/2h_f \cdot \left(\tau^2 + h_f^2\right) - r_d$; h_f is the height of the scallop; interface angle $\varphi = \text{arctg}\left(\tau / \left(r_d + r_f - h_f\right)\right)$.

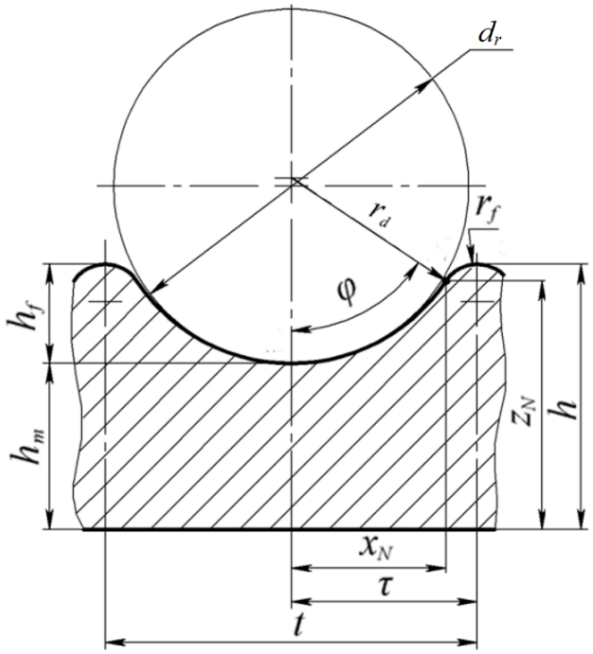

Fig. 2.10. Example of a cross-section of a profiled groove of a MHM drum: d_r - diameter of the rope; h_m - minimum thickness of the shell

In further calculations, let us assume that the radius of the groove bottom r_d is equal to half of the groove pitch τ, as it is accepted at NKMZ. In this case, the expression for calculating the radius of the groove scallop takes the following form:

$$r_f = \frac{\left(\tau - h_f^2\right)}{2h_f}.$$

Consequently, the scallop height h_f cannot exceed half of *the* cutting pitch τ.

Let us construct on the shell an imaginary equidistant surface shifted relative to the neutral surface by the value *e*, and denote by u_0 *(x)* the displacement of its points. To the study of the profiled shell we apply the modified Kirchhoff-Lava kinematic hypothesis, according to which the transverse displacements do not depend on the *z* coordinate, i.e. $w \equiv w(x)$.

The axial displacements can be described by the following formula:

$$u(x,z) \equiv u_0(x) + (e-z)\frac{dw}{dx}.$$

According to the Cauchy relation, the relative longitudinal deformation of the shell is as follows

$$\varepsilon_x(x,z) = \frac{\partial u(x,z)}{\partial x} = \frac{du_0(x)}{dx} + (e-z)\frac{d^2w}{dx^2}.$$

Hereinafter we denote the relation describing the deformation of the equidistant surface $du_0(x)/dx$, by ε_{x_0}.

The expressions that can be used to determine the angle of rotation and curvature of the shell are as follows:

$$\psi(x) = \frac{dw}{dx}; \kappa(x) = -\frac{d^2w}{dx^2}. \qquad (2.27)$$

Then, based on Hooke's law

$$\sigma_x(x,z) = \frac{E}{1-\mu^2}(\varepsilon_x + \mu\cdot\varepsilon_\varphi) = \frac{E}{1-\mu^2}\left(\varepsilon_{x_0} + (e-z)\frac{d^2w}{dx^2} - \mu\frac{w}{R}\right); \qquad (2.28)$$

$$\sigma_\varphi(x,z) = \frac{E}{1-\mu^2}(\varepsilon_\varphi + \mu\cdot\varepsilon_x) = \frac{E}{1-\mu^2}\left(-\frac{w}{R} + \mu\left(\varepsilon_{x_0} + \frac{d^2w}{dx^2}(e-z)\right)\right). \qquad (2.29)$$

Now, using equations (2.26) and (2.27), we find the stresses inside and outside the profiled drum shell, i.e.

$$\sigma_{x\,в}(x) = \frac{E}{1-\mu^2}\left(\varepsilon_{x_0} + \frac{d^2w}{dx^2}\left(e-\frac{h}{2}\right) - \mu\frac{w}{R}\right);$$

$$\sigma_{x\,н}(x) = \frac{E}{1-\mu^2}\left(\varepsilon_{x_0} + \frac{d^2w}{dx^2}(e+f_z(x)) - \mu\frac{w}{R}\right);$$

$$\sigma_{\varphi в}(x)=\frac{E}{1-\mu^2}\left(-\frac{w}{R}+\mu\left(\varepsilon_{x_0}+\frac{d^2w}{dx^2}\left(e-\frac{h}{2}\right)\right)\right);$$

$$\sigma_{\varphi н}(x)=\frac{E}{1-\mu^2}\left(-\frac{w}{R}+\mu\left(\varepsilon_{x_0}+\frac{d^2w}{dx^2}\left(e+f_z(x)\right)\right)\right).$$

Stress intensity according to Mises criterion

$$\sigma=\frac{1}{\sqrt{2}}\sqrt{\left(\sigma_x-\sigma_\varphi\right)^2+\sigma_\varphi{}^2+\sigma_x{}^2}. \qquad (2.30)$$

By substituting the expressions describing longitudinal and circumferential stresses and strains in the shell into equation (2.25), the following conclusions can be drawn:

$$\delta U_k=R\int_0^{l_k}\int_0^{2\pi}\int_{-f_z(x)}^{\frac{h}{2}+h_k}\left[\sigma_x\cdot\delta\left(\varepsilon_{x_0}+(e-z)\frac{d^2w}{dx^2}\right)+\sigma_\varphi\left(-\frac{\delta w}{R}\right)\right]dx\,d\varphi\,dz=$$

$$=2\pi\cdot R\int_0^{l_k}\left(\delta\left(\varepsilon_{x_0}\right)\int_{-f_z(x)}^{\frac{h}{2}+h_k}\sigma_x dz+\delta\left(\frac{d^2w}{dx^2}\right)\int_{-f_z(x)}^{\frac{h}{2}+h_k}\sigma_x e\,dz+\delta\left(-\frac{d^2w}{dx^2}\right)\int_{-f_z(x)}^{\frac{h}{2}+h_k}\sigma_x z\,dz+\left(-\frac{\delta w}{R}\right)\int_{-f_z(x)}^{\frac{h}{2}+h_k}\sigma_\varphi dz\right)dx.$$

Further we introduce the following notations of internal force factors:

$$N_x=\int_{-f_z(x)}^{\frac{h}{2}+h_k}\sigma_x dz\,;N_\varphi=\int_{-f_z(x)}^{\frac{h}{2}+h_k}\sigma_\varphi dz\;;M_x=\int_{-f_z(x)}^{\frac{h}{2}+h_k}\sigma_x\cdot z dz \qquad (2.31)$$

Taking into account equations (2.25) and (2.29), the expression for determining the variation of the potential energy will have this meaning:

$$\delta U_k=2\pi\cdot R\int_0^{l_k}\left(N_x\cdot\delta\varepsilon_{x0}-N_x\cdot e\cdot\delta\kappa+M_x\cdot\delta\kappa+N_\varphi\cdot\delta\varepsilon_\varphi\right)dx\,.$$

Let us formulate an equation similar to Hooke's law to calculate the force factors inside the shell, i.e.

$$M_x = \int\limits_{-f_z(x)}^{\frac{h}{2}+h_k} \frac{E}{1-\mu^2}\left(\varepsilon_{x0} + (e-z)\frac{d^2w}{dx^2} - \mu\frac{w}{R}\right)z dz\,; \tag{2.32}$$

$$N_\varphi = \int\limits_{-f_z(x)}^{\frac{h}{2}+h_k} \frac{E}{1-\mu^2}\left(-\frac{w}{R} + \mu\left(\varepsilon_{x0} + \frac{d^2w}{dx^2}(e-z)\right)\right)dz\,; \tag{2.33}$$

$$N_x = \int\limits_{-f_z(x)}^{\frac{h}{2}+h_k} \frac{E}{1-\mu^2}\left(\varepsilon_{x_0} + (e-z)\frac{d^2w}{dx^2} - \mu\frac{w}{R}\right)dz\,. \tag{2.34}$$

It was also observed that two opposite situations are possible depending on the bending stiffness values of the lobes:

1) the lobes have high bending stiffness and prevent the shell from deforming in the axial direction ( ); $\varepsilon_{x0} = 0$

2) the stiffness of the lobes allows the shell to deform freely in the axial direction ( ). $N_x = 0$

Since the bending stiffness of hoist drum lobes is much lower than the axial stiffness of the shell, the second limiting situation is more likely.

As a result, after transforming the integral (2.34)

$$N_x = \frac{E}{(1-\mu^2)}\left(\left(\varepsilon_{x_0} + e\frac{d^2w}{dx^2} - \mu\frac{w}{R}\right)\left(\frac{h}{2} + h_k + f_z(x)\right) + \frac{1}{2}\frac{d^2w}{dx^2}\left(f_z{}^2(x) - \frac{h^2}{4}\right)\right),$$

therefore

$$\varepsilon_{x_0} = -\frac{\frac{1}{2}\frac{d^2w}{dx^2}\left(f_z{}^2(x) - \frac{h^2}{4}\right)}{\left(\frac{h}{2} + f_z(x)\right)} - e\frac{d^2w}{dx^2} + \mu\frac{w}{R} = -\frac{1}{2}\frac{d^2w}{dx^2}\left(f_z(x) - \frac{h}{2} + 2e\right) + \mu\frac{w}{R}\,. \tag{2.35}$$

Substituting the obtained equation (2.35) into the expressions for determining the bending moment (2.32) and circumferential force (2.33) arising in the drum shell, we obtain such values of the mentioned parameters:

$$M_x = \int\limits_{-f_z(x)}^{+0,5h} \frac{E}{1-\mu^2}\left(-\frac{1}{2}\frac{d^2w}{dx^2}\left(f_z(x)-\frac{h}{2}+2e\right)+\mu\frac{w}{R}+(e-z)\frac{d^2w}{dx^2}-\mu\frac{w}{R}\right)zdz =$$

$$= \int\limits_{-f_z(x)}^{+0,5h} \frac{E}{1-\mu^2}\cdot\frac{d^2w}{dx^2}\left(\frac{h}{4}-\frac{f_z(x)}{2}-z\right)zdz = \frac{E}{1-\mu^2}\cdot\frac{d^2w}{dx^2}\left(\frac{h}{8}z^2-\frac{f_z(x)}{4}z^2-\frac{z^3}{3}\right)\Bigg|_{-f_z(x)}^{0,5h} =$$

$$= -\frac{E}{1-\mu^2}\cdot\frac{d^2w}{dx^2}\left(\frac{h^3}{96}+\frac{f_z(x)h^2}{16}+\frac{{f_z}^2(x)h}{8}+\frac{{f_z}^3(x)}{12}\right);$$

$$N_\varphi = \int\limits_{-f_z(x)}^{+0,5h} \frac{E}{1-\mu^2}\cdot\left(-\frac{w}{R}+\mu\left(-\frac{1}{2}\frac{d^2w}{dx^2}\left(f_z(x)-\frac{h}{2}+2e\right)+\mu\frac{w}{R}+\frac{d^2w}{dx^2}(e-z)\right)\right)dz =$$

$$= \int\limits_{-f_z(x)}^{+0,5h} \frac{E}{1-\mu^2}\cdot\left(-\frac{w}{R}+\mu\left(\frac{d^2w}{dx^2}\left(\frac{h}{4}-\frac{f_z(x)}{2}-z\right)+\mu\frac{w}{R}\right)\right)dz =$$

$$= \frac{E}{1-\mu^2}\cdot\left(-\frac{w}{R}z+\mu\left(\frac{d^2w}{dx^2}\left(\frac{h}{4}z-\frac{f_z(x)}{2}z-\frac{1}{2}z^2\right)+\mu\frac{w}{R}z\right)\right)\Bigg|_{-f_z(x)}^{0,5h} = -\frac{Ew}{R}\cdot\left(\frac{h}{2}+f_z(x)\right);$$

$$N_\varphi = -\frac{Ew}{R}\cdot\left(\frac{h}{2}+f_z(x)\right).$$

The absence of the parameter *e* in the expressions obtained by transformation indicates that there is no need to take into account the displacement of its neutral line in calculations of the axisymmetric deformation of the profiled shell.

Thus, the equations describing the internal force factors in the drum shell take the following form:

$$M_x(x) = D(x)\cdot\kappa(x) = -D(x)\frac{d^2w(x)}{dx^2}; \qquad (2.36)$$

$$N_\varphi(x) = B(x)\cdot\varepsilon_\varphi(x) = -B(x)\frac{w(x)}{R}, \qquad (2.37)$$

where $D(x)$ and $B(x)$ are the bending and ring stiffness functions of the profiled shell, each of which has the following form:

$$D(x) = \frac{E}{1-\mu^2}\cdot\left(\frac{h^3}{96}+\frac{f_z(x)\cdot h^2}{16}+\frac{{f_z}^2(x)\cdot h}{8}+\frac{{f_z}^3(x)}{12}\right); \qquad (2.38)$$

$$B(x) = E \cdot \left(\frac{h}{2} + f_z(x) \right). \tag{2.39}$$

Using the obtained expressions (2.35), (2.38), (2.39), we conclude that equation (2.28), describing the axial stress in the shell, and (2.29) - for the determination of the radial one, take the following form, respectively:

$$\sigma_x(x,z) = \frac{E}{1-\mu^2}\left(\varepsilon_x + \mu \cdot \varepsilon_\varphi\right) = \frac{E}{1-\mu^2}\left(\varepsilon_{x_0} + (e-z)\frac{d^2w}{dx^2} - \mu\frac{w}{R} \right)$$

$$\text{or}\,\sigma_x(x,z) = \frac{E}{1-\mu^2} \cdot \frac{M_x}{D(x)} \cdot \left(\frac{f_z(x)}{2} - \frac{h}{4} + z \right) \tag{2.40}$$

$$\sigma_\varphi(x,z) = \frac{E}{1-\mu^2} \cdot \left(\frac{N_\varphi}{B} \cdot \left(1-\mu^2\right) + \mu \cdot \left(\frac{M_x}{D(x)} \cdot \left(\frac{f_z(x)}{2} - \frac{h}{4} + z \right) \right) \right);$$

$$\text{or}\,\sigma_\varphi(x,z) = \frac{E \cdot N_\varphi}{B} + \mu \cdot \sigma_x(x,z) \tag{2.41}$$

Taking into account the results of transformations obtained by us, we write down the equations for determining the stresses occurring on the inner and outer surfaces of the profiled drum shell, namely:

$$\sigma_{x\,i}(x) = -\frac{E}{1-\mu^2} \cdot \frac{d^2w}{dx^2} \cdot D(x) \cdot \left(\frac{f_z(x)}{2} + \frac{h}{4} \right);$$

$$\sigma_{x\,o}(x) = \frac{E}{1-\mu^2} \cdot \frac{d^2w}{dx^2} \cdot D(x) \cdot \left(\frac{f_z(x)}{2} + \frac{h}{4} \right);$$

$$\sigma_{\varphi\,i}(x) = -\frac{w}{R} - D(x) \cdot \mu \cdot \frac{E}{1-\mu^2} \cdot \frac{d^2w}{dx^2} \cdot \left(\frac{f_z(x)}{2} + \frac{h}{4} \right);$$

$$\sigma_{\varphi\,o}(x) = -\frac{w}{R} + D(x) \cdot \mu \frac{E}{1-\mu^2} \cdot \frac{d^2w}{dx^2} \cdot \left(\frac{f_z(x)}{2} + \frac{h}{4} \right).$$

According to the principle of possible displacements of the drum shell, the sum of the values of the work of external and internal forces resulting from any kinematically probable displacements of the points of the shell as an elastic system

is equal to zero, i.e.

$$\delta U - \delta A = 0. \qquad (2.42)$$

In this regard, the work of external forces causing the displacements of the shell,

$$\delta A = \int_0^{2\pi}\int_0^{l} q \cdot \delta w \cdot d\varphi \cdot dx = 2 \cdot \pi \cdot R \int_0^{l} q \cdot \delta w \cdot dx.$$

Substituting the corresponding expressions into equation (2.42), let us integrate by parts the equation for determining the variation of internal potential energy, viz:

$$\begin{aligned}
\delta U &= 2\pi \cdot R \int_0^{l} \left(-M_x \cdot \delta \frac{d^2 w}{dx^2} - N_\varphi \frac{\delta w}{R} \right) dx = \\
&= 2\pi \cdot R \cdot \left(-M_x \cdot \delta \left(\frac{dw}{dx} \right) \Big|_0^{l} + \int_0^{l} \left(\frac{dM_x}{dx} \cdot \delta \left(\frac{dw}{dx} \right) \right) dx - \int_0^{l} N_\varphi \cdot \frac{\delta w}{R} dx \right) = \\
&= 2 \cdot \pi \cdot R \cdot \left(-M_x \cdot \delta \left(\frac{dw}{dx} \right) \Big|_0^{l} + \frac{dM_x}{dx} \delta w \Big|_0^{l} - \int_0^{l} \left(\frac{d^2 M_x}{dx^2} \cdot \delta w \right) dx - \int_0^{l} N_\varphi \frac{\delta w}{R} dx \right).
\end{aligned}$$

Now equation (2.40) takes this form:

$$-M_x \cdot \delta \left(\frac{dw}{dx} \right) \Big|_0^{l} + \frac{dM_x}{dx} \cdot \delta w \Big|_0^{l} - \int_0^{l} \left(\frac{d^2 M_x}{dx^2} + \frac{N_\varphi}{R} + q \right) \delta w \cdot dx = 0 .$$

We conclude that since the variation values of δw are arbitrary and the sum of the non-integral terms of the equation is zero, taking into account the boundary conditions, the integrand is also zero. Thus, given the following conditions: $\delta w = 0$ and $\delta(dw/dx) \neq 0$, at the points $x = 0$ and $x = l$, we consider it to be true that

$$M_x = 0; \frac{dM_x}{dx} \neq 0 \ .$$

Now the equation for determining the equilibrium of the shell will take the following form:

$$\frac{d^2 M_x}{dx^2} + \frac{N_\varphi}{R} + q = 0 .$$

Substituting expressions (2.36) and (2.37) into the previous formula, we obtain the equation describing the equilibrium of the section of the profiled axisymmetric drum shell, i.e.

$$\frac{d^2}{dx^2}\left(D(x)\frac{d^2w}{dx^2}\right)+\frac{B(x)\cdot w}{R^2}=q. \tag{2.43}$$

In contrast to the application of the method of two scales to the transformation of second-order equations described in this paper, the authors of the present monograph used the method for a fourth-order equation, while performing averaging of the coefficients.

Since the drum shell groove is cut with a constant pitch *t*, the periodicity of the functions *D*(*x*) and *B*(*x*) corresponds to the value *t*. To calculate the characteristics of the shell with length *l* and with a large number of grooves, where *l* >> *t*, *we* can additionally use the parameter $\nu = t/l$, and, in addition to the variable *x*, apply the following: $\xi = x/\nu$.

We will look for the value of *w* in the form of a polynomial, i.e.

$$w(x)=\sum_{i=0}^{M}\nu^{\,i}\cdot w_i(x,\xi),$$

где *M* - order of the polynomial.

Using the method of two scales, the equilibrium equation (2.43) can be written as follows:

$$D_{\text{o}}\frac{d^4w}{dx^4}+\frac{B_{\text{o}}}{R^2}w=q, \tag{2.44}$$

where are averaged values of bending D_{o} and ring B_{o} stiffnesses

$$D_{\text{o}}=\tau\cdot\left(\int_0^{\tau}\left(D(x)\right)^{-1}dx\right)^{-1}; \tag{2.45}$$

$$B_o = \frac{1}{\tau} \cdot \int_0^{\tau} B(x)\,dx\,. \qquad (2.46)$$

Here, half of the pitch of the threading $\tau = t/2$.

Substituting the values of functions (2.38) and (2.39) into the integrals, we obtain analytical equations for determining the averaged values of the annular and bending stiffness of the profiled drum shell, namely:

$$D_a = \frac{E \cdot \tau}{(1-\mu^2)} \left(\int_0^{\tau} \left(\frac{h^3}{96} + \frac{f_z(x) \cdot h^2}{16} + \frac{f_z{}^2(x) \cdot h}{8} + \frac{f_z{}^3(x)}{12} \right)^{-1} dx \right)^{-1}; \qquad (2.47)$$

$$B_a = \int_0^{\tau} \frac{E}{\tau} \left(\frac{h}{2} + f_z(x) \right) dx\,. \qquad (2.48)$$

Unlike the equations describing the equilibrium of a shell made of isotropic material, where the parameters *D* and *B are* related, the characteristic of a profiled shell does not contain such a relationship. This allows us to consider the latter as structurally orthotropic, and its elastic moduli are determined from the following expressions, respectively:

- axially

$$E_1 = \left(12D \cdot (1-\mu^2)\right) \Big/ \left(h^3 + \frac{12D}{E_2} \right). \qquad (2.49)$$

- county direction

$$E_2 = B_o / h\,. \qquad (2.50)$$

After applying these values, the equation for calculating the equilibrium of the profiled shell can be written as a formula describing the same parameter of the structural-orthotropic shell, i.e.

$$\frac{E_1 \cdot h^3}{12(1-\mu_1 \cdot \mu_2)} \frac{d^4 w}{dx^4} + \frac{E_2 \cdot h}{R^2} w = q\,,$$

here Poisson's coefficients defined in the circumferential and axial directions, $\mu_1 = \mu, \mu_2 = \mu \cdot E_1/E_2$ respectively.

The axial stresses that occur in the upper and lower layers of the structural-orthotropic shell at the sections corresponding to the i-th coordinate line can be calculated in this way:

$$\sigma_{xi} = -\frac{E_1 \cdot h \cdot \kappa}{2\left(1-\mu^2\right)}; \sigma_{xo} = \frac{E_2 \cdot h \cdot \kappa}{2\left(1-\mu^2\right)}\ ; \tag{2.51}$$

and the circumferential stresses developing there acquire such values:

$$\sigma_{\varphi i} = -\frac{E_2 \cdot w}{R} - \frac{E_1 \cdot h \cdot \mu \cdot \kappa}{2\left(1-\mu^2\right)}; \sigma_{\varphi o} = \frac{E_2 \cdot w}{R} + \frac{E_1 \cdot h \cdot \mu \cdot \kappa}{2\left(1-\mu^2\right)}. \tag{2.52}$$

Applying a semi-empirical approach to our formulations, we refine the value of the flexural stiffness of the shell by introducing a reduction factor k_p , determined during the computational experiment, and then replace the variables in equations (2.49) and (2.50) D_o by D and B_o by B, provided that $D = k_p D_o$, and $B = B_o$.

To determine the bending stiffness of the finite element model of the drum, let us consider the pure bending of a profiled shell. Based on the theory of thin shell bending, we assume that the Timoshenko-Reissner direct normal hypothesis is valid in our case.

To verify this assumption, let's build a computational model of the profiled shell using SolidWorks Simulation, limiting ourselves to 10 slicing steps (see Fig. 2.11). In order to exclude the non-uniformity of SSS distribution near the right edge of the shell in the zone of bending moment application, we provide as a kinematic boundary condition of symmetry on its three lateral edges. For calculations we choose the section of the profile passing through its leftmost scallop as a control section.

It follows from the calculation results (Fig. 2.11) that the deformed bottom edge of the shell is a circular cylindrical surface, and the normals that pass under the scallop and under the bottom of the groove remain straight.

In order to simplify the calculation model and reduce the calculation time, we will further investigate the so-called half-rope, i.e. a section of the shell whose length is equal to half of the slicing pitch *t*.

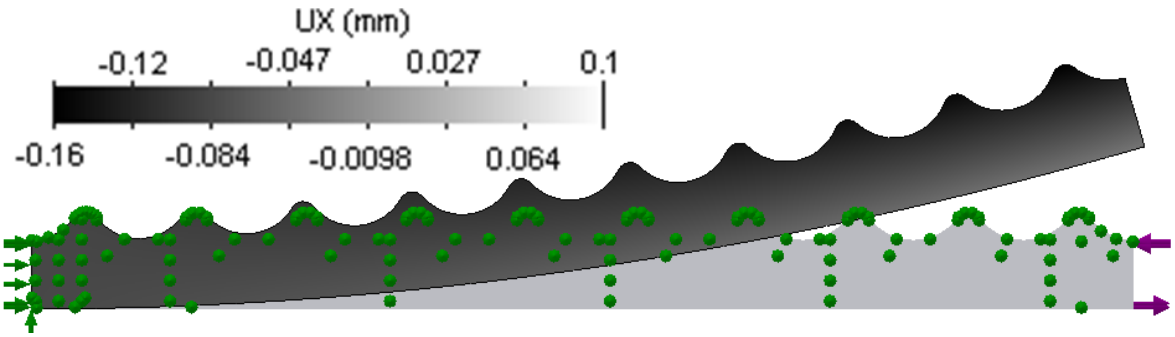

Fig. 2.11. Schematic of the profiled shell
and results of calculation of its parameters

In order to verify to what extent the semi-groove we have selected corresponds to the model (see Fig. 2.11), let us consider two design cases of bending moment application: in the first case the right edge remains flat (Fig. 2.12, *a)*, in the second case it may deform (Fig. 2.12, *b*).

As the graphs in Fig. 2.13 show, the displacements of the right edge of the "half-channel" and the profiled shell in the left section near the embedment, in the case of application of a distributed moment, its deformation does not correspond to the hypothesis of straight normals, and when the moment is applied "rigid bond", the mentioned deformation almost completely coincides with the deformation of the profiled shell.

Comparison of the results presented in Fig. 2.13 allows us to draw the following conclusions:

1. The applicability of the Timoshenko-Reissner hypothesis of direct normals in the bending of a profiled shell of a MHM drum can be considered quite reasonable.

2. The effect of the "rigid link" moment must be taken into account in the design model of the "half-channel".

To determine the required in our calculations reduction factor k_p we will

conduct a two-factor computational experiment on the initial data, which are summarised in Table 2.1. They reflect the parameters of 5 and 6 m diameter drums. The experiment was carried out using SolidWorks Simulation software.

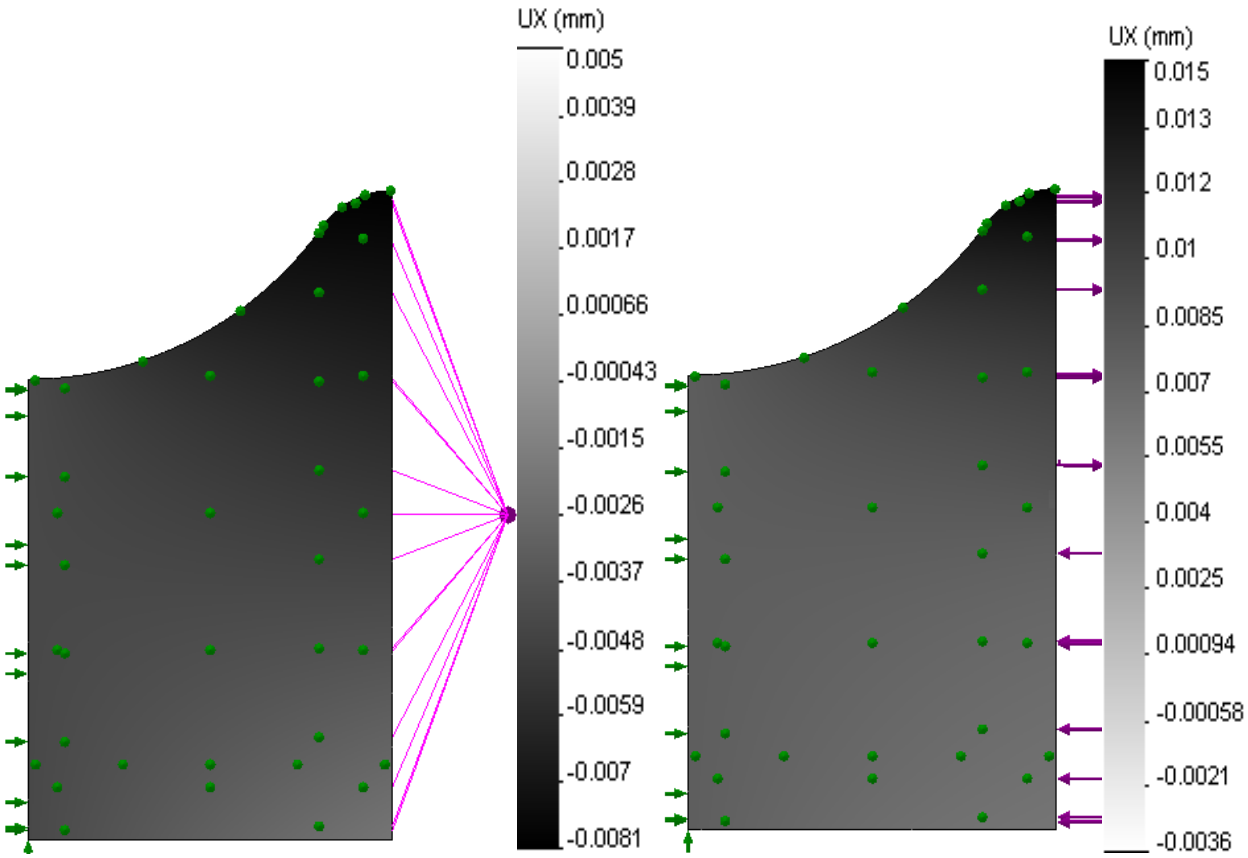

a *b*

Fig. 2.12. Schemes of SSS displacement fields in the "half-rope" and results of calculation of boundary conditions under the influence: *a* - rigid-bond moment; *b* - distributed bending moment

The investigated section of the profiled drum shell is modelled as a flat bending of a plate of the corresponding profile, its thickness b = 3 mm. The diagram of the section is given in Fig. 2.14.

For the calculation we define the following boundary conditions: the front and left faces of the shell are symmetrical; the right face is not bent, but only rotates as a rigid whole under the influence of the applied concentrated moment M, the lower left face of the "half-channel" is fixed.

Fig. 2.15 shows the axial displacement field of a plate with the following parameters: t = 62 mm, h = 55 mm, h_f = 16 mm.

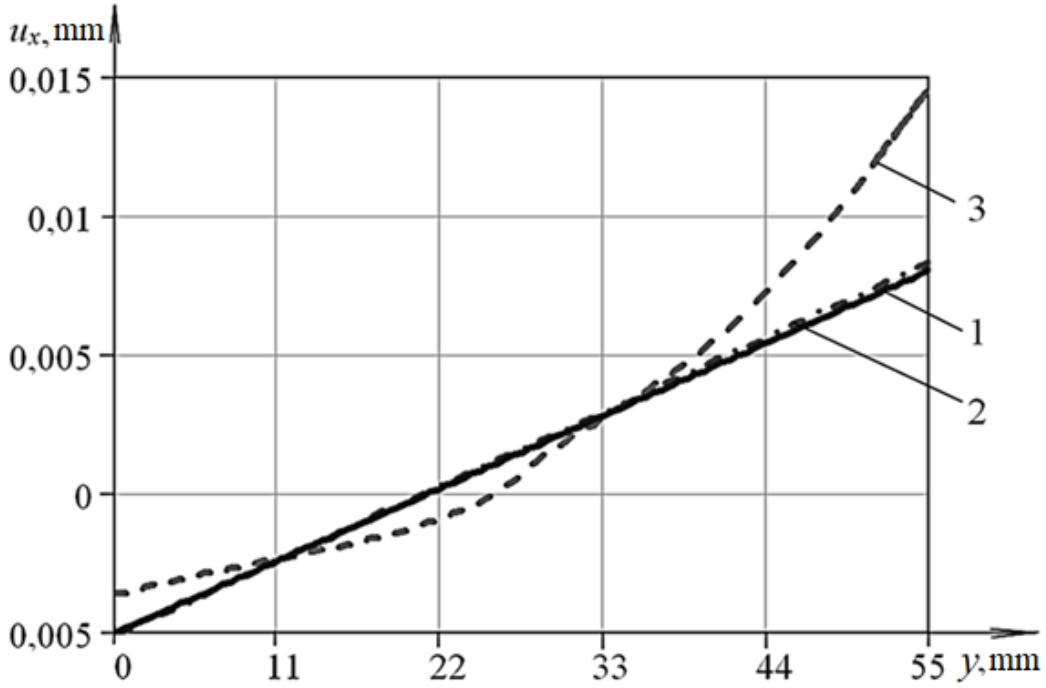

Fig. 2.13. Displacement plots of the right profile of the drum shell:

1 - in the place of the control section of the long shell;

2 - in the "half-canvas" under the influence of the moment "rigid connection";

3 - in the same place in case of distributed moment application

Table 2.1.

MHM drum shell parameters, mm

d_d	d_r	h_f	t
5000	29	9	32
5000	34,5	10	36
5000	36,5	11	40
5000	39,5	12	45
5000	44,5	13,5	50
5000	53,5	15	56
5000	56	16	63
5000	63	18	71
6000	31	10	34

d_d	d_r	h_f	t
6000	34,5	11	37
6000	36,5	12	40
6000	39,5	13	44
6000	43	14	48
6000	46,5	15	52
6000	50,5	16	56
6000	56	16	62
6000	63	16	68

To determine the angle of rotation of the edge ψ, let us measure the distances of displacements of its extreme points v_1 and v_2 in the direction of the horizontal

axis x in this way:

$$\psi = \frac{v_1 + v_2}{h}. \tag{2.53}$$

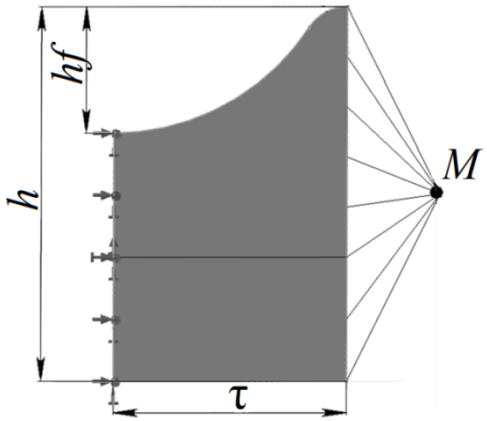

Fig. 2.14. Scheme for conducting a computational experiment to determine the value of k_p

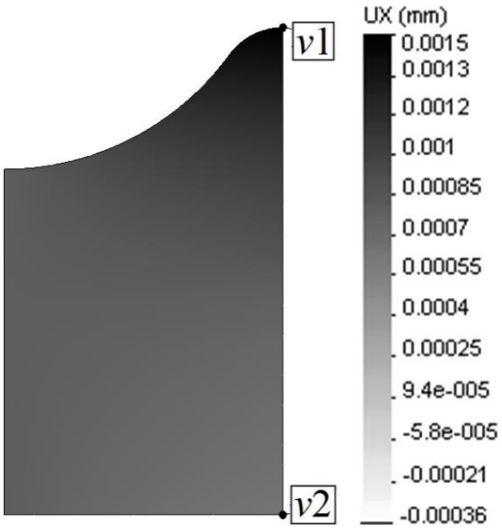

Fig. 2.15. Diagram of axial displacements, occurring in the profiled shell

Then we calculate the turning curvature κ and the bending stiffness D_b using the following formulae:

$$\kappa = \psi / \tau; \tag{2.54}$$

$$D_b = M / \kappa. \tag{2.55}$$

Accordingly, the expression for calculating the reduction factor will take the following form:

$$k_{\text{p}} = D_b / D_{\text{o}} . \qquad (2.56)$$

The computational experiment to determine this value was carried out using the "Design Research" programme module built into SolidWorks. The geometrical parameters of the profile h, h_f and τ acted as variables in calculations, in particular their discrete values were set. For each combination of parameters during the experiment the programme found the distances by which the points were moved and made the corresponding reports, the data from which were then processed using formulas (2.51) - (2.54) to find the desired value ι_b. The results of the calculations are presented in Tables 2.2 and 2.3.

Table 2.2.

Values of coefficient k_{p} taking into account geometrical parameters profile of the shell profile of a 5 m diameter MHM drum

h, mm	d_r, mm							
	29	34,5	36,5	39,5	44,5	53,5	56	63
55	0,892	0,890	0,888	0,887	0,885	0,883	0,881	0,880
50	0,865	0,864	0,862	0,860	0,858	0,857	0,855	0,853
45	0,839	0,838	0,836	0,834	0,833	0,831	0,829	0,828
40	0,822	0,820	0,818	0,817	0,815	0,813	0,812	0,810

To use the method of planning a computational experiment, we introduce such dimensionless geometric parameters: $\eta = h_f / h$; $\theta = t/h$.

Let us call as design points (in the graph of Fig. 2.16, *a of the* dependences of the parameters η and θ), the values of which correspond to the data of Tables 2.2, 2.3. In the same figure, the function $\theta_o(\eta) = 2\eta$, its graph (lower line) limits the area of permissible values of the mentioned quantities.

For optimal planning of the experiment, we rotate the coordinate system (rotation angle $\gamma = 1.31$ rad). We choose the angle value so that the new axis θ' passes between the calculated points.

Therefore, when the axes are rotated by the angle *γ, the* coordinates change as follows:

$$\eta = \eta' \cdot \cos\gamma - \theta' \cdot \sin\gamma;\ \ \theta = \eta' \cdot \sin\gamma + \theta' \cdot \cos\gamma;\ \ \eta' = \eta \cdot \cos\gamma + \theta \cdot \sin\gamma;\ \ \theta' = -\eta \cdot \sin\gamma + \theta \cdot \cos\gamma.$$

Let us set the levels and intervals of variation of the values of the parameters η′ and θ′, summarise them in Table 2.4, and place the points obtained as a result of the computational experiment in Fig. 2.16, *a*.

Table 2.3.

Values of the coefficient k_p taking into account geometrical parameters profile of the shell profile of a 6 m diameter MHM drum

h, mm	d_r, mm								
	31	34,5	36,5	39,5	43	46,5	50,5	56	63
55	0,890	0,889	0,887	0,886	0,885	0,883	0,882	0,881	0,879
50	0,863	0,862	0,861	0,859	0,858	0,857	0,856	0,854	0,853
45	0,837	0,836	0,835	0,834	0,832	0,831	0,830	0,829	0,827
40	0,821	0,819	0,818	0,817	0,816	0,815	0,813	0,812	0,811

Table 2.4.

Output data for the computational experiment on determination of the parameters of the MHM drum

Name and designation of factors	Levels of variation of values					intervals variation intervals
	-1	-0,5	0	0,5	1	
Present value of the scallop height η'	0,3	0,725	1,15	1,602	2	0,425
Present value of the thread pitch θ'	-0,04	-0,015	0,01	0,035	0,06	0,025

For convenience of calculations in the experiment we took into account that the thickness of the sheet *h* = 50 mm. The obtained experimental results are presented in Table 2.5.

To simplify the calculations, instead of the parameters η and θ, we introduce the dimensionless value ε, which reflects the relative depth of the groove, and the

parameter ζ, which characterises its shape. Their values are determined from the following expressions:

$$\varepsilon = h_f / h_m ; \zeta = t / h_f \qquad (2.57)$$

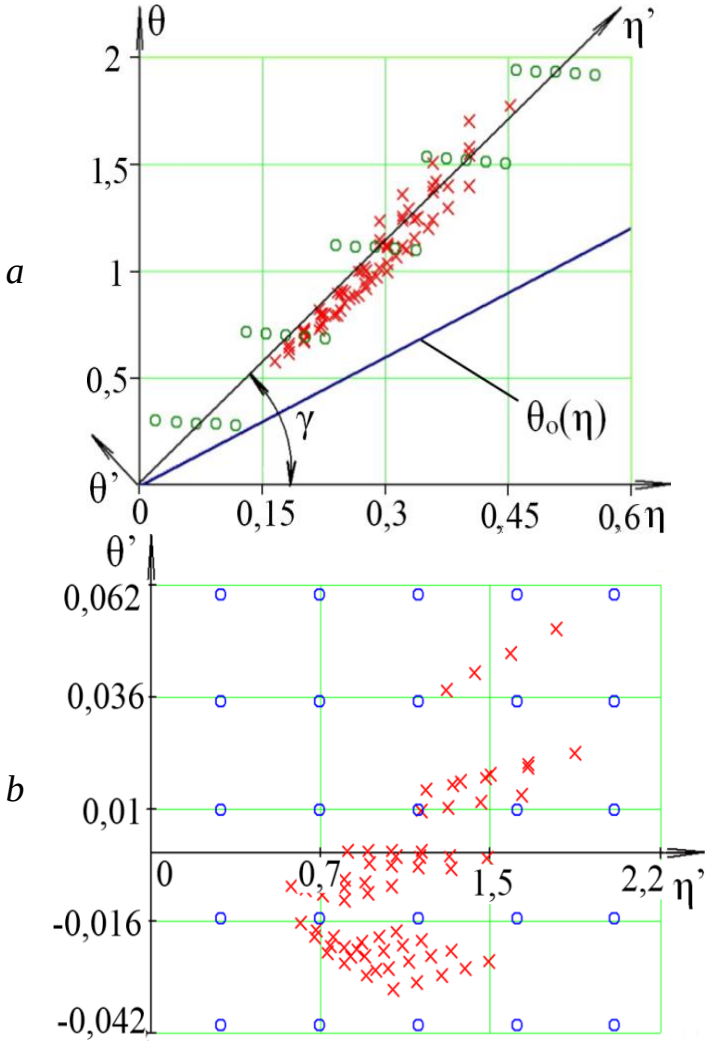

Fig. 2.16. Graphical interpretation of planning computational experiment:

a - in the initial coordinate system; *b* - in the rotated coordinate system;

× - values of parameters from Tables 2.2, 2.3

○ - placement of points for experimentation

Having established the relationship between the new and previous parameters, we obtain the following equations: $\varepsilon = \eta/(1-\eta)$; $\xi = \theta/\eta$.

To process the obtained results, we will use the method of regression analysis

[3]. Let us assume that the approximating polynomial of degree 3 for the function k_p (ε, ζ) will have the following form:

$$k_{\text{p}}(\varepsilon,\zeta) = z_1 + z_2\cdot\varepsilon + z_3\cdot\zeta + z_4\cdot\varepsilon^2 + z_5\cdot\varepsilon\cdot\zeta + z_6\cdot\zeta^2 + z_7\cdot\varepsilon^3 + z_8\cdot\varepsilon^2\cdot\zeta + z_9\cdot\varepsilon\cdot\zeta^2 + z_{10}\cdot\zeta^3,$$

here $\{z\}^T = \{z_1\ z_2\ z_3\ z_4\ z_5\ z_6\ z_7\ z_8\ z_9\ z_{10}\}$, is a vector of unknown parameters determined by the least squares method, according to which the sum of squares of deviations of the polynomial k_{p} (ε, ζ) from the calculated values of $k_{\text{p}i}$, i.e., is minimised.

$$\Delta = \sum_{i=1}^{N}\left(k_{\text{p}}(\varepsilon_i,\zeta_i) - k_{\text{p}i}\right)^2,$$

where N is the number of columns in Table 2.5.

Table 2.5.

Values of parameters of the drum shell parameters of MHM drum, obtained as a result of computational experiment

k_{p}	η	θ	h_f	τ
1	***2***	***3***	***4***	***5***
0,810	0,11600	0,27954	5,80000	6,98850
0,813	0,09185	0,28599	4,59250	7,14975
0,817	0,06769	0,29243	3,38450	7,31075
0,820	0,04354	0,29888	2,1770	7,47200
0,823	0,01938	0,30533	0,96900	7,63325
0,827	0,22559	0,69017	11,2795	17,25425
0,830	0,20143	0,69662	10,0715	17,4155
0,833	0,17728	0,70306	8,86400	17,5765
0,837	0,15312	0,70951	7,65600	17,73775
0,840	0,12897	0,71596	6,44850	17,8990
0,843	0,33517	1,10080	16,7585	27,52000
0,847	0,31102	1,10724	15,5510	27,68100
0,850	0,28687	1,11369	14,3435	27,84225
0,854	0,26271	1,12014	13,1355	28,00350
0,857	0,23856	1,12658	11,9280	28,16450
0,860	0,44476	1,51143	22,2380	37,78575

Continuation of Table 2.5

1	*2*	*3*	*4*	*5*
0,864	0,42061	1,51787	21,0305	37,94675
0,867	0,39645	1,52432	19,8225	38,10800
0,871	0,37230	1,53077	18,6150	38,26925
0,874	0,34814	1,53721	17,4070	38,43025
0,878	0,55435	1,92206	27,7175	48,0515
0,881	0,53019	1,92850	26,5095	48,2125
0,885	0,50604	1,93495	25,3020	48,37375
0,888	0,48188	1,94139	24,0940	48,53475
0,892	0,45773	1,94784	22,8865	48,6960

Equating to zero the partial derivatives of the function Δ, we obtain a system of equations for determining the vector {z}, namely:

$$\begin{cases} \frac{\partial}{\partial z_1}\Delta = 2\sum_{i=1}^{N}\left(k_p(\varepsilon_i,\zeta_i)-k_{pi}\right)=0; \\ \frac{\partial}{\partial z_2}\Delta = 2\sum_{i=1}^{N}\left(k_p(\varepsilon_i,\zeta_i)-k_{pi}\right)\cdot\varepsilon_i=0; \\ \frac{\partial}{\partial z_3}\Delta = 2\sum_{i=1}^{N}\left(k_p(\varepsilon_i,\zeta_i)-k_{pi}\right)\cdot\zeta_i=0; \\ \frac{\partial}{\partial z_4}\Delta = 2\sum_{i=1}^{N}\left(k_p(\varepsilon_i,\zeta_i)-k_{pi}\right)\cdot\varepsilon_i^2=0; \\ \frac{\partial}{\partial z_5}\Delta = 2\sum_{i=1}^{N}\left(k_p(\varepsilon_i,\zeta_i)-k_{pi}\right)\cdot\varepsilon_i\cdot\zeta_i=0; \\ \frac{\partial}{\partial z_6}\Delta = 2\sum_{i=1}^{N}\left(k_p(\varepsilon_i,\zeta_i)-k_{pi}\right)\cdot\zeta_i^2=0; \\ \frac{\partial}{\partial z_7}\Delta = 2\sum_{i=1}^{N}\left(k_p(\varepsilon_i,\zeta_i)-k_{pi}\right)\cdot\varepsilon_i^3=0; \\ \frac{\partial}{\partial z_8}\Delta = 2\sum_{i=1}^{N}\left(k_p(\varepsilon_i,\zeta_i)-k_{pi}\right)\cdot\varepsilon_i{}^2\cdot\zeta_i=0; \\ \frac{\partial}{\partial z_9}\Delta = 2\sum_{i=1}^{N}\left(k_p(\varepsilon_i,\zeta_i)-k_{pi}\right)\cdot\varepsilon_i\cdot\zeta_i{}^2=0; \\ \frac{\partial}{\partial z_{10}}\Delta = 2\sum_{i=1}^{N}\left(k_p(\varepsilon_i,\zeta_i)-k_{pi}\right)\cdot\zeta_i^3=0, \end{cases}$$

which we transform to the standard form, i.e. $\left[K\right]\cdot\left\{z\right\}=\left\{G\right\}$.

Now let us write down the equations for calculating the components of the system in this form:

$$[K]=\begin{vmatrix} N & \sum_{i=1}^{N}\varepsilon_i & \sum_{i=1}^{N}\xi_i & \sum_{i=1}^{N}\varepsilon_i^2 & \sum_{i=1}^{N}\varepsilon_i\cdot\xi_i & \sum_{i=1}^{N}\xi_i^2 & \sum_{i=1}^{N}\varepsilon_i^3 & \sum_{i=1}^{N}\varepsilon_i^2\cdot\xi_i & \sum_{i=1}^{N}\varepsilon_i\cdot\xi_i^2 & \sum_{i=1}^{N}\xi_i^3 \\ \sum_{i=1}^{N}\varepsilon_i & \sum_{i=1}^{N}\varepsilon_i^2 & \sum_{i=1}^{N}\varepsilon_i\cdot\xi_i & \sum_{i=1}^{N}\varepsilon_i^3 & \sum_{i=1}^{N}\varepsilon_i^2\cdot\xi_i & \sum_{i=1}^{N}\varepsilon_i\cdot\xi_i^2 & \sum_{i=1}^{N}\varepsilon_i^4 & \sum_{i=1}^{N}\varepsilon_i^3\cdot\xi_i & \sum_{i=1}^{N}\varepsilon_i^2\cdot\xi_i^2 & \sum_{i=1}^{N}\varepsilon_i\cdot\xi_i^3 \\ \sum_{i=1}^{N}\xi_i & \sum_{i=1}^{N}\varepsilon_i\cdot\xi_i & \sum_{i=1}^{N}\xi_i^2 & \sum_{i=1}^{N}\varepsilon_i^2\cdot\xi_i & \sum_{i=1}^{N}\varepsilon_i\cdot\xi_i^2 & \sum_{i=1}^{N}\xi_i^3 & \sum_{i=1}^{N}\varepsilon_i^3\cdot\xi_i & \sum_{i=1}^{N}\varepsilon_i^2\cdot\xi_i^2 & \sum_{i=1}^{N}\varepsilon_i\cdot\xi_i^3 & \sum_{i=1}^{N}\xi_i^4 \\ \sum_{i=1}^{N}\varepsilon_i^2 & \sum_{i=1}^{N}\varepsilon_i^3 & \sum_{i=1}^{N}\varepsilon_i^2\cdot\xi_i & \sum_{i=1}^{N}\varepsilon_i^4 & \sum_{i=1}^{N}\varepsilon_i^3\cdot\xi_i & \sum_{i=1}^{N}\varepsilon_i^2\cdot\xi_i^2 & \sum_{i=1}^{N}\varepsilon_i^5 & \sum_{i=1}^{N}\varepsilon_i^4\cdot\xi_i & \sum_{i=1}^{N}\varepsilon_i^3\cdot\xi_i^2 & \sum_{i=1}^{N}\varepsilon_i^2\cdot\xi_i^3 \\ \sum_{i=1}^{N}\varepsilon_i\cdot\xi_i & \sum_{i=1}^{N}\varepsilon_i^2\cdot\xi_i & \sum_{i=1}^{N}\varepsilon_i\cdot\xi_i^2 & \sum_{i=1}^{N}\varepsilon_i^3\cdot\xi_i & \sum_{i=1}^{N}\varepsilon_i^2\cdot\xi_i^2 & \sum_{i=1}^{N}\varepsilon_i\cdot\xi_i^3 & \sum_{i=1}^{N}\varepsilon_i^4\cdot\xi_i & \sum_{i=1}^{N}\varepsilon_i^3\cdot\xi_i^2 & \sum_{i=1}^{N}\varepsilon_i^2\cdot\xi_i^3 & \sum_{i=1}^{N}\varepsilon_i\cdot\xi_i^4 \\ \sum_{i=1}^{N}\xi_i^2 & \sum_{i=1}^{N}\varepsilon_i\cdot\xi_i^2 & \sum_{i=1}^{N}\xi_i^3 & \sum_{i=1}^{N}\varepsilon_i^2\cdot\xi_i^2 & \sum_{i=1}^{N}\varepsilon_i\cdot\xi_i^3 & \sum_{i=1}^{N}\xi_i^4 & \sum_{i=1}^{N}\varepsilon_i^3\cdot\xi_i^2 & \sum_{i=1}^{N}\varepsilon_i^2\cdot\xi_i^3 & \sum_{i=1}^{N}\varepsilon_i\cdot\xi_i^4 & \sum_{i=1}^{N}\xi_i^5 \\ \sum_{i=1}^{N}\varepsilon_i^3 & \sum_{i=1}^{N}\varepsilon_i^4 & \sum_{i=1}^{N}\varepsilon_i^3\cdot\xi_i & \sum_{i=1}^{N}\varepsilon_i^5 & \sum_{i=1}^{N}\varepsilon_i^4\cdot\xi_i & \sum_{i=1}^{N}\varepsilon_i^3\cdot\xi_i^2 & \sum_{i=1}^{N}\varepsilon_i^6 & \sum_{i=1}^{N}\varepsilon_i^5\cdot\xi_i & \sum_{i=1}^{N}\varepsilon_i^4\cdot\xi_i^2 & \sum_{i=1}^{N}\varepsilon_i^3\cdot\xi_i^3 \\ \sum_{i=1}^{N}\varepsilon_i^2\cdot\xi_i & \sum_{i=1}^{N}\varepsilon_i^3\cdot\xi_i & \sum_{i=1}^{N}\varepsilon_i^2\cdot\xi_i^2 & \sum_{i=1}^{N}\varepsilon_i^4\cdot\xi_i & \sum_{i=1}^{N}\varepsilon_i^3\cdot\xi_i^2 & \sum_{i=1}^{N}\varepsilon_i^2\cdot\xi_i^3 & \sum_{i=1}^{N}\varepsilon_i^6\cdot\xi_i^3 & \sum_{i=1}^{N}\varepsilon_i^4\cdot\xi_i^2 & \sum_{i=1}^{N}\varepsilon_i^3\cdot\xi_i^3 & \sum_{i=1}^{N}\varepsilon_i^2\cdot\xi_i^4 \\ \sum_{i=1}^{N}\varepsilon_i\cdot\xi_i^2 & \sum_{i=1}^{N}\varepsilon_i^2\cdot\xi_i^2 & \sum_{i=1}^{N}\varepsilon_i\cdot\xi_i^3 & \sum_{i=1}^{N}\varepsilon_i^3\cdot\xi_i^2 & \sum_{i=1}^{N}\varepsilon_i^2\cdot\xi_i^3 & \sum_{i=1}^{N}\varepsilon_i\cdot\xi_i^4 & \sum_{i=1}^{N}\varepsilon_i^5\cdot\xi_i^2 & \sum_{i=1}^{N}\varepsilon_i^3\cdot\xi_i^3 & \sum_{i=1}^{N}\varepsilon_i^2\cdot\xi_i^4 & \sum_{i=1}^{N}\varepsilon_i\cdot\xi_i^5 \\ \sum_{i=1}^{N}\xi_i^3 & \sum_{i=1}^{N}\varepsilon_i\cdot\xi_i^3 & \sum_{i=1}^{N}\xi_i^4 & \sum_{i=1}^{N}\varepsilon_i^2\cdot\xi_i^3 & \sum_{i=1}^{N}\varepsilon_i\cdot\xi_i^4 & \sum_{i=1}^{N}\xi_i^5 & \sum_{i=1}^{N}\varepsilon_i^3\cdot\xi_i^3 & \sum_{i=1}^{N}\varepsilon_i\cdot\xi_i^5 & \sum_{i=1}^{N}\varepsilon_i\cdot\xi_i^5 & \sum_{i=1}^{N}\xi_i^6 \end{vmatrix}$$

$$\{G\}^T=\left|\sum_{i=1}^{N}\iota_{\text{э}i}\ \sum_{i=1}^{N}\iota_{\text{э}i}\cdot\varepsilon_i\ \sum_{i=1}^{N}\iota_{\text{э}i}\cdot\zeta_i\ \sum_{i=1}^{N}\iota_{\text{э}i}\cdot\varepsilon_i^2\ \sum_{i=1}^{N}\iota_{\text{э}i}\cdot\varepsilon_i\cdot\zeta_i\ \sum_{i=1}^{N}\iota_{\text{э}i}\cdot\zeta_i^2\sum_{i=1}^{N}\iota_{\text{э}i}\cdot\varepsilon_i^3\ \sum_{i=1}^{N}\iota_{\text{э}i}\cdot\varepsilon_i^2\cdot\zeta_i\ \sum_{i=1}^{N}\iota_{\text{э}i}\cdot\varepsilon_i\cdot\zeta_i^2\ \sum_{i=1}^{N}\iota_{\text{э}i}\cdot\zeta_i^3\right|.$$

Using the Gauss elimination method [3], we obtain the regression function for determining the reduced value of the bending stiffness of the drum shell, viz:

$$k_{\text{p}}(\varepsilon,\zeta)=1{,}347\ -0{,}5\cdot\varepsilon-0{,}295\cdot\zeta+0{,}61\cdot\varepsilon^2+0{,}016\cdot\varepsilon\cdot\zeta+0{,}074\cdot\zeta^2- \\ -0{,}195\cdot\varepsilon^3-0{,}021\cdot\varepsilon^2\cdot\zeta+0{,}007\cdot\varepsilon\cdot\zeta^2-0{,}006\cdot\zeta^3. \qquad (2.58)$$

Let us evaluate the error of the obtained regression dependence in terms of the absolute RMS ε_{rms} and maximum relative β deviation of the parameter values determined by regression analysis and experimentally, in particular,

$$\varepsilon_{rms}=\frac{\sqrt{\sum_{i=1}^{N}\Delta_i^2}}{N}=2{,}064\cdot10^{-2};\beta_{\max}=\frac{\varepsilon_{\text{rms}}}{\min\left(\iota_{\text{э}i},i=1...N\right)}\cdot100\ \%=0{,}39\ \%\ ,$$

here $\Delta_i=\iota_{\text{э}}(\varepsilon_i,\zeta_i)-\iota_{\text{э}i}$.

The small values of absolute RMS and maximum relative errors obtained in

these calculations can serve as a basis for the legitimacy of using in the experiment the regression dependence derived by us.

Fig. 2.15 presents a graphical interpretation of the dependence of the reduction factor k_p on the parameters ε and ζ in the range of varying values of the mentioned quantities.

As the diagram shows, the value of the bending stiffness of the shell can decrease by 19 %, which can be explained by the absence of normal stresses at the groove contour points of this shell. That is why the value of the bending stiffness was less than the value obtained by applying the Kirchhoff-Liave statistical hypothesis. Thus, it became necessary to introduce a reduction factor into the calculations.

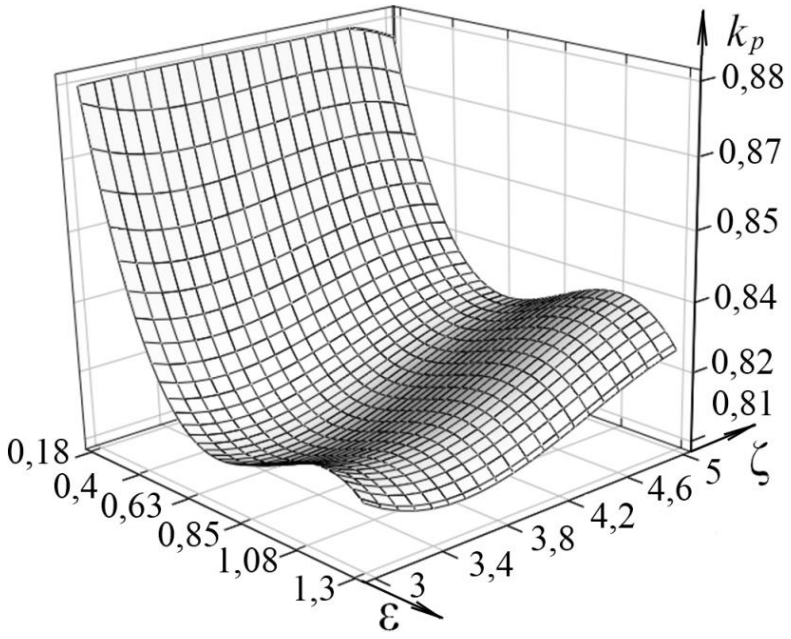

Fig. 2.15. Diagram of dependence of the reduction factor k_p on the parameters ε and ζ

For a more detailed analysis of the function k_p (ε, ζ), let us consider its curves (Fig. 2.16), which correspond to the minimum and maximum values of the dimensionless parameters ε, ζ.

As can be seen from the dependence of the reduction factor k_p on the dimensionless profile parameters ε and ζ (Fig. 2.16), as the scallop height decreases, the value of the first quantity tends to 1. And at the moment when ε = 0.5, it can be

considered that k_p = 0.82 (with an error of 3 %).

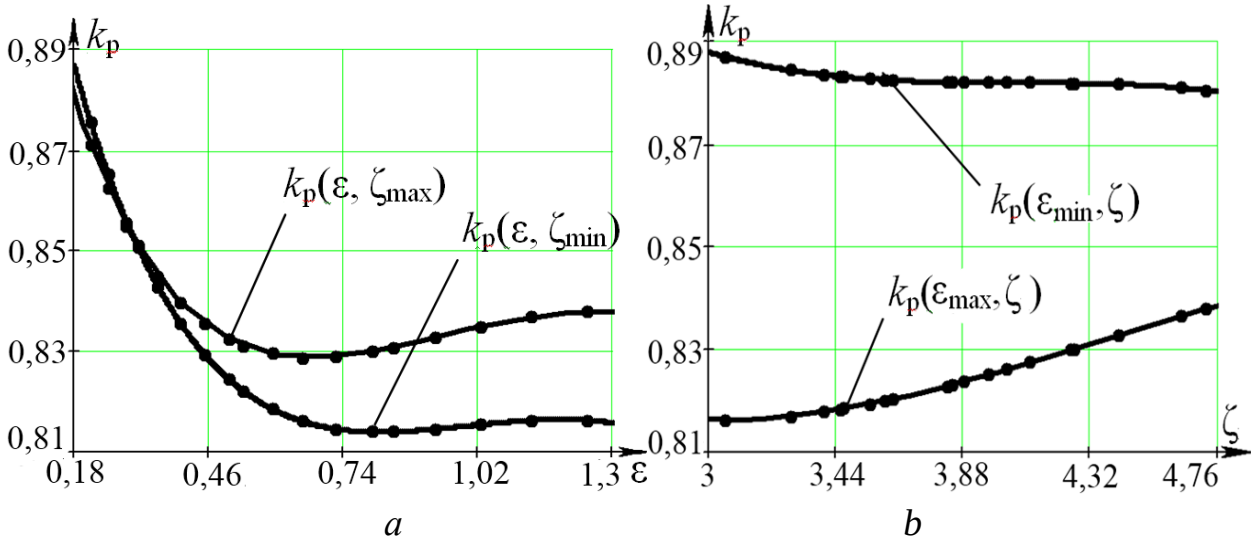

Fig. 2.16. Graphs of change in values of the reduction ratio

As a result, the expression describing the bending stiffness can be represented as follows:

$$D = \left(\begin{array}{l} 1{,}347 - 0{,}5\cdot\varepsilon - 0{,}295\cdot\zeta + 0{,}61\cdot\varepsilon^2 + 0{,}016\cdot\varepsilon\cdot\zeta + \\ +0{,}074\cdot\zeta^2 - 0{,}195\cdot\varepsilon^3 - 0{,}021\cdot\varepsilon^2\cdot\zeta + 0{,}007\cdot\varepsilon\cdot\zeta^2 - 0{,}006\cdot\zeta^3 \end{array}\right)\times$$
$$\times\frac{E\cdot\tau}{\left(1-\mu^2\right)}\cdot\left(\int_0^{\tau}\left(\frac{h^3}{96}+\frac{f_z(x)\cdot h^2}{16}+\frac{{f_z}^2(x)\cdot h}{8}+\frac{{f_z}^3(x)}{12}\right)^{-1}dx\right)^{-1}. \qquad (2.59)$$

Expression (2.57), obtained using a semi-empirical approach, takes the form of the product of the averaged stiffness and the reduction factor, for the expression of which an approximation relationship is constructed on the basis of a computational experiment.

Let's compare the value of bending stiffness of the drum shell 2Ts-6×2,4, obtained by formula (2.59), with the results of calculations according to the method developed in PJSC "NKMZ" (where the minimum wall thickness was taken into account), and according to the Zinchenko method.

For example, taking into account such parameters of the shell: h_m = 30 mm, h_f = 15 mm and τ = 24 mm, bending stiffness D = 5,12-10^5 N-m (the result of

applying the method of PJSC "NKMZ"). Calculations made with the help of the method developed by the authors gave the following result: D = 6,43-10^5 N-m, which is 25 % more than the previous one.

At the same time, the calculated parameters of the drum shell profile 2Ts-6×2,4 produced by PJSC "NKMZ", in particular its equivalent thickness are close to the values of this characteristic obtained by Zinchenko's method. At the same time, the method developed by the authors allows to determine the bending stiffness of the shell of any profile. For this reason, the values of bending stiffness of a profiled shell given in the work of Fedorova 3.M. and Zinchenko S.N. raise doubts, because the value of stiffness of a smooth shell is underestimated by 12 times.

The new method has shown that the obtained value of cylindrical stiffness is 25 % higher than the results of calculations performed using the predecessor methods. This effect is caused by the possibility to take into account in the new method the geometrical shape of the profile and the FEM calculations on a finer grid.

2.4.3 Construction of physical models of drum reinforcements as discrete circular compression and torsion springs

In order to realise this task, it is necessary to determine the dependence of the stiffness characteristics of reinforcements on their geometrical parameters.

A computational experiment using FEM was chosen as the solution method.

The assumptions made in the calculations were as follows:

1. The connection of the drum lobes to the hub can be replaced by a "rigid termination" connection.

2. All reinforcements are subjected to radial pressure and bending moment.

In the creation of the mechanical model of the frontal we take into account the assumption of axisymmetric character of SSS arising in it, and this allows us to perform an equivalent replacement of the frontal by compression springs with stiffness λ and torsion springs with stiffness χ (see the scheme of Fig. 2.17).

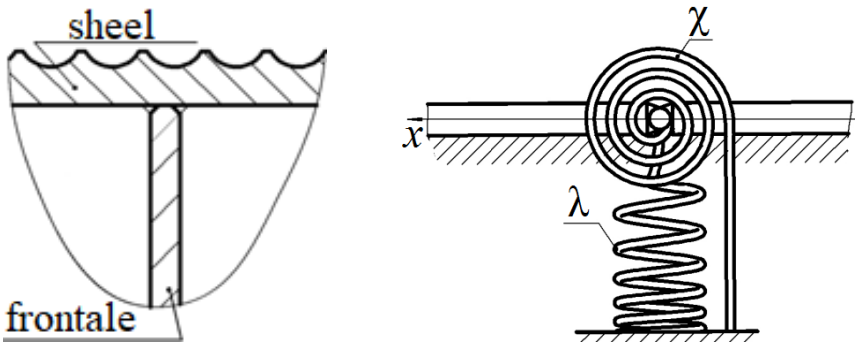

Fig. 2.17. Replacing the joint between the shell and head with compression and torsion springs

Now we can calculate the bending and radial stiffness of frontal by means of computational experiment by finite element modelling using SolidWorks Simulation software. Fig. 2.18 shows the scheme for calculating the parameters of the frontal with thickness h_l, external radius R_l and radius of the centre hole for hub mounting R_c.

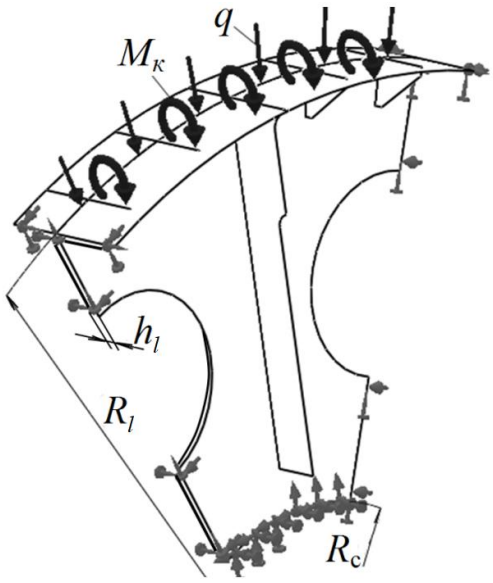

Fig. 2.18. Data for the computational experiment

The following boundary conditions concerning the edges of the lobes were accepted in the calculations: prohibition on the movement of the central hole; on rotations of the lobes around the drum axis and along its radius at the edges formed by the sections; impossibility of translational circumferential movements. At the same time, it was taken into account that a circumferential torque $M_к$ is applied

to the outer circular edge of the object and a uniformly distributed pressure q acts.

The bending stiffness of the frontal is calculated as the ratio of the applied moment $M_к$ to the average angle of rotation ψ of its outer circular edge, i.e.

$$\chi = 4M_к / \pi \cdot R_l \cdot \psi . \quad (2.60)$$

We can define the radial stiffness as the ratio of the applied pressure q to the average value of the radial displacement $w_л$ of the outer circular edge, which corresponds to this expression:

$$\lambda = \frac{q \cdot h_l}{w_l} . \quad (2.61)$$

We introduce dimensionless parameters peculiar to the drum frontal, namely: dimensionless radius $\rho = R_l / R_c$; dimensionless thickness $\delta = h_l / R_c$ . .

Then we set the step (interval) of measurements and levels of variation of values of the entered values (see Table 2.6).

Table 2.*6*.

Defined initial conditions for conducting the numerical experiment

Parameter	Level of variation			Step
	-1	0	1	
ρ	2,5	3,1	3,7	0,6
δ	0,024	0,038	0,05	0,012

We also take such parameters as outputs for the numerical experiment:

dimensionless ring stiffness $\tilde{\lambda} = \frac{\lambda}{B} = \frac{\lambda}{E \cdot h_l}$; (2.62)

dimensionless bending stiffness $\tilde{\chi} = \frac{\chi}{D} = \frac{12 \cdot \chi (1 - \mu)}{E \cdot h_l^3}$ (2.63)

Using a finite element model of the drum frontal, a computational experiment was carried out, during which it was possible to determine the values of radial displacements of the shell (Fig. 2.19, *a*) and the angle of rotation of its outer edge (Fig. 2.19, *b*).

The obtained results were processed using the method of least squares, as a consequence of which we found dependences of the values of bending and radial stiffness on the parameters R_l and h_l, which correspond to these equations:

$$\tilde{\lambda}(\rho) = 54{,}5 - 22{,}3 \cdot \rho + 3 \cdot \rho^2; \qquad (2.64)$$

$$\tilde{\chi}(\rho, \delta) = 0{,}71 - 0{,}041 \cdot \rho - 2{,}35 \cdot \delta - 0{,}065 \cdot \rho^2 - 7{,}1 \cdot \rho \cdot \delta + 224{,}5 \cdot \delta^2. \qquad (2.65)$$

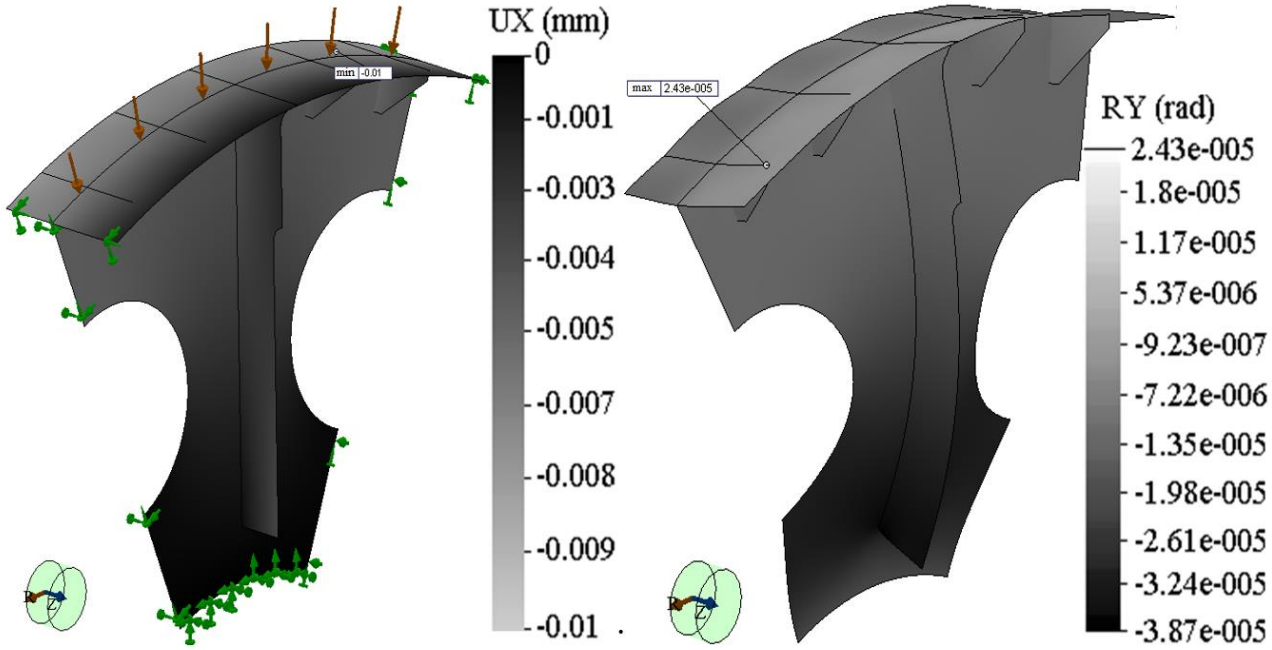

a *b*

Fig. 2.19. The result of numerical analysis of processes, occurring in the drum frontal (using FEM)

At that, the absolute RMS error of approximation does not exceed 1.6 %, and the maximum relative error is 5.3 %.

In the same way as the joint of the drum shell with the frontal was investigated,

let us consider its joints with the spandrel and bearing rib, which can be represented as annular plates having certain stiffness characteristics.

The analytical expressions for determining the values of radial and bending stiffnesses of the spar and flange, respectively, are as follows:

$$\lambda_{\text{br}} = \frac{B_{\text{br}} \cdot \left(b_{\text{br}}^2 - a_{\text{br}}^2\right)}{\left(1+\mu\right) \cdot \left(a_{\text{br}}^2 \cdot b_{\text{br}} + \left(1+2\mu\right) \cdot b_{\text{br}}^3\right)};\ \chi_{\text{br}} = \frac{D_{\text{br}} \cdot \left(b_{\text{br}}^2 - a_{\text{br}}^2\right) \cdot \left(1-\mu^2\right)}{b_{\text{br}}^3 \cdot \left(1-\mu\right) + b_{\text{br}} \cdot a_{\text{br}}^2 \cdot \left(1+\mu\right)}. \quad (2.66)$$

$$\chi_{\text{f}} = \frac{D_{\text{f}} \cdot \left(b_{\text{f}}^2 - a_{\text{f}}^2\right) \cdot \left(1-\mu^2\right)}{a_{\text{f}}^3 \cdot \left(1-\mu\right) + b_{\text{f}}^2 \cdot a_{\text{f}} \cdot \left(1+\mu\right)};\ \lambda_{\text{f}} = \frac{B_{\text{f}} \cdot \left(b_{\text{f}}^2 - a_{\text{f}}^2\right)}{\left(1+\mu\right) \cdot \left(a_{\text{f}} \cdot b_{\text{f}}^2 + \left(1+2\mu\right) \cdot a_{\text{f}}^3\right)}, \quad (2.67)$$

where a_{br} , a_{f} is the inner radius of the spar and flange respectively; b_{br} , b_{f} is the outer radius of the same elements; annular stiffness of the plate $B = E \cdot h$; bending stiffness of the plate $D = E \cdot h^3 / 12(1-\mu^2)$; h is the thickness of the reinforcing element.

In order to build a mechanical model of the braces and ribs, we will use the assumption of axisymmetric character of the SSS arising there, which makes it possible to replace them by rings of equivalent thickness h_{ring}, the volume of which is equal to the volume of the mentioned reinforcing elements.

The equivalent thickness of the ring can be determined using this formula:

$$h_{ring} = \frac{2 \cdot V_{\text{rfrc}} \cdot n}{l_{\text{rfrc}} \cdot R}, \quad (2.68)$$

where V_{rfrc} is the reinforcement volume; l_{rfrc} is the reinforcement length; *n is the* number of reinforcements arranged in a circle.

Thus, it was possible to construct mechanical models of the drum reinforcing elements. In this case, the flanges and spandrels are represented as elastic supports operating in compression and torsion. In addition, analytical dependences for determining the parameters of the elastic supports were obtained. In the calculation

results, the absolute RMS error was 1.6 %, and the maximum relative error was 5.3 %.

2.5 Setting the algorithm for determining the design loads, arising in the MHM drum

Let us set the condition, by which the number of the load rope coil k corresponds to the number of the loading variant v.

Let us assume that in the calculation of the parameters of the MHM drum, such a loading variant is used, at which the maximum intensity of stresses arising in its structural-orthotropic shell is achieved.

The method for determining design loads involves the following steps:

1 Using equations (2.48) - (2.50), (2.58), (2.64) - (2.68), determine the parameters of the structural-orthotropic shell, in particular, the values of bending D and annular B stiffnesses, elastic moduli E_1 , E_2 , Poisson's coefficients μ , μ_{12} ; as well as the parameters of elastic supports, i.e. bending χ and annular stiffness λ.

2. Depending on the values of the parameters of the structural-orthotropic shell and elastic supports, the components of the pliability matrix [W] are calculated using equations (2.22) - (2.24).

3. Applying the values of the components of the pliability matrix [W], according to the mathematical model of rope winding (2.8) - (2.17) determine the matrix of loading variants with such components: $P_{j,k}$, j = 1,..., N - number of the groove, k = 1,..., $N_г$ - number of the loading variant.

4. For all variants of drum loading, the following formulas are used to determine the vector {σ}, each *k-th* component of which reflects the maximum intensity of stresses σ_k, occurring in the shell and corresponding to the k-th loading variant. Thus, according to the calculated load, the modelled structural-orthotropic axisymmetric shell experiences stresses that can be determined by the following formulas:

- Axial (longitudinal) in the upper and lower layers

$$\sigma_{xu_i} = \frac{E_{2_k} \cdot \kappa_i}{1 - \mu_1 \cdot \mu_2}\left(\frac{h_m}{2} + \frac{h}{4}\right); \quad \sigma_{xl_i} = -\frac{E_{2_k} \cdot \kappa_i}{1 - \mu_1 \cdot \mu_2}\left(\frac{h_m}{2} + \frac{h}{4}\right); \tag{2.69}$$

● Circular (circular)

$$\sigma_{\varphi l_i} = -\frac{E_{1_k} \cdot w_i}{R} - \frac{E_{2_k} \cdot \mu_1 \cdot \kappa_i}{1 - \mu_1 \cdot \mu_2} \cdot \left(\frac{h_m}{2} + \frac{h}{4}\right); \; \sigma_{\varphi u_i} = -\frac{E_{1_k} \cdot w_i}{R} + \frac{E_{2_k} \mu_1 \cdot \kappa_i}{1 - \mu_1 \cdot \mu_2}\left(\frac{h_m}{2} + \frac{h}{4}\right). \tag{2.70}$$

5. The loading variant, at which the vector component {σ} reaches the maximum value, is determined as the main one for FEM calculation of forces arising in the MHM drum.

2.6 Conclusions to Section 2

1. The method of determining the design loads when winding the rope on the cylindrical drum and its unwinding is based on the condition of modelling the mentioned process in the form of successive putting on the drum and removing from it pre-stretched smooth elastic rings, the stiffness of which is equal to the longitudinal stiffness of the rope, while the cylindrical drum is considered to be supported by axisymmetric structural-orthotropic shell. The data for determining the SSS arising in the drum are selected taking into account the variants of its loading corresponding to different positions of lifting vessels in the shaft.

2. The mathematical model described above was constructed in such a way that the initial radius of each ring was determined in the expectation that the force generated in it after putting it on is equal to the rope tension force.

3. The developed recurrence process of solving the system of equations describing the mathematical model makes it possible to determine the value of the linear force that occurs when each ring is put on.

4. A mathematical model of the deformation process of the reinforced drum shell in the form of a system of linear algebraic equations has been constructed; as a result of its analytical solution, the pliability matrix [*W*] has been obtained, and it

has been found that its components depend on the unknown parameters of the structural-orthotropic shell and elastic supports.

5. It was proved that by modelling the SSS, spiral grooves on the drum can be replaced by annular grooves, and in the range of obtained values of the investigated parameters the error does not exceed 10 %.

6. The variation of the relative error in the determination of the results of the intensity of the stresses and the displacement distance of the shell when the grooving angle is unchanged and when dimensionless parameters (drum width, shell and head thickness) are taken into account does not exceed 0.6 %.

7. As shown by the analysis of the results of the computational experiment on the study of the SSS arising at the operation of two cylindrical drums, which have spiral and annular grooves, under the influence of radial pressure and due to the change of the cutting angle from 2.6° to 3.6°, the relative errors of the obtained values when replacing the spiral groove with a sequence of annular grooves monotonically increase, not exceeding 6 % relative to the maximum displacements, and 10 % taking into account the maximum intensity of stresses.

3 LABORATORY VALIDITY STUDIES METHODS FOR DETERMINING MHM DRUM LOADS

3.1 Problem statement

Modern literature sources do not reflect the methods of conducting and results of experimental studies on the weakening of the tension of rope coils on the cylindrical drum due to its radial deformations. The fact is that the determination of the magnitude of these deformations in the process of operation of mine hoisting installations is a very difficult task due to the specifics of the work of these machines, in addition, requires significant financial costs.

In this regard, to confirm the reliability of the method proposed by the authors to determine the calculated loads when winding the rope on a cylindrical drum, we use a laboratory setup that simulates this process, and then conduct a computational experiment. In laboratory tests we proceed from the fact that the method as a scientific tool should ensure that there are no discrepancies in the results obtained in the process of repeated experiments.

One of the main tasks of the method is the selection of design parameters for the maximum stresses in the structural-orthotropic shell of the drum based on loading variants and their subsequent finite element analysis. In order to assess the adequacy of the values of stresses occurring in the structural-orthotropic shell and those calculated using the finite element model, it is reasonable to compare them on the example of the processes occurring in the wedged part of the drum of a PR-type machine.

We ensure the solution of the task by carrying out the following actions:

1. Evaluation of the proposed method by testing using a laboratory setup modelling the process of rope winding on a drum.

2. Justification of the choice of design parameters of the shell on the example of the drum of the TsR machine.

3.2 Modelling of the rope winding process on a laboratory installation

Laboratory studies were carried out to test the effect of the method developed by the authors by the criterion of closeness of the values of radial deflections of the drum shell of the laboratory unit obtained by experimental and calculated means.

Such an algorithm for solving the stated problem was defined:

- justify the parameters and develop the design of the laboratory unit, draw up the programme and test methods;
- Determine the deflection values of the drum shell by means of measurements on a laboratory apparatus;
- determine the deflection values of this shell by calculation;
- to evaluate the error of the results obtained using the developed method.

3.2.1 Justification of the parameters of the laboratory setup

From what was stated in Section 3.1, it follows that to carry out the experiment it is necessary to create a laboratory setup, make a programme and develop a test methodology. Designing of the laboratory set-up we start with justification of its basic parameters. First of all, it is necessary to reproduce the process of rope winding with the help of drum shell and rope models. For their correct use, it is necessary to clearly formulate some relations between the parameters of the laboratory model and the real design. In determining the design conditions of the laboratory setup we use the theory of dimensions and similarity.

The mathematical model of the structural-orthotropic drum shell was based on the following conditions: a thin-walled axisymmetric shell is used (corresponds to the following inequality: $h/R \le 1/20$), radial deflections w of which are less than its thickness ($w/h < 0{,}5$), the shell is considered to be long enough ($L \ge 2\pi/\beta$), and deformation of its material corresponds to Hooke's law, i.e. $Ew/R < \sigma_т$, where $\sigma_т$ - yield strength of the cable material; h - thickness of the shell; R - radius of the shell;

E - modulus of elasticity of the material; L - length of the shell; β - variability parameter of the shell [$\beta > -\ln(0,1)/t$].

In order to take into account, the peculiarities of the process of winding the hoisting rope on the drum, we will provide such values of additional criteria:

- stress-strain state variability $e^{-\beta t} > 0.1$;

- measurement accuracy $\frac{w}{h} > \frac{R \cdot T}{E \cdot h \cdot d}$;

- number of turns $L/t \geq 50$;

- compliance of the rope parameters with Hooke's law, with $t < 0,25 \cdot \pi \cdot \psi \cdot d^2 \cdot \sigma_t$, where ψ = 0.69 - rope filling factor; d - *rope* diameter.

To determine the relationship between the characteristics of the model and the real structure, we use the π-theorem. In this connection, let us assume that the deflection of the middle part of the shell caused by annular compression in interaction with a rope of diameter d and tensile force T *is* described by the following function:

$$w = f(h, L, R, d, E, T). \tag{3.1}$$

Application of the π-theorem shows that four π-variables must be used to formulate this problem. Let the parameter π_1 contain a definable variable w, then expressions to describe π-variables take such values:

$$\pi_1 = \frac{w}{h};\ \pi_2 = \frac{h}{R};\ \pi_3 = \frac{R}{L};\ \pi_4 = \frac{L}{d};\ \pi_5 = \frac{T}{E \cdot d \cdot h}.$$

Now we can formulate the problem by applying the obtained expressions, viz:

$$\frac{w}{h} = \varphi\left(\frac{h}{R}, \frac{R}{L}, \frac{L}{d}, \frac{T}{E \cdot d \cdot h}\right).$$

Since the obtained equation is valid for both the real structure and the model, it can be assumed that it describes the ratio of parameters of the former, and an equation similar to it, i.e.

$$\frac{w_m}{h_m} = \varphi\left(\frac{h_m}{R_m}, \frac{R_m}{L_m}, \frac{L_m}{d_m}, \frac{T_m}{E_m \cdot d_m \cdot h_m}\right),$$

- second. On the basis of the obtained expressions we will introduce such conditions for the design of the MHM drum:

$$\frac{h_m}{R_m} = \frac{h}{R}; \frac{R_m}{L_m} = \frac{R}{L}; \frac{L_m}{d_m} = \frac{L}{d}; \frac{T_m}{E_m \cdot d_m \cdot h_m} = \frac{T}{E \cdot d \cdot h}.$$

Whence it follows that

$$h_m = R_m \frac{h}{R}; R_m = L_m \frac{R}{L}; d_m = L_m \frac{d}{L} \tag{3.2}$$

The fourth design condition is the basic condition for determining the required load acting on the model, viz:

$$T_m = \frac{E_m \cdot d_m \cdot h_m}{E \cdot d \cdot h} \cdot T. \tag{3.3}$$

Considering the above, the equation predicting the deflection of the model takes the following form:

$$w_m = h_m \cdot \frac{w}{h}. \tag{3.4}$$

Consequently, in order to achieve the required deflection value in the real structure, it is necessary to multiply the measured results of this parameter in the model by the ratio of the shell thickness values of the real drum and the modelled one.

To determine the basic parameters of the laboratory model, let us consider a simplified scheme of interaction of an elementary section of rope with the shell (Fig. 3.1) far from the attachment points. In this scheme, both objects look like rings put on each other with tension.

$T_к$ is the tensile force of the rope and T_{sh} is the compressive force of the sheath.

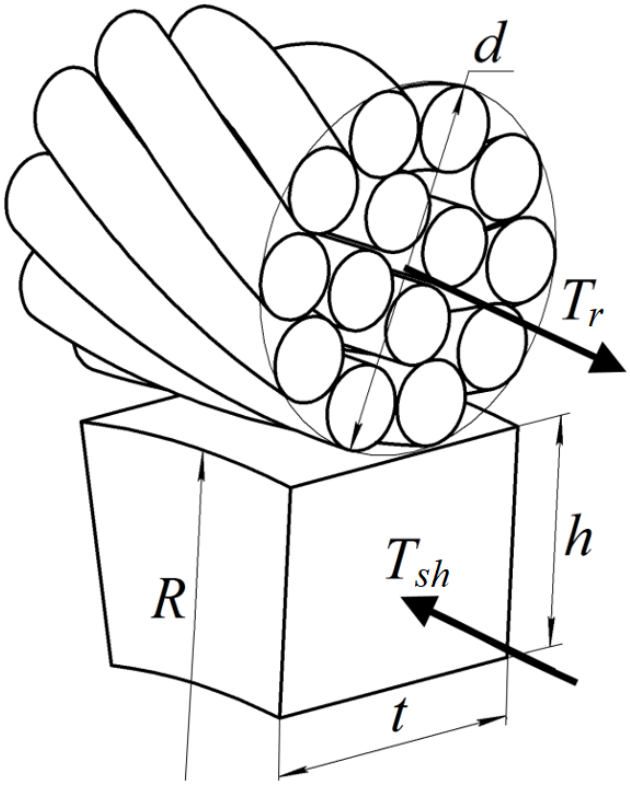

Fig. 3.1. Schematic for calculation of parameters in the system "rope-pipe"

It follows from the equilibrium condition that

$$T_r = T_{sh} = \frac{w}{R} \cdot E \cdot h \cdot t. \tag{3.5}$$

The deflection of the shell is determined using the following expression:

$$w = \frac{T_r \cdot R}{E \cdot h \cdot t}. \tag{3.6}$$

Assuming that $\pi_6 = w/R$, the following condition is true:

$$\frac{w_m}{R_m} = \frac{w}{R} = \frac{T_r}{E \cdot h \cdot t}. \tag{3.7}$$

Taking into account the criterion of accuracy of measurements that the deflection of the shell model w_m = 0,75 mm, and the modulus of elasticity of the material E_m = 8-10^8 Pa, we obtain the values of its other parameters calculated using the above expressions, namely: R_m = 150 mm; L_m = 200 mm; h_m = 2,5 mm;

d_m = 3 mm; T_m = 130 N.

Taking into account the similarity criteria, we developed an experimental rope winding bench with the following parameters:

Single coiling rope of TK type GOST 3063-80	
Schematic of its construction: 1×19(1+6+12), diameter	3 mm
Rope length	100 m
Polypropylene shell	
(GOST 26996-86) (PP), modulus of elasticity	$8 \cdot 10^8$ Pa
Drum diameter	300 mm
Tension force	30; 65; 95; 130 N
Total number of turns	69
Number of friction turns	3

In Fig. 3.2 we see the scheme of the laboratory installation for studying the process of rope winding on the drum. Here, two flanges 2, symmetrically located relative to the centre of the drum, were attached to the surface of a metal drum 4, which has the possibility of free rotation relative to its horizontal axis on roller supports 5, and the end walls of the shell were rigidly attached to their outer edges.

In the central part of the cylindrical drum shell 4, four radial holes with threads were drilled every 90°. In these holes were screwed bushings with screwed indicators of clock type 3, the dials of which were located inside the drum shell, and the tips of the measuring rods rested on the inner surface of the plastic shell 1.

In order to keep the tension force of the rope 8 coiled on the surface of the shell 1 constant, a block system of load suspension 9 was used. Before the tests, the rope was wound on a spool 10, and its free end passed through two fixed 6 and one movable block 7, and at the same time was fixed on the flange 2 of the drum. A weight 9 is suspended on the movable block 7. In the process of drum rotation and rope winding, the bobbin 10 is in a braked state, and the rope is subjected to a tension force approximately equal to half the weight of the weight 9. The winding of the rope on the shell 1 is accompanied by the simultaneous lifting of the weight 9 together with the block 7. When the height range of the movable block 7 is

completely exhausted, the drum rotation is stopped and the reel 10 is released, thus ensuring the return of the weight 9 to the lower end position, after which the rope winding cycle is repeated.

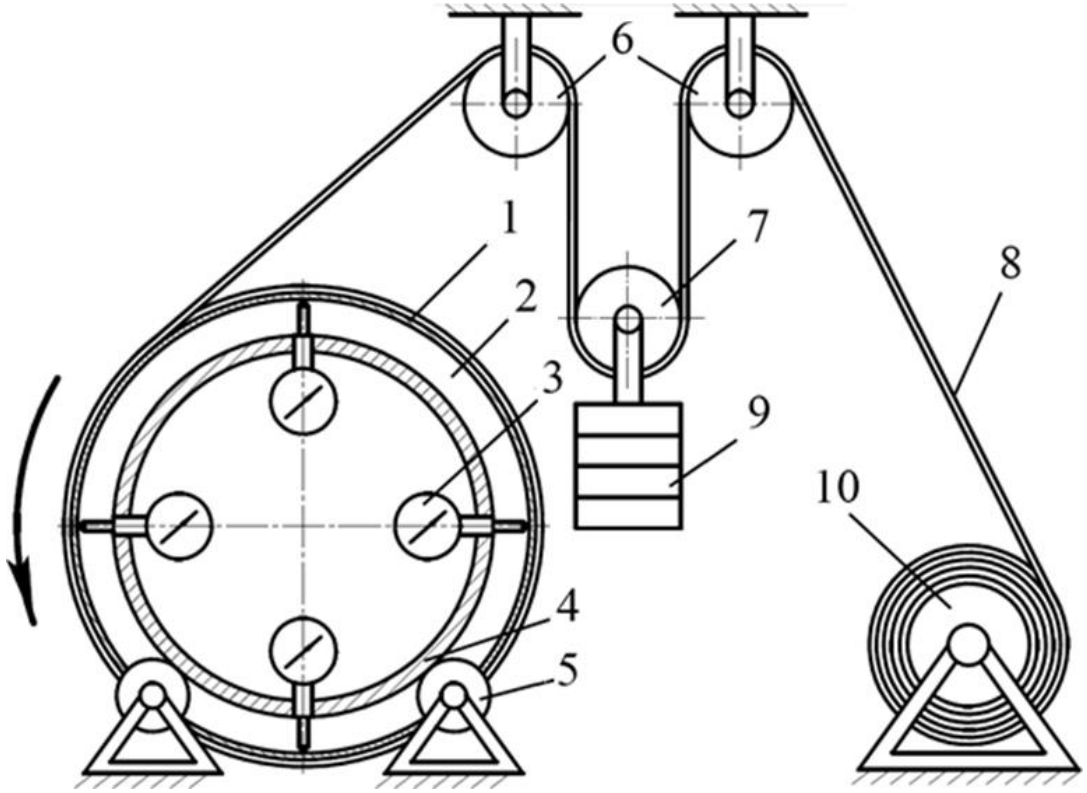

Fig. 3.2. Laboratory set-up for the study of rope winding on the drum

Fig. 3.3 shows the general view of the laboratory setup, and Fig. 3.4 shows the location of clock-type indicators inside the drum of the lifting machine model.

In order to accurately determine the values of the rope tension force in the process of its winding on the drum, excluding the influence of friction in the rotating parts of the suspension blocks, this index was measured in the rope branch directly wound on the drum. For this purpose, a dynamometer (Fig. 3.5) was installed on the rope section between the drum and the suspension block, and then the rope was wound within the length of the free end of the branch.

As a result of the substantiation of parameters of the sheath and rope models according to the theory of dimensionality and similarity, the following parameters of the laboratory installation for the study of rope winding on the drum were found: the radius of the polypropylene sheath is 150 mm; the length of the sheath is 200

mm; the thickness of the sheath is 2.5 mm; the diameter of the rope is 3 mm. The tests were carried out according to the programme and method developed by the authors.

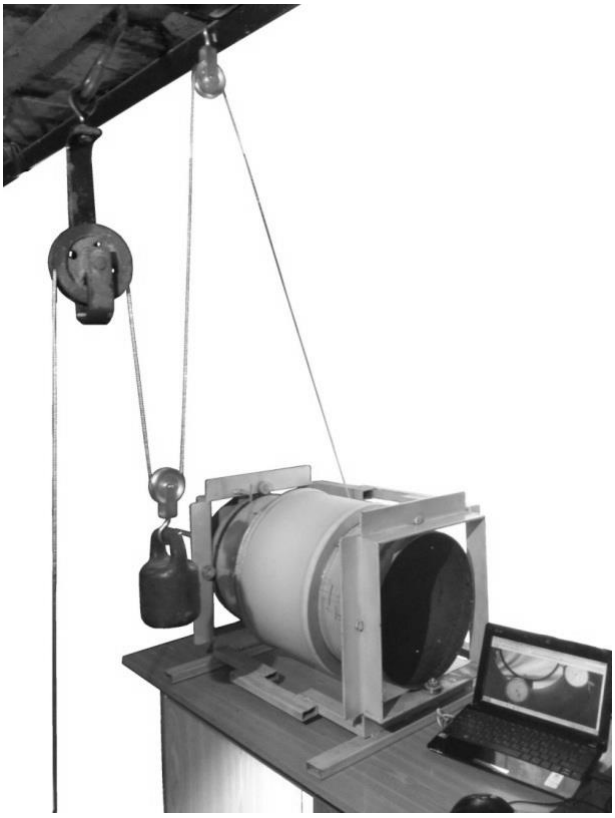

Fig. 3.3. General view of the laboratory installation

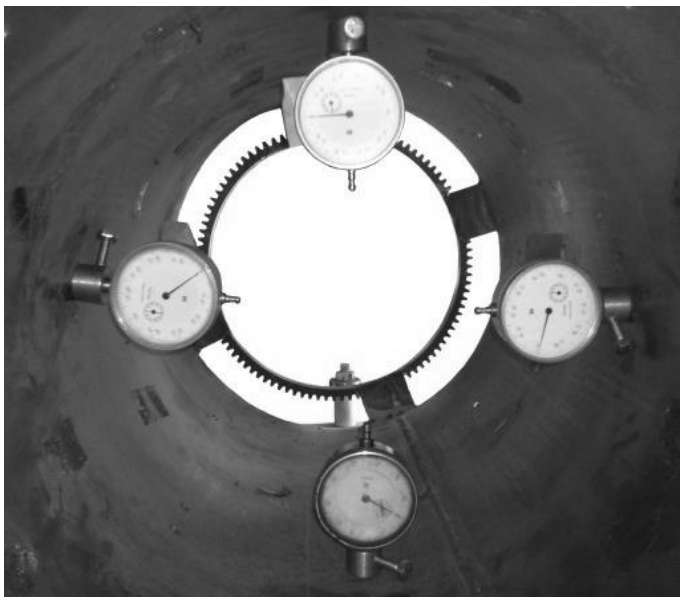

Figure 3.4.Location of clock-type indicators inside the drum of lifting machine model

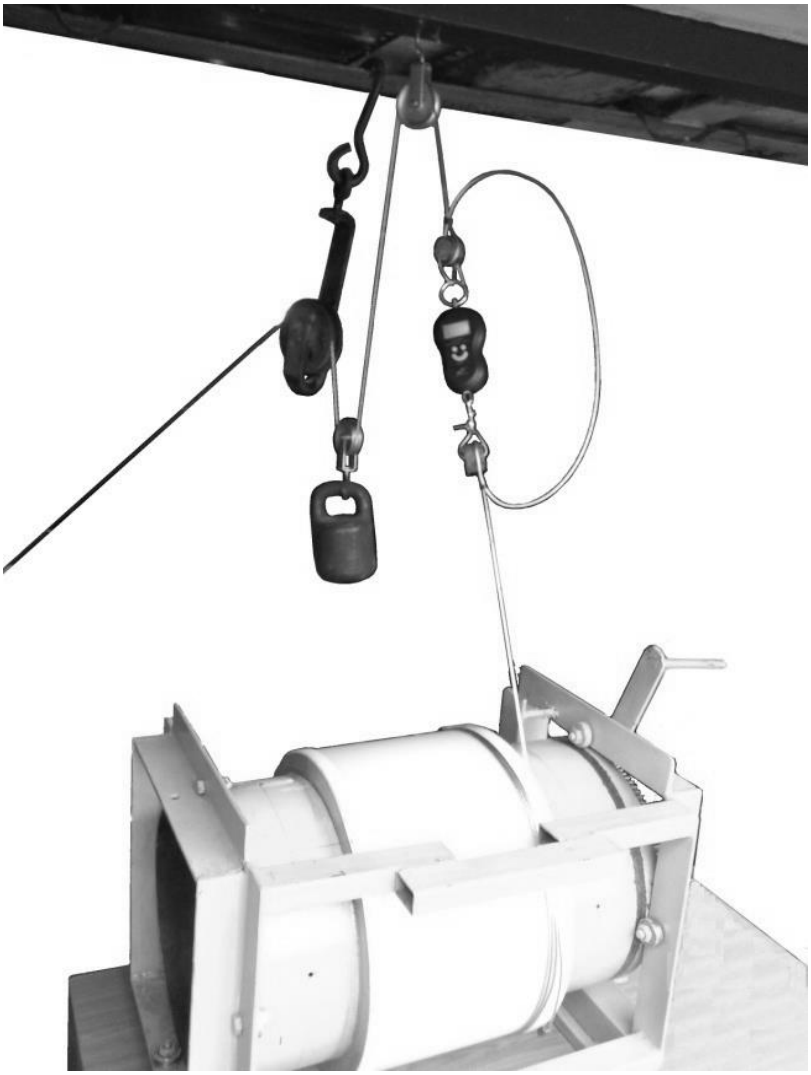

Fig. 3.5. Measuring the tension force in the winding rope branch

3.2.2 Determination of the deflection values of the drum shell using a laboratory installation and

In accordance with the programme and test methodology developed by the authors, an experiment simulating the process of rope winding on the drum was carried out on a laboratory installation. In the process of experimental works, the change in the values of radial deflection of the middle part of the drum shell under the action of the force that occurred in the wound rope was observed and recorded. Fig. 3.6 presents curves showing these changes. The graphs were constructed based on the results of the experiment, in which the tension of the wound rope was 130 N (here *i* is the number of the wound rope coil).

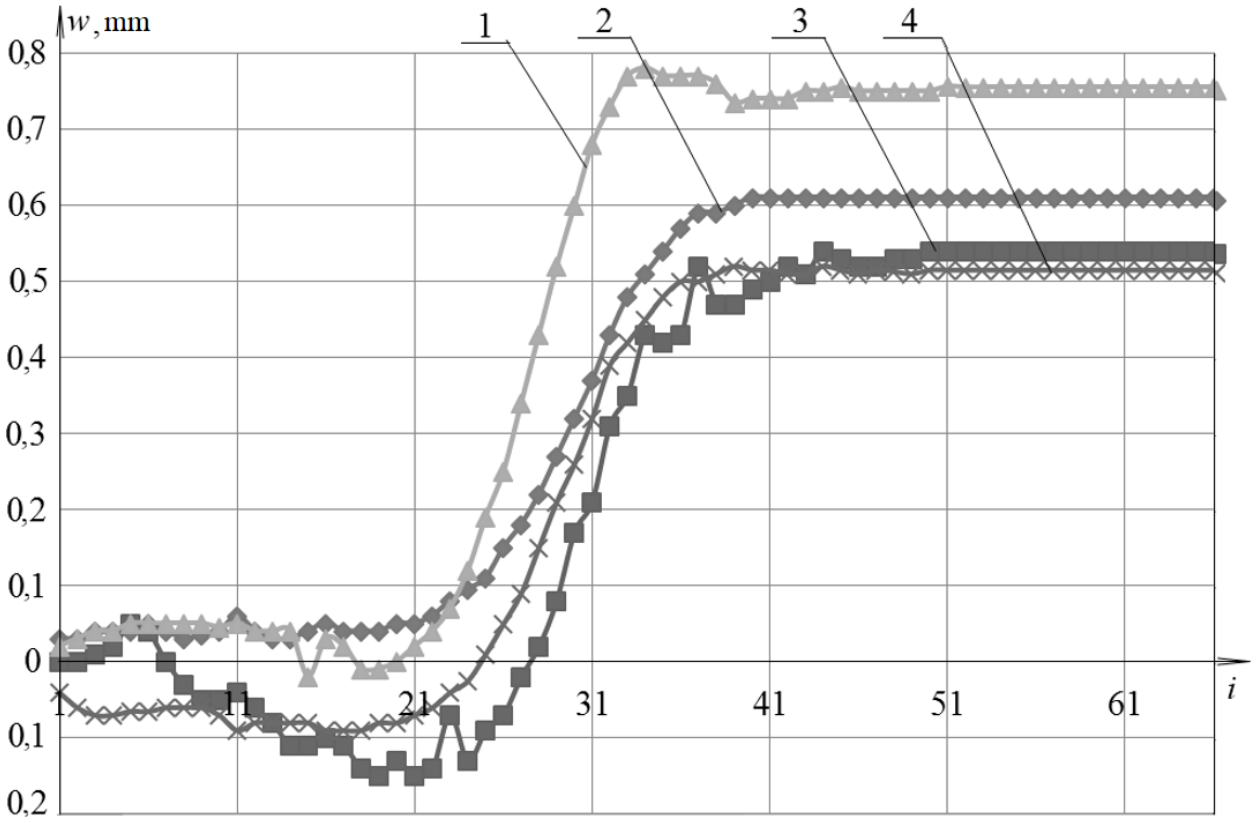

Fig. 3.6. Graphs of radial displacements of the shell when winding the rope with tension equal to 130 N:

1, 2, 3, 4 - readings of I, II, III and IV sensors of the installation respectively

The analysis of the results showed that the curves plotted from the data of each of the four sensors of the laboratory setup have approximately the same shape, but quantitatively different. To explain the reasons for this circumstance, let us consider the deflection values in the polar coordinate system when winding the 30th and 50th turns (Fig. 3.7). The graph shows that the scatter of indicator readings relative to the average deflection values on the opposite sides of the shell (0° and 180° coordinate section) exceeds the average values, and on the 90° and 270° section it is lower than them. At the same time, the points of readings of the opposite sensors are almost symmetrical with respect to the centre of the circles of the coordinate system. This is caused by deviations from the cylindrical shape of the shell itself, as well as by the violation of the ideal configuration of the discs on which it is planted. In this connection, in further studies we will use the averaged values of the readings of the four sensors.

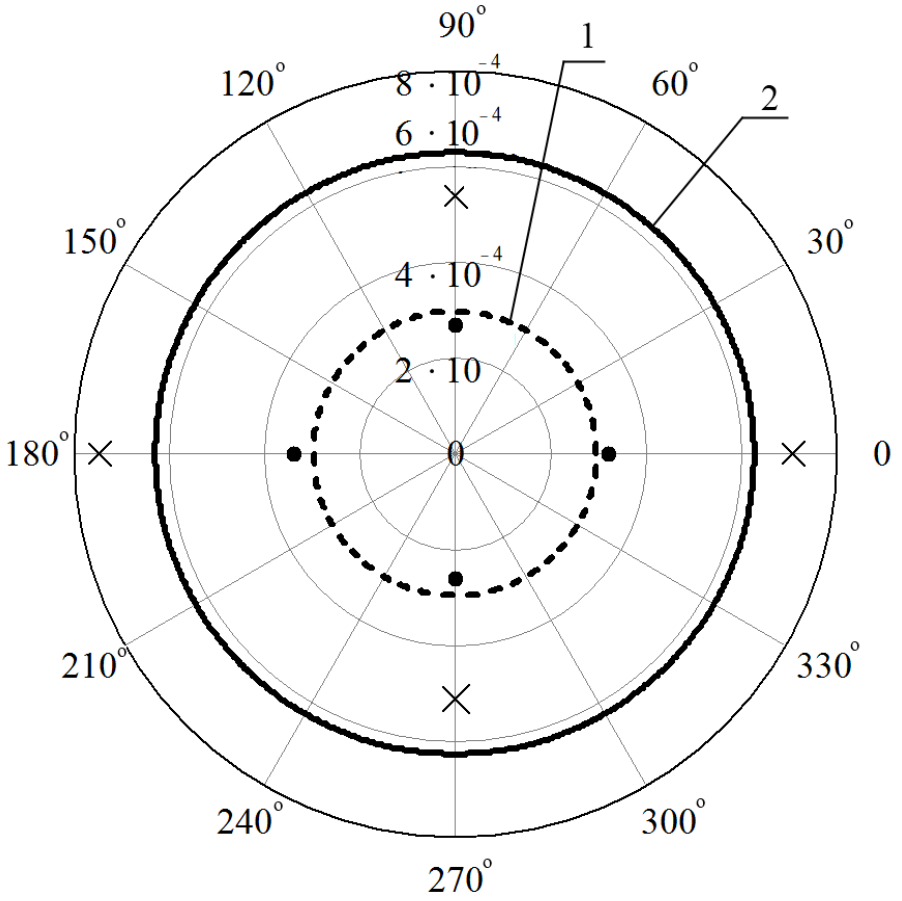

Fig. 3.7. Scheme of drum shell displacements in indicator points and their average values during winding of 30th (1 – •), 50th (2 - ×) turns

The analysis of the curves showed that the values of the shell deflection consist of the sum of three values. Firstly, it is a deterministic axisymmetric component, its value depends on the coil number; secondly, it is a deterministic component arising under the influence of the non-axisymmetric shape of the shell (its value does not depend on the coil number); and thirdly, it is a random value as a consequence of the measurement error.

The error of calculations was evaluated by comparing the experimental results and parameter values calculated by the proposed method. For this purpose, we performed statistical processing of experimental results.

Suppose that the random variables determining the deflection values of the drum shell during winding of each coil are such that their mathematical expectations are equal to zero, and they can differ from each other only by the values of dispersions.

To confirm our hypothesis, let us test it by applying the Kochren criterion, according to which the ratio of the maximum variance to the sum of all refined variance values should be less than its critical value. For this purpose, at a given significance level of the parameter α, we calculate the parameter G_{obs} - the observed value of the criterion as the ratio of the refined maximum variance to the sum of all its values S^2, and find the critical point G_{cr}. The distribution of values of the parameter G_{cr} depends on the number of samples N_p and the number of degrees of freedom $f = n - 1$, where *n is* the number of experiments. Thus,

$$G_{obs} = S^2_{\max} \Big/ \sum_{i=1}^{N_p} S_i^2 .$$

At 95% confidence level, the following inequality holds: $G_{cr} < G_{obs}$(0.280 < 0.283), and the difference in sample variance is significant.

Let us try to prove the correctness of the hypothesis using Fisher's criterion. So, the control of adequacy of the obtained dependence includes three stages:

1. Determination of the adequacy variance, i.e.

$$S^2_{ad} = \sum_{i=1}^{n} \frac{w_i - w^*}{f},$$

here w_i is the experimental value of the elastic modulus of the cable.

2. Determine the reproducibility variance (weighted average) using the following expression:

$$S^2_{rep} = \sum_{i=1}^{n} w_i \cdot f_i \Big/ \sum_{i=1}^{n} f_i .$$

3. Checking the homogeneity of variance values of adequacy and reproducibility, for which it is necessary to preliminarily establish the calculated value of Fisher's criterion and compare it with the tabulated one, namely:

$$\Phi = S^2_{ad} \big/ S^2_{rep} < \Phi_a \left(f_{ad}, f_{rep} \right).$$

At the 95 % confidence level, the following inequality holds: $\Phi_a > \Phi$ (3.75 > 2.98), so the dispersion values of the test results in different sections of the shell are significantly different.

In this connection, the samples of values in separate sections are independent, that is why statistical processing of each of them as a set of functions dependent on one parameter should be carried out separately.

Let's study the law of distribution of values of a random variable by Pearson's criterion. We calculate the number of intervals between experiments using the formula from the manual, i.e.

$$N = 1 + 3{,}32 \cdot \log(n). \tag{3.8}$$

The value of the number of intervals obtained as a result of calculations is 5.089. As we can see, the entire range of values of the random variable is divided into five intervals, so the number of degrees of freedom is four. Taking this into account, at a confidence probability of 95%, the value of Pearson's criterion $\chi^2_{кр}$ will be equal to 9.5. Let us calculate the actual values of frequencies and distributions of the theoretical random variable, for which we will make the calculation Tables 3.1 - 3.3.

At a confidence level of 95 %, the following inequality is observed: $\chi_{obs} < \chi_{cr}$ (0.84 < 9.5). Similarly, the results of the experiment to determine the deflection of the drum shell under the influence of each of the winding turns of the rope were processed. This allows us to conclude that, taking into account the Pearson criterion, there is no reason to reject the hypothesis of the normal law of distribution of random values of the shell deflection under the influence of any number of wound coils.

The graph comparing the values of statistical and theoretical density distribution of shell deflection values when the rope tension is 30 N is shown in Fig. 3.8. The number of measurements for each interval is plotted on the ordinate axis. The distribution of random variables is shown as a histogram, and the theoretical distribution as a frequency polygon.

Table 3.1.

Frequency values of random variables affecting the deflection of the shell of the MHM drum

Interval number i	Interval boundaries		Variant	Frequenc	$x_i - \overline{x}^*$	$x_{i+1} - \overline{x}^*$
	x_i	x_{i+1}	$\overline{x}_i^* = \frac{x_i + x_{i+1}}{2}$	n_i		
1	$1{,}336\text{-}10^{-4}$	$1{,}356\text{-}10^{-4}$	$1{,}346\text{-}10^{-4}$	1	-	$-3\text{-}10^{-6}$
2	$1{,}356\text{-}10^{-4}$	$1{,}376\text{-}10^{-4}$	$1{,}366\text{-}10^{-4}$	4	$-5\text{-}10^{-6}$	$-1\text{-}10^{-6}$
3	$1{,}376\text{-}10^{-4}$	$1{,}396\text{-}10^{-4}$	$1{,}386\text{-}10^{-4}$	6	$-3\text{-}10^{-6}$	$1\text{-}10^{-6}$
4	$1{,}396\text{-}10^{-4}$	$1{,}416\text{-}10^{-4}$	$1{,}406\text{-}10^{-4}$	3	$-1\text{-}10^{-6}$	$3\text{-}10^{-6}$
5	$1{,}416\text{-}10^{-4}$	$1{,}436\text{-}10^{-4}$	$1{,}426\text{-}10^{-4}$	1	$1\text{-}10^{-6}$	-
Sum of frequen.				**15**		

Table 3.2.

Distribution of values of the random variable determining the deflection of of the shell of the MHM drum

Interval number i	Normalised interval boundaries		Laplace function values		Probability of hitting the interval	Estimated frequency
	$z_i = \frac{x_i - \overline{x}}{\sigma^*}$	$z_{i+1} = \frac{x_{i+1} - \overline{x}^*}{\sigma^*}$	$\Phi(z)_i$	$\Phi(z)_{i+1}$	$P_i = \Phi(z_{i+1} - \Phi(z)_i$	$n_i' = n \cdot P_i$
1	$-\infty$	-1,751	-0,4982	-0,4601	0,038	0,572
2	-1,751	-0,583	-0,4601	-0,2203	0,24	3,596
3	-0,583	0,584	-0,2203	0,2203	0,441	6,61
4	0,584	1,751	0,2203	0,4601	0,24	3,596
5	1,751	∞	0,4601	0,4982	0,038	0,572
Sum of frequen.					**1**	**15**

Conclusions

1. The results of the experimental winding of the rope on the drum with the measurement of the deflection of the central part of its shell showed that the points reflecting the readings of the opposite sensors are almost symmetrical with respect to the centre of the circles, which makes it possible to use in further calculations the average values of the readings of the four sensors.

Table 3.3.

Results of laboratory study of the MHM parameters

Interval number i	Frequencies		$(n_i - n_i')^2$	$\frac{(n_i - n_i')^2}{n_i'}$	n_i^2	$\frac{n_i^2}{n_i'}$
	n_i	n'_i				
1	1	0,572	0,183	0,320	1	1,748
2	4	3,596	0,163	0,045	16	4,449
3	6	6,61	0,373	0,056	36	5,446
4	3	3,596	0,355	0,099	16	4,449
5	1	0,572	0,183	0,320	1	1,748
Sum of frequen.	**15**	**15**		**χ^2 = 0.84**		**17,84**

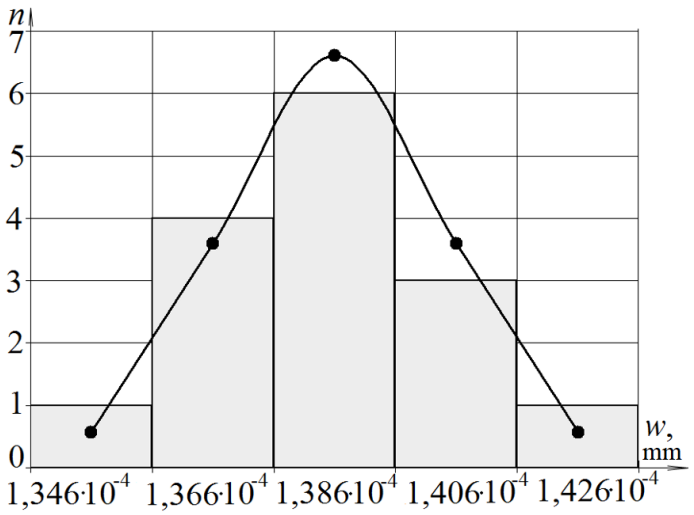

Fig. 3.8.Histogram of distribution of values of radial deflection of the drum shell of the MHM drum

2. The distribution of the values of the radial deflection of the drum shell in the sample under consideration obeys the normal law and at a confidence probability of 95 % the deviation of the confidence interval boundaries from the mathematical expectation does not exceed 3 %.

3.2.3 Determination of the deflection values of the drum shell of the cinder by calculation

As mentioned above, the main parameter measured using the laboratory setup is the deflection values in the central part of the drum shell, which will be compared

with the values of the same parameter obtained by calculation using the method of determining the rope load on the MHM drum. The use of this method involves the development and application of a physical model of the shell rigidly clamped at both ends. Fig. 3.9 shows the calculation scheme of this model.

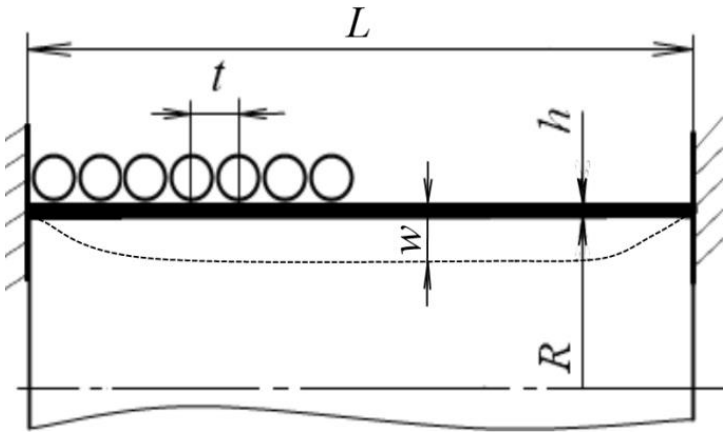

Figure 3.9. Calculation scheme of the physical model of the shell of the MHM drum: *L* - length; *R* - radius; *h* - thickness; *t* - rope winding step (in case of tight winding it is equal to its diameter *d*); *w* - shell deflection

To perform the calculations, let us divide the sheath into elementary sections, the length of each of which is equal to the rope winding step *t*. Let the number of winding turns is *K*, then the number of these sections is *K* - 1. The boundary conditions for the parameters of each section of the sheath are as follows:

$$w_1(0) = 0;\ \varphi_1(0) = 0;$$

$$\left.\begin{aligned} w_k(l) &= w_{k+1}(0); \\ \varphi_k(l) &= \varphi_{k+1}(0); \\ M_k(l) &= M_{k+1}(0); \\ Q_k(l) &= Q_{k+1}(0) - T; \end{aligned}\right\} \quad (k = 1,\ldots, K\text{-}2); \qquad (3.9)$$

$$w_{K-1}(l) = 0;\ \varphi_{K-1}(l) = 0,$$

here rope tension $T = q\text{-}R\text{-}t$; *q* is the pressure of the rope turns; *l is* the length of each section of the shell.

The equilibrium equation of the *k-th* section of the shell takes this form:

$$\frac{d^4 w_k}{dx^4} + 4\beta^4 \cdot w_k = 0, \qquad (3.10)$$

here k = 1,..., K - 2; displacement damping factor $\beta = \sqrt[4]{E \cdot h / 4 \cdot R^2 \cdot D}$; flexural stiffness of the shell $D = E \cdot h^3 / 12\left(1 - \mu^2\right)$.

Solving the equilibrium equations (3.10) and substituting the result into the boundary conditions (3.9), we obtain a system of linear algebraic equations of such dimensionality: N = 4K - 4, to determine the vector of integration constants *{C}* in matrix form, i.e.

$$[A]\text{-}\{C\}=\{B\}, \qquad (3.11)$$

where [*A*] is the matrix of the system, the values of its components are presented in Table 3.4; *{B}* is the vector of forces.

The suppleness matrix is defined from the following expression:

$$[W] = [K]\text{-}[A]^{-1} \text{-}[G, \qquad (3.12)$$

where specific radial force $G_{i,j}$ = ; $\delta_{i,8j-2} \cdot F / R$ $\delta_{i,8j-2}$ is the Kronecker symbol; unit load F = 1 N; shell deflections $K_{i,j} = C_{4k-2} + C_{4k}$, with $k = 2j$, $1 \le i \le K$, $1 \le j \le N$.

The further algorithm for calculating the shell deflection values does not differ from that used in the mathematical model (see Section 2.3.2).

For convenience of substantiating the adequacy of the models, it is sufficient to obtain the dependence of deflections only in the middle section of the shell on the number of rings to be put on.

When winding the *k-th* coil, the value of the resulting deflection is determined by the following equation:

$$u_{\frac{K}{2},k} = \sum_{j=1}^{k} P_{j,k} \cdot W_{i,j} \ , \qquad (3.13)$$

where $P_{j,k}$ is the tension in the *j-th coil* when winding the *k-th coil*.

Fig. 3.10 shows the graphs of variation of the shell deflection values obtained by calculation using the developed method at different values of rope tension. As we can see, the curves of the deflection of the central part of the shell can be divided into three sections: 1 - zero (1 - 22nd turns), which reflects the winding of the rope near the termination, which practically does not cause deflection; 2 - transitional (22 - 37th turns) - the situation when the deflection value is proportional to the number of turns; 3 - the section of the curve, which shows the steady deflection (37 - 66th turns), here the process does not depend on the number of turns.

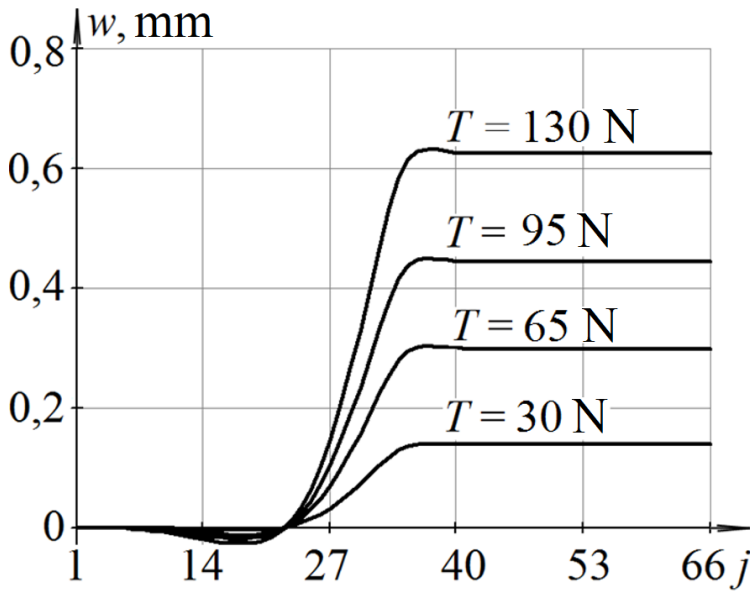

Fig. 3.10. Curves of dependence of deflection in the central part oftheshell drum on the number of winding *j*

Conclusion

1. Using the proposed method, it was possible to determine the values of the radial deflection of the drum shell under the influence of the rope load. The rope tension was varied in the range of 30...130 N, and the value of the maximum deflection was 0.14...0.63 mm.

3.2.4 Estimation of calculation error

The objectives of our study imply analysing the values of the radial deflection of the drum shell as a consequence of the rope winding on it. The values obtained

by calculation (Section 3.2.3) and empirical method (Section 3.2.2) were considered and statistically processed. On their basis, curves reflecting the values of the shell

Table 3.4.

Values of the values contained in the rope winding system matrix

Boundary conditions	Components of the matrix [A]
$w_1(0) = 0$; $\varphi_1(0) = 0$	$A_{1,1} = 0;\ A_{1,2} = -D;\ A_{1,3} = 0;\ A_{1,4} = -D;$ $A_{2,1} = -D \cdot \beta;\ A_{2,2} = -D \cdot \beta;\ A_{2,3} = -D \cdot \beta;\ A_{2,4} = D \cdot \beta;$
$w_k(l) = w_{k+1}(0)$; $\varphi_k(l) = \varphi_{k+1}(0)$;	$A_{4k-1,4k-3} = D \cdot e^{\beta \cdot l} \cdot \sin(\beta \cdot l);\ A_{4k-1,4k-2} = D \cdot e^{\beta \cdot l} \cdot \cos(\beta \cdot l);$ $A_{4k-1,4k-1} = D \cdot e^{-\beta \cdot l} \cdot \sin(\beta \cdot l);\ A_{4k-1,4k} = D \cdot e^{-\beta \cdot l} \cdot \cos(\beta \cdot l);$ $A_{4k-1,4k+1} = 0;\ A_{4k-1,4k+2} = -D;\ A_{4k-1,4k+3} = 0;\ A_{4k-1,4k+4} = -D;$ $A_{4k,4k-3} = D \cdot \beta \cdot e^{\beta \cdot l} \cdot (\cos(\beta \cdot l) + \sin(\beta \cdot l));$ $A_{4k,4k-2} = D \cdot \beta \cdot e^{\beta \cdot l} \cdot (\cos(\beta \cdot l) - \sin(\beta \cdot l));$ $A_{4k,4k-1} = D \cdot \beta \cdot e^{-\beta \cdot l} \cdot (\cos(\beta \cdot l) - \sin(\beta \cdot l));$ $A_{4k,4k-2} = -D \cdot \beta \cdot e^{-\beta \cdot l} \cdot (\cos(\beta \cdot l) + \sin(\beta \cdot l));$
$M_k(l) = M_{k+1}(0)$; $Q_k(l) = Q_{k+1}(0)$;	$A_{4k,4k+1} = -D \cdot \beta;\ A_{4k,4k+2} = -D \cdot \beta;\ A_{4k,4k+3} = -D \cdot \beta;$ $A_{4k,4k+2} = D \cdot \beta;$ $A_{4k+1,4k-3} = 2 \cdot \beta^2 \cdot D \cdot e^{\beta \cdot l} \cdot \cos(\beta \cdot l);$ $A_{4k+1,4k-2} = -2 \cdot \beta^2 \cdot D \cdot e^{\beta \cdot l} \cdot \sin(\beta \cdot l);$ $A_{4k+1,4k-1} = -2 \cdot \beta^2 \cdot D \cdot e^{-\beta \cdot l} \cdot \cos(\beta \cdot l);$ $A_{4k+1,4k} = 2 \cdot \beta^2 \cdot D \cdot e^{-\beta \cdot l} \cdot \sin(\beta \cdot l);$ $A_{4k+1,4k+1} = -(2 \cdot \beta^2 \cdot D);\ A_{4k+1,4k+2} = 0;$ $A_{4k+1,4k+3} = 2 \cdot \beta^2 \cdot D;\ A_{4k+1,4k+4} = 0;$ $A_{4k+2,4k-3} = -2 \cdot D \cdot \beta^3 \cdot e^{\beta \cdot l} \cdot (\cos(\beta \cdot l) - \sin(\beta \cdot l));$ $A_{4k+2,4k-2} = 2 \cdot D \cdot \beta^3 \cdot e^{\beta \cdot l} \cdot (\cos(\beta \cdot l) + \sin(\beta \cdot l));$ $A_{4k+2,4k-1} = -2 \cdot D \cdot \beta^3 \cdot e^{-\beta \cdot l} \cdot (\cos(\beta \cdot l) + \sin(\beta \cdot l));$ $A_{4k+2,4k} = -2 \cdot D \cdot \beta^3 \cdot e^{-\beta \cdot l} \cdot (\cos(\beta \cdot l) - \sin(\beta \cdot l));$ $A_{4k+1,4k+1} = 2 \cdot \beta^3 \cdot D;\quad A_{4k+2,4k+2} = -2 \cdot \beta^3 \cdot D;$ $A_{4k+2,4k+3} = 2 \cdot \beta^3 \cdot D;\quad A_{4k+2,4k+4} = 2 \cdot \beta^3 \cdot D;$

$w_{K-1}(l) = 0$, $\varphi_{K-1}(l) = 0$	$A_{N-1,N-3}=D\cdot e^{\beta\cdot l}\cdot\sin(\beta\cdot l)$; $A_{N-1,N-2}=D\cdot e^{\beta\cdot l}\cdot\cos(\beta\cdot l)$; $A_{N-1,N-1}=D\cdot e^{-\beta\cdot l}\cdot\sin(\beta\cdot l)$; $A_{N-1,N}=D\cdot e^{-\beta\cdot l}\cdot\cos(\beta\cdot l)$; $A_{N,N-3}=D\cdot\beta\cdot e^{\beta\cdot l}\cdot(\cos(\beta\cdot l)+\sin(\beta\cdot l))$; $A_{N,N-2}=D\cdot\beta\cdot e^{\beta\cdot l}\cdot(\cos(\beta\cdot l)-\sin(\beta\cdot l))$; $A_{N,N-1}=D\cdot\beta\cdot e^{-\beta\cdot l}\cdot(\cos(\beta\cdot l)-\sin(\beta\cdot l))$; $A_{N,N}=-D\cdot\beta\cdot e^{-\beta\cdot l}\cdot(\cos(\beta\cdot l)+\sin(\beta\cdot l))$;

radial deflection were constructed (Fig. 3.11). In the figures, the solid line shows the theoretical results obtained using the author's calculation method. The experimental results are labelled as a set of dots. Comparison of both curves confirms a high degree of proximity of calculated and real (established by measurements) values of the main indicators. As we can see, all calculated deflection values corresponding to different tension values fall within the confidence interval of the experimental values with a probability of 95 %.

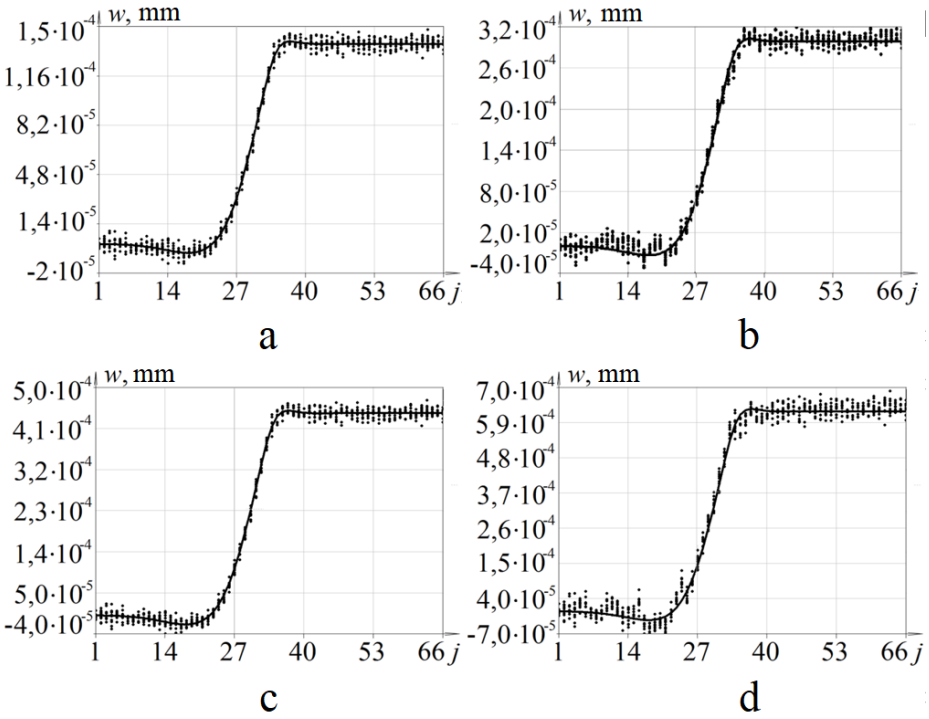

Fig. 3.11. Curves of dependence of the values of radial deflection of the shell on the number of the coil wound on the drum, if the tension force is:

a - 30 N; *b* - 65 N; *c* - 95 N; *d* - 130 N

To estimate the error of calculation of the shell deflection values, let us compare the average values of this parameter at the moment of winding of 40...66th turns (this is the working range), obtained experimentally and theoretically, in calculation for the values of the rope tension force and 90 % confidence level (Table 3.5).

The table shows that with a confidence level of 90 % the discrepancy of values does not exceed 7 %.

Our evaluations confirm the reliability of the proposed method, since there is a high degree of closeness between the calculated and experimental values of its main index. The error in determining the deflection of the shell at successive winding of the rope in comparison with the physical experiment is not higher than 7 %.

Table 3.5.

Data for the study of the deflection of the MHM drum shells

Rope tension force, N	Theoretical deflection value, mm	Experimental deflection value, mm	Uncertainty, %
30	1,291	1,386	6,8
65	2,912	3,075	5,3
95	4,115	4,344	5,4
130	6,148	6,432	4,4

3.3 Justification of the choice of a set of design parameters research on the example of a drum of the lifting machine TsR - 6×3,4/0,6

First, let's determine the design loads on the wedged part of the MHM drum TsR - 6×3,4/0,6 (see Fig. 3.12).

In a method of the solution, it is provided that the rope is wound on a cylindrical drum.

In the solution we use the initial data given in Table 3.6.

Following the methodology outlined in the paper, we plot the dependence of the change in the rope tension force on the position of the lifting vessels in the shaft

according to the five-period tachogram of skip lifting-descent.

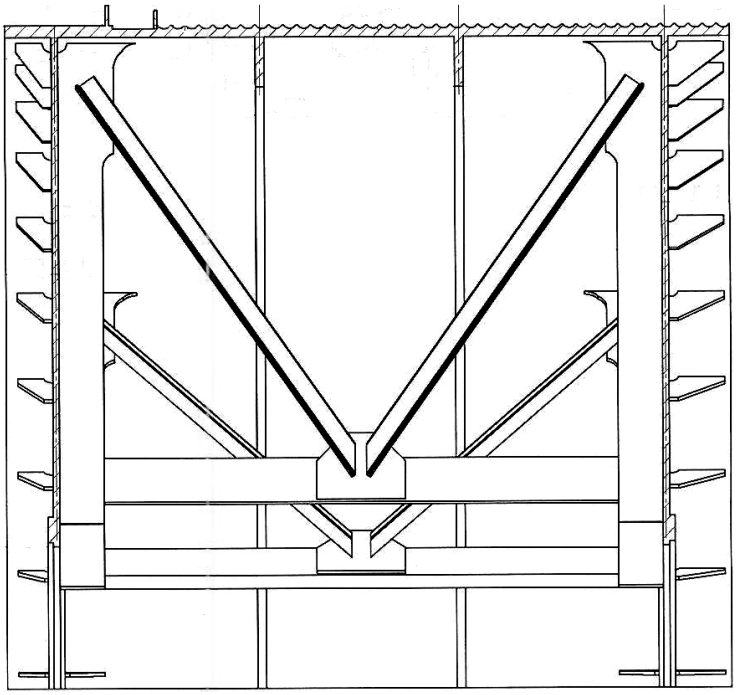

Fig. 3.12. Sketch of the jammed part of the MHM drum of type TsR-6×3,4/0,6

Table 3.6

Technical characteristics of MHM type TsR - 6×3,4/0,6

Passport details		Parameters of the jammed part of the drum	
Lift height	697 м	Number of turns of working rope N_w	34
Skip weight	12000kg	Number of turns of idle rope N_x	34
Rock mass	15300kg	Number of free grooves N_f	5
Counterweight	19650kg	Number of friction turns N_{fr}	3
Rope diameter (GOST 7669-80)	57 mm	Total number of grooves N	44

Let's consider two cases of rope winding sequence: A - rope with a load is wound first on the slack part of the drum and then on the slack part; B - the same rope is wound only on the slack part, and the idle rope is wound on both parts of the drum, starting from the slack part.

The working rope winding starts with the 1st coil on the rewinding part of the

drum (winding variant A). Since in the framework of this task the wedged part of the drum is of interest, we designate the first number of the working rope coil wound on its first groove.

Then tension in the 1st turn of the working rope (at this stage the vessel moves in curves)

$$T_1^* = \left(M_r - 3M_v + M_s + M_l\right) \cdot \left(g + a_{0,7}\right), \tag{3.14}$$

where M_r - mass of one rope branch; mass of one rope coil M_v = ρ-π-D_d linear mass of one metre of rope; D_d - diameter along the drum winding axis; M_{ves} - mass of lifting vessel; M_l - mass of load (rock); g - acceleration of free fall; $a_{0,7}$ - acceleration of deceleration when moving along the curve.

Tension of the working coils at the moment of lifting the load

$$T_i^* = \left(M_r - \left(i + 2\right) \cdot M_v + M_{ves} + M_l\right) \cdot g, \tag{3.15}$$

here are numbers of working turns at load lifting i = 2...30.

Tension force in the rope from 31st to 33rd turns (vessel enters unloading curves)

$$T_i^* = \left(M_r - \left(i + 2\right) \cdot M_v + M_{ves} + M_l\right) \cdot \left(g - a_{0,7}\right), \tag{3.16}$$

where the numbers of turns corresponding to the beginning of vessel movement along the curve, i = 31...33; $and_{0,7}$ is the increase of deceleration at vessel entry into unloading curves.

Tension force in the 34th turn (vessel moves along the curve)

$$T_{34}^* = \left(M_r - 36 \cdot M_v + M_{ves} + M_l\right) \cdot \left(g - a_{0,3}\right). \tag{3.17}$$

The working rope is not wound on the drum grooves from 35th to 44th.

Winding of the idle rope (case B) takes place from the 44th coil on the wedged part of the drum. The numbers of the coils and the grooves on which they are wound

coincide.

Friction coils are 44...40. We assume that the tension in them is distributed according to the linear law, and in 44th its force is equal to zero, and in 43rd is 4/5 of the tension, which is observed in the sixth working coil of the rope. The described process reflects the magnitude of the rope tension change in the friction spiral turns according to Euler's law. HThroughout the entire cycle of lifting/lowering the vessel, the tension force in these coils does not change, i.e.

$$T_i^{**} = T_{39}^{**} \cdot e^{-\mu\gamma} \; S_i = S_б \cdot e^{-\mu\gamma}, \tag{3.18}$$

where the numbers of friction turns i = 43...40; T_{39}^{**} - tension in the 39th turn; μ - coefficient of friction of the rope on the drum surface; γ - central angle of the drum, defining the considered section of the rope and counted from the point of its run-up (the first turn).

Tension in the 39th turn (at this stage the vessel moves along the curve)

$$T_{39}^{**} = \left(M_r + M_c\right) \cdot \left(g + a_{0,3}\right), \tag{3.19}$$

where M_c is the mass of the counterweight.

Rope tension force in turns 38 to 36 (corresponds to the vessel's exit from the unloading curve)

$$T_i^{**} = \left(M_r + M_c - \left(39 - i\right)M_v\right) \cdot \left(g + a_{0,7}\right), \tag{3.20}$$

where i = 38...36.

Tension in working rope coils during skip descent

$$T_i^{**} = \left(M_r + M_c - \left(39 - i\right)M_v\right) \cdot g\,, \tag{3.21}$$

where i = 35...7.

Rope tension force between 6th and 4th coil (vessel enters unloading curves)

$$T_i^{**} = \left(M_r + M_c - \left(39 - i\right)M_v\right) \cdot \left(g - a_{0,7}\right), \qquad (3.22)$$

here i = 6...4.

Tension force in the 3rd turn of the rope (vessel moves along the curve)

$$T_3^{**} = \left(M_r + M_c - 36 \cdot M_v\right) \cdot \left(g - a_{0,3}\right). \qquad (3.23)$$

The idle rope is not wound on the first and second grooves of the drum.

According to the results of the study of the MHM type TsR - 6×3,4/0,6 in Fig. 3.13 shows the diagram of tension forces of working and idle ropes when they are wound on the *k-th* groove of the wedged drum. The data calculated with the help of expressions (3.14 - 3.23) were used in the construction of the diagram. Negative numbers of groove numbers correspond to winding the rope on the slip drum.

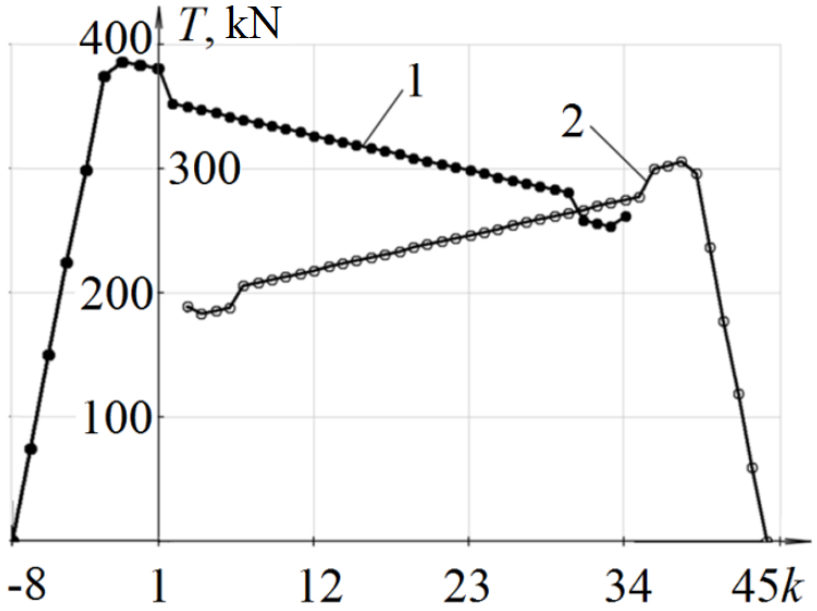

Fig. 3.13. Diagram of dependence of the tension force of the working (1) and idle (2) ropes on the drum on the number of the groove *k, on* which they are wound up

To determine the design loads on the MHM drum, we apply the method developed in Section 2.5, which involves solving several problems. Let's consider each of them.

1) Determination of stiffness parameters.

First we calculate the reduction factor using expression (2.55), i.e.

$$k_{\text{p}} = 1{,}347 - 0{,}5 \cdot \varepsilon - 0{,}295 \cdot \zeta + 0{,}61 \cdot \varepsilon^2 + 0{,}016 \cdot \varepsilon \cdot \zeta + \\ + 0{,}074 \cdot \zeta^2 - 0{,}195 \cdot \varepsilon^3 - 0{,}021 \cdot \varepsilon^2 \cdot \zeta + 0{,}007 \cdot \varepsilon \cdot \zeta^2 - 0{,}006 \cdot \zeta^3 = 0{,}887,$$

where ε and ζ are defined by formulae (2.57).

Then we calculate the stiffness values of the averaged shell using equations (2.56) and (2.45), viz:

$$D_{\text{o}} = k_{\text{p}} \cdot \frac{E \cdot \tau}{\left(1 - \mu^2\right)} \cdot \left(\int_0^{\tau} \left(\frac{h^3}{96} + \frac{f_z(x) \cdot h^2}{16} + \frac{{f_z}^2(x) \cdot h}{8} + \frac{{f_z}^3(x)}{12} \right)^{-1} dx \right)^{-1} = 1{,}4 \cdot 10^6 \,\text{N} \cdot \text{m};$$

$$B_{\text{o}} = \frac{E}{\tau} \int_0^{\tau} \left(\frac{h}{2} + f_z(x) \right) dx = 9{,}44 \cdot 10^9 \,\frac{\text{N}}{\text{m}}.$$

Applying expressions (2.46), (2.47), we find the values of the modulus of elasticity of the structural-orthotropic shell and Poisson's ratio according to the directions:

- axial

$$E_1 = \frac{12D\left(1 - \mu^2\right)}{h^3 + \frac{12D}{E_2}} = 9{,}39 \cdot 10^{10} \,\frac{\text{N}}{\text{m}^2}; \qquad \mu_1 = \mu = 0.3;$$

- county

$$E_2 = B_{\text{o}} / h = 1{,}72 \cdot 10^{11} \,\text{Н/м}^2; \; \mu_2 = \mu \cdot E_1 / E_2 = 0{,}164 \quad .$$

The dimensionless values of annular λ and bending χ stiffnesses of the frontal *are* calculated using formulas (2.59) - (2.62), namely:

$$\lambda = E \cdot h_l \cdot \left(54{,}5 - 22{,}3 \cdot \rho + 3 \cdot \rho^2\right) = 1{,}5 \cdot 10^9 \,\text{N/m};$$

$$\chi = \frac{E \cdot h_l^3}{12 \cdot \left(1 - \mu\right)} \cdot \left(0{,}71 - 0{,}041 \cdot \rho - 2{,}35 \cdot \delta - 0{,}065 \cdot \rho^2 - 7{,}1 \cdot \rho \cdot \delta + 224{,}5 \cdot \delta^2\right) = 8{,}84 \cdot 10^6 \,\text{N} \cdot \text{m},$$

To determine the annular and bending stiffness of the reinforcements, we apply expressions (2.63) and (2.64), i.e.

$$\lambda_{\text{br}} = \frac{E \cdot h_{\text{br}} \cdot \left(b_{\text{br}}^2 - a_{\text{br}}^2\right)}{(1+\mu)\cdot\left(a_{\text{br}}^2 \cdot b_{\text{br}} + (1+2\mu)\cdot b_{\text{br}}^3\right)} = 2,4\cdot 10^8 \frac{\text{N}}{\text{m}};$$

$$\chi_{\text{br}} = \frac{E \cdot h_{\text{br}}^3 \cdot \left(b_{\text{br}}^2 - a_{\text{br}}^2\right)\cdot\left(1-\mu^2\right)}{12(1-\mu)\cdot\left(b_{\text{br}}^3 \cdot (1-\mu) + b_{\text{br}} \cdot a_{\text{br}}^2 \cdot (1+\mu)\right)} = 6,72\cdot 10^5 \,\text{N}\cdot\text{m};$$

$$\lambda_{\text{lf}} = \frac{E \cdot h_{\text{lf}} \cdot \left(b_{\text{lf}}^2 - a_{\text{lf}}^2\right)}{(1+\mu)\cdot\left(a_{\text{lf}} \cdot b_{\text{lf}}^2 + (1+2\mu)\cdot a_{\text{lf}}^3\right)} = 3,15\cdot 10^7 \frac{\text{N}}{\text{m}};$$

$$\chi_{\text{lf}} = \frac{E \cdot h_{\text{lf}}^3 \cdot \left(b_{\text{lf}}^2 - a_{\text{lf}}^2\right)\cdot\left(1-\mu^2\right)}{12(1-\mu)\cdot\left(a_{\text{lf}}^3 \cdot (1-\mu) + b_{\text{lf}}^2 \cdot a_{\text{lf}} \cdot (1+\mu)\right)} = 4,65\cdot 10^4 \,\text{N}\cdot\text{m};$$

$$\lambda_{\text{rf}} = \frac{E \cdot h_{\text{rf}}^3 \cdot \left(b_{\text{rf}}^2 - a_{\text{rf}}^2\right)}{(1+\mu)\cdot\left(a_{\text{rf}} \cdot b_{\text{rf}}^2 + (1+2\mu)\cdot a_{\text{rf}}^3\right)} = 2,88\cdot 10^7 \frac{\text{N}}{\text{m}};$$

$$\chi_{\text{rf}} = \frac{E \cdot h_{\text{rf}}^3 \cdot \left(b_{\text{rf}}^2 - a_{\text{rf}}^2\right)\cdot\left(1-\mu^2\right)}{12(1-\mu)\cdot\left(a_{\text{rf}}^3 \cdot (1-\mu) + b_{\text{rf}}^2 \cdot a_{\text{rf}} \cdot (1+\mu)\right)} = 3,32\cdot 10^4 \,\text{N}\cdot\text{m}.$$

2) Construction of the pliability matrix of the MHM drum shell.

To automate the process of calculating the coefficients of the ductility matrix, the solution of equation (2.21) was programmed in the MathCAD application package, where the following sequence of operations is provided: the system matrix [*A*] is formed by substituting the general solution into the boundary conditions; the vector of forces {B} of dimension *N is* determined, as well as the vectors of integration constants *{C}*; the matrix [*W*] is constructed.

To verify the accuracy of the described model, the components of the ductility matrix were compared with experimental data. An example is presented in Fig. 3.14, a diagram of the change in the drum shape under the action of a unit specific force applied to its fifteenth groove. It was observed that the RMS error in determining the ductility matrix using the proposed mathematical model does not exceed 2.4 %.

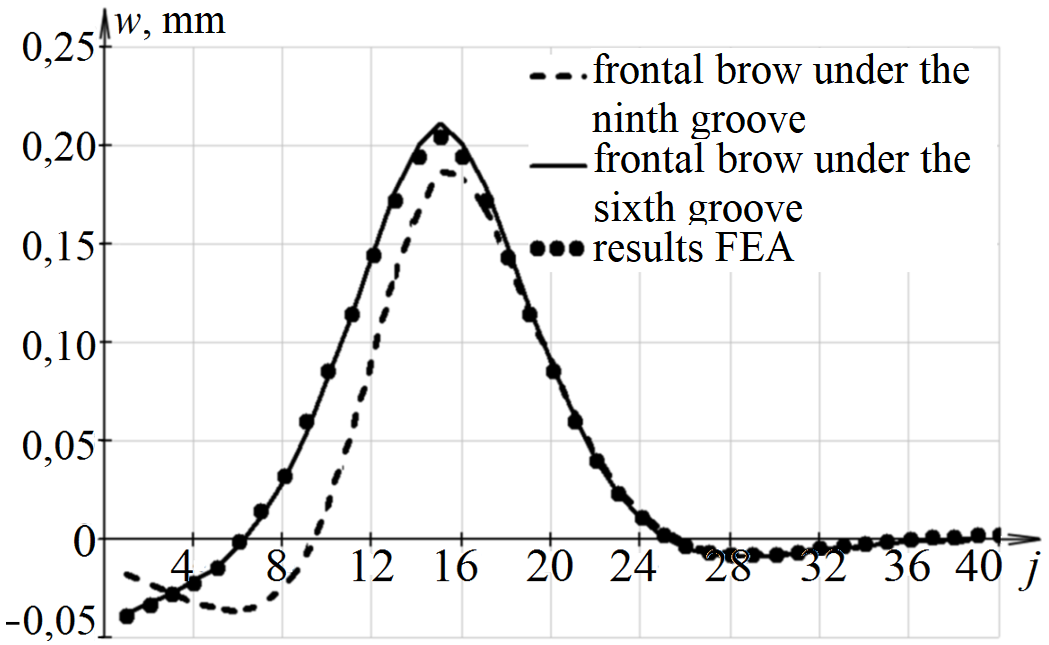

Fig. 3.14. Graph of change in the shape of the drum shell

As shown in Fig. 3.14, the maximum deflection decreased by 11.5 % as a result of moving the shell lobe from the sixth groove to the ninth groove. To perform such a study in the manner previously proposed in this paper would require more than a hundred computational experiments and the use of a full finite element model of the drum.

As an example, Fig. 3.15 shows graphs of dependence of $W/v_к$ on parameters *i* and *j*, where

$$v_к = R^2/B \cdot t .$$

In order to visualise the dependence of the pliability matrix on the deformation of the *j-th* groove under the influence of the circumferential force on the *i-th* groove, we construct a diagram (Fig. 3.16).

As can be seen in Fig. 3.16, in the diagram of the ductility matrix several sections corresponding to different stress states of the MHM drum can be distinguished.

Once again, we recall that the visualisation of the process indicates the maximum pliability of the cantilevered section of the MHM drum shell.

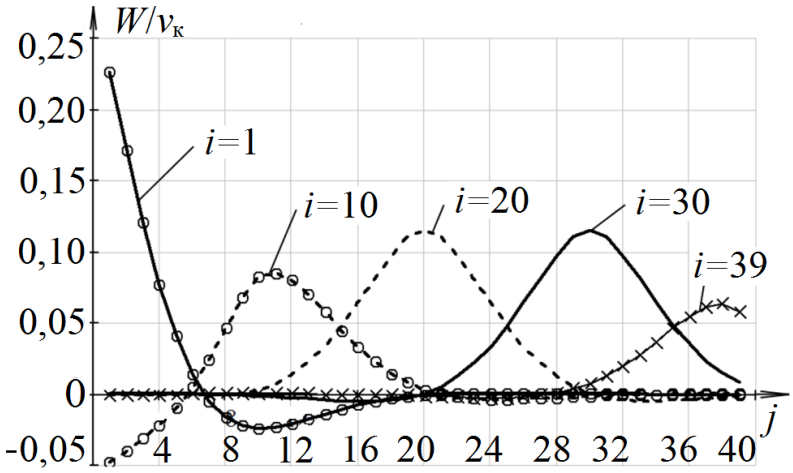

Fig. 3.15. Graph of change of the shape of the drum MHM type TsR - 6×3,4/0,6

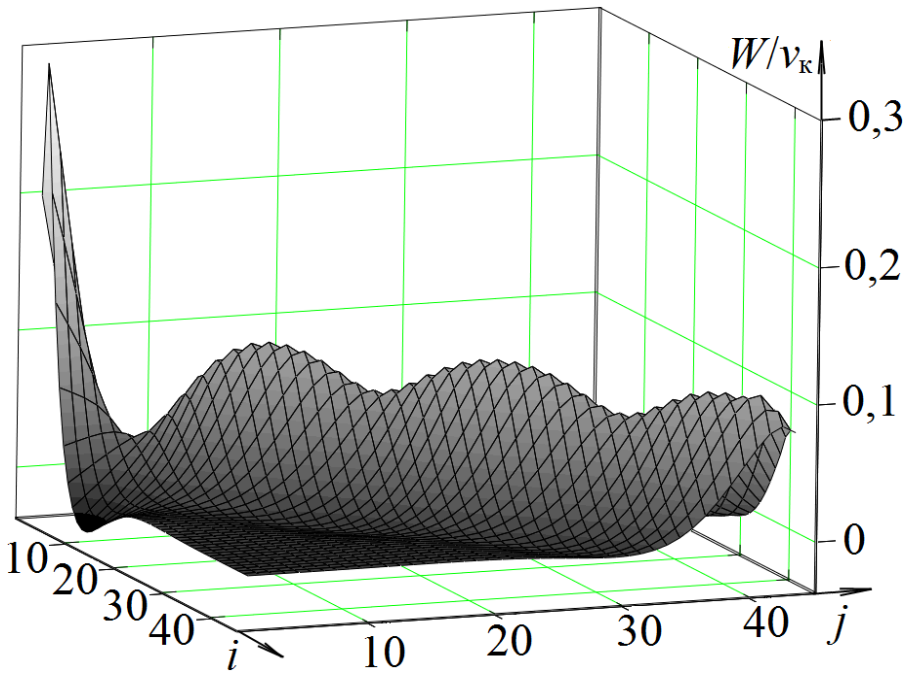

Fig. 3.16. Diagram of the pliability matrix of the MHM drum of type TsR-6×3,4/0,6

3) Determination of the design loads acting on the shell of the MHM drum.

Calculation of radial rope pressure on the drum was performed using the following methods: K.S. Zabolotny (here the loosening of the tension of the rope turns was not taken into account), NKMZ (assuming that the loosening of the tension of the rope turns across the width is constant due to the deformation of the unsupported drum) and NSU (the loosening of the rope turns during the deformation of the supported drum was taken into account).

According to the results of calculations, the graphs reflecting the pressure distribution over the width of the wedged drum depending on the number of groove, at such stages of the MHM operation were constructed: the beginning of the loaded skip lifting (Fig. 3.17), the average position of the skip in the shaft (Fig. 3.18), the end of the skip lifting (Fig. 3.19).

Let us analyse in detail the first case (Fig. 3.17), when the loaded rope is in the barrel and the drum takes only the radial pressure coming from the coils of the idle rope.

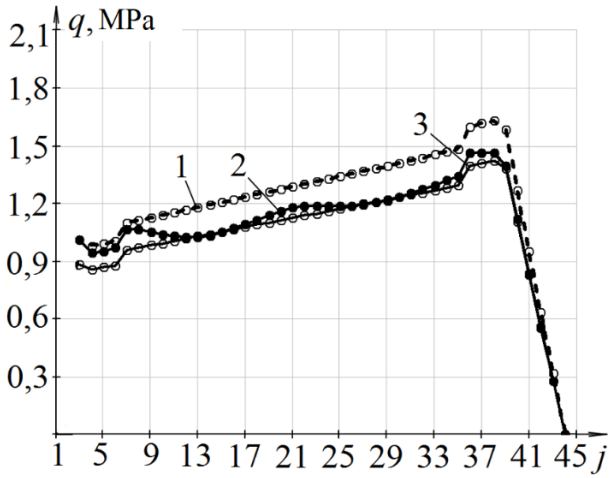

Fig. 3.17. Radial pressure distribution curves of the idle rope over the width of the wedged drum (at the beginning of the working rope lifting).
results of calculations according to the methods:1 - K.S. Zabolotny, 2 - NMU, 3 - NKMZ are used for construction

By analysing curve 1, some patterns can be observed. The winding of the idle rope starts from the 39th groove of the drum. And on the 40th - 44th winding coils of friction of this rope, while the load coming from them increases to the value of rope pressure in the 39th groove according to the linear law. This can be explained by the accelerated movement of the counterweight at the beginning of the rope lift. In the section of the drum from the 35th to the 7th groove, the rope is wound at a constant speed and the load decreases linearly with the formation of each coil due to the decreasing length of the rope plumb. At the 3rd to 7th groove there is a decrease in pressure caused by the counterweight braking.

The radial load corresponding to curve 3 is equal to that reflected by curve 1, only multiplied by the correction factor for rope pressure reduction ($\psi_0 = 0.873$).

The analysis of curve 2 allows us to formulate certain regularities. Thus, due to the high radial stiffness of the brow in its vicinity, the rope pressure value approaches the values corresponding to curve 1. When the rope is removed from the lobes or spandrels by eight turns, the radial pressure is reduced by 15 % to the values reflected in curve 3. Since the radial stiffness of the spars is much lower than that of the lobes, the radial pressure in the adjacent section occupies an intermediate position between the parameter values corresponding to curves 1 and 3 (approximately 0.9 of the values forming curve 1).

Let's analyse the second case we have chosen for calculation (the stage of the skip mid-lift). Here, on the left side of the jammed drum the working rope is wound on the left side of the drum, and on the right side the idle rope is left, so that the first rope is wound from the 1st to the 18th groove, and the second one from the 24th to the 44th groove, so that there are five free grooves between them (see Fig. 3.18).

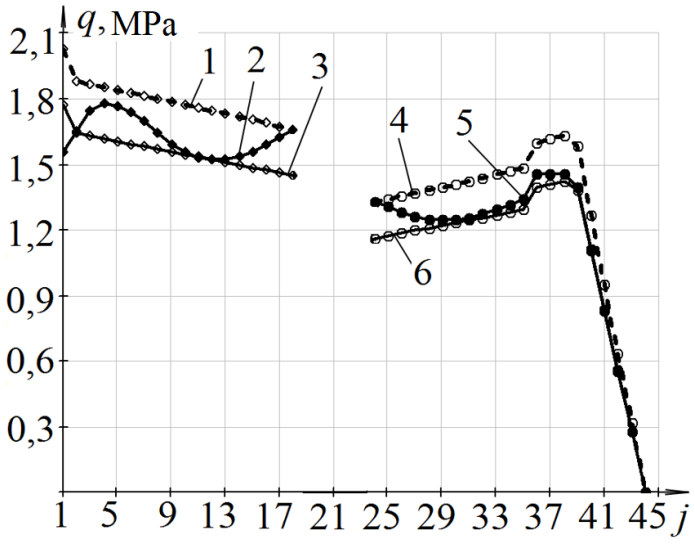

Fig. 3.18. Radial pressure distribution curves of coiled ropes (1, 2, 3 - working; 4, 5, 6 - idle) across the width of the wedged drum in the middle of the loaded skip liftingFor construction we used results of calculations according to the following methods: K.S. Zabolotniy - 1, 4; NMU - 2, 5; NKMZ - 3, 6

Curves 4 and 6 in Fig. 3.18 are parts of curves 1 and 3 in Fig. 3.17.

Curve 1 (Fig. 3.18) corresponds to the forces exerted by the coils of the working rope. Increase in radial pressure of the rope on the 1st groove is connected with accelerated movement of the skip at the beginning of its lifting.

In the section from the 2nd to the 18th groove, the rope is wound at a constant speed and the load decreases linearly during the formation of each coil due to the decreasing length of the rope plumbness.

The radial load corresponding to curve 3 is similar to that illustrated by curve 1, but multiplied by a correction factor for rope pressure reduction ($k = 0.873$).

Calculation performed according to the NSU method (curve 2 in Fig. 3.18) showed that the maximum radial pressure relaxation occurs in the first groove of the drum and is 30 %. This is due to the fact that the first groove is located at the free edge of the shell where maximum ductility is observed. The spoon between the grooves increases the stiffness of the shell, so that the radial pressure on the fourth and fifth grooves, to the left of the spoon, is maximised and is weakened by only 4 %. Under the action of the wound coils, the radial pressure exerted by the working rope in the section from the 5th to the 17th groove is weakened by about 15 %, while the load exerted by the idle rope, already from the 3rd to the 17th groove, is reduced by 13.2 %. The results of calculations carried out according to the method described by us (as opposed to those obtained by applying the methods of K.S. Zabolotny and NKMZ), allow us to draw important conclusions. At the rope winding section (see Fig. 3.18, curve 2, reflecting the pressure in the 18th groove) and at the place of its winding (see curve 5 - in the 24th groove, respectively), the radial pressure does not weaken. This can be explained by the absence of rope coils between both branches on the drum. And in the neighbouring coils of the winding and unwinding ropes the radial pressure decreases according to the exponential function.

Let's analyse the third case of calculation (stage of skip lifting completion), when the working rope is wound on the left part of the jammed drum, and on the right part of the drum the friction coils of the idle rope are left, i.e., the first of them

is wound from the 1st to the 34th groove, and the second one from the 40th to the 44th groove, and there are five free grooves between the ropes.

The shape of curves 1 and 3 in Fig. 3.19 corresponds to the shape of curves 1 and 3 in Fig. 3.18 with the peculiarity that the latter reflect the radial pressure weakening occurring in the section from the 31st to the 34th drum groove associated with the skip braking at the end of lifting.

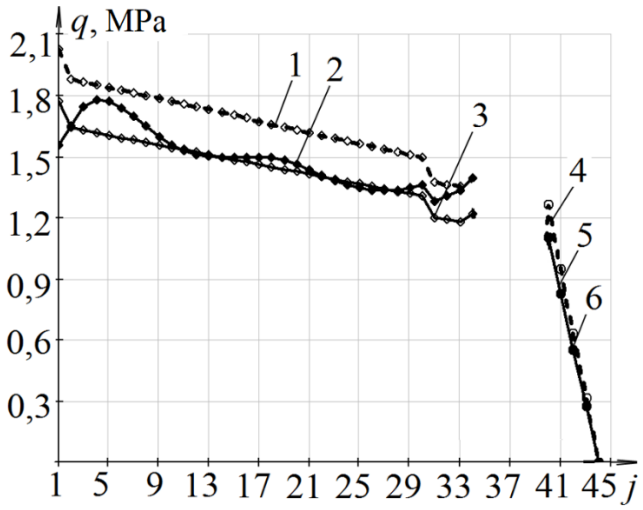

Fig. 3.19. Radial pressure distribution curves of coiled ropes (1, 2, 3 - working; 4, 5, 6 - idle) across the width of the wedged drum at the end of the loaded skip lifting. The results of calculations according to the methods of: K.S. Zabolotny - 1, 4; NSU - 2, 5; NKMZ - 3, 6 were used in the construction.

The results of the calculation performed using the NSU method showed that the changes in the shape of curve 2 in Fig. 3.19 (corresponding to the pressure in the frontal area) are similar to the changes in the shape of curve 2 in Fig. 3.18. Thus, in the area of the unsupported drum shell, the radial pressure is weakened to a value that corresponds to curve 3 by 16 %. At the same time, near the spandrels, the radial pressure decreases by 11 %.

The curves in Figs. 3.17, 3.18, 3.19 corresponded to the forces occurring when the working rope was wound on the sixth (k = -3), eighteenth (k = 18) and 34th groove (k = 34). Fig. 3.20 shows a graph of the force distribution as a function of two

variables: *k* is the number of the drum groove on which the coil is wound and *j is the* number of the groove in which the resulting pressure is determined.

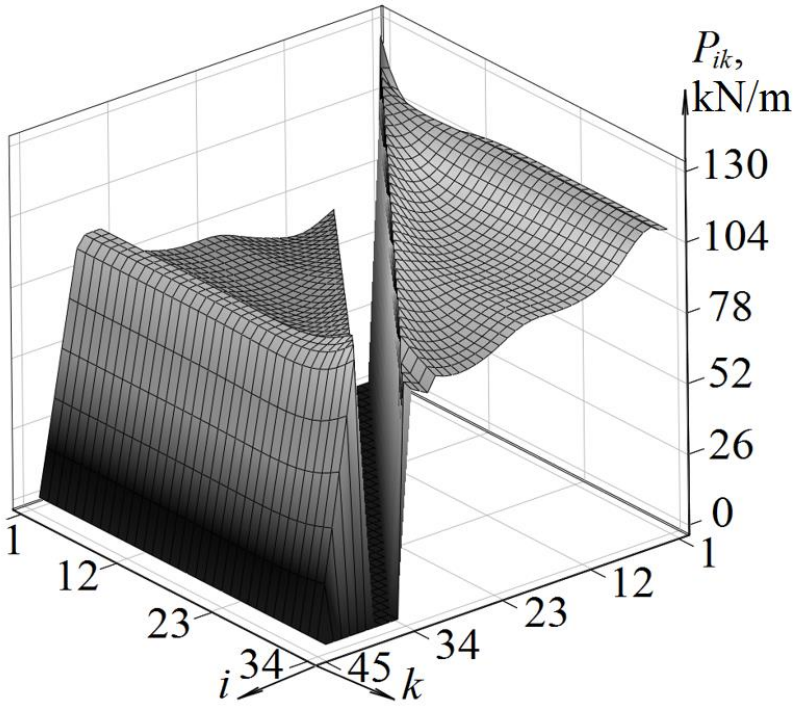

Fig. 3.20. Diagram of dependence of the linear load $P_{i,k}$ on the shell of *the* MHM drum on the parameters *i* and k

As can be seen from the graph in Fig. 3.20, the rope load occurring in the section from the 4th to the 6th coil (frontal zone) reaches the maximum value. This is due to the increased radial stiffness of the brow and the amount of tension in the upper section of the working rope. The character of the radial pressure change due to the location (number) of the winding *k-th coil*, when the skip occupies an intermediate position in the shaft, corresponds to the character of curves 4 and 5 in Fig. 3.19. 3.19. The necessity to determine the values of radial pressure corresponding to the full range of changes in the number of the winding *k-th coil is* caused by the fact that it is necessary to detect the most dangerous condition, at which maximum stresses occur in the drum shell. For example, in order to analyse the effect of a spar on the performance of a structure, it is necessary to test the spar under maximum load conditions.

4) Determination of stresses in the structural-orthotropic shell of the drum.

Let us formulate how the maximum averaged stresses occurring in the structural-orthotropic shell depend on the number of the *i-th winding coil*. For this purpose, we first describe the expressions for determining the deflection and curvature at the *k-th* section of the composite structural-orthotropic shell, namely:

$$w_k(x)=e^{\beta_k\cdot x}\cdot\left(C_{4k-3}\cdot\sin(\beta_k\cdot x)+C_{4k-2}\cdot\cos(\beta_k\cdot x)\right)+e^{-\beta_k\cdot x}\cdot\left(C_{4k-1}\cdot\sin(\beta_k\cdot x)+C_{4k}\cdot\cos(\beta_k\cdot x)\right);$$

$$\kappa_k(x)=-2\cdot\beta_k^2\cdot\left[\begin{array}{l}\left(C_{4k-1}\cdot e^{-\beta_k\cdot x_k}+C_{4k-3}\cdot e^{\beta_k\cdot x_k}\right)\cdot\cos(\beta_k\cdot x_k)+\\+\left(C_{4k-2}\cdot e^{\beta_k\cdot x_k}+C_{4k}\cdot e^{-\beta_k\cdot x_k}\right)\cdot\sin(\beta_k\cdot x_k)\end{array}\right],$$

here is the displacement damping coefficient $\beta_k=\sqrt[4]{B_k/4\cdot R^2\cdot D_k}$; R is the shell radius; x_k is the length of the *k-th* beam.

Proceeding from the fact that between the two grooves of the profiled shell two sections of the composite structural-orthotropic shell are placed, we conclude that there is a relationship between the numbers of the *i-th* groove and the *k-th* section at the left end of which this groove is located, i.e. k = 2i - 1.

Applying expressions (2.66) and (2.67), we determine the values of axial stresses in the upper and lower layers of the structural-orthotropic shell, i.e.

$$\sigma_{xu_i}=-\frac{E_{1_k}\cdot\kappa_i\cdot h}{2\left(1-\mu^2\right)};\qquad \sigma_{xl_i}=\frac{E_{2_k}\cdot\kappa_i\cdot h}{2\left(1-\mu^2\right)}\ .$$

We take into account that the corresponding circumferential stresses have these values:

$$\sigma_{\varphi u_i}=-\frac{E_{2_k}\cdot w_i}{R}-\frac{E_{1_k}\cdot\mu\cdot\kappa_i\cdot h}{2\left(1-\mu^2\right)};\qquad \sigma_{\varphi l_i}=\frac{E_{2_k}\cdot w_i}{R}+\frac{E_{1_k}\cdot\mu\cdot\kappa_i\cdot h}{2\left(1-\mu^2\right)}.$$

In addition, the stress intensity according to the Mises criterion can be described by the following expressions:

- in the upper layers of the structural-orthotropic shell

$$\sigma_{u_i} = \frac{1}{\sqrt{2}}\sqrt{\left(\sigma_{xu_i} - \sigma_{\varphi u_i}\right)^2 + \sigma_{\varphi u_i}{}^2 + \sigma_{xu_i}{}^2};$$

- in its lower layers

$$\sigma_{l_i} = \frac{1}{\sqrt{2}}\sqrt{\left(\sigma_{xl_i} - \sigma_{\varphi l_i}\right)^2 + \sigma_{\varphi l_i}{}^2 + \sigma_{xl_i}{}^2}.$$

Below (Fig. 3.21) are the results of mathematical modelling of the process of change of stresses occurring in the upper $\sigma_в$ and lower $\sigma_н$ layers of the structural-orthotropic shell taking into account the numbers of the winding *i-th coil* and *j-th* groove.

The diagrams we have constructed show that the maximum stresses that occur in the upper (Fig. 3.21, *a*) and lower (Fig. 3.21, *b*) layers of the structural-orthotropic shell reach their maximum value in the frontal zone. The results of mathematical modelling of the process show that the most dangerous conditions occur in the working rope in the section from the 18th to the 34th groove.

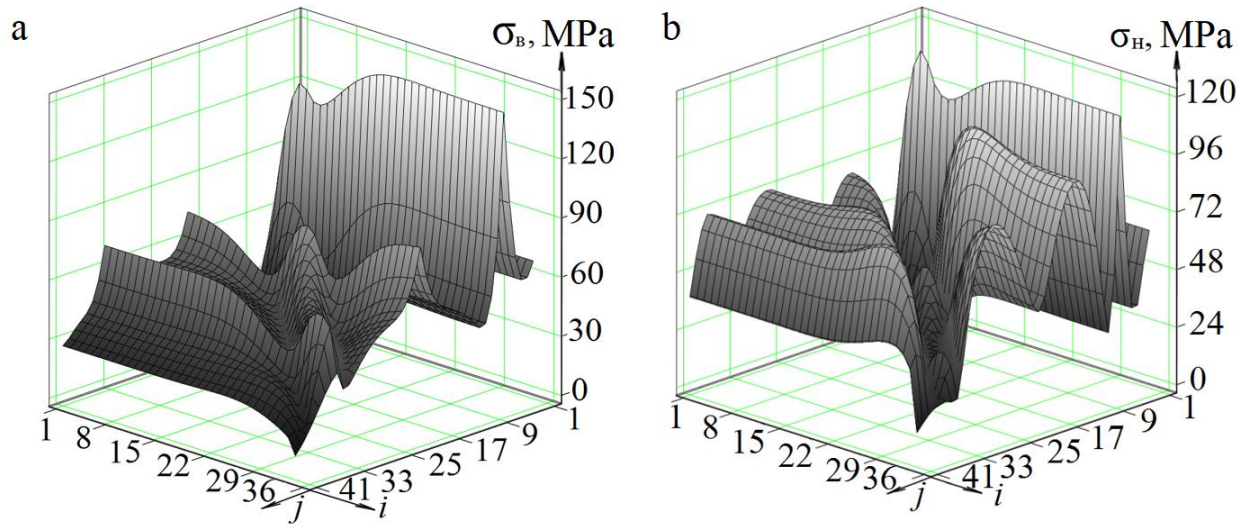

Fig. 3.21. Diagrams of dependence of stresses σ on parameters *i* and *j*

Fig. 3.22 shows the curves of change of forces as well as the resulting stresses and deflections of the sheath in the process of winding the 18th coil of the slaveo of the rope.

As shown in the figure, the pressure σ_{max} in the fourth groove is higher than in the sixth groove (where the frontal is attached). This phenomenon follows from the monotonically decreasing tension of the working rope depending on its location (groove number). Point 1 on the curve σ_{max} corresponds to the tension that occurs when the shell interacts with the frontal located between the sixth and seventh grooves. The break in this curve reflects the impact of the shear force from the side of the spar, a similar break in the curve corresponds to the place of its interaction with the spar (point 5), which occurs near the twentieth groove. Moreover, due to the low radial stiffness of the spar, this shearing force will be weaker. For this reason, the shape of the curve σ becomes more gentle. In addition, points 3 and 7 on the curve correspond to the maximum deflections of the drum shell, occurring between the lobe and the spar. And points 2, 4 and 6 of the curve reflect a significant decrease in bending stresses compared to annular stresses, as they correspond to the change in the sign of the curvature of the shell deformation.

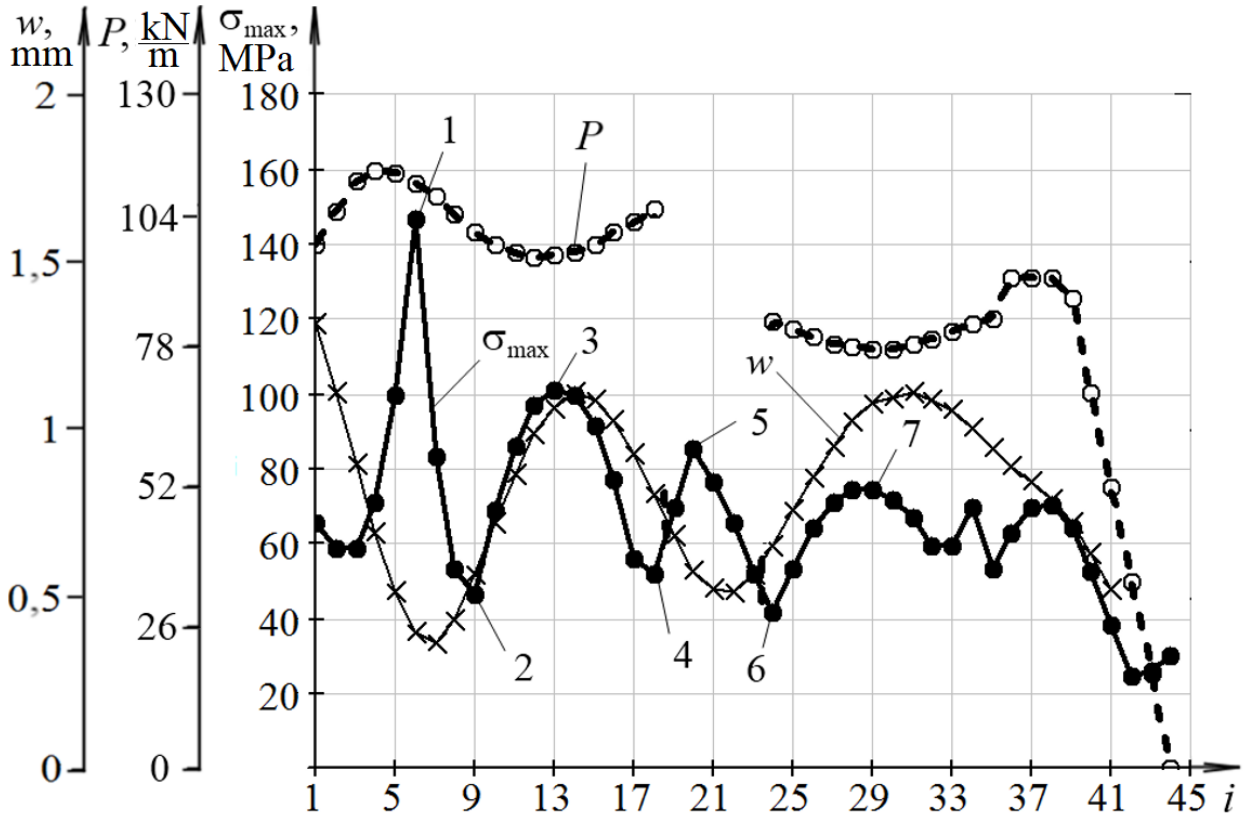

Fig. 3.22. Curves of dependence of forces *P*, stresses σ_{max} and deflections *w* on the place of their occurrence (groove number *i*)

5) Selection of parameters for calculating the SSS in the MHM drum.

The vector {σ} (Fig. 3.23), each component of which corresponds to the maximum intensity of the stresses developing there, is determined for all variants of the drum shell loading. At the same time, the variant that corresponds to the maximum value of the vector {σ} component is used in FEM calculations.

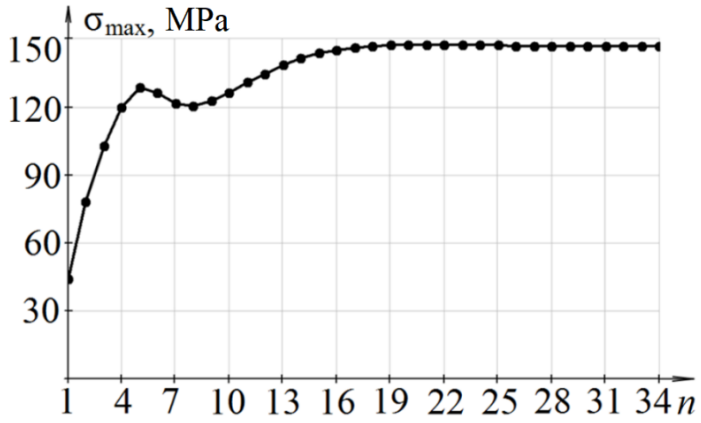

Fig. 3.23. Graph of the vector of maximum stresses in the shell of the MHM drum

Judging by the shape of the curve in Fig. 3.23, the stresses in the structural-orthotropic shell continuously increase, reaching an asymptotic value of 150 MPa.

6) Calculation of drum SSS using FEM.

Fig. 3.24 shows the results of stress calculation in the finite element model of the wedged part of the drum TsR - 6×3.4/0.6, corresponding to the eighteenth variant of loading.

From the analysis of the data obtained, it can be seen that the maximum stresses are distributed on the bottoms of the grooves above the right frontal, and the maximum value achieved (190 MPa) significantly exceeds the maximum permissible value.

To verify the adequacy of the method of determining the design loads, let us compare the graphs of stresses occurring in the upper (Fig. 3.25, *a*) and lower (Fig. 3.25, *b*) layers of the structural-orthotropic shell, as well as reproduced in the solid model of the wedged part of the drum, which was created using FEM by means of SolidWorks Simulation.

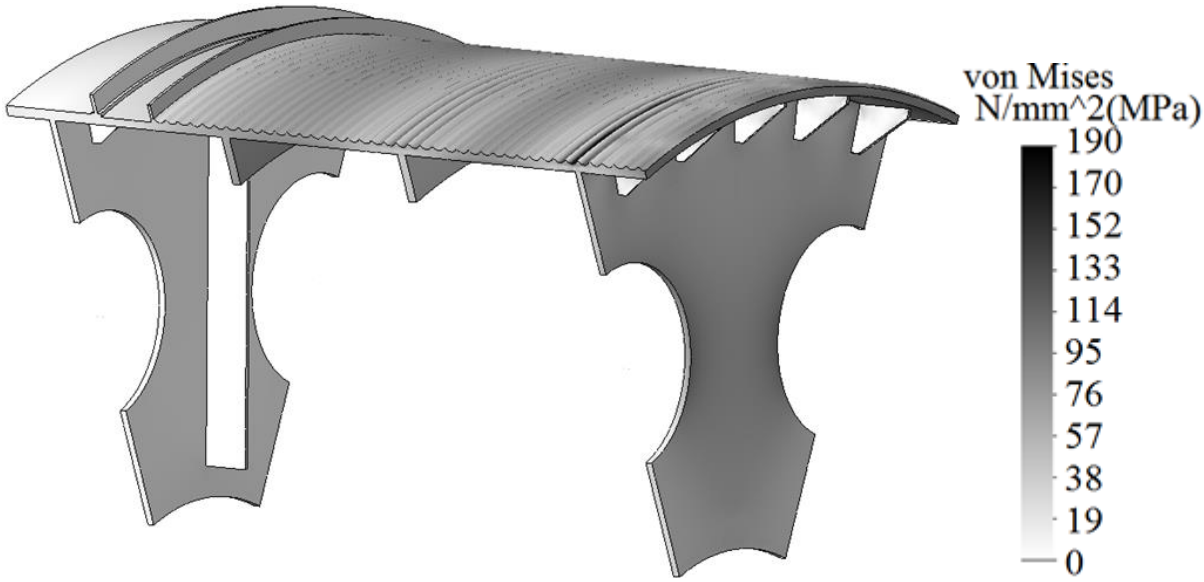

Fig. 3.24. Calculation results of the stress-strain state of the drum of the machine of the TsR type

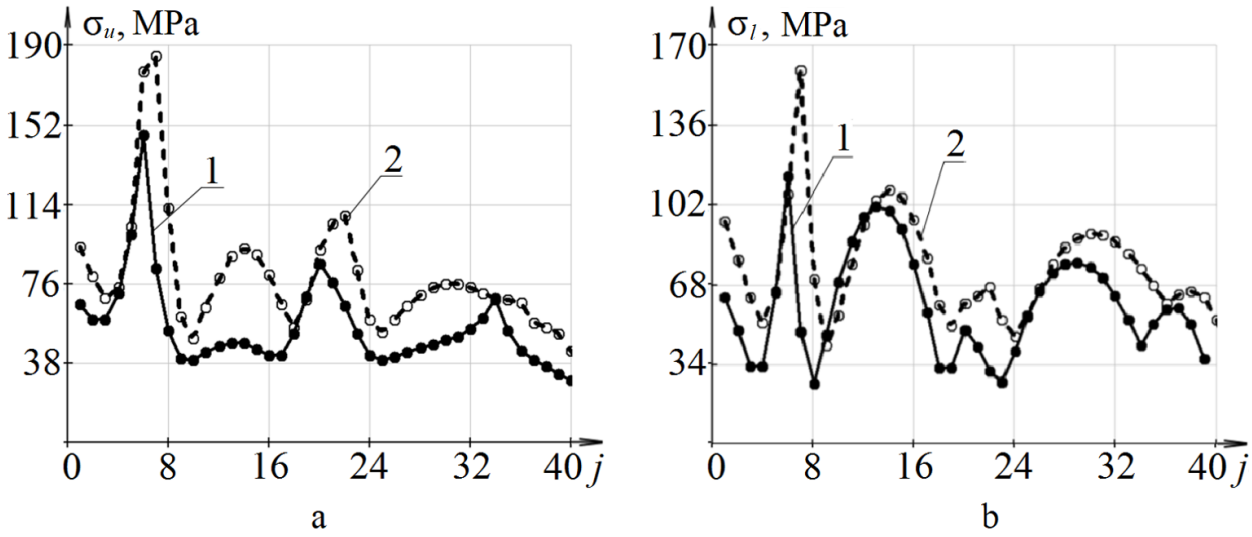

Fig. 3.25. Stress curves in the upper (*a*) and lower (*b)* layers of the shell plotted on the basis of data obtained using:

1 - mathematical model of the structural-orthotropic shell;

2 - solid model of the drum

Comparing the graphs of stresses (Fig. 3.25, *a*, *b*) occurring in the profiled drum and in the structural-orthotropic shell under the influence of the same forces, we see that the configuration of the curves is similar, and the stresses in the averaged shell are lower than in the solid model. This is explained by the fact that tangential stresses occur at the base of the ridge of the profiled shell, which are not taken into account

in the structural-orthotropic shell, and longitudinal forces act only at the groove bottom. Thus, the mathematical model of the structural-orthotropic shell developed by the authors allows us to obtain averaged values of stresses, often they will be lower than the real ones, this makes it possible to qualitatively assess the nature of their distribution in the MHM drum.

3.4 Conclusions to Section 3

1. On the basis of the theory of similarity and with the use of appropriate dimensions, the following parameters of the laboratory installation for studying the process of rope winding on the drum are justified: the radius of the shell 150 mm; the length of the shell 200 mm; the thickness of the shell 2.5 mm; the diameter of the rope 3 mm.

2. Using the developed method, the values of radial deflections of the drum shell under the influence of rope load were determined. At that, the rope tension varied in the range of 29.4...133 N, and the maximum deflection was in the range of 0.14...0.63 mm.

3. The experimental winding of the rope on the drum, during which the deflections of the central section of its sheath were measured, shows that the points of readings of the opposite sensors are practically symmetrical with respect to the centre of the circles of the coordinate system, so that the average values of the readings of the four sensors can be used.

4. The values of radial deflections of the drum shell in the sample are distributed according to the normal law, so, with a confidence probability of 95 %, the deviation of the boundaries of the confidence interval of the obtained data from the mathematical expectation does not exceed 3 %.

5. The error in determining the values of the shell deflections using the method proposed by the authors, when a sequential winding of the rope is provided, compared to the results of the physical experiment is not more than 9 %.

6. The plots of stresses occurring in the profiled drum, plotted using FEM and based on the method proposed by the authors, are marked by qualitative similarity, while the quantitative difference is due to the fact that tangential stresses occur at the base of the scallop of the profiled shell.

7. In the method developed by the authors, the mathematical model of the structural-orthotropic drum shell serves as a basis for obtaining average stress values, which makes it possible to select design parameters for the subsequent determination of the SSS arising in the drum by applying the FEM.

4 DEVELOPMENT OF ENGINEERING METHODOLOGY FOR CALCULATIONAND DESIGN OF CYLINDRICAL BARABANS OF MHM'S

4.1 Problem statement

In the previous section, a method for determining the design loads occurring during rope winding on the cylindrical drum of the MHM was outlined [4 - 7].

The authors set themselves the task of developing, on the basis of the proposed approaches, an engineering method of calculation and design of cylindrical drums of MHM, which will allow to choose optimal values of maximum stresses arising in the drum from a variety of loading options with minimum labour input, and on their basis to determine rational design parameters of the drum according to the criterion of ensuring minimum stresses in the drum.

4.2 Algorithm for developing an engineering methodology

To realise the problem at hand, the mathematical models of the reinforced drum deformation and rope winding described by equations (2.8) to (2.65) were used as a computational algorithm, according to the sequence presented in Section 2.5.

The mathematical models were compiled using the MathCAD 14 high-level algorithmic language, the block diagram of the calculation sequence can be seen in Fig. 4.1.

As we can see in Fig. 4.1, the calculation algorithm consists of blocks corresponding to the following actions: input of initial parameters of the machine 2, determination of tensile forces occurring in the upper section of the rope 3, calculation of stiffness parameters of the structural-orthotropic shell and elastic supports of the drum 4, determination of components of the system matrix 5; as well as the following auxiliary algorithms-functions: determination of the ductility matrix 6, linear linear linear forces occurring during the winding process working 7, idle 8 ropes, their simultaneous winding and unwinding 9, calculation of maximum

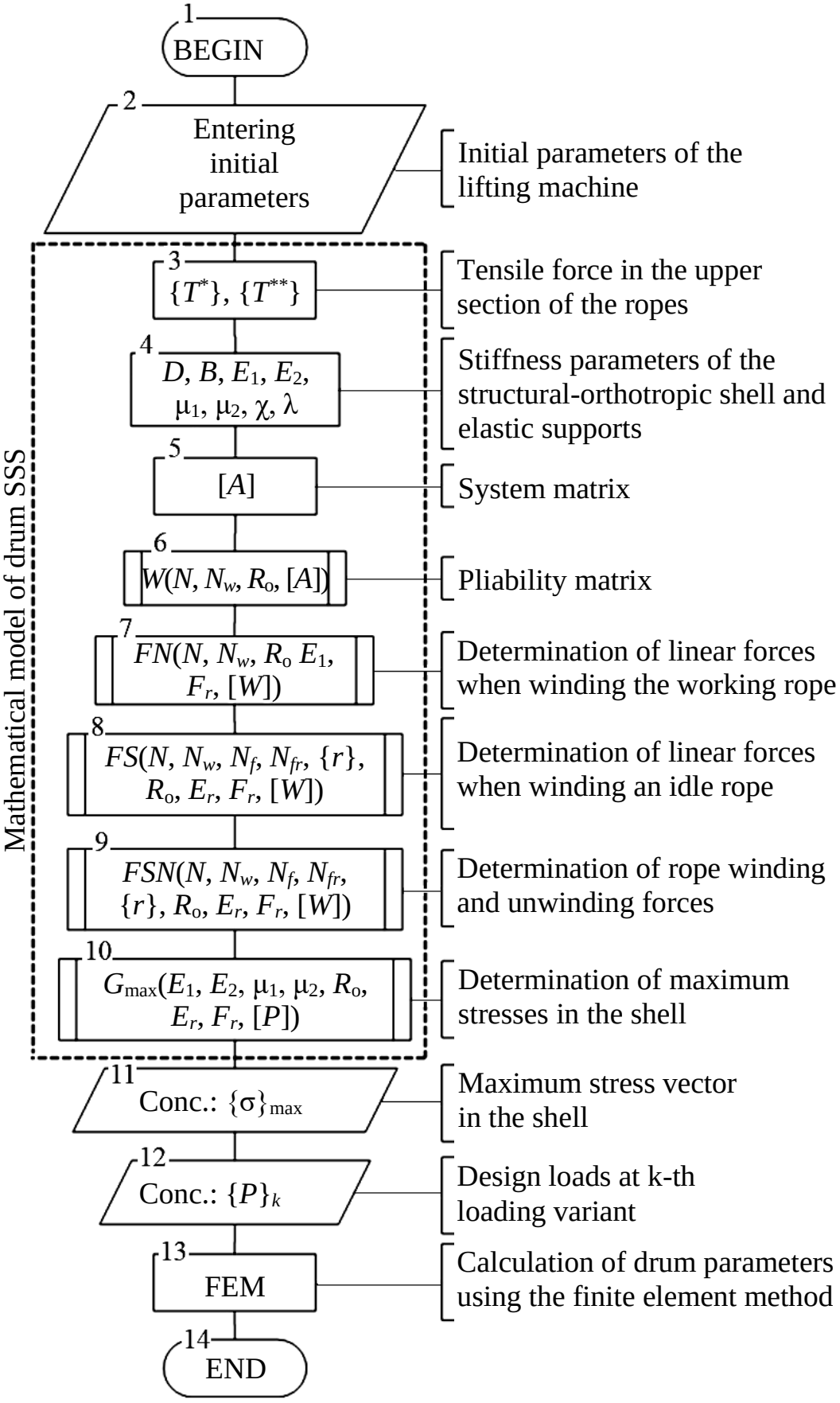

Fig. 4.1. Algorithm of determination of design loads arising in the drum, according to the method developed by the authors

stresses in the sheath 10; in addition, the scheme provides blocks corresponding to the output of the vector of maximum stresses 11 and design loads 12, allowing to set the values of the drum parameters by means of FEM 13.

Let us consider in detail the step-by-step implementation of the head algorithm (Fig. 4.1). According to the initial parameters of the machine (block 2), applying expressions (3.14) - (3.23), we determine the tensile forces applied to the upper section of the ropes (block 3), and using equations (2.49) - (2.50), (2.58), (2.64) - (2.68), we calculate such stiffness parameters of the structural-orthotropic shell (block 4): flexural D and annular B stiffnesses, elastic moduli E_1 , E_2 , Poisson's coefficients μ , μ_{12} ; parameters of the elastic supports of the drum, in particular, flexural χ and annular stiffness λ. Parameters D and B participate in the formation of the matrix of the system [A] (block 5).

After completion of the described actions, by equations (2.22) - (2.24) determine the components of the ductility matrix [W] (block 6), the algorithm of calculation of which is presented in the form of a block diagram in Fig. 4.2. The algorithm includes one outer and two inner cycles. Within the inner loop, the force vector is formed, after which it is possible to find the integration constants C by applying the function lsolve (A, B). The mentioned constants are substituted into the next cycle, where the vector of components of the pliability matrix [W] is formed, and then the described actions are repeated until the number j *is* equal to the total number of grooves of the drum N.

The obtained components of the pliability matrix are substituted into the mathematical model of rope winding (2.8) - (2.17), from which it is possible to determine the matrix of loading variants with components $P_{j,k}$ and the vector of values of radii of undeformed rings $\{r\}$. The mathematical model of the rope utilisation process provides for the execution of algorithms corresponding to winding (Fig. 4.3), unwinding (Fig. 4.4) and simultaneous winding-unwinding (Fig. 4.5) of the rope.

At the next stage of calculations, the values of design loads are substituted into the system of equations (2.22), after solving which the matrix of integration constants [C] is determined. Then the obtained result should be substituted into the expression

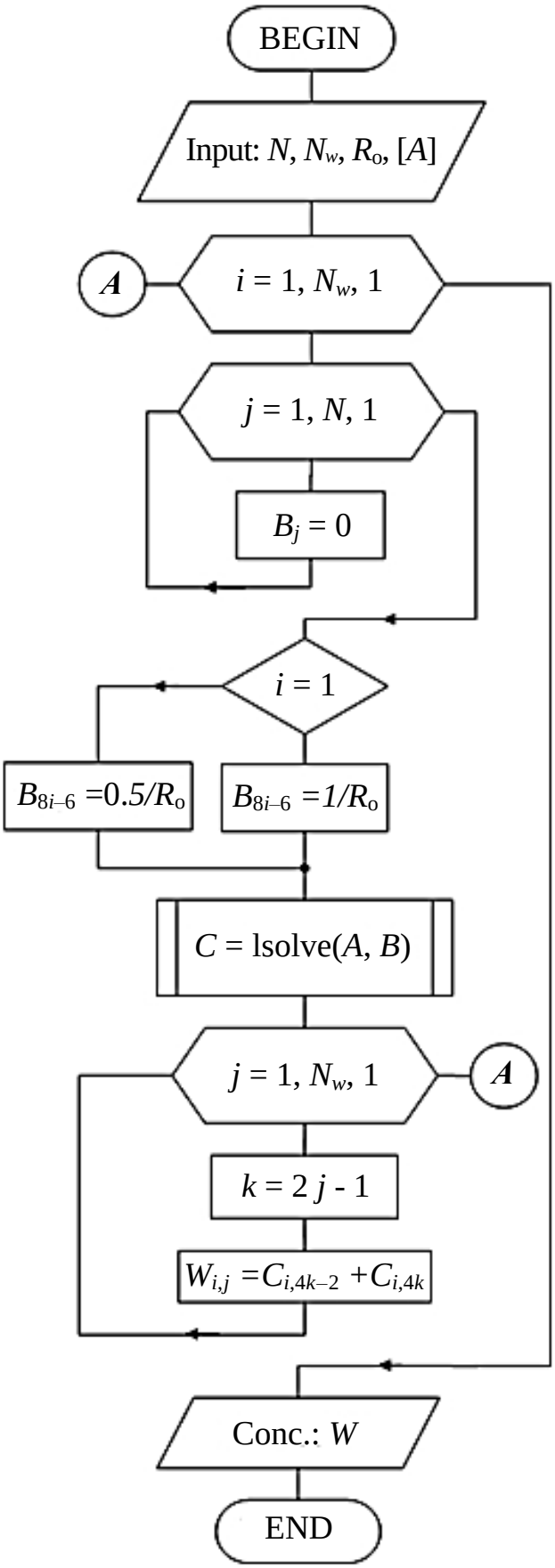

Fig. 4.2. Block diagram of the subroutine *W*for the algorithm of constructing of the pliability matrix of the MHM drum shell

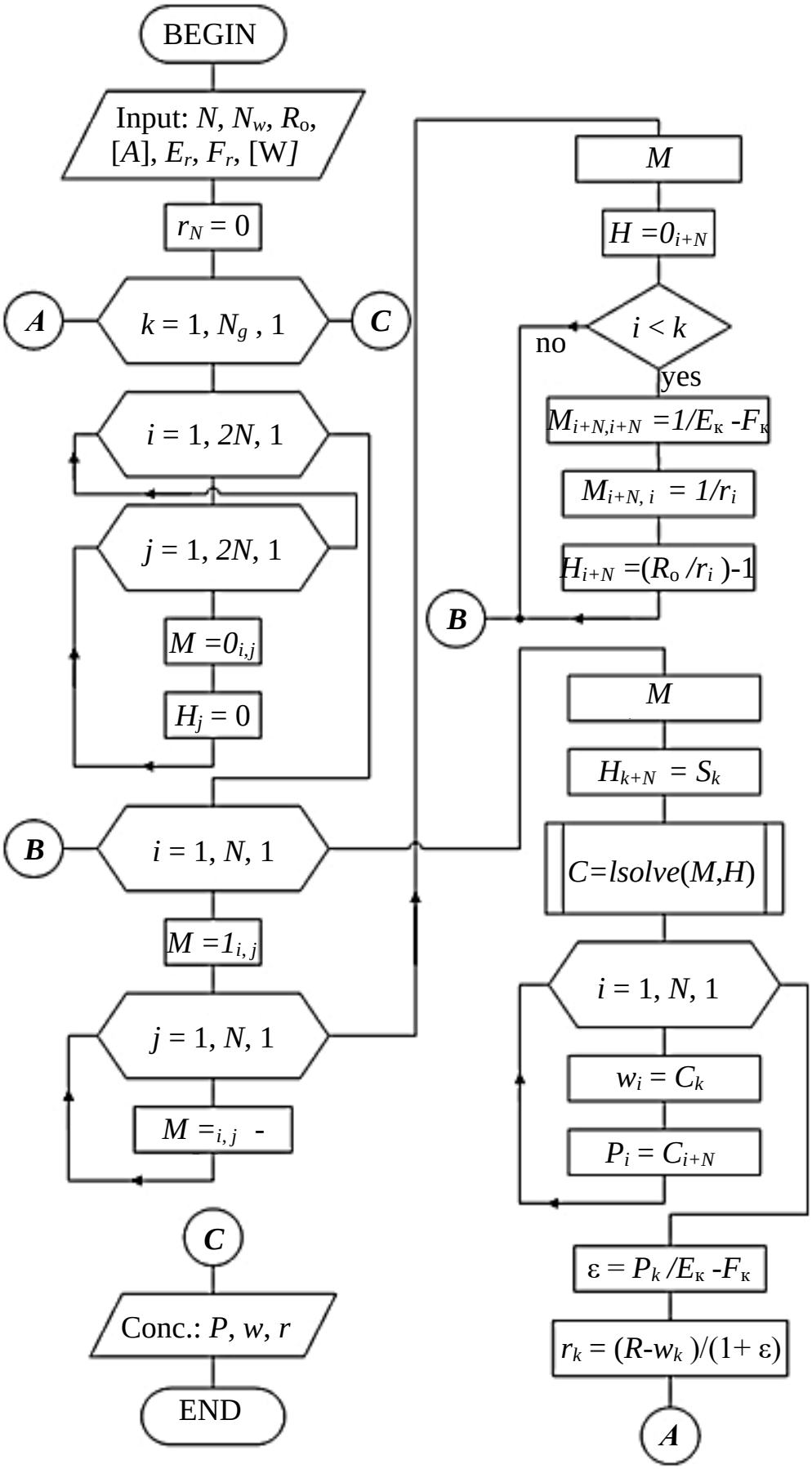

Fig. 4.3. Block diagram of the *FN* subroutine for the algorithm of determining the design loads arising in the process of winding the rope on the MHM drum

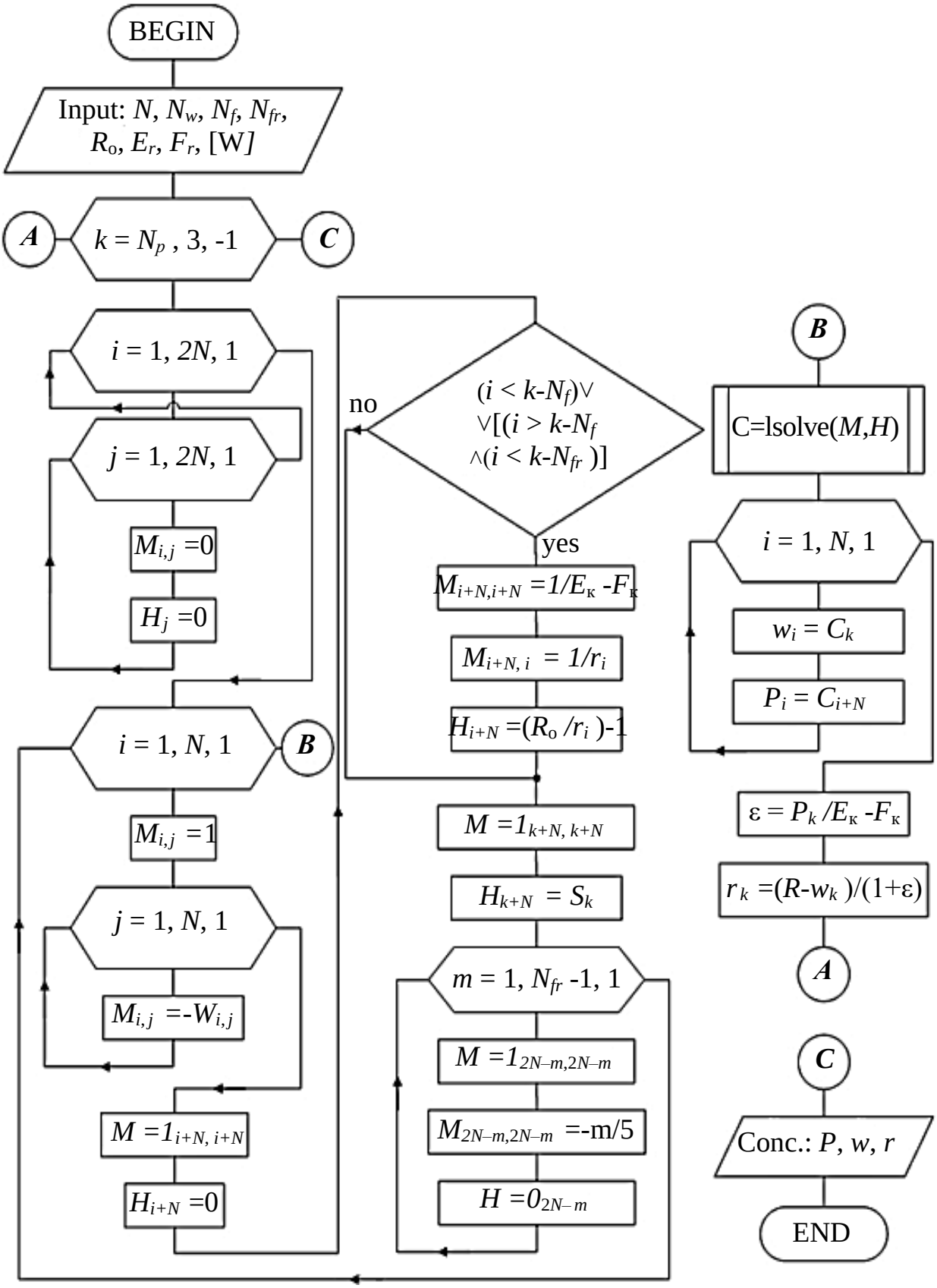

Fig. 4.4. Block diagram of the *FS* subroutine for the algorithm of determining the design loads generated in the process of unwinding the rope from the MHM drum

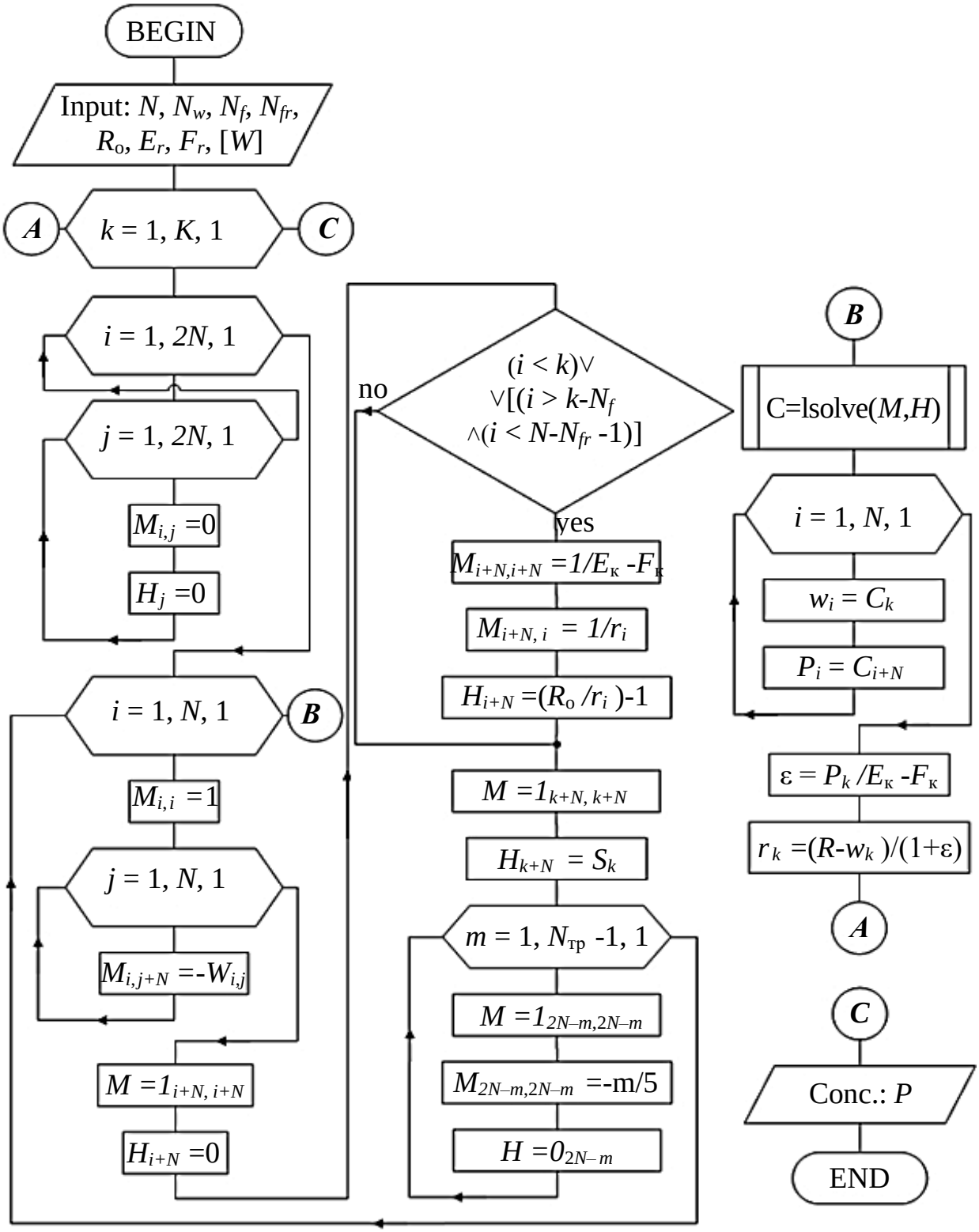

Fig. 4.5. Block diagram of the *FSN* subroutinefor the algorithm of determining design loads occurring in the process of winding-unwinding of the MHM rope

(2.18), applying which the values of the shell deflection are found and its curvature is determined by its derivative. The calculation results are substituted into the expressions for determining the axial (2.69) and circumferential (2.70) stresses in the

upper and lower layers of the shell. The obtained solution results are used to calculate the reduced stress values according to the fourth theory of strength, from which the maximum ones are selected. The algorithm described above can be represented as a block diagram (see Fig. 4.6).

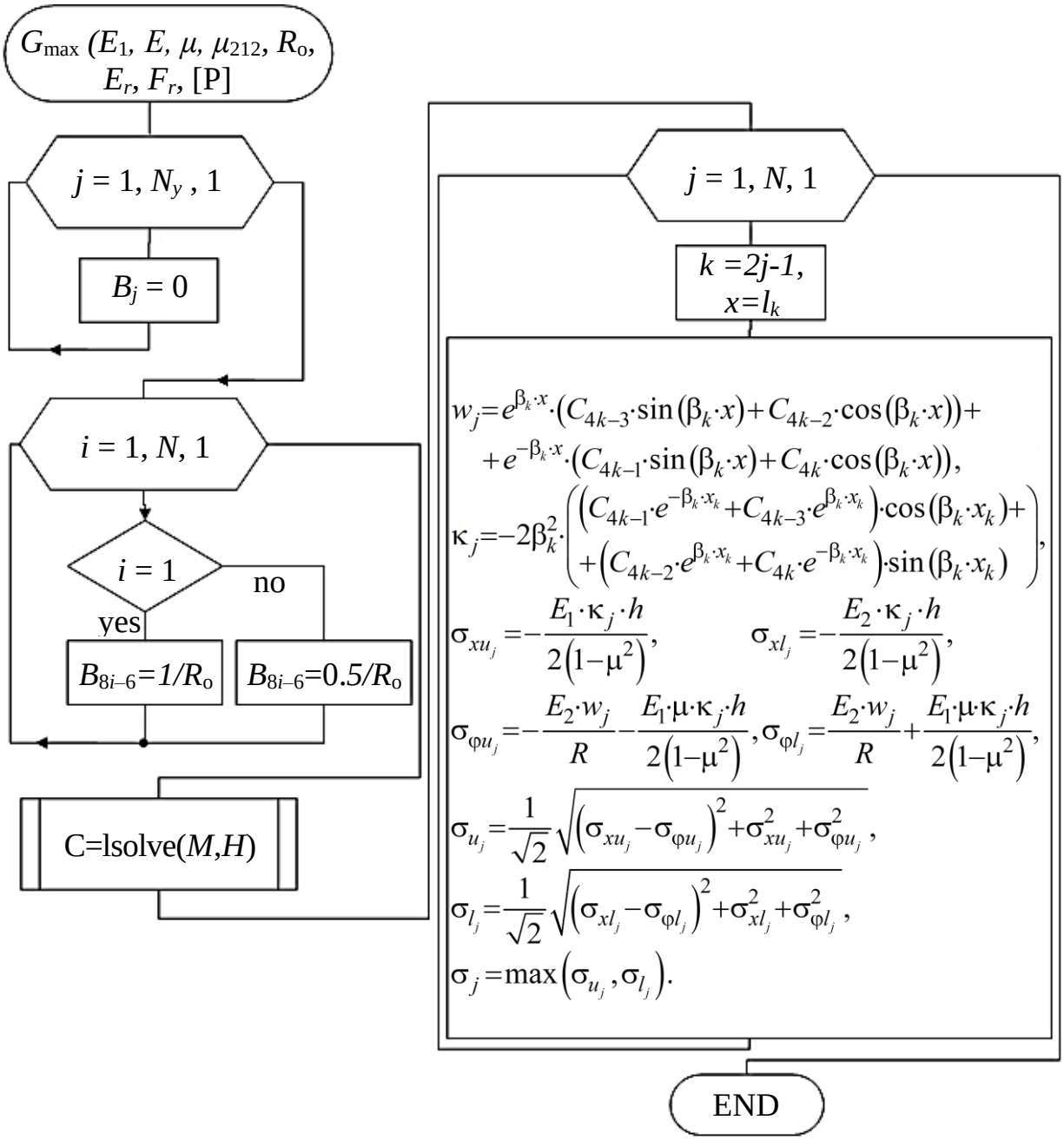

Fig. 4.6. Block diagram of the subroutine G_{max} for aalgorithmfor determining maximum stresses developing in the shell of the MHM drum

The given algorithm for determining the design loads arising in the process of winding and unwinding of the MHM rope is implemented in the form of a programme

"Designer's Workstation" in the Mathcad algorithmic language. The calculation results obtained with the help of this programme are used as boundary conditions for determining the SSS of the drum using the finite element method.

4.3 Conclusions to Section 4

1. In the section on the basis of the proposed approaches the engineering methodology of calculation and design of cylindrical drums of MHM is developed, which will allow to choose optimal values of maximum stresses arising in the drum from a set of loading variants with minimum labour input, and on their basis to determine rational design parameters of the drum on the criterion of ensuring minimum stresses in the drum.

2. The methodology developed by the authors is implemented in the work of designers at PJSC "NKMZ" for evaluation of different variants of drum design and its optimisation, and verification calculation of its parameters should be performed by means of FEM.

5 INVESTIGATION OF THE INFLUENCE OF THE PARAMETERS OF THE MHM DRUM ON STRESS-STRAIN STATES ARISING THERE

5.1 Problem statement

We develop the methodology for calculating parameters and selecting a rational design of cylindrical drums of MHM on the basis of analysis of dependences between generalised values of their characteristics and stresses arising in the structural-orthotropic shell.

In particular, we will consider how the position of the drum lobes affects the magnitude of the maximum stresses in the shell and, based on the results of the research, formulate recommendations regarding the design of the drum. Next, we will analyse the relationship between the parameters of the supporting elements of the drum (spandrels) and the head and the stresses occurring in the shell.

As a result, we determine the influence of the parameters of the drum reinforcing elements on the stress intensity.

5.2 Analysing the relationship between the location of the drum lobes and the magnitude of maximum stresses

Let us first consider how the maximum stress intensity in the drum depends on the frontal placement parameter l (Fig. 5.1)

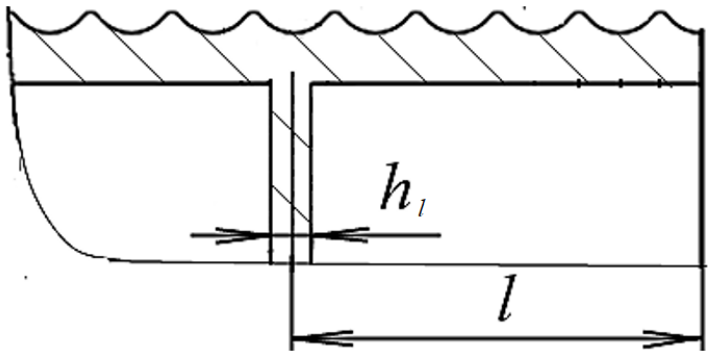

Fig. 5.1. Investigated parameters of the MHM frontal

In the process of the study, the assumptions provided in the method developed above (para. 2.5) for determining the design loads acting on the cylindrical drum of the MHM during its operation are adopted.

The studies were performed according to the engineering methodology developed by the authors (see Section 4).

Fig. 5.2 shows the results of the application of this technique in the form of plots of the dependence between the maximum intensity of stresses in the drum and the distance of the frontal (its multiple of the groove pitch *t* was 0.5 ... 5.5) from the cutting plane on the wedged part of the drum TsR - 6×3.4/0.6 (see Fig. 5.2). Here is denoted *k* - number of loading.

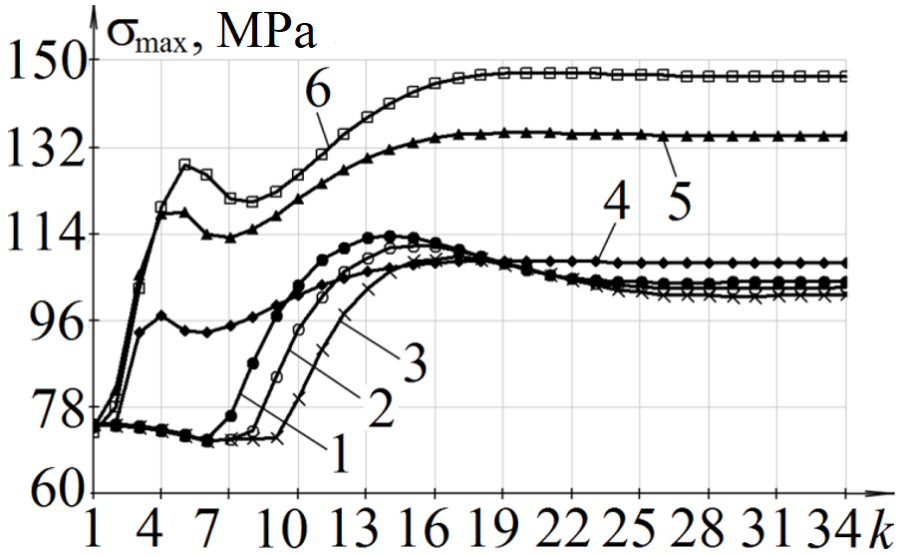

Fig. 5.2. Graphs of dependence of the maximum stresses occurring in the drum shell on the loading variant corresponding to such values of the parameter *l*: 1 - 0,5*t*; 2 - 1,5*t;* 3 - 2,5t; 4 - 3,5*t;* 5 - 4,5t; 6 - 5,5t

It was observed that when the lobe was spaced at 3.5*t*, the maximum stresses were reduced by 48% compared to that of the baseline drum design (5.5*t*).

It took only one hour to construct the graphs using the method proposed by the authors, whereas using the FEM, the same work can be done only in 300 hours.

The analysis of the obtained dependencies allows us to make the following observations:

- 0.5 ... 3.5 of the cutting pitch, the maximum stresses in it decrease as the number of the loading variant increases in the range of 1 ... 12, and then smoothly increase, reaching the asymptotic value of 100 MPa;
- if the multiplicity of distances is 4.5 ... 5.5 of the slicing step, the maximum stresses under the same conditions continuously increase and reach the asymptotic value in the range of 132 ... 150 MPa after the 18th loading variant.

There is a need to optimise the distance *l*, which defines the position of the frontal on the side of the tipped part of the drum, at which it is possible to achieve the minimum of maximum stresses σ_{max} , occurring in the shell of the tipped part of the drum TsR - 6×3,4/0,6.

In this case, we assume that, being a variable parameter, the dimensionless distance between the frontal near the location of the drum cut and this cut l_β = l-β.

The following dimensionless maximum stresses that occur in the drum shell are taken as the target function: $\Gamma = \sigma / \sigma_{maxasym}$.

Then we find such a value of the parameter l_β, at which the dimensionless maximum stresses will be minimal, i.e.

$$L^* = \min_{\Gamma \in \mathbb{X}} \|\Gamma\|,$$

here; $\|\Gamma\| = \max\left\{\left|\Gamma\left(l_\beta\right)\right| : l_\beta \in [0{,}1;1{,}7]\right\}$ $\mathbb{X}$ is a valid set of real numbers.

After conducting the computational experiment and processing its results, we managed to construct a curve of dependence of the maximum stresses occurring in the drum shell on the reduced value of the length of its cantilever part (Fig. 5.3).

The minimum value of stresses in the drum shell is achieved when the relative length of the cantilevered part of the drum $l_\beta = 0.7$.

The analysis of the dependence (Fig. 5.3) shows that if the cantilever is long ($l_\beta > 0.7$), the maximum stresses occur above the frontal, which unlike the shell, experiences a negligible bending force. At with a short arm, when the dimensionless distance from the rope being wound to the shovel is $l_\beta < 0.7$, the bending stresses at

the middle section of the shell reach their maximum and can approach the asymptotic value.

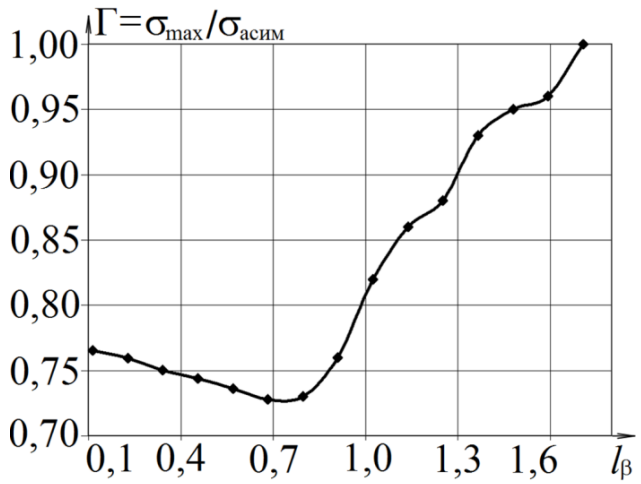

Fig. 5.3. Graph of dependence of maximum stresses in the shell on the reduced value of the length of the cantilever part of the drum

Using FEM, we determine by how much the maximum stresses in the shell will be reduced if the distance from the lobe to the edge of the drum is 0.5 slicing steps, compared to the basic design (where the distance is 5.5 slicing steps).

Fig. 5.4 shows the results of calculation of SSS values in the finite element model of the basic design of the wedged part of the drum type TsR - 6×3,4/0,6 [5, 6], corresponding to the 18th loading variant, and the modified design based on the 13th loading variant.

Having analysed the results of calculation of SSS of the wedged part of the drum TsR - 6×3,4/0,6, we see that the stresses in the basic design are 53 % higher than in the modified one.

Fig. 5.5 shows the plots of stresses that occur in the upper (Fig. 5.5, *a*) and lower (Fig. 5.5, *b*) layers of the shell, plotted by different methods: using the mathematical model developed by the authors and using FEM.

The data of Fig. 5.5 show a qualitative similarity of the curves, with the stress values obtained using the analytical model being smaller than those obtained using the finite element model.

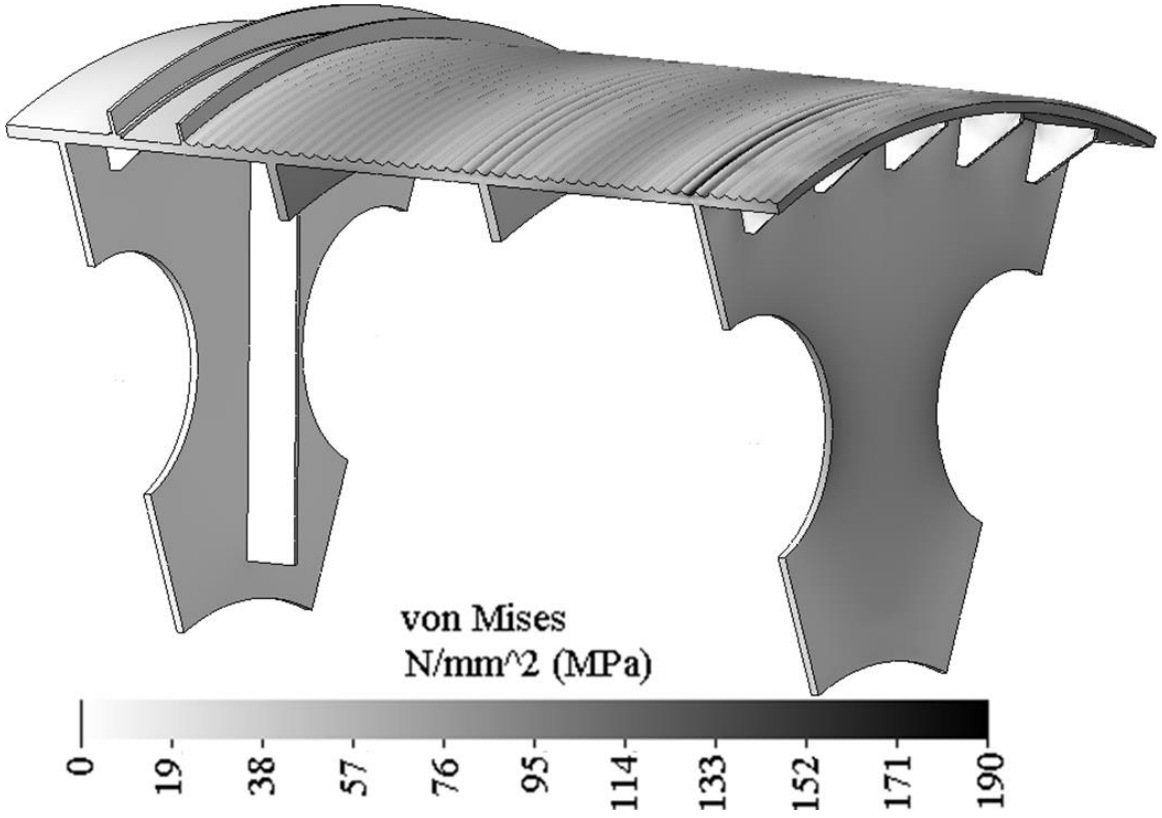

a

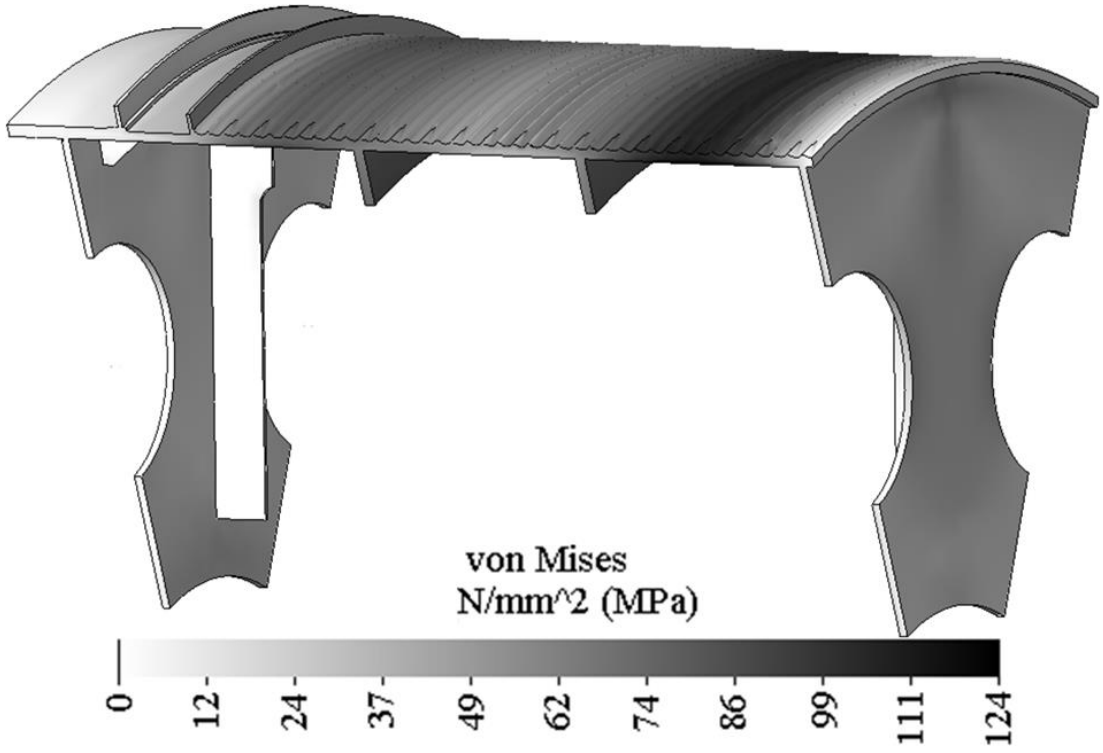

b

Fig. 5.4. Results of calculation of SSS arising in the drum (by FEM):

a - of the basic structure;

b - of the structure with the frontal moved to the edge

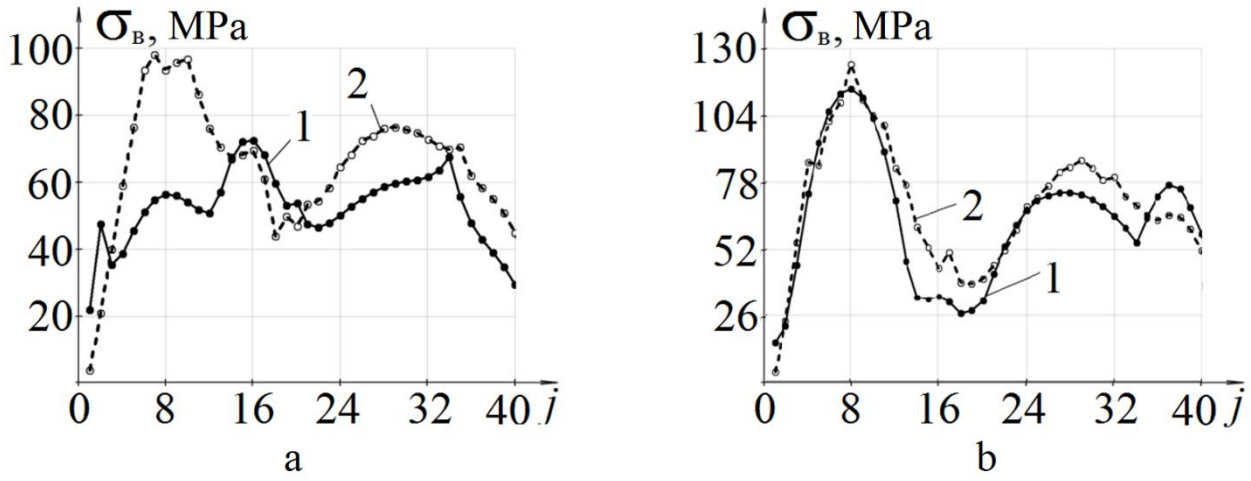

Fig. 5.5. Stress curves in the upper (a) and lower (b) layers of the shell of the wedged part of the drum TsR - 6×3,4/0,6, plotted using two methods:
1 - proposed by the authors;
2 - finite element analysis of the solid model of the drum

So, we can summarise the results of the performed research, in particular, we have established that two qualitatively different mechanisms of the processes occurring in the wedged drum are possible with a change in the dimensionless length of the cantilever part of the shell. In the presence of a long cantilever ($l_\beta > 0.7$), the maximum stresses occur above the frontal, which, unlike the shell, is subjected to insignificant bending. If the dimensionless distance from the winding rope to the brow $l_\beta > 2.7$, the bending stresses above the brow reach their maximum and approach the asymptotic value.

When the wire rope runs into the short cantilevered part of the shell ($l_\beta < 0.7$), a bending of the frontal occurs, accompanied by a slight bending of the shell, so that the resulting bending stresses are smaller than those observed above the right spar under the influence of the winding of the idle rope. Subsequently, the annular stresses in the area between the right *frontal* and the spar grow due to the coiling of the working rope in this area and reach their asymptotic value when the dimensionless distance from the rope to the frontal $l_\beta > 3.7$.

5.3 Investigation of the influence of spandrels on the stresses occurring in the drum shell

Let us consider how the characteristics of the spandrels can influence the maximum stress intensity and the stability of the drum. As an example, consider the stress plots presented in Fig. 5.6 plots of stresses occurring in the basic structure of the wedged part of the drum TsR - 6×3,4/0,6, as well as in the structure without spandrels. Here, two curves are shown on each graph, one of them is plotted according to the results of calculations using the authors' methodology, and the other one is plotted according to the FEM data.

The analysis of the graph shows that in the design without spandrels (Fig. 5.6, *b*) compared to the basic design (Fig. 5.6, *a*), the maximum stresses are lower by 20 %, while the error in determining the maximum stress intensity using the author's method and FEM does not exceed 14 %. The increase of stresses σ_{max} occurs in the drum where the spandrels are installed.

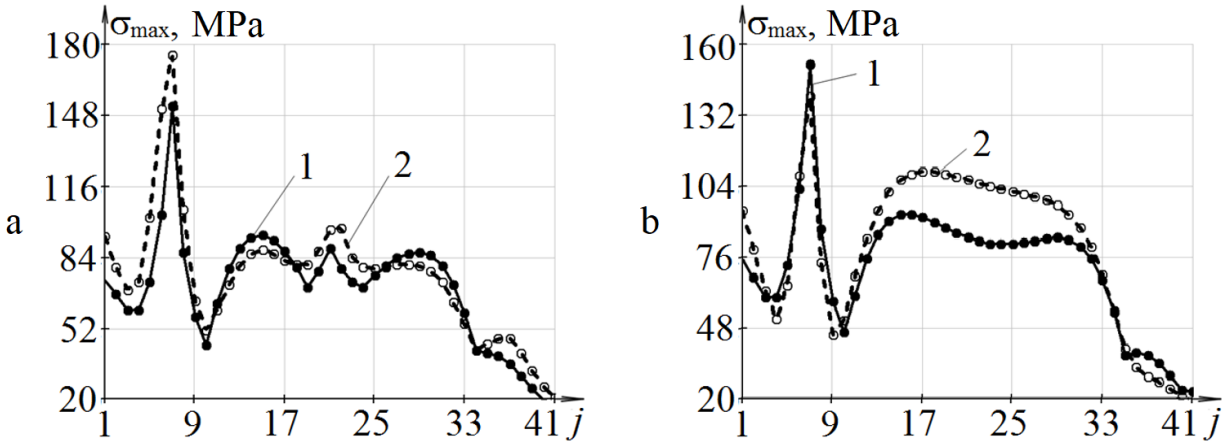

Fig. 5.6. tress intensity curves in the shellof the TsR machine constructed using the methoddeveloped by the authors (1) and according to the FEM data (2): *a* - in the study of the basic structure; *b* - the structure without spars.

Checking the structure without spars (Fig. 5.7) shows that the drum will lose stability under the influence of a load exceeding the applied load by a factor of 3.44

(load factor = 3.44). The data of Fig. 5.7 shows that the drum is more likely to lose stability in the axial direction than in the radial direction.

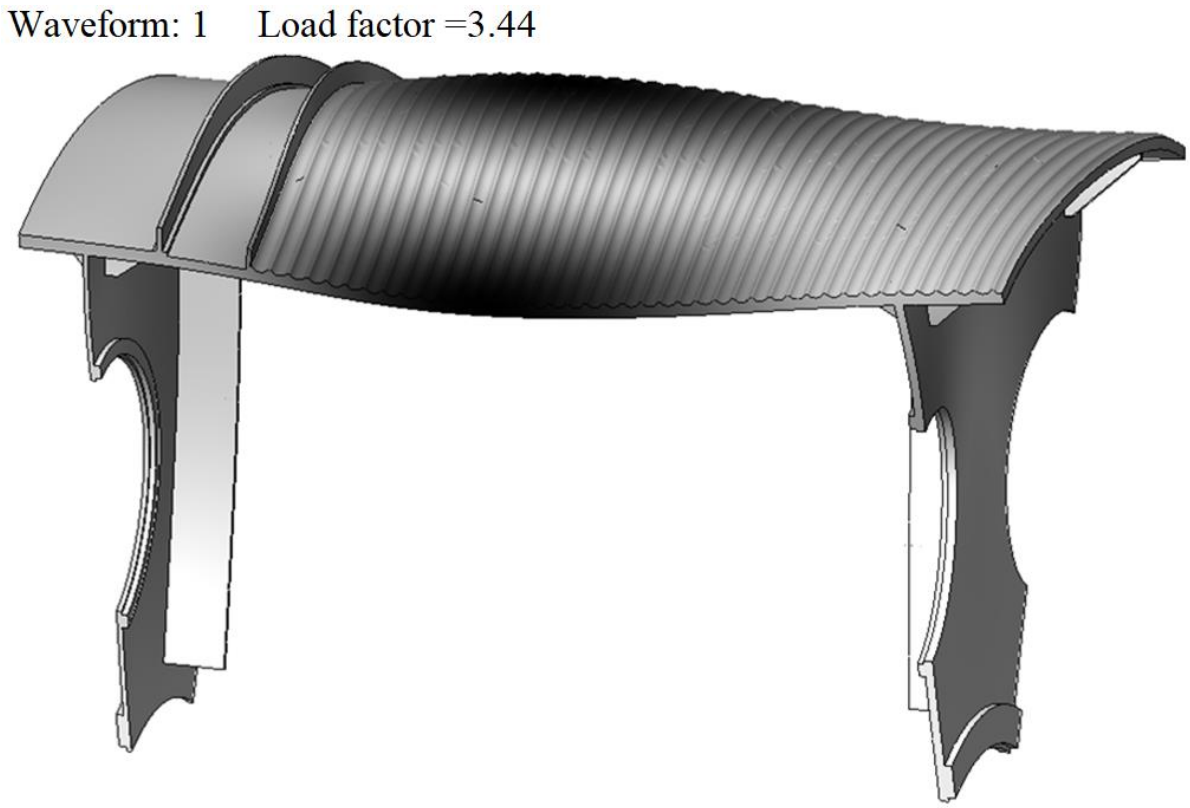

Fig. 5.7. Results of stability test of the wedged part of the drum TsR - 6×3,4/0,6 without spars

Thus, it is considered inappropriate to use spandrels as this may be the cause of increased stresses in the drum shell.

5.4 Analysing the influence of the radial stiffness of the frontal on the maximum stress intensity

As it was noted above (para. 5.2), in drums with a long cantilever part, the maximum stresses occur above the head, causing its insignificant bending. Let us consider the possibility of reducing the maximum stresses in the shell by providing a fixed length of the cantilever by changing the stiffness of the frontal. To obtain general results, we introduce such dimensionless parameters: the reduced value of the maximum stress intensity $\Gamma = \sigma / \sigma_{maxasym}$; the reduced value of the frontal

stiffness $Z = \lambda/V$.

Taking into account the peculiarities of TsR-type machine designs, the minimum value of the frontal stiffness was chosen, i.e. $Z = 0.016$. Then the relative radial stiffness of the frontal was gradually increased by this value until the reduced value of the stress intensity Γ reached its asymptotic level with an accuracy of 0.1 %. Fig. 5.8 shows the results of the computational experiment and the approximating function, obtained by interpolation, of the experimental results, viz:

$$\Gamma(Z) = 1 - e^{-\alpha 1 \cdot Z - \alpha 2},$$

here the coefficients $\alpha_1 = 1.2$ and $\alpha_2 = 0.74$, they were calculated by the least squares method by minimising the squares of deviations, and if $Z = 0.6$, the value of the parameter Γ will not be lower than 0.9.

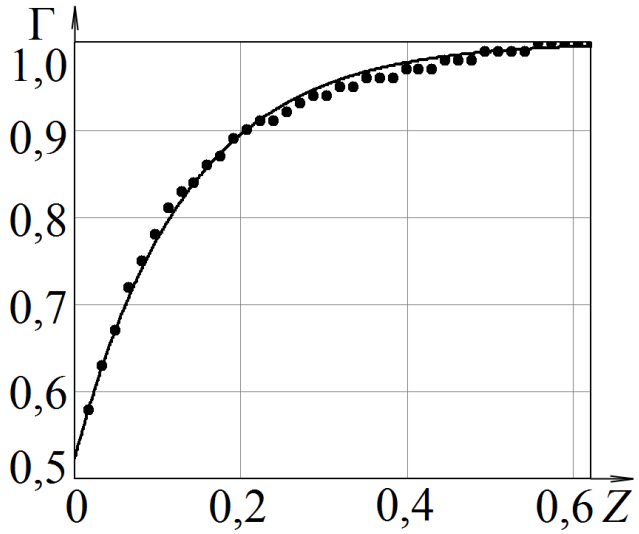

Fig. 5.8. Graph of dependence of maximum stresses,
arising in the MHM drum on the radial stiffness of the frontal

It follows from the above that if the fraction of the radial stiffness of the frontal exceeds 0.6 of the radial stiffness of the shell, the stresses remain unchanged, reaching their asymptotic value. If this stiffness is reduced, the stresses decrease exponentially, e.g., at a relative stiffness equal to 0.2, they are 90 % of the maximum.

5.5 Structural support of radial stiffness reduction of the MHM drum frontal

Let's consider for example the MHM of type TsR - 6×3,4/0,6. The stresses arising in the basic structure of the wedged part of the drum ($Z = 0.159$) exceed the permissible values. When the radial stiffness is reduced by 50 %, the stresses in the shell are reduced by 12.6 % and become below the permissible values.

Let's determine which structural elements should have a frontal with reduced radial stiffness ($Z = 0.079$).

For this purpose, let us use the diagram of construction of the head and the drum (Fig. 5.9). As can be seen, to the frontal 1 together with the shell 2 inside the drum there are ribs 3 welded between the mounting holes, and outside and inside between the ribs there are braces 4 welded.

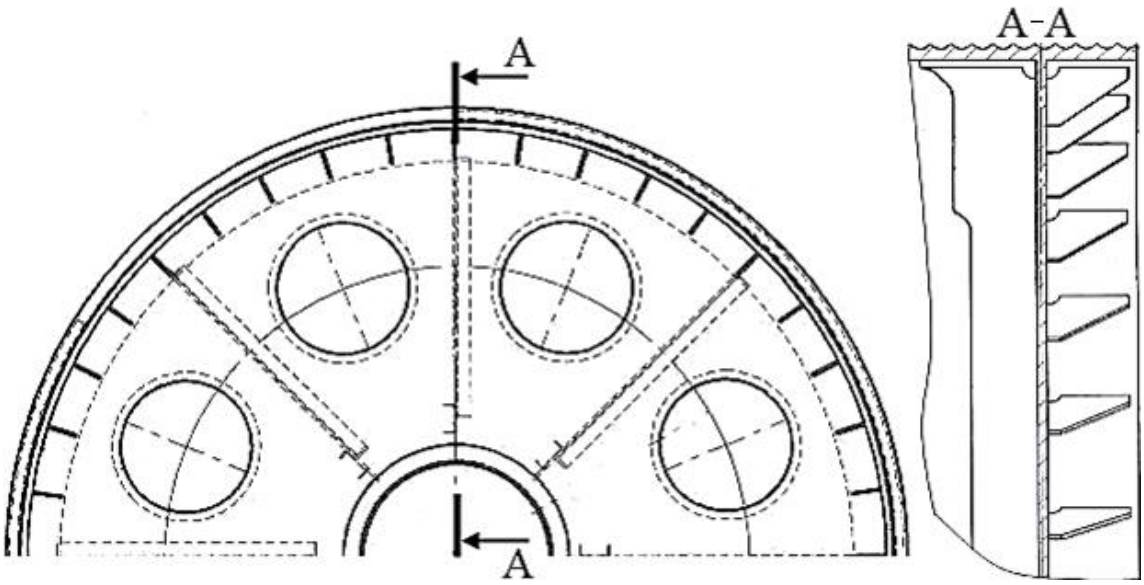

Fig. 5.9. Schematic diagram of the frontal and drum construction

Let us assume that the presence of ribs and braces does not significantly affect the radial stiffness of the frontal. Let's try to reduce the thickness of the frontal twice (16 mm) and carry out a verification calculation of the stresses arising in this case (Fig. 5.10). It is shown that the maximum stresses are concentrated at the rounding of the rib and amount to 172.2 MPa (Fig. 5.10, *a*), which exceeds the permissible

values by a factor of 1.26. The stability analysis (Fig. 5.10, *b*) showed that the structure will lose it under the influence of the load, which is 0.72 of the design load.

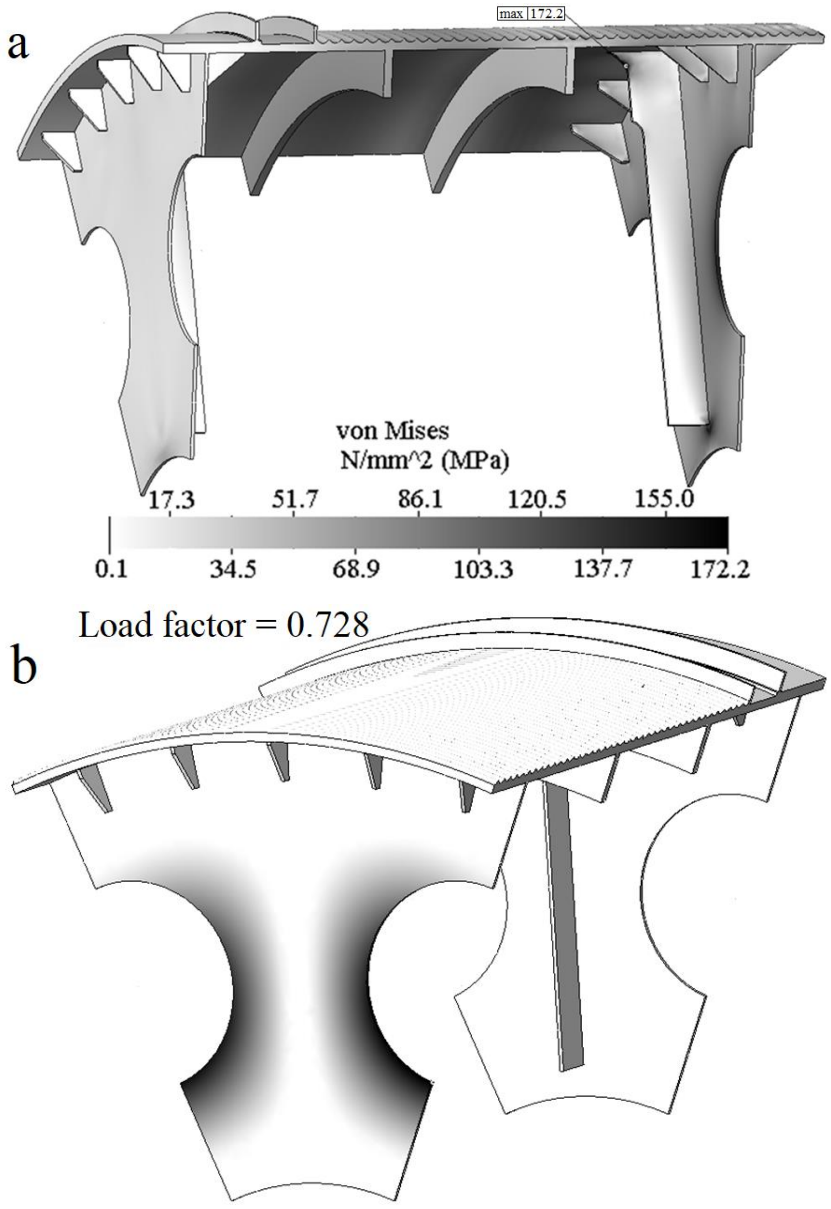

Fig. 5.10. Results of determining the drum SSS parameters:
a - stress intensity; b - stability coefficient

Having considered the SSS indicators of the rib (Fig. 5.10, *a*), we see that in its upper part it is necessary to increase the bending stiffness by increasing the width of this element and the radii of roundings, as a result of which the stress concentration is reduced in this place. Here it is necessary to take into account that the lower part of the rib has excessive bending stiffness, which means that extra metal must be

removed. The local loss of stability of the lobes (Fig. 5.10, *b*) is eliminated by adding additional rings on the outer side of each of them.

Fig. 5.11 shows the calculation results of the modernised drum design.

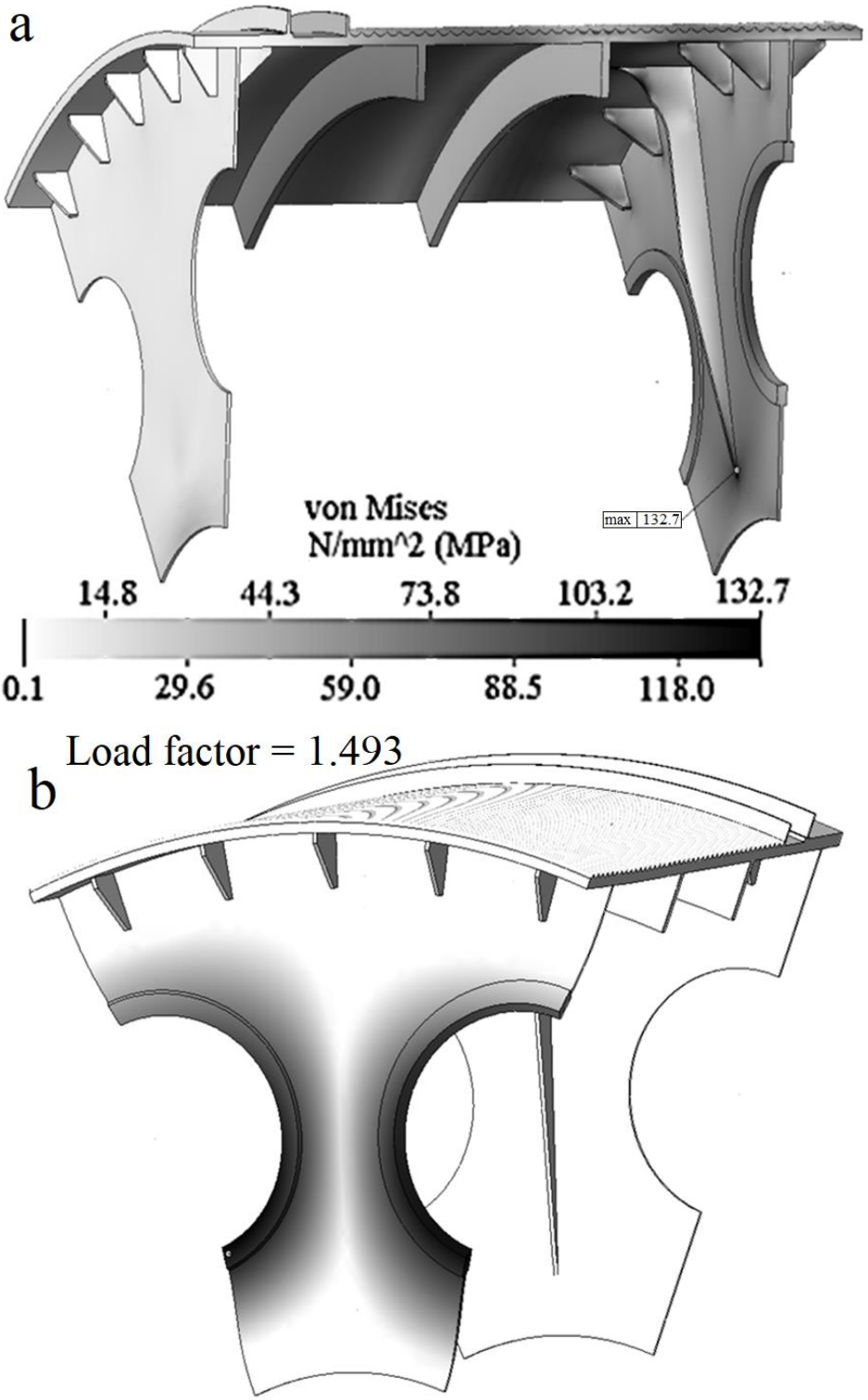

Fig. 5.11. Results of calculation of parameters of the modernised drum: a - stress intensity; b - stability coefficient

As evidenced by the data of Fig. 5.11, *a*, the maximum stresses are concentrated at the junction of the rib with the frontal and reach 132.7 MPa, which is below the maximum permissible value. The analysis of stability parameters (Fig. 5.11, *b*) showed that installation of additional rings around the mounting holes of the drum reinforces the structure twice, and the load factor was approximately 1.5.

Thus, by halving the thickness of the frontal, changing the shape of the ribs and reinforcing the frontal by means of rings, we have obtained a very functional modernised drum design, the mass of which is 4661 kg less compared to the basic design.

The above-mentioned results were used in the creation of the methodology of calculation and design of the MHM, approved by NMU specialists and agreed with the engineering service of PJSC "NKMZ".

As we can see, the implementation of technical solutions developed by the authors allows to improve the functional parameters of the MHM drum, to increase the safety of the design, to reduce its weight.

5.6 Conclusions to Section 5

1. The studies have shown that in mine hoists of the TsR type the parameters of the stress-strain state of the drum significantly depend on the length of the cantilever part of its shell *l* near the cutting plane of this structure, as well as on the value of the variability coefficient β, which is the square root of the ratio between the annular and bending stiffness of the shell. If there is a long cantilever ($l_\beta > 0.7$), the maximum stresses occur above the drum lobe, and their intensity increases with increasing length of the cantilever part. If there is a short cantilever ($l_\beta < 0.7$), on the contrary, the stresses decrease with increasing cantilever length. Consequently, the optimum by the criterion of achieving the minimum of maximum stresses is the length of the cantilever corresponding to the following condition: $l_\beta = 0.7$. And it was noted that the optimisation of the length of the drum console in the MHM of type TsR - 6×3,4/0,6 allows to reduce the maximum stresses arising there by 35 %.

2. The inexpediency of using spandrels as drum reinforcements was justified, as in this case there is an increase of stresses in the shell due to the increase of bending stresses at the areas of their installation.

3. The values of the maximum stress intensity have an exponential dependence on the given values of the radial stiffness of the frontal. In addition, considering the wedged part of the MHM drum of the type TsR - 6×3,4/0,6, the radial stiffness of the brow of which exceeds 0,6 part of the radial stiffness of the shell, we note the constancy of the stresses reaching their asymptotic value. A decrease in this stiffness leads to an exponential decrease in stresses. For example, if the relative stiffness is 0.2, the stresses are 90 % of the maximum.

4. The result of reducing the radial stiffness of the frontal, e.g. by making it thinner, is a reduction of stresses in the shell. The resulting additional stresses in each rib of the frontal and the local loss of stability in the holes between the ribs were reduced by changing the shape of the ribs and introducing additional reinforcement rings around the hole. Thus, a fully functional design of the frontal was created, which contributes to the reduction of stresses in the wedged part of the drum.

5. The given examples of determination of design parameters of the structure testify to high efficiency of the developed methodology introduced in the practice of designing at PJSC "NKMZ" for estimation of various variants of the drum design and its optimisation, at the same time verification calculation of its parameters is recommended to be performed using FEM.

6 CALCULATION METHODOLOGY OF THE MHM DRUMS OF NON-STANDARD DESIGNS

6.1 Analysis of recent research and publications

Due to the need to increase the lifting depth and the associated complication of the drum design, the calculation of the axial displacements of brake discs for the use of disc brakes requires the development of a methodology for calculating the drum of a hoisting machine for axial stiffness based on the analysis of the operation of individual components, the creation of their simplified models and the calculation of the displacements of the drum model and the subsequent calculation of stresses in the output components. Finite element analysis on a mesh of acceptable quality requires the use of high-performance PCs and expensive computer packages such as CATIA 5. Hence the development of new methods for calculating such structures that are available for use with mid-range packages such as SolidWorks Simulation.

The research works related to the development of hoisting and transporting machines are carried out at the National Technical University “Dniprovska Polytechnic”. The scientific research results in the field of mechanics of new mine hoisting machine structures are of great practical importance. Other studies are devoted to determining the dependence of dynamic parameters on the technical state parameters of the individual units in the installation [8].

The following scientists, such as B.A. Morozov, B.G. Klimov, B.I. Davidov, B.S. Kowalski, Z.M. Fedorova, A.P. Nesterov, F.L. Shevchenko, S.M. Zinchenko, K.S. Zabolotnyi, M.A. Rutkovskiy were engaged in research on hoisting machines. Almost all the works of these scientists are devoted to the study of stresses in the drum elements of mine hoisting machines (MHM).

Scientific works, the analysis of which is given in [9], are devoted to the development of scientific methods for substantiating the design parameters of mine hoisting machines. The authors dealt with the following issues: braking devices on its stress-strain state (SSS) [10], developing a method for calculating the design loads [11-12]. They were ingaged into increasing the rope capacity of a single-drum mine

hoisting installation [13], as well as substantiating the parameters of equipment for dehydration of ropes in mine hoisting installations [14]. In addition, the method for calculating the force factors in the turns of multilayer winding of rubber-cable ropes has been improved [15].

In the work, a semi-empirical approach has been developed, which leads to obtaining a simpler analytical mathematical model of an object that provides reliable results. With this approach, the object is described through a simplified model, which uses coefficients determined experimentally and selected in such a way that, in this range of parameter changes, the calculated and experimental data are in good agreement. However, when determining the axial displacements of the braking fields caused by the own weight of the drum and the tension of the ropes, which run off and run on, the analytical method is not suitable and it becomes necessary to develop a specialized computational approach.

Fig. 6.1 shows the design of such a drum, model TsR-6.75×6.2/1.95 [16]. This unit makes it possible to lift the extracted mineral from a depth of up to 1477 metres, while its useful load capacity is 15 tonnes. The figure shows that the drum is divided into three segments: two of them are connected and form the jammed part, while the third segment is an interchangeable part. Inside the drum there is a repositioning mechanism that allows the repositioning part to be separated from the main shaft of the machine to adjust the length of the rope, which is important when changing horizons or when cutting rope for testing.

The spacer 6 and jammed 7 parts of the drum have a screw groove for the rope on the outer surface of the shell. The upper wire rope attached to the jammed part can only be wound up to the slit, i.e. to the splitter part. The lower rope, attached to the splitter part, passes through the cut. The sheath 3 is a rolled sheet steel cylinder with a helical groove cut into its outside for rope winding. The headstocks 8 are connected to the main shaft 4 by means of bolts with four inner and two outer hubs 2, and to the shell by welds.

To improve the rigidity of this drum model, various reinforcing elements are used, including I-beam rings and sheet metal elements (so-called frames 11 or ring

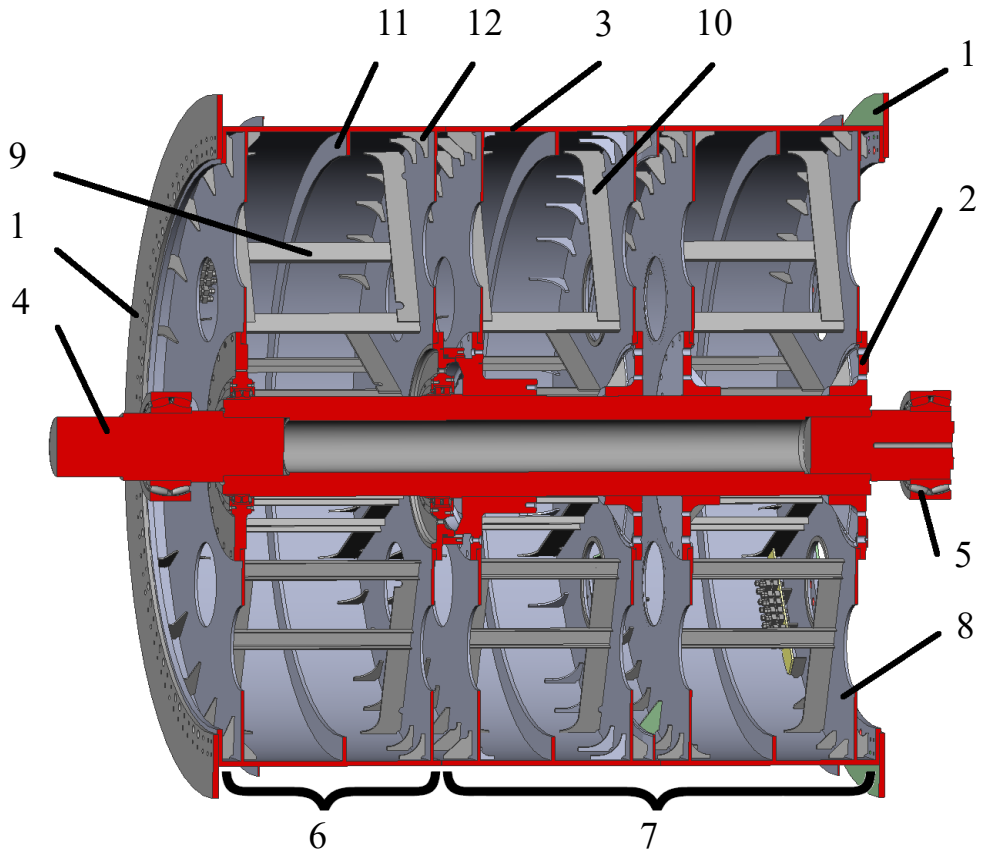

Fig. 6.1. Section of the drum of the angle grinder type TsR -6.75×6.2/1.95:
1 - brake discs; 2 - hubs; 3 - shell; 4 - shaft; 5 - bearings;
6 - drum part; 7 - jammed drum part;
8 - frontal plates; 9 - channels; 10 - ribs; 11 - frames; 12

ribs). To relieve the welds between the shell and the gussets on the inside, additional reinforcements in the form of scarves 12 are used. The stiffness between the shell and the surface between the holes of the headers is strengthened by welding ribs 10, which have a rectangular shape or a curved transition.

When lifting a load, the upper and lower ropes act as the working and idle ropes, respectively, and when changing the cycle, the opposite is true: the upper rope is idle and the lower rope will be working.

Lifts of the TsR type can be equipped with different braking systems [11, 17]: shoe or disc brakes, the choice of which is determined by the technical specifications. Disc brakes have a number of advantages over shoe brakes: they are more compact, they do not have a lever system (which is typical for shoe brakes), and they have a

higher response speed, which makes them preferable for use in mine hoists. In particular, the TsR-6.75×6.2/1.95 is equipped with a disc brake system. This system consists of a pair of racks with brake blocks (Fig. 6.2), which interact with brake discs located at the ends of the drum. These posts can be located either on the front side or on both sides of the drum of the mine hoist depending on the amount of braking torque.

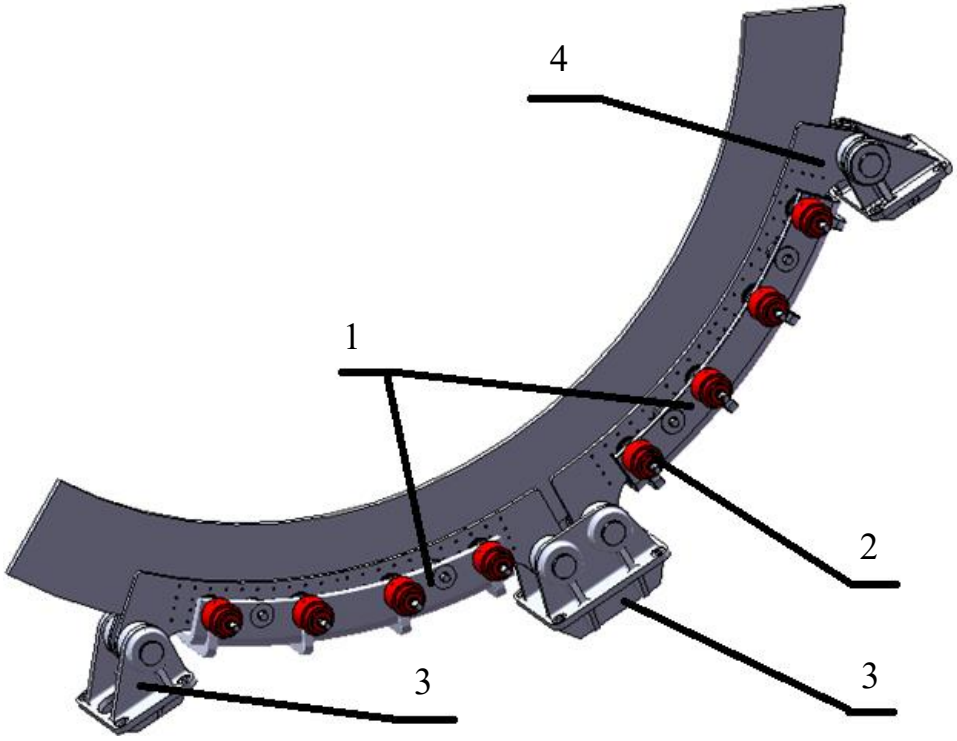

Fig. 6.2. Rack with brake modules:
1 - body; 2 - disc brake cylinder; 3 - rack; 4 - cheek

During operation of a split drum (as opposed to a two-drum system), the working rope is wound and the idler rope is unwound simultaneously. In order to prevent the working and idle ropes from crossing during operation, a gap is provided between them, approximately equal to the length of the drum splitter. When the rope reaches the transition from the splitter part to the jammed part, it enters a special groove due to the increased pitch of the last turn of this part. Passing through the cut, the rope moves to the jammed part of the drum and enters the shaped section of the first groove and, pressing against its edge, moves to the standard groove of the

jammed part of the drum.

Taking into account the increase in the depth of mining, the drums of the MHM type TsR, in order to increase the rope capacity, require lengthening of both their parts: the jammed and the splitter parts. For example, for a TsR-6.75×6.2/1.95 device, the total working length of the drum reaches 6200 mm, while the interchangeable part is 1950 mm long, with a distance of 38 so-called "empty" turns between the working and idle ropes. Increasing the length of the drum is a potential problem, as longer lengths contribute to a decrease in structural rigidity under working loads, especially in the axial direction. Reducing the axial stiffness of the drum during operation means that end runout at the edges of the drum will increase. This, in turn, is a negative factor when installing a disc brake, because the disc brake has installation rules that do not allow end runout of the brake disc to exceed 1.5-2 mm, with a distance of 3 mm between the disc and the pad.

As noted by Z. M. Fedorova, torsional stresses due to torque transmission can be neglected when calculating drum shells, as they are very small, and bending stresses due to rope tension should be taken into account only for long shells if the ratio of drum length *B* to diameter *D is high*:

$$\frac{B}{D} > 3\ldots4.$$

To increase the rope capacity of a winder drum, its length must be increased. Based on the recommendations for the design of mine hoist drums, the angle of deviation should be no more than 1°30′. By increasing the length of the drum, the angle of deviation also increases, and if its value is greater than 1°30′, there is a problem with rope winding on the casing, namely, the rope slipping off the groove. On the other hand, if the length of the drum is increased, to bring the deviation angle back to the recommended value, it is necessary to increase the length of the rope string by moving the machine away from the shaft or increase the height of the header. According to the design recommendations, the maximum string length

should not exceed 65 m, since increasing the string length beyond 65 m contributes to the appearance of axial and, as a result, transverse vibrations of the rope string, which can lead to a malfunction in the rope winding on the drum. When the length exceeds 65 m, it is customary to install intermediate support for the string in the form of rollers, which will wear out and require additional maintenance for normal operation.

On the other hand, by increasing the length of the drum, the axial movement of its ends increases, which, when using disc brakes, can cause a serious problem. As already mentioned, for the TsR-6.75×6.2/1.95, which operates in conjunction with disc brakes, for safe operation of the machine, the amount of end runout of the brake discs should not exceed 1.5-2 mm, with a gap between the disc and the pad of 3 mm.

To demonstrate the relevance of the problem of determining the axial stiffness of drums of this type, an experiment was performed on the example of a computer model of a TsR-6.75×6.2/1.95 drum (Fig. 6.1), in which the relationship between the length of the shell and the value of the axial displacement of its end under external pressure was found.

To do this, a shell with parameters similar to the drum of the TsR-6.75×6.2/1.95 machine was created and pressure was applied to the outer surface, modelling the action of the coiled rope (Fig. 6.3).

Let's calculate and analyse the axial displacement diagram shown in Fig. 6.4. We can see that the side face moves in the axial direction, i.e. the shell is lengthened, with a displacement of 9.389 mm at a length of 7202 mm, with a diameter-to-length ratio of the shell.

Let's carry out three more calculation cases in which we will reduce the length of the shell by 25%. As a result of the calculations, we will derive the dependence of the axial displacement value on the ratio of the drum length to the shell diameter (Fig. 6.5).

The result is a shell end runout of 6,942, 4,494 and 2,061 mm for the 5402, 3602 and 1802 mm long shells.

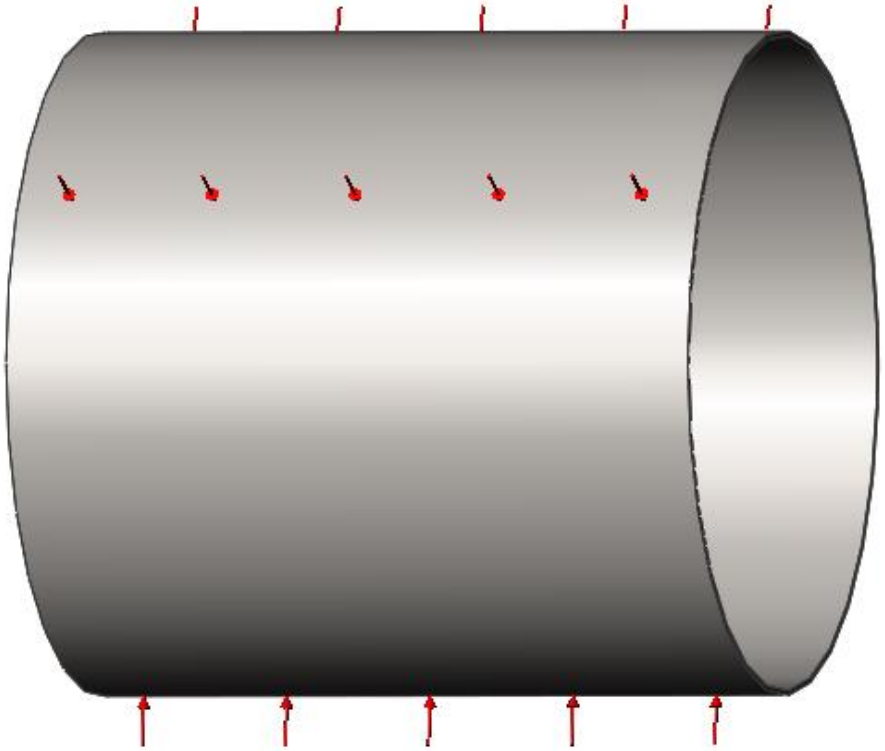

Fig. 6.3. External pressure that simulates the operation of the wound rope on the shell

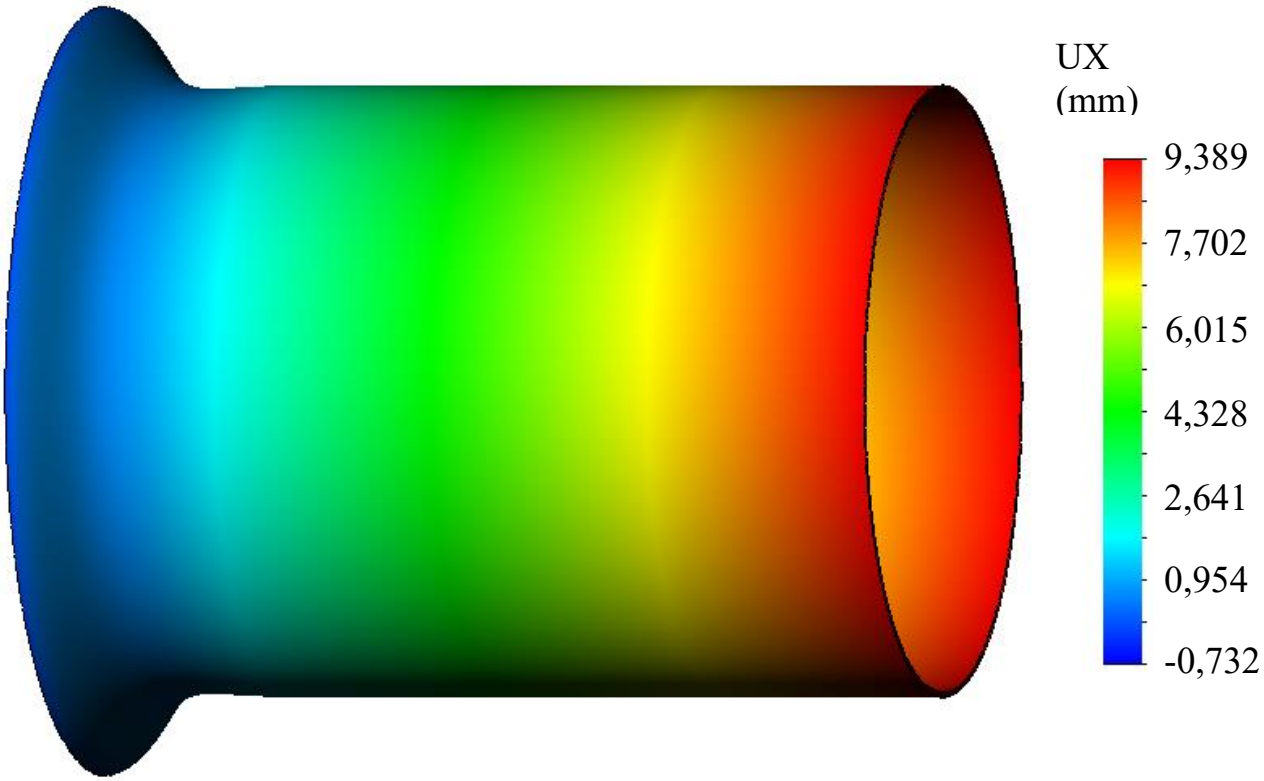

Fig. 6.4. Diagram of axial displacement of the casing under external pressure

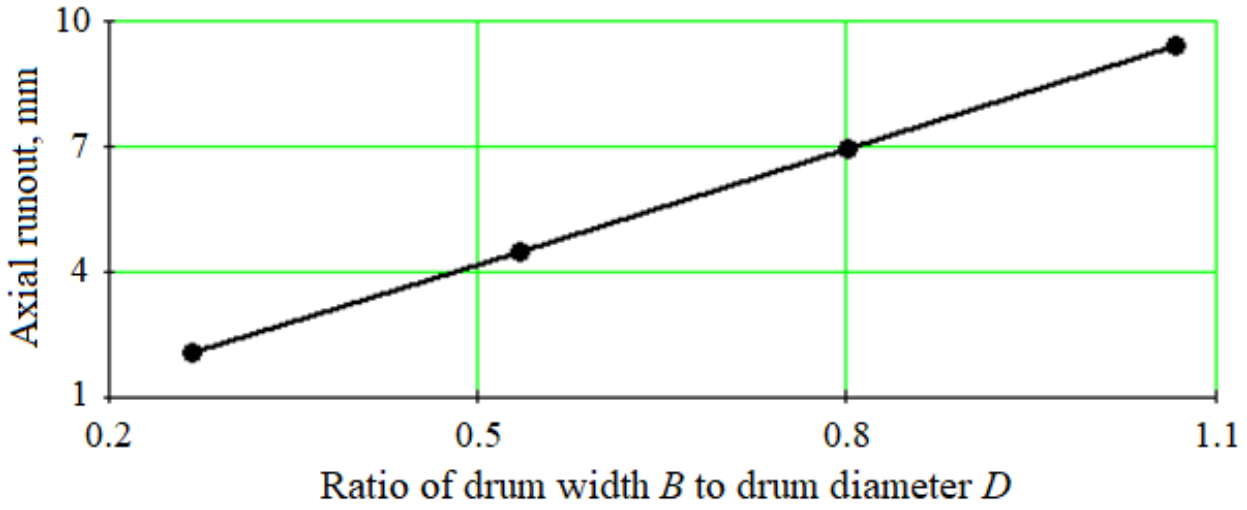

Fig. 6.5. Diagram of axial displacement versus drum length to shell diameter ratio

Analysing the graph, we conclude that the greater the value of the shell length ratio, the greater the displacement of the sidewall at a constant external pressure.

In this regard, it can be said that an increase in the length of the drum of a mine hoisting machine can lead to a large value of the brake disc end runout during operation, which may make it impossible to use disc brakes. All of the above proves the relevance of the study of axial stiffness for the possibility of using disc brakes in hoisting machines with long drums.

In the process of developing the method, a semi-empirical method was used to determine the design loads in the drum. The following assumptions were made: the tension force of the rope remains constant within one coil; the rope winding on the drum was modelled as a sequential application of discrete rings with a certain tension; the force in the rope coil that is wound on the drum is equivalent to the tensile force in the rope sheave; friction between the rope coils and the drum can be neglected.

In connection with the above, the following research objectives have been set:

1. Development of a computer finite element model of a long drum.

2. Investigation of the influence of lifting machine parameters on the stress-strain state of a long cylindrical drum.

3. Development of methodological recommendations for design**.**

We use the method for calculating multilayer composite structures developed by V.V. Bolotin and Yu. M. Novichkov:

1) a simplified homogeneous model is studied with corresponding boundary conditions;

2) the model SSS is analyzed and the most stressed areas are selected; the areas with the highest SSS are selected and boundary conditions for them are determined;

3) these areas from a homogeneous material are calculated and this material characteristics are determined;

4) a model from this material with specified boundary conditions is created and its calculation is performed;

5) the stresses are found at the boundaries of the selected areas and their calculation is performed for the real material.

The MHM drums belong to the class of thin-walled strengthened structures with elements of various thickness. This leads either to a large quantity of nodes with a mesh with a given maximum aspect ratio, or to a mesh with fewer nodes but a higher maximum aspect ratio. The MHM drums of a complicated structure are characterized by a large quantity of relatively thin strengthening elements.

The so-called “averaging method” has been widely used in solving the problems of celestial mechanics, the main technique of which is that the right-hand sides of complex differential equations are replaced with “smoothed“, averaged functions that do not contain rapidly changing system parameters.

In the statics and dynamics of ribbed shells, this method was used by I.V. Andrianov, V.A. Lesnichaya and L.I. Manevich.

When calculating complex structures such as aircraft fuselages and ship hulls, numerous solution methods that are economical in terms of machine time and resources should always use information about the analytical nature of the task.

Structural anisotropy schemes have been widely used in engineering calculations, according to which the initial shell is replaced with a smooth one with some of the specified parameters.

Inhomogeneities of the design or structure of the material are usually repetitive, periodic, therefore, valuable information about the system behavior can be obtained by replacing it with a simpler one with some of the specified (averaged) characteristics, which is typical when changing to structural orthotropy scheme. In this case, correct information can be obtained about such global characteristics as frequencies of vibrations or displacements, local ones such as stresses, determined with a large error. At the same time, the very determination of these parameters is a non-trivial task.

The essence of using the averaging method in structural mechanics can be briefly described by the following algorithm:

1. The initial structure is presented in the form of a set of nodes that allow a priori representation of their load and SSS.

2. The averaging parameter is chosen, usually the thickness of the shell or frontal, etc.

3. Parametric models of each such node are constructed.

4. Typical calculation cases are selected for all nodes, for example for strengthened drums – this is an axially-symmetrical compression or bending of the drum as a beam.

5. The values of optimization parameters are determined for each node, at which the averaged node stiffness in the selected calculation case of loading coincides with the initial strengthened node stiffness.

6. For each calculation case of loading the strengthened structure, an assembly is performed from the corresponding averaged nodes.

7. The calculations are compared and the most dangerous one is chosen.

6.2 Selecting the boundary conditions and calculating the initial model for the TsR-6.75×6.2/1.95 mine hoisting machine drum.

A distinctive feature of the drums under consideration is that they consist of two wedged parts and one interchangeable part. This drum has two shells, six fronts

supported by braids and ribs, six frames, two flanges, two brake discs, a shaft with hubs and two spherical double row roller bearings (Figure 6.6).

To develop a calculation methodology, we will represent the drum as a structure consisting of ten components: 1 - shaft with hubs; 2 - spherical bearing; 3 - left ring with braids of the interchangeable part; 4 - left shell ring with a rib; 5 - right ring with braids of the interchangeable part; 6 - left ring with wedged part braids; 7 - shell ring with rib; 8 - ring with two lobes; 9 - right shell ring with rib; 10 - right ring with wedged part braids.

The design of the drum under consideration uses two spherical double-row bearings that allow the shaft to rotate in three directions and prohibit its vertical movement.

When calculating the radial stiffness of the bearings, we will neglect the concentrated forces of the coiled and twisted ropes, and take into account only the weight of the drum with the rope, which is 2207 kN.

$$P_c = P_d + P_r = 2207 \text{ kN},$$

where P_d = 2049.3 - weight of the drum, kN

P_r - rope weight, kN:

$$P_r = H \cdot m_r \cdot g = 1157.9 \text{ kN},$$

where *H is* the lifting height, m

m_r - weight per linear metre of rope, kg

g is the acceleration of free fall, m/s^2.

It is assumed that eight rollers are in contact, so we use one eighth of the bearing load to calculate the FEA.

$$F_{b1} = 137.9 \text{ kN}.$$

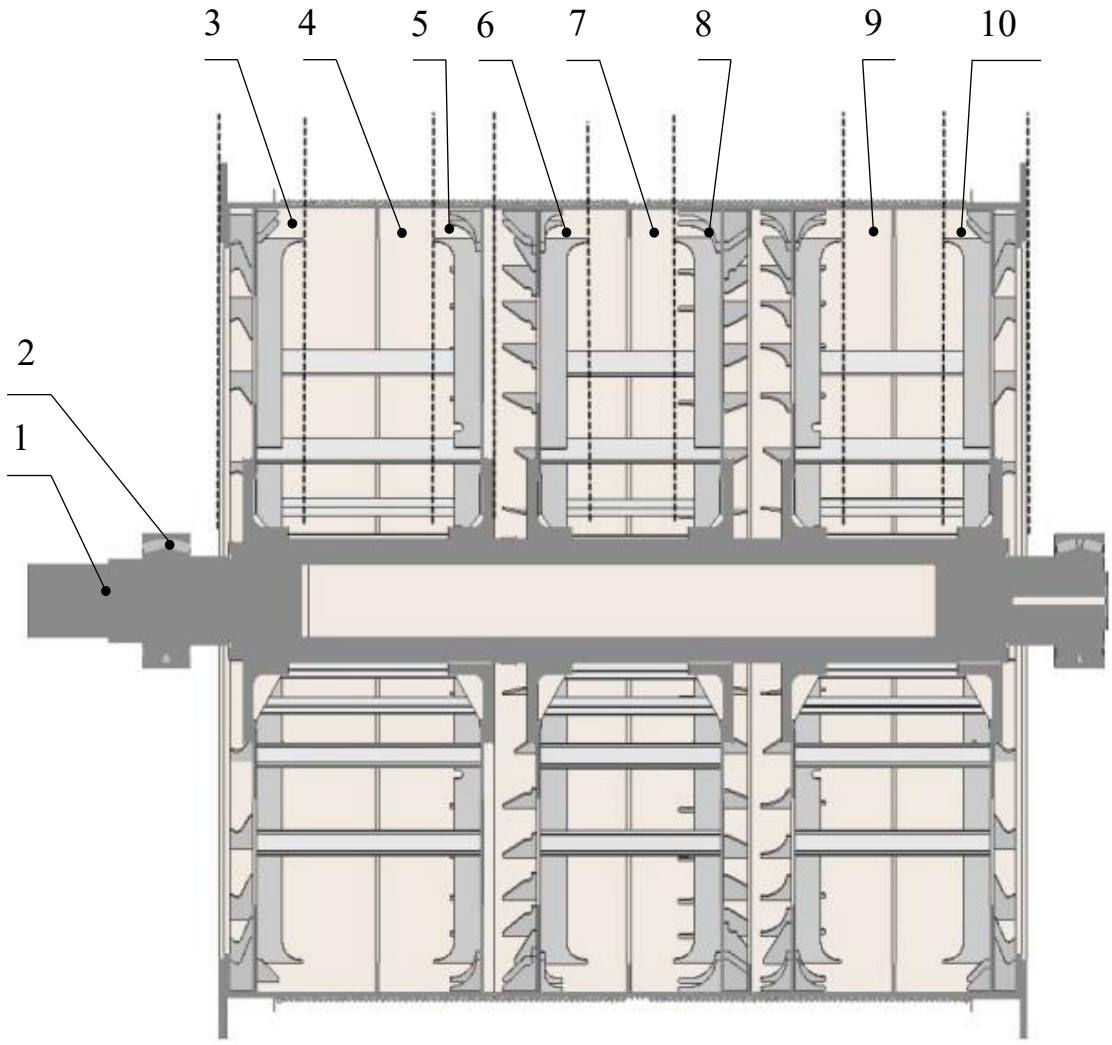

Fig. 6.6. Drum construction

The load acting on the bearing roller:

$$q = \frac{F_{b1}}{h} = 7.45 \cdot 10^5 \text{ N/m},$$

where*:* h = 185.1 - length of the bearing roller, mm,

For the analytical calculation of the radial stiffness of the bearing, we will represent one roller and the inner ring of the bearing as two cylinders with diameters D_1 , equal to 85 mm, and D_2 , equal to 847.5 mm. Figure 6.7 shows a diagram of the contact interaction between the two cylinders. The dashed line with two points represents the undeformed cylinders with diameters D_1 and D_2 .

Initial distance between cylinder axes:

$$L_1 = \frac{D_1 + D_2}{2} = 466.3 \text{ mm},$$

Apply a linear load *q to the* axis of the first cylinder. The axis of the second cylinder is fixed. After the load is applied, the cylinders move closer together, forming a flat contact surface with a width of *2B*. denote by L_2 distance between the cylinder axes after deformation and by axes, which is equal

$$\delta = L_1 - L_2, \text{ mm}$$

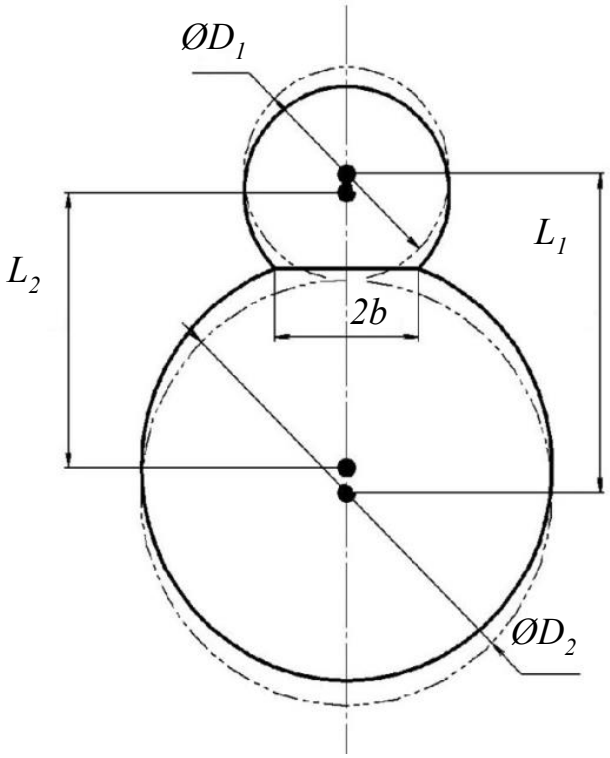

Fig. 6.7. Diagram of contact interaction between the roller and the inner ring of the bearing

The following expressions follow from the Hertz-Belyaev theory.

The elastic constant of tangent bodies:

$$\mu = \frac{1 - \nu_1^2}{E_1} + \frac{1 - \nu_2^2}{E_2} = 8.9 \cdot 10^{-12} \text{ Pa.}^{-1}$$

Half-width of the contact strip [1]:

$$b = 1.128 \cdot \sqrt{\mu \cdot q \cdot 0.5 \cdot \frac{D_1 \cdot D_2}{D_1 + D_2}} = 5.709 \cdot 10^{-4} \text{ m.}$$

$$\delta = \frac{2 \cdot q}{\pi} \cdot \left[\frac{1 - v_1^2}{E_1} \cdot \ln\left(\frac{D_1}{b} - 0.107 \right) + \frac{1 - v_2^2}{E_2} \cdot \ln\left(\frac{D_2}{b} - 0.407 \right) \right] = 0.0261 \text{ mm,}$$

where: E_1 , E_2 = 2.1-10^5 - elastic moduli of the first and second bodies, MPa;

v_1, v_2 = 0.25 - Poisson's ratios of the first and second bodies;

B - half-width of the contact strip.

Analytical stiffness of bearing assemblies:

$$C = \frac{F_{b1}}{\delta} = 5.284 \cdot 10^9 \text{ N/m,}$$

Following the recommendations for self-aligning rolling bearings, the axial stiffness should be equal to the radial stiffness.

As a parametric model of the bearing, we will use the SolidWorks Simulation tool "Bearing support".

The fourth, seventh and ninth drum assemblies are rings consisting of a grooved shell with a rope supported by an annular frame. As a model of these assemblies, we consider a homogeneous shell with equivalent stiffness.

Since we are modelling the shell with an axisymmetric model, it is sufficient to limit ourselves to a fragment bounded in the circumferential direction by five degrees.

We use the original structure as a model of the frame, and apply the following algorithm to model the shell with grooves and rope.

In axial bending of the drum, three main sections can be distinguished: the upper section, where tensile stresses prevail, the lower section, where compression stresses prevail, and the middle section, where bending stresses prevail. The

boundary conditions for axisymmetric bending (Figure 6.8a) are as follows: the left side face of the shell is fixed with respect to normal and radial displacements, and a radially directed force is applied to the right side face. As a result of the calculation, we will find the average radial displacements of the right side face.

The second design case is axisymmetric tension. The boundary conditions are shown in Figure 6.8 b: the left face is fixed against axial displacements, and an axial force is applied to the right face. As a result of the calculation, we obtain the average axial displacement of the right edge.

Let's set the task of finding the equivalent thickness *H of a* homogeneous shell from the point of view of axisymmetric bending.

Let's calculate the axisymmetric bending of a homogeneous shell with thicknesses H_1 and H_2 (along the bottom and tops of the grooves). Then, using linear interpolation, we will find the thickness of the homogeneous shell and perform a test calculation. If the obtained value of the radial displacements differs from the interpolation results by more than 10%, an additional calculation should be performed with the average thickness between the thicknesses H_1 and H_2 and use quadratic interpolation.

For the rope casing, in the case of axisymmetric bending of a fragment limited in the circumferential direction to five degrees, an average radial displacement of 0.001534 mm was obtained at a load of 1 MN, and for axisymmetric tension - 0.000196 mm at a load of 10 kN. As a result of linear interpolation, the thickness values were obtained: H_{bend} is 44.53 mm and H_{str} is 42.53 mm. The verification calculation gave an error in bending of 0.2% (Figure 6.9 a) and in tension of 0.22% (Figure 6.9 b).

For the computational model, the thickness of the shell is assumed to be equal to the smaller of the obtained thicknesses (42.53 mm).

In order to develop a calculation method that allows obtaining an acceptable result on a medium-power computer, the drum was previously calculated on a powerful computer, with mesh characteristics based on curvature, which were: maximum element size - 50 mm, minimum element size - 10 mm, total nodes -

3352229, total elements - 1874904, maximum aspect ratio - 11.26, percentage of elements with an aspect ratio >10 - 0.000213.

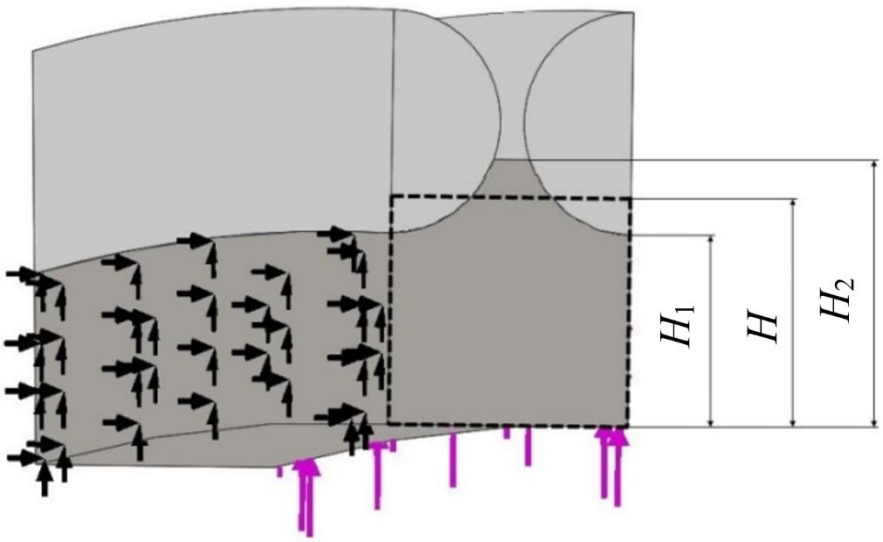

a

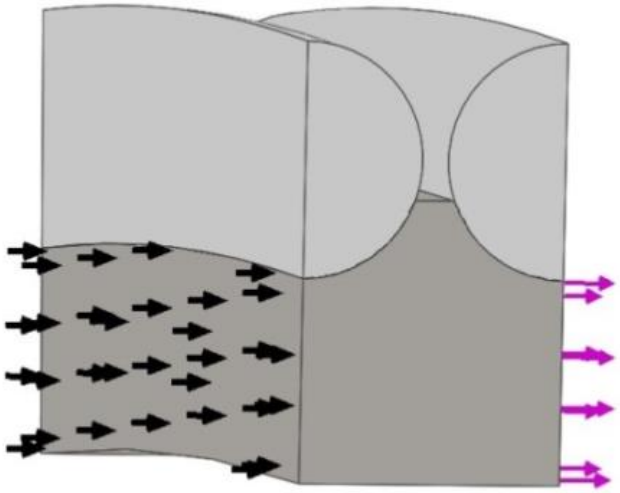

b

Fig. 6.8. Boundary conditions in axisymmetric bending (a)
and in axisymmetric tension (b)

As boundary conditions, we consider the loading of the drum by gravity, two tensile forces from the running and running ropes, and pressure from the coiled rope.

Due to the small width of the gap between the two parts of the drum (3 mm), we will neglect the stiffness of the rope connecting these parts.

To reduce the resource intensity of the problem, we will apply tensile forces reduced by half not to the ropes, but to the sub-facets formed by the intersection of the rope and the drum (Figure 6.10). In this case, to eliminate the peculiarities of the resulting cross-sectional shape, we will replace the rope with a body of square cross-section.

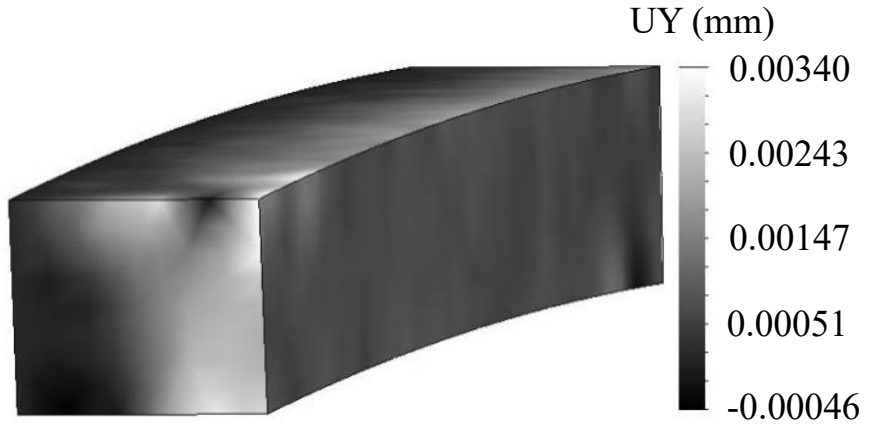

a

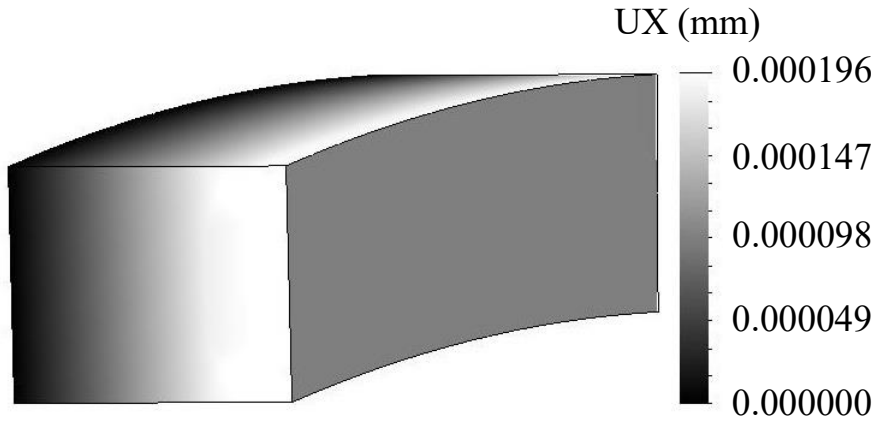

b

Fig. 6.9. Verification calculations of radial displacements in axisymmetric bending (a) and axial displacements in axisymmetric tension (b)

The tensile forces from the running and running ropes are located:

$$T_2 = T_{\max} - 0.5 \cdot P_r = 371.1 \text{ kN},$$

$$T_3 = T_{\min} + 0.5 \cdot P_r = 61.05 \text{ kN},$$

where $T_{\max}$ is the maximum static tension of the rope, kN:

$T_{\min}$ is the minimum static tension of the rope, kN:

$$T_{\min} = T_{\max} - T_{diff} = 140 \text{ kN},$$

where T_{diff} = 310 is the difference in rope tension, kN.

The angles of inclination to the horizon are 38° and 43° for the running and running ropes, respectively.

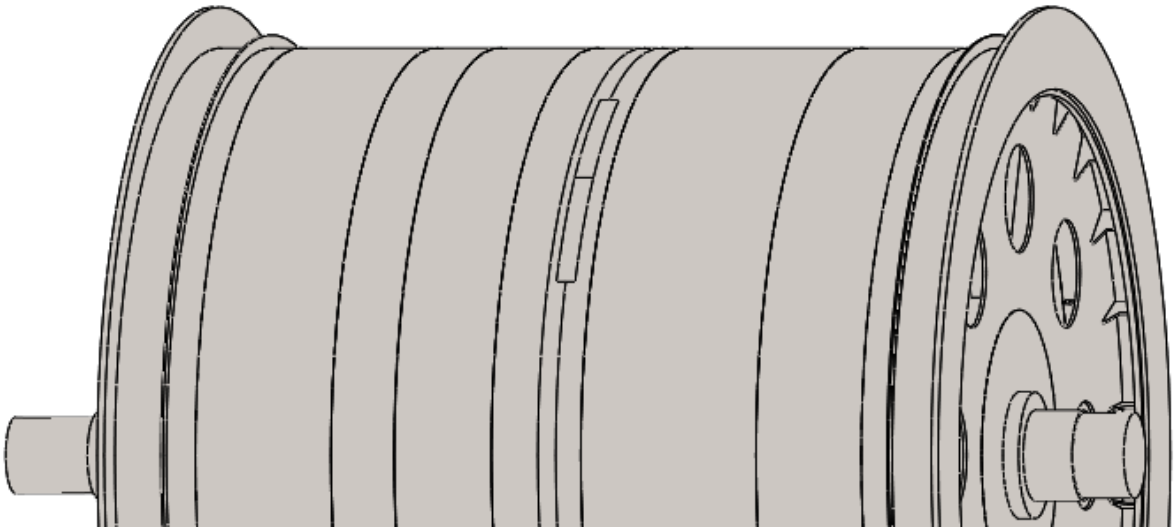

Fig. 6.10. Subgames for the application of the tensile force of the rope

The pressure distribution from the rope being coiled and wound is symmetrical about the centre of the drum (Figure 6.11):

$$p_{av} = \left(T_{\max} - 0.25 \cdot P_r\right) / R \cdot t = 2.385 \cdot 10^6 \text{ Pa},$$

$$p_1 = p_4 = T_{\max} / R \cdot t = 2.614 \cdot 10^6 \text{ Pa},$$

$$p_2 = p_3 = T_2 / R \cdot t = 2.156 \cdot 10^6 \text{ Pa},$$

where T_2, T_{max} is the static tension of the rope at points 2 and 3, N

R - drum radius, mm

t - groove cutting pitch, mm.

In Figure 1.6, the following values are assumed: x_1 = 1.205 m; x_2 = 4.071 m; x_3 = 4.224 m; x_4 = 7.405 m;

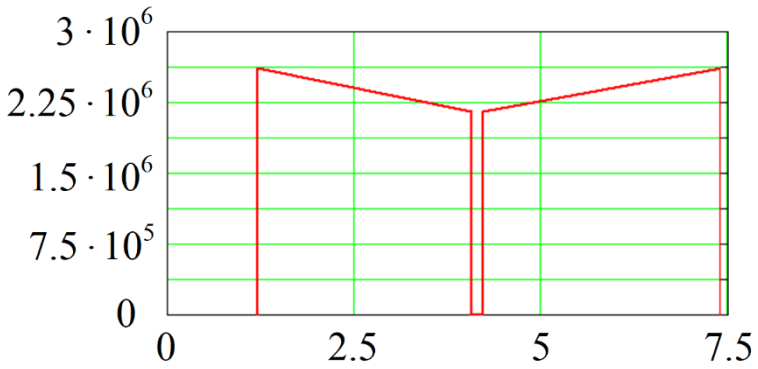

Fig. 6.11. Diagram of rope pressure distribution over the width of the drum

The pressure from the wound rope must be set unevenly, since the weight of the wound rope will cause a difference in pressure from the edge to the middle of the drum (design case). To account for the unevenness, use the linear interpolation formula:

$$p(x) = \begin{cases} 2.385\ MPa \cdot (0.588 + 0.055\ м^{-1} \cdot x), & \text{де } x_3 \le x \le x_4 \\ 2.385\ MPa \cdot (1.067 - 0.061\ м^{-1} \cdot x), & \text{де } x_1 \le x \le x_2 \end{cases}$$

Since gravity does not match the original model, it was decided to change the material density of the parametric model:

$$\rho_{simp} = m_{orig} / V_{simp} = 9030.764\ \text{kg/m}^3 .$$

where m_{orig} is the weight of the original drum model, kg

V_{simp} is the volume of a simplified drum model, m^3.

According to the calculation results, it turns out that under the load from lifting the loaded skip from the right side of the drum (Figure 6.12 a), the maximum axial

displacements of the right and left edges of the brake discs are 0.854 mm and 1.921 mm, respectively.

The batten is a thin-walled disc that works in bending, and it is advisable to check its effect on the overall deformed state of the assembly, since its consideration leads to an increase in the number of nodes.

The diagram in Figure 6.12 b shows that the flanges do not have a major impact on the overall deformed state.

The maximum axial movement is 2.013 mm and the error is 4.8%.

6.3. Application of the averaging method for calculating the displacements of a drum of a non-standard design for amilling machine TsR -6.75x6.2/1.95

Let's illustrate the application of the method to the calculation of a specific lifting machine.

Based on the algorithm of the averaging method, let's break down the drum structure into ten nodes (see Figure 6.6).

It is unacceptable to choose the thickness of the shell as an averaging parameter, since it is impossible to take into account the influence of ribs on the behaviour of a particular node by changing this parameter, so we choose the thickness of the shell equal to the original one, and take into account the influence of reinforcing elements by changing the thickness of the frontal sheet.

Based on the analysis of the deformed shape (Figure 6.12), we select two design cases for nodes 3, 5, 6, 8 and 10 - shear and loading with a uniform external pressure.

As boundary conditions for the model of the assembly in the "shear" design case, we consider its loading by a bending moment of uniformly distributed and oppositely directed forces on the end faces equal to 1 MN. The edge of the frontal plate is fixed at the point where it is connected to the hub (Figure 6.13 a). Boundary conditions for the design case "pressure" - loading of the outer cylindrical face of the shell with a pressure directed radially to the centre equal to 1 MPa, the fixed face is similar to the previous design case (Figure 6.13 b).

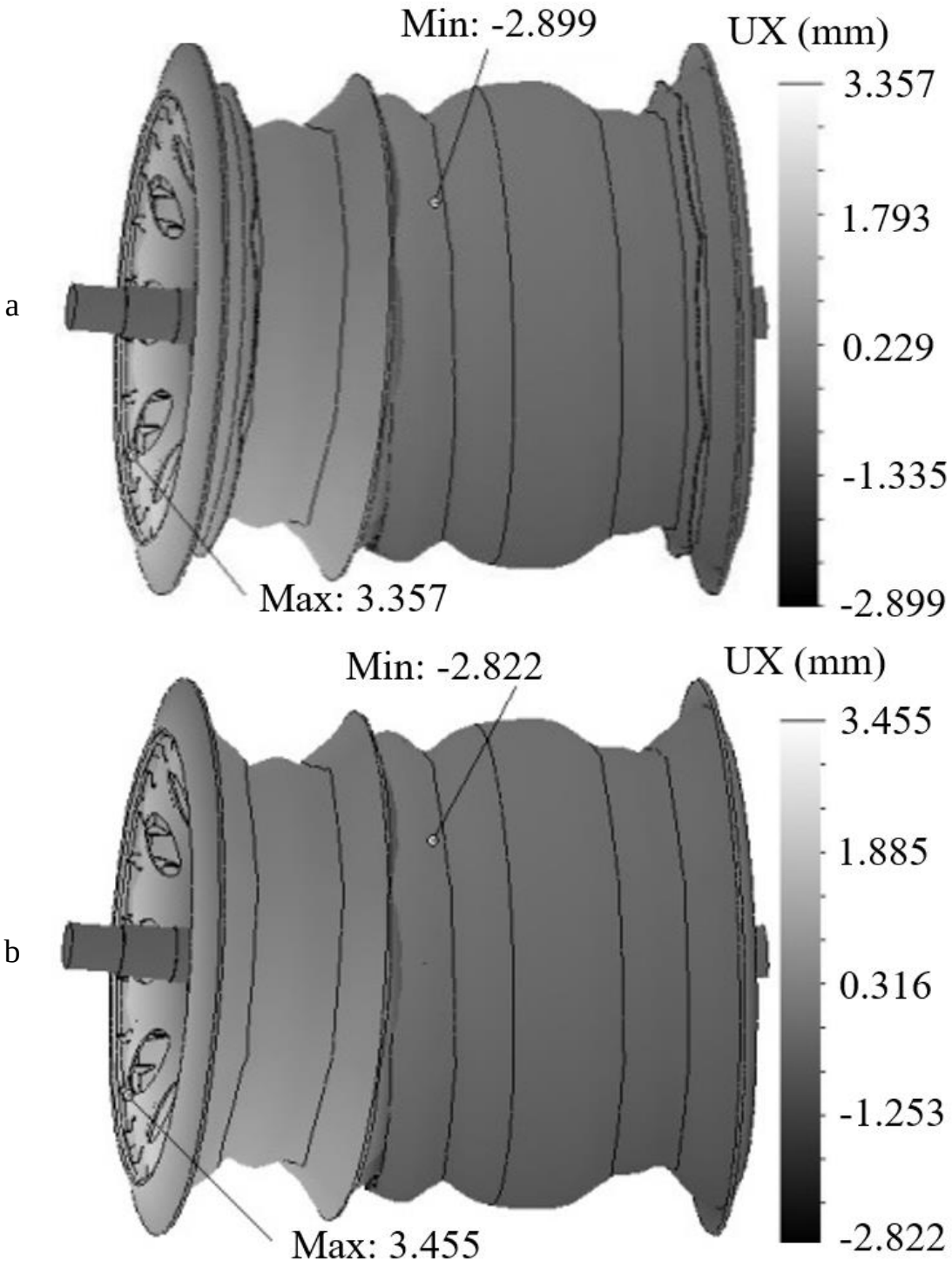

Fig. 6.12. Diagram of axial displacements of the drum with a flange (a) and without a flange (b)

As an averaging parameter, let's use the variable thickness of the frontal plate in the design of the assembly without braids and ribs (Figure 6.14 b), to find which we use the difference in the average vertical displacements of the outer right and left edges of the shell:

$$\Delta = y_r - y_l,$$

where y_n and $y_л$ *are the* average vertical displacements of the outer right and left edges of the shell.

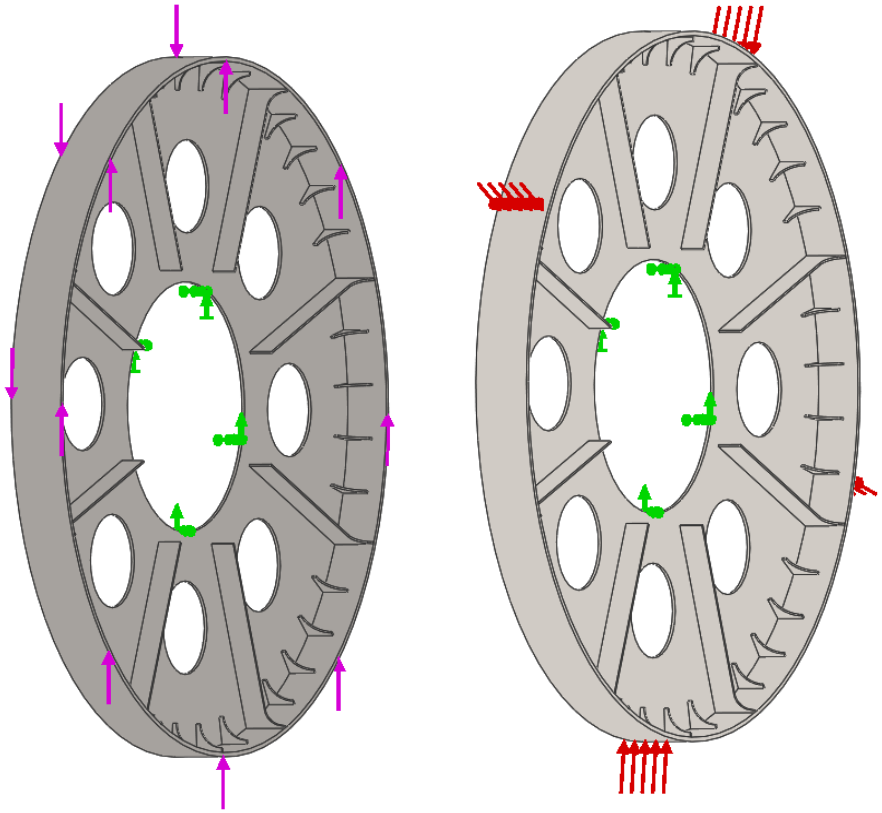

a b

Fig. 6.13. Boundary conditions for the calculation of node 5: a) design case "shear"; b) design case of uniform pressure loading

The difference in the average vertical displacements of the left and right outer edges of the shell will be used as a measure of the rotation of the assembly during shear.

For a parametric node, we find the thickness of the frontal lobe *b* of the parametric model of node 5 from the quadratic interpolation of three calculations, in the first of which, by the method of iteration, we select a thickness of the frontal lobe b such that the difference in average vertical displacements is 5-10% greater than

the difference in displacements for the original node, and in the next two, we increase the thickness by 5 mm in each case.

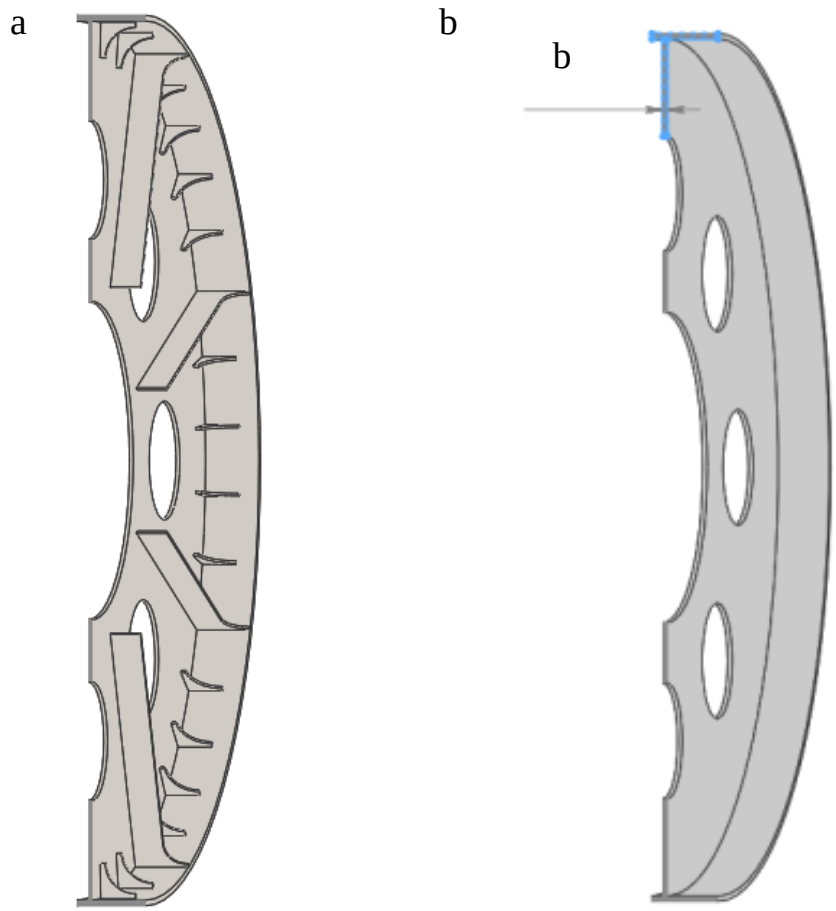

Fig. 6.14. Section of node 5: a) original structure; b) parametric model

As a second design case, we will consider loading with an external pressure of 1 MPa. The maximum radial displacement of the outer edge of the assembly shell, located at the maximum distance from the frontal plate in the axial direction, will serve as a parameter for finding the thickness of the frontal plate.

Similarly to the "shear" case, we will find the thickness of the frontal lobe *b of the* parametric model of node 5 from the quadratic interpolation of the three calculations.

Due to the unequal masses of the original design of the assembly and its parametric model, further calculation will give a large error, so we will find the true material density of the parametric assembly for both design cases from the formula:

$$\rho_{simp} = \frac{m_{orig}}{V_{simp}},$$

where m_{orig} is the mass of the initial model of the node, kg

V_{simp} is the volume of a simplified model of the node, m^3.

Node 6 differs from node 5 in that the kerchiefs are located on both sides of the frontal area. The boundary conditions for the "shear" design case are selected similarly to node 5. As a result of the calculation, we find the difference in the average vertical displacements of the end edges. As the second design case, we consider loading with an external pressure of 1 MPa. After that, for each of the calculations performed, we find the rational thicknesses of the gussets using quadratic interpolation, similarly to the previous node.

A distinctive feature of node 8 is the high stiffness caused by the presence of two frontal lobes. The parametric model is also designed with two frontal lobes. Similarly to the above cases, we perform two calculations for the original and parametric nodes - "displacement" and "pressure" - and find the difference in the average vertical displacement and the maximum radial displacement, respectively. After that, for each of the calculations performed, we find the rational thicknesses of the lobes using quadratic interpolation, similarly to the previous node.

In contrast to the above nodes, node 3 has a flange and a brake disc. The boundary conditions are similar to node 5, but the side face of the brake disc is used as one of the end faces. For the original and parametric node, we perform two calculations of "displacement" and "pressure" with the same boundary conditions as in the previous cases considered and find the difference in the average vertical displacement and the maximum radial displacement, respectively. After that, for each of the calculations, we use quadratic interpolation to find the rational thicknesses of the frontal lobes similarly to the previous nodes.

Node 10 is the mirror image of node 3 and is modelled with the same model.

Create an assembly of a simplified model of the drum of the hoisting machine from the parametric models of nodes 3-10, shaft with hubs (node 1) (Figure 6.15).

6.4. Testing of the developed methodology for determining the axial stiffness of a drum of a non-standard design of the TsR-6.75x6.2/1.95 machine

As an example of a drum of a hoisting machine of a complicated design, let's choose the drum of the TsR-6.75×6.2/1.95 machine, which has reinforcements in the form of 48 ribs, 224 braids, 20 mm thick, 48 braids, 16 mm thick and 64 braids, 14 mm thick.

Figure 6.6 shows a general view of the drum of a single rope single motor hoist with a single-layer split cylindrical drum of a gearless design with a single layer winding.

Type of hoist - skip-skip, hoisting height - 1477.657 m, drum diameter - 6750 mm, jammed part width - 4250 mm, interchangeable part width - 1950 mm, maximum static rope tension - 450 kN, maximum difference in rope tension - 310 kN, groove pitch - 51 mm.

The drum consists of a wedged and an interchangeable part, on which two ropes are wound - a running and a running rope. There is a 3 mm gap between these parts. BRIDON "Dayform" 34LR/PI (34×19) steel multi-strand cargo rope, 46 mm in diameter.

The shaft is mounted in two spherical bearings 241/710. There is a cylindrical part on the right side of the shaft for connection to the actuator.

Bearing modelling is similar to the calculation of the original drum model.

For the initial node 5, the difference in average vertical displacements is equal (Figure 6.16 a):

$$\Delta = 7.209 - \left(-1.598\right) = 8.807 \text{ mm.}$$

The thickness of the frontal plate is 38 mm and the corresponding difference in maximum vertical displacement of the edges is 8.734 mm. In this case, the error, i.e. the difference between the difference in the average vertical displacements of the original reinforced node and the parametric model, was 0.8%. The diagram of the

verification calculation of node 5 (design case "shear") is shown in Figure 6.16 b.

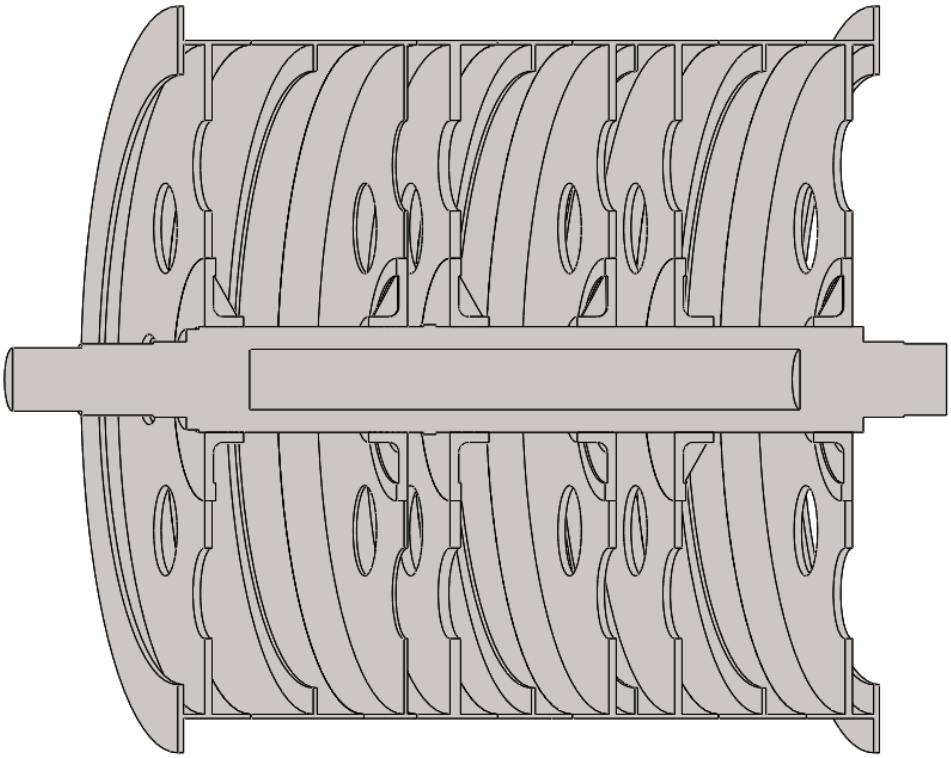

Fig. 6.15. Parametric model of the hoist drum

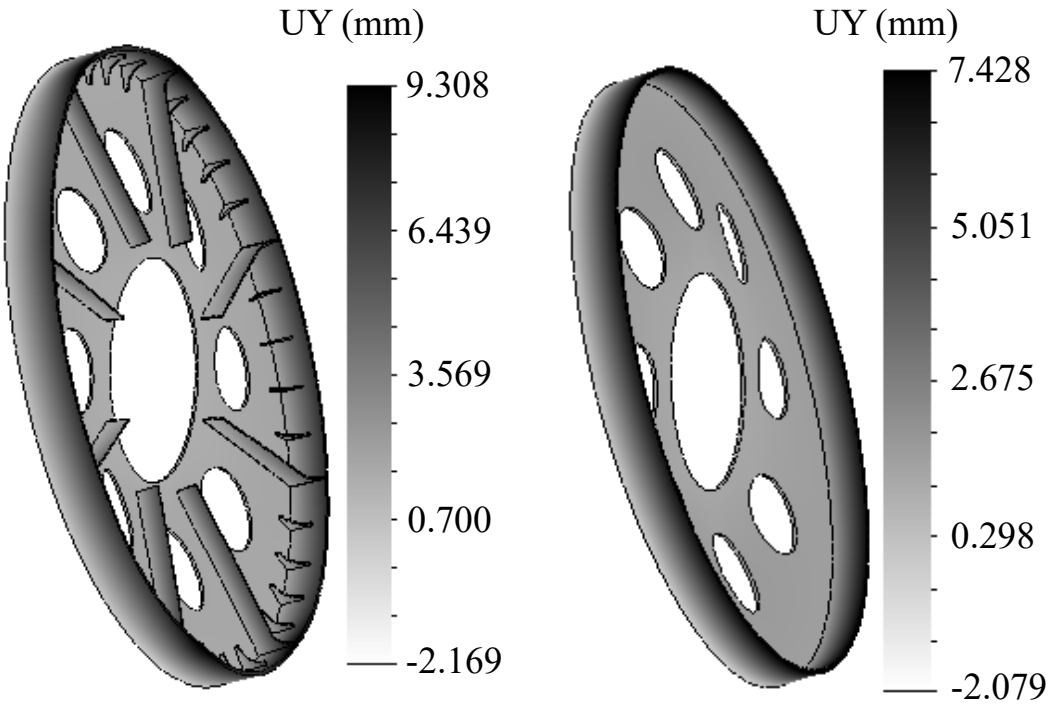

a b

Fig. 6.16. Vertical displacement diagram of the original model (a and verification calculation (b) of node 5

The density of the parametric model for the design case "shear" is 9855.96 kg/m^3 .

Similarly to node 5 for the design case "shear", we carry out verification calculations for nodes 6, 8 and 3 (10) and find the values of the thicknesses of the lobes for these nodes (Table 6.1).

In Table 6.1, the letter δ_1 denotes the difference in the average vertical displacements of the edges of the original assembly, mm; s is the thickness of the frontal area of the averaged model, mm; δ_2 is the difference in the average vertical displacements of the edges of the averaged model of the assembly, mm; Δ is the error, %.

The material density for nodes 6, 8 and 3 (10) is 10470.39 kg/m^3 , 8280.21 kg/m^3 , 9126.06 kg/m^3 , respectively.

Table 6.1.

Values of lamina thicknesses for the design case "shear"

node number	δ_1	s	δ_2	Δ
5	8.807	38	8.734	0.8
6	16.617	39.374	16.665	0.3
8	1.231	55.174	1.230	0.08
3 (10)	9.013	45.231	9.007	0.07

For the output node 5, the value of the average radial displacement is -1.749 mm (Figure 6.17 a).

The thickness of the frontal lobe of the averaged model is 36.284 mm and the corresponding maximum edge displacement is -1.748 mm. In this case, the error, i.e. the difference between the maximum radial displacements of the original reinforced node and the parametric model, was 0.06%. The diagram of the verification calculation of node 5 (design case "pressure") is shown in Figure 6.17 b.

The density of the parametric model for the design case "pressure" is 10051.68 kg/m^3 .

The material density for nodes 6, 8 and 3 (10) is 5196.19 kg/m^3 , 6689.91 kg/m^3, 6941.43 kg/m^3 , respectively.

Similarly to node 5 for the design case "pressure", we carry out verification calculations for nodes 6, 8 and 3 (10) and find the values of the thicknesses of the lobes for these nodes (Table 6.2).

In Table 1.2, the letter δ_3 denotes the maximum radial displacement of the edge of the original node, mm; s is the thickness of the lobe of the averaged model, mm; δ_4 is the maximum radial displacement of the edge of the averaged model of the node, mm; Δ is the error, %.

To create a finite element model of the drum, a medium-power computer was used, on which the calculation was limited to the number of finite element mesh nodes equal to 750000.

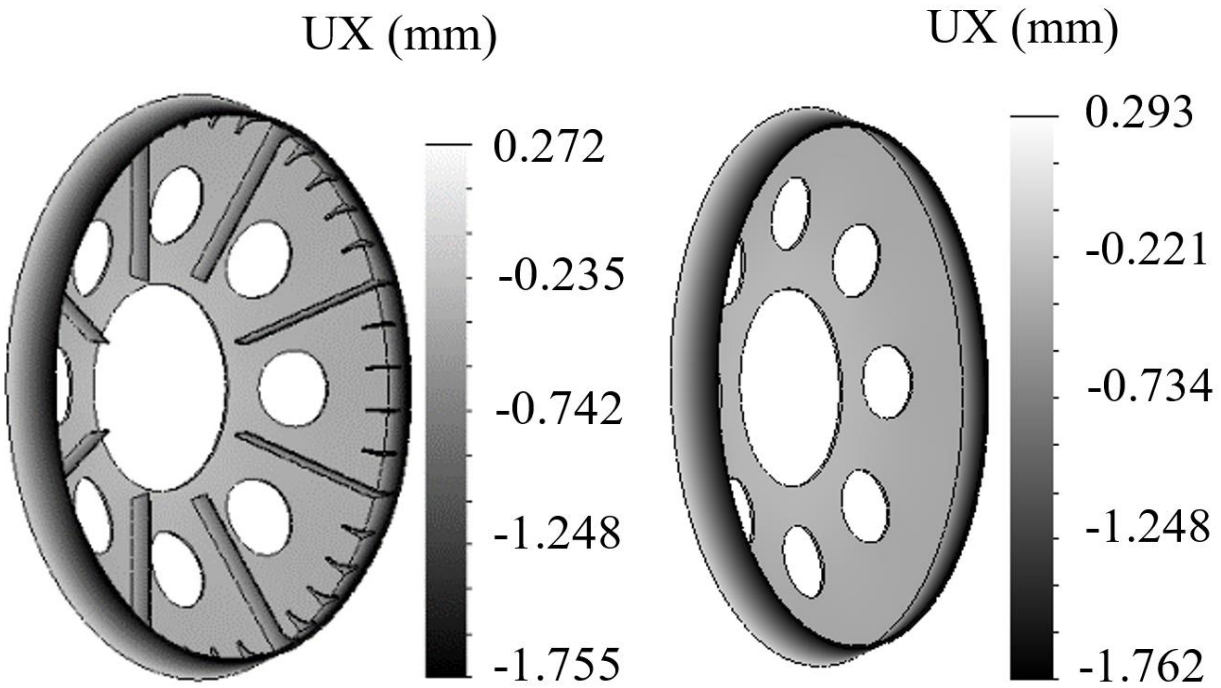

a b

Fig. 6.17. Radial displacement diagram of the original model (a and verification calculation (b) of node 5

Based on the found values of the parameters of the models of each node, we will create sketches of the corresponding bodies of revolution with the subsequent cutting of eight symmetrically located holes in the frontal area.

As a parametric model of the shaft with hubs (item 1, Figure 6.6), we select the original design of the assembly.

Table 6.2.

Values of the thicknesses of the frontal lobes for the design case "pressure"

node number	δ_3	s	δ_4	Δ
5	-1.749	36.284	-1.748	0.06
6	-1.048	109.444	-1.048	0
8	-1.078	75.416	-1.080	0.19
3 (10)	-1.121	76.469	-1.121	0

As a result of creating finite element meshes, curvature-based meshes with a maximum element size of 100 mm were obtained for the design cases "shear" and "pressure" with characteristics:

- for "shift": the number of nodes is 645107, the maximum aspect ratio is 23.547;

- for "pressure": the number of nodes is 662055, the maximum aspect ratio is 23.422.

The calculation was performed using the FFEPlus software. The calculation time was 10.5 minutes.

As a result of the calculations, the axial displacements of the brake disc edges of the drum were obtained:

- calculated case "displacement": for the wedged part (Figure 6.18 a), the maximum positive value is 0.654 mm, the minimum negative value is 0.355 mm, for the interchangeable part (Figure 6.18 b), the maximum positive value is 1.766 mm, the minimum negative value is 0.176 mm.

- calculated case "pressure": for the wedged part (Figure 6.19 a), the maximum positive pressure is 0.584 mm, the minimum negative pressure is 0.433 mm, for the interchangeable part (Figure 6.19 b), the maximum negative pressure is 1.327 mm, the minimum negative pressure is 3.246 mm.

The maximum error was 8.1% for shear and 69% for pressure.

6.5 Conclusion to the chapter

Disc brakes have a number of advantages over shoe brakes: they are more compact, they do not have a lever system (which is typical for shoe brakes), and they have a higher release rate, which makes them preferable for use in mine hoists. In particular, the TsR-6.75×6.2/1.95 is equipped with a disc brake system. On the other hand, the main disadvantage is the maximum permissible brake disc runout during operation, which is 1.5-2 mm.

Increasing the rope capacity of the drum by lengthening its casing, one may face the problem of significant end runout. In the experiment, a direct correlation was obtained between the length of the drum and the amount of end runout, which shows that the longer the length of the shell, the greater the amount of end runout, which in turn can make it impossible to use disc brakes in the hoist complex.

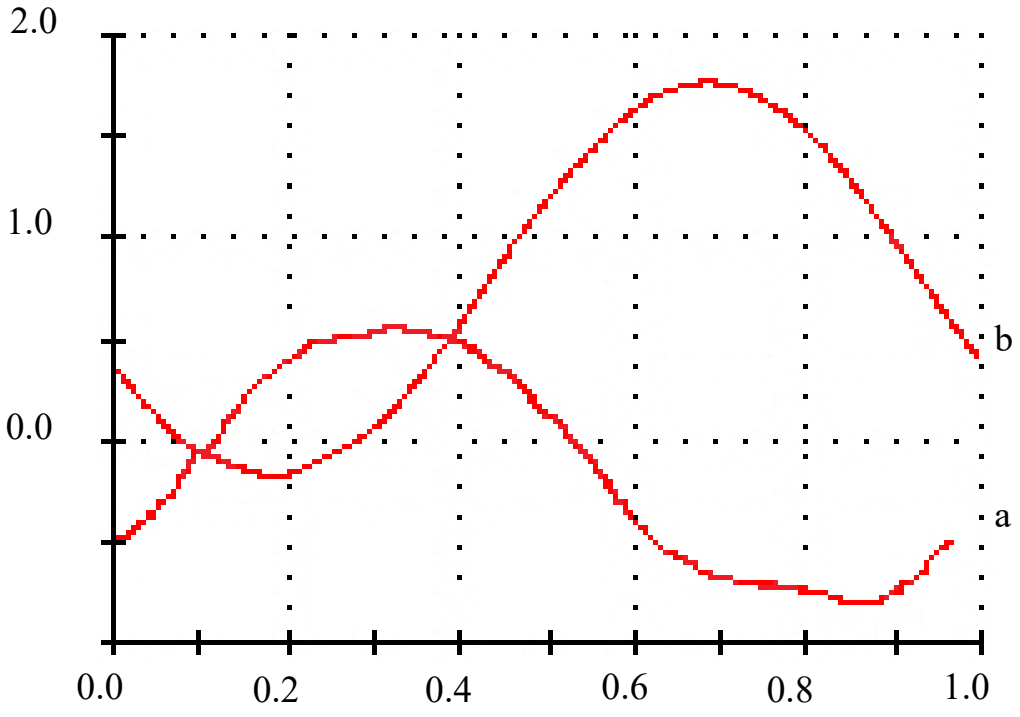

Fig. 6.18. Axial displacements of the brake disc edges in the design case "shear":

a) wedged part of the drum;

b) the repositioned part of the drum

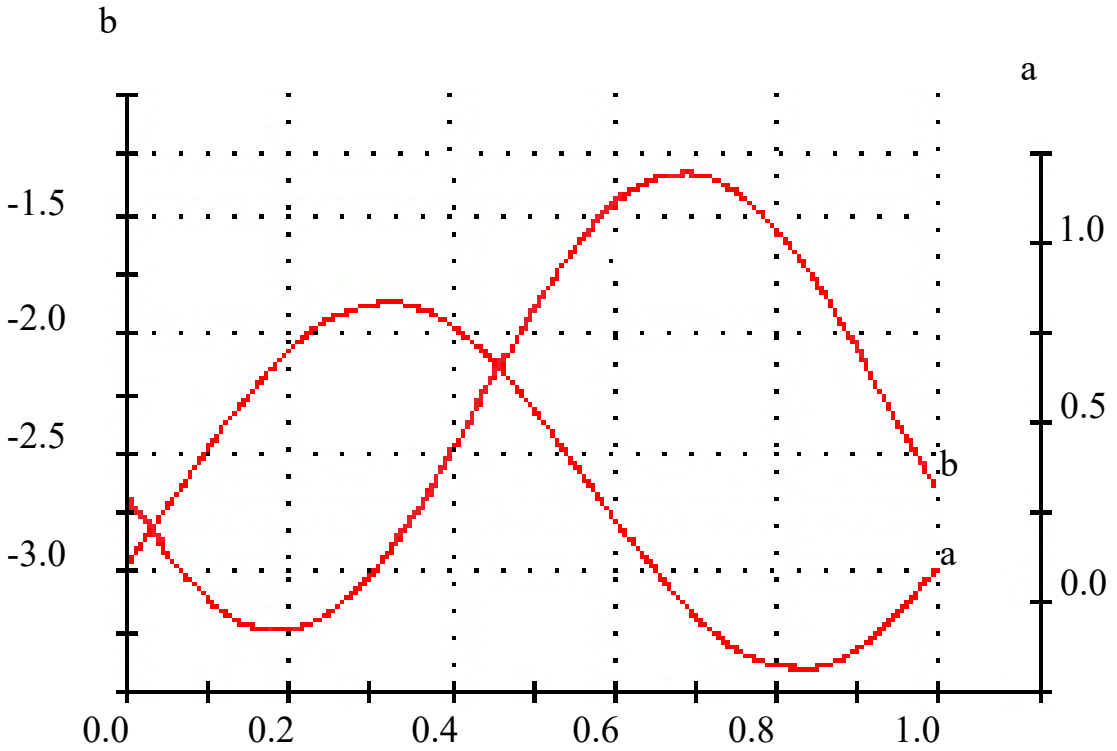

Fig. 6.19. Axial displacements of the brake disc edges in the design case "pressure": a) wedged part of the drum;
b) the repositioned part of the drum

In addition, the lengthening of the drum increases the deviation angle, which should not exceed 1°30′ for normal operation. To bring the deviation angle back to the recommended value, either move the machine away from the shaft or increase the height of the headframe, which means increasing the length of the rope string. If the length of the string exceeds the recommended 65 m, this can lead to axial and, as a result, transverse vibrations of the rope string, which can lead to a malfunction in the rope winding on the drum. This problem is solved by installing intermediate support supports, which in turn wear out and require additional maintenance.

A method for calculating long drums was developed - the averaging method. In the averaging method, a significant role is played by the choice of the so-called test load, which is used to load a single element (assembly) of the structure with the selected method of fastening. Thus, two types of loading were selected for the considered designs of drum assemblies: uniform external pressure and shear when the assemblies were fixed along the boundary of their connection with the hub. Then,

the thickness of the lining was determined to ensure the appropriate stiffness in the first and second cases. It turned out that the error in the maximum axial displacement of the brake disc edges was 8.1% for the assembly with an average frontal area in the first case and 69% in the second. This indicates that in fact the assemblies are subjected to combined loading and the use of the first or second case separately leads to an unacceptable error, which requires the development of other calculation methods.

CONCLUSIONS

The content of the monograph covers the solution of an urgent scientific problem of substantiation and development of a method for determining the design loads arising in the process of winding a rope on a cylindrical drum of a wire rope machine, taking into account the influence of geometric and stiffness characteristics of its supported structure. In solving this problem, the authors studied the stress-strain states of the structure under the influence of the wound turns, using a computer algorithm (designer's workstation) as the basis for the engineering methodology being developed. The result of this task was the ability to determine the parameters and design rational structures of the drums of the angle grinder.

In the course of the research, scientific results were obtained, conclusions were drawn and recommendations were developed, namely

1. Taking into account the complexity of creating modern designs of drum mine hoists and the problems that arise during their operation, the authors have established the expediency of using a simplified generalised parametric model of this installation in their design. In implementing this approach, the development of an effective methodology for determining the design loads on the drum was very useful, taking into account the geometric and stiffness characteristics of the supports introduced into the drum structure, as well as changes in its stress-strain state under the influence of rope winding.

2. A scientifically based method for determining the design loads arising from the winding and unwinding of a rope on a cylindrical drum was developed on the basis of a new approach that provides for modelling these processes in the form of successive putting on and taking off pre-stretched smooth elastic rings from the drum, and removal from it of pre-stretched smooth elastic rings, the stiffness of which is equivalent to the longitudinal stiffness of the rope, with the cylindrical drum considered as a reinforced axially symmetric structurally orthotropic shell (its parameters were calculated using a semi-empirical approach). The set of

characteristics for determining the drum's SSS was selected from the variants of its loading corresponding to different positions of the lifting vessels in the mine shaft.

3. The reliability of the method proposed by the authors was ensured due to the high degree of closeness of the calculated values of its main drum indicator to those obtained by measurements during the experiment on a laboratory setup. It was found that the error in determining the deflections of the drum sheath during sequential rope winding compared to the results of a physical experiment does not exceed 9 %.

4. The application of the developed method was made possible by the use of a computer algorithm (designer's workstation), which, according to, allows, on the basis of mathematical models of deformation of the supported drum and the rope winding process, to perform very accurate calculations of parameters and design rational structures of cylindrical drums of the wire rope machine. The dependencies between the generalised characteristics of the drums and the values of the resulting stresses in the structurally orthotropic shell were taken into account. The method became part of the engineering methodology for calculating the parameters and design of cylindrical drums approved by the scientific management of the National University of Science and agreed with the engineering service of NKMZ.

5. The studies carried out using the above-mentioned methodology have shown that in mine hoisting machines of the CR type, the stress-strain state of the drum significantly depends on the length of its cantilever part l near the plane of the cut of this structure and the stress variability factor β, which is determined by extracting the square root of the ratio of the values of the annular and bending stiffness of the shell. The cantilever length that meets the following condition was found to be optimal: $l_\beta = 0.7$. For example, optimising the length of a cantilever in a machine TsR - 6×3.4/0.6 results in a 35 % reduction in maximum stresses.

6. The use of frames as reinforcements was deemed inappropriate due to the increase in stresses in the drum shell, which in turn increased bending stresses where they could be installed, and it did not lead to a loss of stability of the drum.

7. The calculations carried out by the authors showed an exponential dependence between the values of the reduced maximum stress intensity and the

reduced radial stiffness of the head. Analysis of this dependence in relation to the wedged part of the drum of the TsR-6×3.4/0.6 made it possible to clarify that if the radial stiffness of the frontal plate exceeds the radial stiffness of the shell by 0.6 times, the stresses are constant and reach their asymptotic value, while a decrease in this stiffness causes an exponential decrease in stresses. In particular, at a relative stiffness of 0.2, they are 90 % of the maximum.

8. It also turned out that reducing the radial stiffness of the frontal plate by reducing its thickness reduces the stresses in the shell. The resulting additional stresses are concentrated in each rib. In addition, there is a local loss of stability in the holes between the ribs. To ensure structural reliability, we changed the shape of the rib and introduced additional reinforcing rings around the hole, as this reduces the stresses in the wedged part of the drum and prevents local loss of stability.

9. The methodological recommendations based on the results of calculations and experiments are used in the work of NKMZ designers to create new designs of the casing boring machines (the act of implementation of research and development work was approved by the Chief Engineer of the PJSC NKMZ's GC and MHM production on 12.04.2013).

10. Axial displacements were determined for the drum of the non-standard design of the TsR-6.75×6.2/1.95 mine hoisting machine due to the use of disc brakes in the machine design. The maximum axial displacements of the brake discs were 0.854 mm and 1.921 mm for the right and left edges, respectively.

11. Due to the large number of FEM mesh nodes of the original model (3352229 nodes), to simplify the calculation, an averaging method was applied, which consisted in replacing the reinforcement with ribs and braids with thickened fronts for two design cases - "shear", which modelled the effect of the tension force of the running and running rope strands and the action of its own weight, and "external pressure", which modelled the effect of the pressure of the wound rope on the drum. The drum was conventionally divided into 10 nodes and for nodes 3, 5, 6, 8 and 10, the rib and braid reinforcement was replaced by a thickened headband, with the condition of equality of stiffness to the type of shear strain and radial

stiffness of the original and simplified node for the "shear" and "external pressure" design cases, respectively. The results of the calculations carried out with the nodes averaged for the "shear" design case showed that the error of the simplified drum model relative to the original drum model was 8.1%, and for the calculation of the drum with the nodes averaged for the "external pressure" design case, the error was 69%, with the number of nodes for the simplified drum models being 645107 for "shear" and 662055 for "pressure".

REFERENCES

1. Fidrovs′ka N.M. Naukovi kontseptsiyi rozrakhunkiv kanatnykh barabaniv : avtoref. dys. … d-ra tekhn. nauk : 05.05.05. Kharkiv. 2012. 32. s.
2. Freund L.B., Suresh S. Thin Film Materials (Stress, Defect Formation and Surface Evolution). Cambridge : Cambridge University Press, 2003. 820 p.
3. Draper N.R., Smith H. Applied regression Analysis. 1 ed. New York : Wiley, 1966. 407 p.
4. Baraban shakhtnoyi pidnimal′noyi mashyny : pat. 7808 Ukrayina : MPK7 V 66 V 15/06. № 20041109393 ; zayavl. 15.11.2004 ; opubl. 15.07.2005, Byul. № 7. – 2 s. : kresl.
5. Baraban shakhtnoyi pidyomnoyi mashyny : pat. № 61682A Ukrayina, MPK7 V 66 D 1/30, V 66 B 15/00. № 2003032683 ; zayavl. 27.03.2003 ; opubl. 17.11.2003, Byul. № 11. – 3 s. : kresl.
6. Baraban shakhtnoyi pidyomnoyi mashyny : pat. № 58251 Ukrayina, MPK V 66 V 15/00. № u201010354 ; zayav. 25.08.2010; opubl. 11.04.2011; Byul. № 7. – 2 s. : kresl.
7. Shakhtna odnobarabanna pidyomna ustanovka : pat. № 76865 Ukrayina, MPK V 66 V 15/00. № 20041109347 ; zayavl. 15.11.2004 ; opubl. 15.09.2006, Byul. № 9. – 2 s. : kresl.
8. Iljin, S., Samusya, V., Iljina, I., Iljina, S. Influence of dynamic processes in mine winding plants on operating safety of shafts with broken geometry. *New Developments in Mining Engineering 2015: Theoretical and Practical Solutions of Mineral Resources Mining.* 2015. P. 425–429. https://www.taylorfrancis.com/chapters/edit/10.1201/b19901-73/influence-dynamic-processes-mine-winding-plants-operating-safety-shafts-broken-geometry-iljin-samusya-iljina-iljina
9. Zabolotny, K., Zhupiev, O., Molodchenko, A. Analysis of current trends in development of mine hoists design engineering. *New Developments in Mining Engineering 2015: Theoretical and Practical Solutions of Mineral Resources*

Mining. 2015. P. 175–179. https://www.taylorfrancis.com/chapters/edit/10.1201/b19901-31/analysis-current-trends-development-mine-hoists-design-engineering-zabolotny-zhupiev-molodchenko

10. Popescu, F.D., Radu, S.M., Andraș, A., Brînaș, I., Budilică, D.I., Popescu, V. Comparative Analysis of Mine Shaft Hoisting Systems' Brake Temperature Using Finite Element Analysis (FEA). *Materials.* 2022. Vol. 15, Iss 9, 3363. https://doi.org/10.3390/ma15093363

11. Zabolotnyi, K., Zhupiiev, O., & Molodchenko, A. Development of a model of contact shoe brake-drum interaction in the context of a mine hoisting machine. *Mining of Mineral Deposits.* 2017. Vol. 11, no. 4. P. 38-45. https://doi.org/10.15407/mining11.04.038.

12. Zabolotnyi, K., Panchenko, O., Zhupiiev, O., Haddad, J.S. Justification of the algorithm for selecting the parameters of the elastic lining of the drums of mine hoisting machines. *E3S Web of Conferences.* 2019. 123, 01021. https://doi.org/10.1051/e3sconf/ 201912301021

13. Ilin, S., Adorska, L., Pataraia, D., Samusia, V., Ilina, S., Kholomeniuk, M. Control of technical state of mine hoisting installations. *E3S Web of Conferences*. 2020. 168, 00045. https://doi.org/10.1051/e3sconf/202016800045

14. Zabolotny, K., Zinovyev, S., Zupiev, A., Panchenko, E. Rationale for the parameters equipment for rope dehydration of mining hoisting installations. *New Developments in Mining Engineering 2015: Theoretical and Practical Solutions of Mineral Resources Mining*. 2015. P. 275-283.

15. Zabolotny, K., Panchenko, E. Definition of rating loading in spires of multilayer winding of rubberrope cable. *New Techniques and Technologies in Mining – Proceedings of the School of Underground Mining*. 2010. P. 223-229. https://doi.org/10.1201/b11329-38.

16. K. S. Zabolotnyi, O. L. Zhupiiev, V. V. Symonenko. Substantiating The Methods For Calculating The Split Cylindrical Drums Of Mine Hoisting Machines

With Increased Rope Capacity. *Naukovyi Visnyk Natsionalnoho Hirnychoho Universytetu*. 2022. № 5. P. 60-67. https://doi.org/10.33271/nvngu/2022-5/060

17. Zabolotnyi, K., Zhupiiev, O., Molodchenko, A. (2018). The effect of stiffness of shoe brake elements on the distribution of contact pressures. *Naukovyi Visnyk Natsionalnoho Hirnychoho Universytetu*. 2018. № 2. P. 39-45. DOI:10.29202/nvngu/2018-2/3

Scientific publication

Zabolotnyi Kostiantyn, **Symonenko** Vitalii
Panchenko Olena, **Rutkovskiy** Maksym

JUSTIFICATION OF THE CALCULATION METHOD FOR CYLINDRICAL DRUMS OF MINE HOISTING MACHINES

Monography

Editor O.N. Ilchenko

Published «Jurfond» Dnipro, av. D. Yavornitskogo, 60

Acc. and pub. sh. 5,8.

Prepared for printing and printed in a higher education institution
Dnipro University of Technology
Certificate of entry into the State Register DK № 1842 from 11.06.2004 p.
49005, Dnipro, av. D. Yavornytskoho, 19.

Zabolotnyi K.S.

J95 **Justification of the Calculation Method for Cylindrical Drums of Mine Hoisting Machines**: monograph / K.S. Zabolotnyi, V.V. Symonenko, O.V. Panchenko, M.A. Rutkovskiy; Ministry of Education and Science of Ukraine, National Technical University "Dnipro Polytechnic." - D: Dnipro, Jurfond, 2024. - 190 p.

ISBN 978-966-934-571-4

The paper presents the results of research aimed at substantiating and developing a method for determining the design loads when winding a rope on a cylindrical drum of mine hoisting machines, taking into account the influence of the geometric and strength characteristics of its reinforced structure and the change in the stress-strain state that occurs there under the influence of rope turns. It is proved for the first time that by determining the average values of stresses in the structurally orthotropic shell of the drum, it is possible to select data for further refined calculation of its parameters by the FEM method. A methodology for calculating drums of non-standard designs of mine hoisting machines has been developed and substantiated on the example of the drum of the TsR-6.75×6.2/1.95 machine. The error of the method of simplified calculation: the method of averaging with increased thickness of the lobes is estimated.

For students, teachers, engineers, technicians, scientists and designers involved in heavy engineering.

UDC 622.673.1:621.778.27